Preparation of the satellite receiving station at Ny-Ålesund for upcoming satellite missions by means of new made-to-measure antenna operation software

vorgelegt von
Diplom Geophysiker
Carsten Falck
geb. in Bad Segeberg

von der Fakultät VI - Planen Bauen Umwelt
der Technischen Universität Berlin
zur Erlangung des akademischen Grades

Doktor der Ingenieurwissenschaften

- Dr.-Ing. -

genehmigte Dissertation

Promotionsausschuss:

Vorsitzender:	Prof. Dr. rer. nat. Jens Wickert
Gutachter:	Prof. Dr.-Ing. Frank Flechtner
Gutachterin:	Prof. Dr.-Ing. Sabine Klinkner
Gutachter:	Prof. Dr.-Ing. Klaus Brieß

Tag der wissenschaftlichen Aussprache: 5. Dezember 2017

Berlin 2018

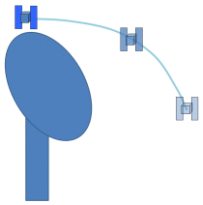

“There are two things children should get from their parents: roots and wings.”

(Source uncertain, but commonly accredited to Johann Wolfgang von Goethe)

Abstract

The German Research Centre for Geosciences GFZ operates a satellite-receiving station at Ny-Ålesund, Spitsbergen since 2001. Valuable support for several satellite missions was provided by the station on a best effort basis, while technical and software related issues, as well as uncertainties regarding important system properties, hindered any project participations with more binding commitments. The upcoming US-German GRACE-Follow On satellite mission with on-board GNSS-RO and gravity measurements and subsequent “near real-time” respectively low latency processing chains raised the demand to integrate the Ny-Ålesund station as the primary data receiving station of the mission’s ground segment. This required the demonstration of improved station performance and reliability with a perspective of sustainability as well as the determination of important antenna system parameters, such as the ratio of antenna gain to system noise (*G/T*). Analysis of receiving problems at the station in the past and considerations on methods to determine the station antennas characteristics suggested that improved antenna operation software was the most important and straightforward element on the planned way. Disappointing experiences with antenna operation programs of third parties, e.g., from shortcomings of functions, flexibility and support, indicated that the effort for an in-house development would pay off.

Consequently new software for the semi-automatic operation of the antennas at the satellite-receiving station at Ny-Ålesund was developed within this work. Main development objectives were the elimination of antenna operation problems which occurred in the past, to improve the station reliability, and to introduce program features for the support of required antenna measurements, e.g., such that use the sun as a natural radio signal source. Other focal

points during the development were the program-internal timing routines, a compact, informative and operation-safe graphical user interface (GUI) and advanced operation logging features. Lessons learned by the operation of software from other parties in the years since 2001 were respected and even some hardware related issues with the antenna systems at Ny-Ålesund were solved by means of the new software.

The new software “NYA-Sattrack” provides all required and desired functions, including some unconventional features. One example is the option to use two different external satellite orbit prediction programs and two sets of prediction elements (twoline elements). An operator can switch between the corresponding pass predictions at any time, even during a satellite contact with already moving antenna. This might be useful, e.g., in a Launch and Early Orbit Phase (LEOP), when different predictions from different sources and with uncertain quality have to be used. Another example is the generation of graphical logs for each satellite contact. An operator can check these logs very fast and simultaneously with normal, text-based logs through a built-in log-viewer function. An eventually desired adaptation to other antenna system types with different technical properties is explicitly supported by the software design as all antenna-specific program code is allocated to individual software interface modules (Dynamic Link Libraries). The new program “NYA-GPS-SYNC” maintains the accuracy of the antenna operation computer clock to support precise operation timing.

The two different antenna positioning systems (Elevation over Azimuth and X over Y) of the satellite-receiving station at Ny-Ålesund are operated routinely with NYA-Sattrack since July 2014 and each of the antennas tracks more than 25 satellite passes per day. The number of outages related to antenna operation issues and the manual effort for the operation of the antennas has decreased significantly since introduction of NYA-Sattrack. The new program features of NYA-Sattrack, e.g., such as the sun-tracking mode combined with scan modes, strongly supported the determination of important antenna system characteristics and the detection of a source of radio interference. All achievements of this work have a benefit for supported missions, e.g., due to a better knowledge about technical boundary conditions for contact planning and less data losses during data reception. NYA-Sattrack significantly improved the reliability, efficiency and sustainability to support current and future satellite missions and the Ny-Ålesund ground station is ready to work as the primary downlink station for the GRACE-FO mission, due for launch in February 2018.

Zusammenfassung

Das Helmholtz-Zentrum Potsdam Deutsches GeoForschungsZentrum GFZ betreibt seit 2001 eine Satelliten-Empfangsstation bei Ny-Ålesund auf Spitzbergen. Die Station hat, so gut es ging, wertvolle Dienste für etliche Satellitenmissionen geleistet. Verbindliche Verpflichtungen in Projekten konnten aber, wegen hard- und softwaretechnischer Probleme und den nur unsicher bekannten Leistungsparametern der Station, nicht eingegangen werden. Die aufkommende US-amerikanisch-deutsche GRACE-Follow On Satellitenmission für GNSS-RO- und Schwerefeldmessungen und die sich daran anschließenden nahe-Echtzeit Datenverarbeitungsketten führten zu dem Wunsch, die Ny-Ålesund Station als primäre Empfangsstation im Bodensegment der Mission zu integrieren. Dies erforderte den Nachweis von verbesserten Betriebseigenschaften, sowie verbesserter Betriebszuverlässigkeit und Zukunftssicherheit, und die Bestimmung wichtiger Antennenparameter, wie dem Verhältnis von Antennengewinn zu Systemrauschen (*G/T*). Analysen zu Empfangsproblemen an der Station in der Vergangenheit und Überlegungen zur Bestimmung der Antennencharakteristika legten nahe, dass der wichtigste und direkteste Schritt auf diesem Weg eine verbesserte Software für den Betrieb der Antennen sein würde. Wegen in verschiedener Hinsicht enttäuschenden Erfahrungen mit Antennenbetriebssoftware von Dritten, z.B. aufgrund unzureichender Funktionen und mangelnder Flexibilität und Unterstützung, wurde angenommen, dass sich der Aufwand für eine eigene Programmentwicklung auszahlen würde.

Infolgedessen wurde mit dieser Arbeit eine neue Software für den halb-automatischen Betrieb der Antennen an der Satelliten-Empfangsstation Ny-Ålesund entwickelt. Die wichtigsten Punkte dabei waren die Lösung der in der Vergangenheit beobachteten Betriebsprobleme mit den Antennen, bzw. die Verbesserung der Zuverlässigkeit der Station, und Funktionen für Messungen an und mit den Antennen, z.B. mit Nutzung der Sonne als natürliche Quelle für Radiosignale. Andere Schwerpunkte der Entwicklung waren die zeitlichen Abläufe im Programm, eine kompakte, informative und betriebssichere graphische Nutzerschnittstelle (GUI) und erweiterte Möglichkeiten zum Protokollieren (Loggen) des Betriebs. Dabei wurden die seit 2001 mit dem Betrieb von extern beschaffter Software gemachten Erfahrungen berücksichtigt und sogar durch Hardware verursachte Probleme beim Betrieb der Antennen in Ny-Ålesund durch die neue Software gelöst.

Das neue Programm „NYA-Sattrack“ stellt alle benötigten und gewünschten Funktionen bereit, inklusive einiger ungewöhnlicher Funktionen. Ein Beispiel ist die Möglichkeit zur Nutzung von zwei unterschiedlichen externen Programmen zur Bahnvorhersage mit unterschiedlichen Bahnelementen (twoline elements). Ein Operator kann so jederzeit zwischen den beiden entsprechenden Bahnvorhersagen wechseln, sogar während eines Satellitenkontakts mit sich bereits bewegenden Antennen. Dies könnte z.B. in der ersten Zeit nach einem Satellitenstart nützlich sein, wenn unterschiedliche Bahnberechnungen mit unsicherer Genauigkeit von unterschiedlichen Quellen verwendet werden müssen. Ein anderes Beispiel ist die Erzeugung graphischer Logs für die einzelnen Satellitenkontakte. Diese Logs lassen sich von einem Operator sehr schnell überprüfen, durch eine integrierte Anzeigefunktion sogar zusammen mit den textbasierten Logdateien. Eine möglicherweise gewünschte Anpassung des Programms für andere Antennen mit unterschiedlichen Betriebseigenschaften wird dadurch unterstützt, dass antennenspezifischer Programmcode in Programmerweiterungen (Dynamic Link Libraries) platziert wurde. Das neue Programm “NYA-GPS-SYNC” kontrolliert die Uhr des Computers für die Antennensteuerung und sorgt so für einen zeitlich präzisen Betrieb.

Die beiden unterschiedlichen Antennenpositionierungssysteme an der Satelliten-Empfangsstation Ny-Ålesund (Elevation über Azimut und X über Y) werden seit Juli 2014 routinemäßig mit NYA-Sattrack betrieben. Jede der beiden Antennen bedient mehr als 25 Satellitenkontakte pro Tag. Seit der Einführung von NYA-Sattrack haben betriebsbedingte Ausfälle stark abgenommen, ebenso der manuelle Aufwand zum Betrieb der Antennen. Die neuen Funktionen von NYA-Sattrack, wie z.B. das Verfolgen der Sonne mit einer Antenne in Kombination mit speziellen Bewegungsmustern, haben die Bestimmung wichtiger Antennenparameter und das Erkennen einer funktechnischen Störquelle ermöglicht. Alle erzielten Ergebnisse nützen indirekt auch den unterstützten Missionen, z.B. durch bessere Kenntnis der technischen Randbedingungen für die Planung von Kontakten und geringere Datenverluste beim Datenempfang. NYA-Sattrack hat die Zuverlässigkeit, Effektivität und Nachhaltigkeitsperspektive der Station für die Unterstützung aktueller und zukünftiger Satellitenmissionen stark verbessert, so dass diese nun für den geplanten Einsatz als primäre Empfangsstation für GRACE-FO bereit ist (geplanter Start im Februar 2018).

Table of Content

1 Preface

The GFZ German Research Centre for Geosciences was founded in the reunited nation of Germany in 1992 as the new national institute for the sciences of the solid Earth. It is located on the Telegrafenberg in Potsdam where also the preceding institutes and observatories settled, beginning with the Royal Prussian Geodetic Institute in 1870. The function of the GFZ as a major research institution includes the operation of major infrastructure, e.g., such as related to satellite missions.

GFZ participated in several satellite missions since the foundation and in 1995 GFZ‘s first own satellite GFZ-1 was ejected into space (from Russian MIR station). It had a number of laser reflectors to be tracked by laser ranging stations on the ground, but no active onboard elements. GFZ’s first own satellite project with an active space segment was PRARE (Precise Range and Range Rate Experiment), which was installed on 3 satellites (ERS-1, Meteor 3-7, ERS-2) and operated in the years from 1995 until 2007. GFZ was responsible for the design, implementation and operation of the satellite mission CHAMP (in orbit 2000 – 2010) and plays an important role for the mission GRACE (two satellites launched in 2002), including a participation in the US/German Science Data System and mission operations. Special GPS receivers on TerraSAR-X and TanDEM-X, for high rate measurements with occulting GPS satellites (GPS-RO method) and the determination of the inter-satellite baseline with sub-mm accuracy (for high precision Digital Elevation Modeling), are operated by GFZ. Highly efficient satellite laser reflectors for satellite laser tracking were developed in house and installed on many satellites, e.g., Kompsat-5 (2013) or the three satellites of the ESA-mission SWARM (2013), which was also initiated with strong contributions by GFZ. More satellite missions with participation of GFZ are on the way, e.g., GRACE Follow-On (2018) and EnMAP (2018). GFZ operates a laser ranging station at Potsdam and a satellite-receiving station at Ny-Ålesund, Spitsbergen, both supporting the scientific output and operational tasks of several satellite-related projects and many working groups worldwide.

2 Motivation

The author was involved in the scientific-technical operation of the satellite CHAMP since 2001. The CHAMP mission had a procedural link to the, at that time, single antenna installation at Ny-Ålesund, which was in operation since 2001. This so called “CHAMP-antenna” was initially operated in cooperation between GFZ and DLR, at least for a few years, when it was also used to receive the DLR-satellite BIRD. In praxis, organisational, financial and scheduling aspects of the operation at Ny-Ålesund were covered by GFZ, but technical know-how, also regarding antenna operation software and maintenance works was contributed by DLR.

In spring 2002 there was already the last maintenance visit of DLR-staff at Ny-Ålesund and the author visited the site for the first time. In 2005 the cooperation contract between DLR and GFZ regarding the jointly owned “CHAMP-antenna” system (later named NYA-1) expired. Meanwhile the practical cooperation in the partnership had already phased out too, mainly due to the retirement of related technical staff at DLR, and so GFZ had to increase own technical competence for the satellite-receiving activities. In this context GFZ replaced aged hardware and installed a lot of supplementary equipment and upgrades, including new telemetry receivers, and even a second antenna system (named NYA-2). The antenna site at Ny-Ålesund grew to a small receiving station with increased capacity under full and exclusive control by GFZ and served more satellite missions (GRACE, SAC-C, TerraSAR-X and TanDEM-X). All receiving activities were executed on a best effort basis, meaning without stringent contractual commitments.

The professionality and capabilities of the satellite-receiving station Ny-Ålesund were considerably higher than those of, e.g., a typical ground-station at a university, but also undoubtable lower than those of professional ground-stations as operated by ESA and NASA. The main reasons for the shortfall behind professional stations were, beside some obvious technical details (e.g., no uplink), the not yet competitive operation reliability, caused by technical and software problems, and the lack of a verified system specification, mandatory for professional work, e.g., to allow link budget calculations.

The most serious problems with the NYA-1 antenna resulted in outages of receiving operations and the loss of some data within one satellite-receiving contact or even the failure of many satellite contacts over periods of several days. Other problems resulted in significant

and continuous, yet principally superfluous effort for system operation, monitoring and maintenance. Some workarounds and software patches were introduced, but a satisfying system performance and operational reliability was never reached. Each of the different programs for the operation of the both antennas had limited and not extendable capabilities and was not sustainable for various reasons. In fact, also some components of the station, especially the NYA-1 antenna operation computer (hard- and software), were hardly serviceable any more, but could not be replaced as the old antenna operation software was tailored for that old computer environment (e.g., special device driver).

The described unsatisfying status of the station was still somehow sufficient to support data processing chains and operational tasks of the mentioned satellite missions, although with a dark perspective, but not to fulfil critical satellite mission tasks or to accept serious contractual commitments. It was then the upcoming US-German GRACE-FO satellite project which pushed ideas to use the satellite-receiving station Ny-Ålesund for frequent data downlinks as an important operational component of the GRACE-FO ground segment. The integration of Ny-Ålesund was expected to support the mission operation and, even more important, the scientific output of “near real-time” product generation chains (GPS-RO and gravity). The mandatory procedures for mission components (e.g., critical reviews by external (NASA) experts) suggested that this goal could be reached only by demonstration of increased station operation reliability and a traceable specification of important system characteristics.

It was the aim of this work to upgrade the satellite-receiving station Ny-Ålesund by means of new developed antenna operation software, as this measure was identified to be most critical to continue operations at low costs and to reach a level of professionality that would allow the participation in higher ranked future projects, such as GRACE-FO. The developed software or at least the developed ideas and solutions may also be useful for other ground stations, especially when they are operated with comparable low personal and financial effort.

3 NYA station support for science and satellite operations

This section describes the context between the operational characteristics of the satellite-receiving station at Ny-Ålesund, commonly addressed by its mnemonic NYA, and the derived benefit for satellite missions and related projects. The concomitant deduction is that quality and quantity of scientific output of satellite projects depend, beside other factors, also on operational issues, which profit significantly from frequent, reliable and affordable satellite contacts, such as provided by NYA. The positive impact on satellite operations is highlighted by examples from praxis. Corresponding relationships to the productivity of related scientific projects are derived from the characteristics of missions and scientific instruments, measurement methods and related operational issues. Pointers to upcoming missions and projects sketch the expected role of NYA in the next future.

3.1 Important operation factors and features of the NYA ground station

The usefulness of a satellite ground station for satellite missions is primarily determined by technical characteristics (described in detail in chapter 4.1), but also by other factors. The NYA ground station has some distinctive features, which are described in the following and which, despite its admittedly limited infrastructures, allow extraordinary valuable and effective support for several projects.

3.1.1 Frequent satellite contacts

One important feature of NYA, the large number of possible contacts between the station and polar orbiting satellites, follows from the geographical location (78° 55′ North, 11° 56′ East) and the corresponding satellite orbit parameters. Figure 1 (generated with software STK = Satellite Tool Kit) sketches the areas of visibility of the ground stations WHM at Weilheim, Germany (yellow circles), NST at Neustrelitz, Germany (green circles), and NYA at Ny-Ålesund, Spitsbergen (red circles) for minimum antenna elevations of 5° and a satellite altitude of 500 km. The restriction to elevations above 5° is commonly used at ground stations, e.g., to avoid problems from signal propagation effects at low elevations (e.g., ground reflections) and masking of the local horizon. The altitude of 500 km corresponds to the initial altitude of the GRACE satellites and is representative for other LEO (Low Earth Orbit) satellites as well. The ground tracks of GRACE-1, which are projections of its orbits onto the surface of the Earth, are displayed as blue lines for a period of 24 hours. Some of the satellite ground tracks (orbits) cross the areas of visibility of all three ground station, which

allows contacts with them. However, most of the orbits are outside the areas of visibility for WHM and NST, while all orbits can be accessed from NYA. In result NYA allows at least 15 contacts per day with LEO satellites in polar orbits (like the GRACE satellites), while WHM and NST cannot make more than about 4 effectually useable contacts per day with the same satellites. The frequent satellite contacts at NYA allow the generation of products from satellite data with low latencies ("near real-time") and are in praxis not replaceable by other measures.

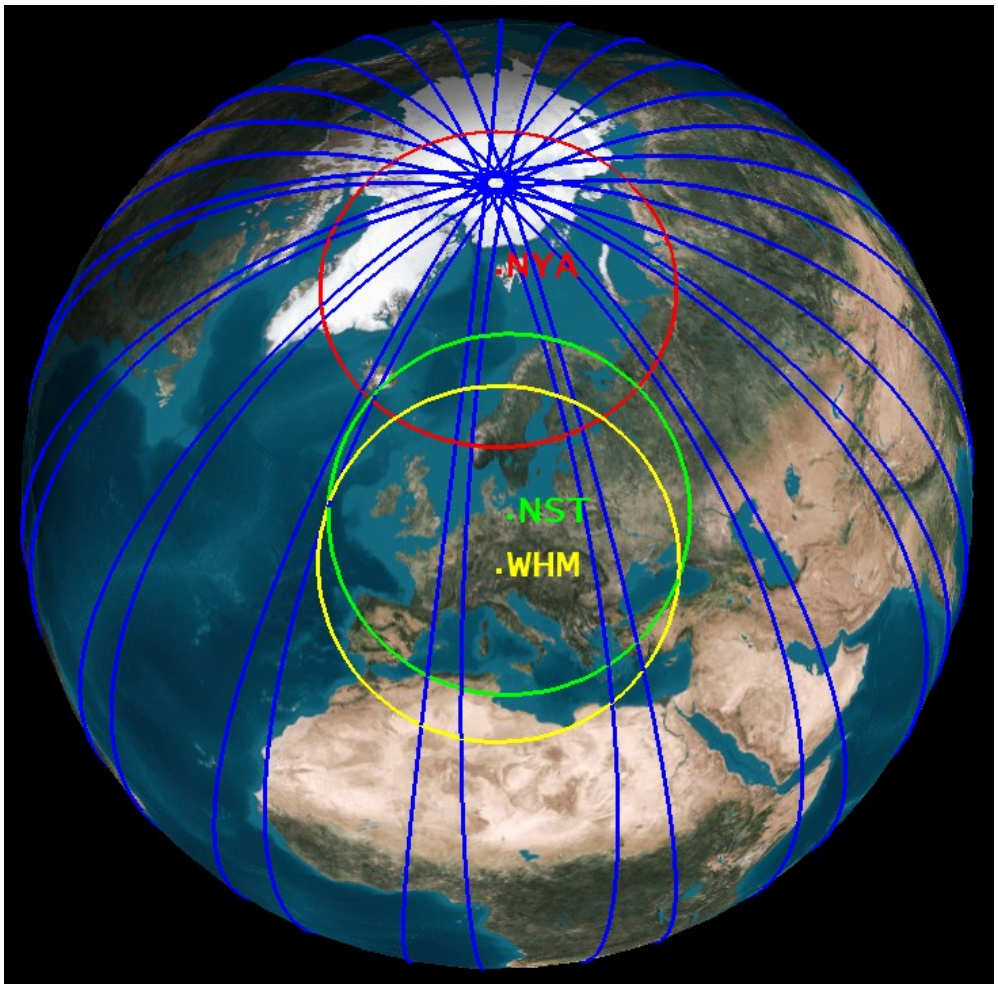

Figure 1: Visibility of GRACE at ground stations WHM, NST (both DLR) and NYA (GFZ)

3.1.2 Two antennas and two receivers

The NYA station has two antennas and two main receivers which can be operated very flexible according to actual requirements. The operation modes of antennas and receivers are currently planned for one week in advance, but can be changed at any time and through only one simple structured interface (Jobfile concept, 5.5). Figure 2 (screen dump from web-based

service, developed by W. Köhler, GFZ) illustrates the distribution of scheduled satellite contacts with respect to time and involved antennas. Each day of the week is represented by one horizontal bar. Each “day-bar” is subdivided into two bars which show operation times of NYA-1 (upper bar) and NYA-2 (lower bar), color coded according to individual satellites (vertical bars).

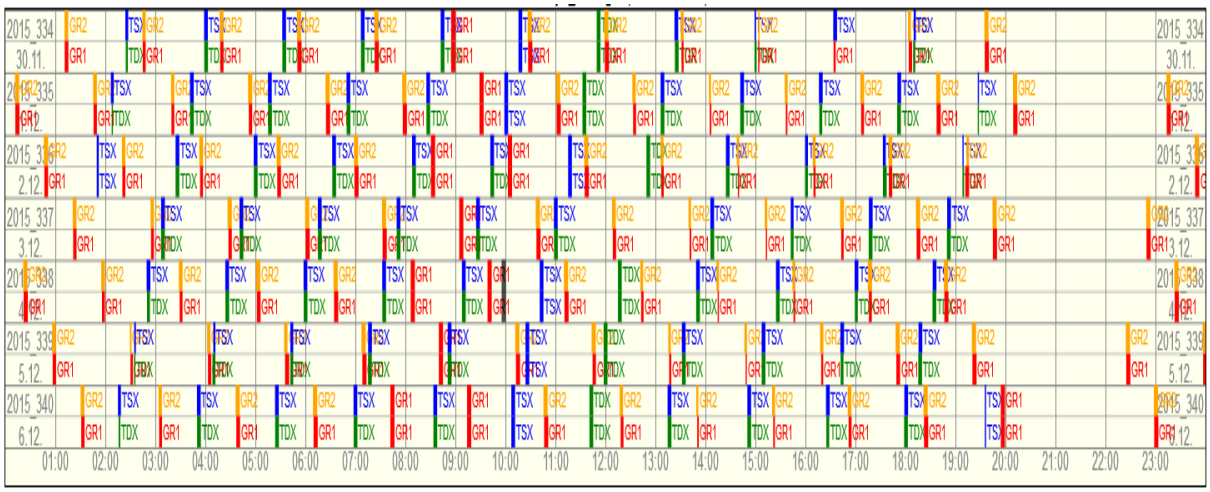

Figure 2: Display of scheduled satellite contacts with the two NYA antennas (© GFZ)

One antenna per satellite may be used if two satellites to be tracked appear close to another in time. This is always the case for the both GRACE satellites, which fly on the same orbit with a nominal along track distance of 220 km and the TerraSAR-X / TanDEM-X twin formation, flying with a nominal inter satellite distance of up to 200 m only. Consequently this mode of operation is used for most contact times and displayed in Figure 2, e.g., at the time of first contacts with GRACE-1 and GRACE-2 on 30.11.2015 at about 1:00 UTC. Only one of the mentioned satellites could be received at a time, respectively per orbit, if there would be only one antenna at NYA. This would increase the mean data access latencies by at least one orbit period for each satellite in a twin-like orbit constellation. The availability of two antennas and two receivers at the NYA station allows to access data from both satellites in a close formation like GRACE simultaneously, resulting in data latencies of one orbit period, at the maximum.

The both NYA antennas can also be used simultaneously to follow the track of one satellite, so that data is received at the station even if one of the receiving chains (antenna with receiver etc.) has technical problems. Examples in Figure 2 are the contacts on 6.12.2015 at about 19:40 UTC (TerraSAR-X) and at about 20:00 UTC (GRACE-1), when each of the satellites was received by both antennas. This kind of operation provides redundancy and reduces the

probability for data losses significantly (product of failure probabilities of each chain). It may be used when contacts are very important, e.g., during special satellite maneuvers or if satellites need special attention (e.g., at critical battery status).

3.1.3 Low operation costs

Another key feature of NYA is the low operation costs, which result from the unmanned, yet fully controllable, semi-automatic operation of the station. Most known satellite ground stations are operated with local staff at considerably high costs, even when all systems and processes at the station are highly automated. The low station operation costs of NYA allow low cost support for satellites with small project budgets (e.g., satellites built by universities, see chapters 3.4.2 and 3.4.1) in the frame of a scientific cooperation with GFZ. Also projects with larger budgets profit from the low NYA operation costs as some particular satellite data based products may hardly be financed through satellite projects or third party funding. Good examples are the GPS-RO (radio occultation) near real-time (NRT) products for numerous weather services, derived from NRT data of special GPS-receivers onboard GRACE and other satellites.

3.2 Satellite projects with regular NYA support (past and present)

Several satellite missions were and are supported by NYA. This section gives some basic information for all of these missions and some more details, e.g., about instruments and products for missions with higher importance for the NYA station and GFZ.

3.2.1 CHAMP

The German CHAMP (Challenging Minisatellite Payload for Geoscience and Application) satellite mission was managed and operated by GFZ. CHAMP was launched into a polar orbit (inclination: 87.18 degrees, period 94 minutes) from Plesetsk (Russia) on 15 July 2000. The altitude was initially about 450 km, decreased below 350 km at the end of the scientific operations, and the satellite decayed on 19 September 2010 (Figure 12). The original satellite operation plans were oriented at the designed satellite lifetime of 5 years. These plans were changed later, when the excellent performance of CHAMP (Reigber, et al. 2006) offered a mission extension, even though some of the onboard systems showed evidence of degradation. The increasingly required intensive care for all onboard systems was based on an extended contract with GSOC (German Space Operation Center), which was connected with

additional costs for GFZ, and the support through NYA with frequent contacts (no additional costs).

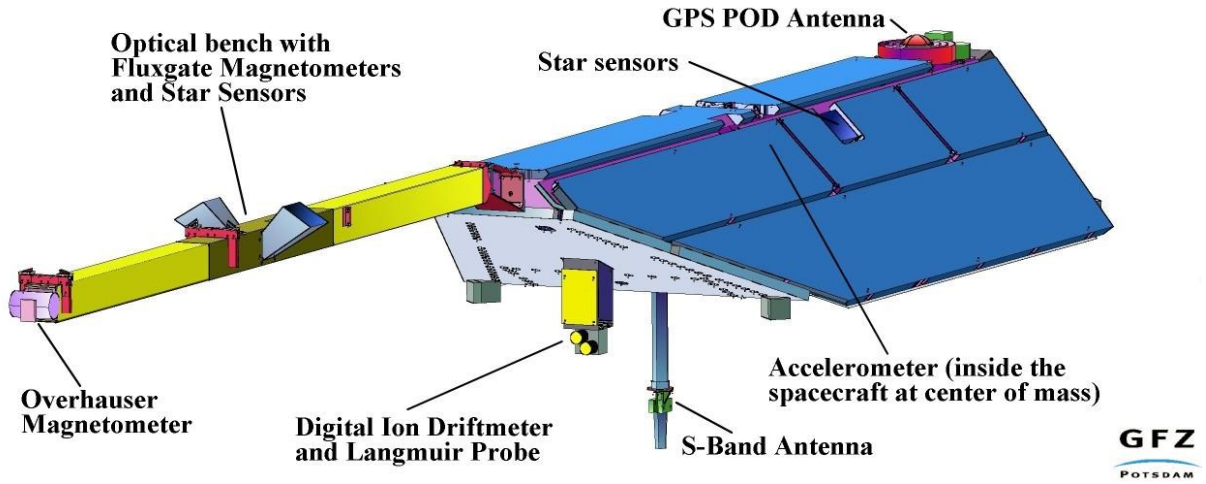

Figure 3: Instruments on satellite CHAMP (© GFZ)

Several scientific instruments on CHAMP (Figure 3) delivered data for science related to the solid Earth and atmospheric research. A GPS receiver delivered data for precise orbit determination (POD) and related orbit perturbations, which were used to determine the Earth's gravity field. The effects of non-gravitational forces acting on the satellite, e.g., atmospheric drag, which contribute to such perturbations, were determined with an accelerometer, placed in the satellite center of mass. Two vector magnetometers (Fluxgate) and one absolute magnetometer (Overhauser) were used to determine the magnetic field. The vector magnetometers were mounted on optical benches together with star sensors, which determined the satellite attitude. One of these magnetometer-star sensor arrangements and the Overhauser magnetometer were installed on a nonmagnetic boom to keep it away from disturbing signals of other satellite systems. A Digital Ion Driftmeter (DIDM) and a Langmuir Probe measured parameters to determine properties of the electric field. A second GPS antenna (additionally to the antenna for POD) was mounted at the satellite rear side and tracked GPS satellites intensively during short intervals (e.g., about two minutes) when they were disappearing below the Earth horizon, which caused an occultation of the received signals (Figure 4). These GPS-RO measurements provided data for the determination of atmospheric and ionospheric properties, e.g., vertical profiles of temperature and humidity (Wickert et al. 2001) or the electron density (Jakowski, et al. 2002). In addition 3D electron density distributions of the topside ionosphere could be derived from the slant-related total

electron content (derived from GPS data as recorded with the POD antenna data (Heise, et al. 2002).

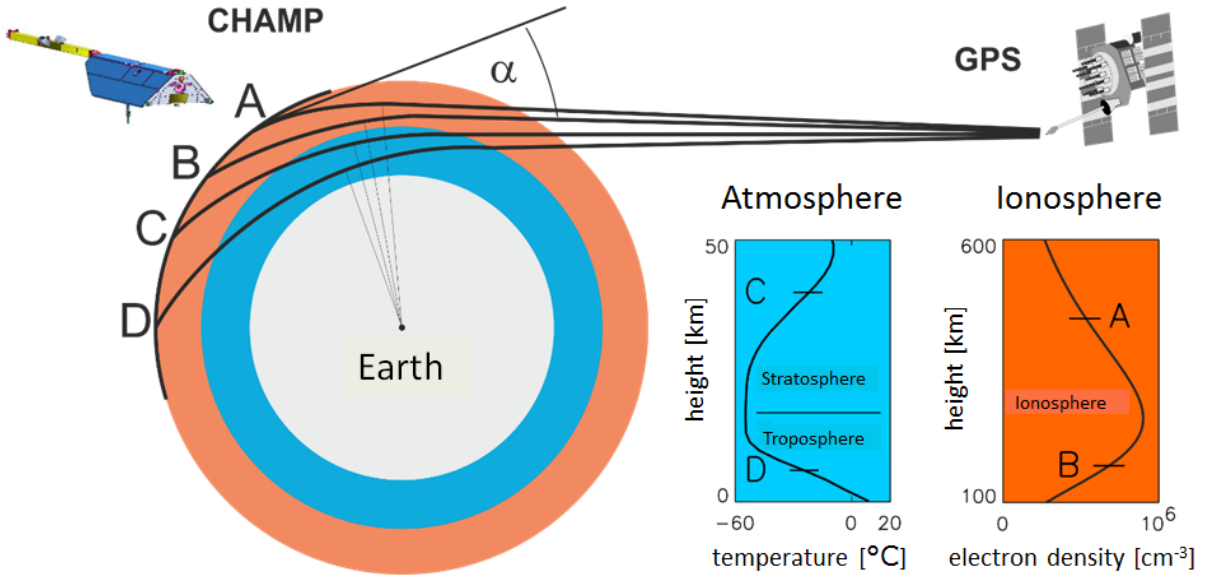

Figure 4: GPS-based sounding of atmosphere and ionosphere (adopted from Wickert 2002)

The importance of GPS-RO data among 25 different meteorological observation types, which are operationally used at ECMWF (European Centre for Medium-Range Weather Forecasts), was investigated in 2014 (Cardinali and Healy 2014). It was concluded that *"The fifth largest impact either in the analysis or in the forecast is provided by GPS-RO data, despite only contributing ~3% of the observations assimilated in the system."* It can be assumed that the importance of GPS-RO data will grow with a higher availability of GPS-RO data, e.g., from more satellite missions with appropriate instrumentation, especially when these are operated in correspondingly optimised constellations.

The CHAMP mission was the first one, which provided continuously around 200 daily globally distributed vertical profiles, derived from GPS-RO measurements (Wickert et al. 2001). GFZ developed, in cooperation with DLR, an automated data processing system (Wehrenpfennig et al. 2001, Wickert 2002, Schmidt et al. 2010) to provide vertical meteorological profiles from CHAMP operationally to international weather services and the atmospheric research community. The system was developed and validated already before the CHAMP launch and was also used for the RO data analysis of other missions (Wickert et al. 2009 a). The quality of the CHAMP data products, generated by GFZ, was validated within numerous studies (Wickert et al. 2004) before they were operationally assimilated by the

weather services, e.g., the DWD (Deutscher Wetterdienst) or ECMWF (Healy, et al. 2007) since September 2006. Weather services have tight time constraints for the delivery of their products. This implies even tighter time constraints for the provision of the observation data to be assimilated into the forecasts. This applied also to the GPS-RO measurements from CHAMP. Thus, it was mandatory to provide processed GPS-RO data from CHAMP with a latency of maximum 3 hours after the time of measurement, including the data downlink, data transfer to GFZ at Potsdam and the POD and RO data processing (Wickert 2002). The 3 hours requirement could not be satisfied with the regular CHAMP mission ground segment, which operated ground stations in Germany only (Neustrelitz, Weilheim). These stations could not have more than 4 contacts per day with CHAMP due to its low altitude and high inclination orbit and the revolution of the Earth (explained in section 3.1.1), resulting in data delivery delays of up to 12 hours.

The additional use of commercially operated satellite ground stations, either located on polar or sub polar latitudes, for frequent GPS-RO raw data downlink contacts with CHAMP was not possible due to the high costs (e.g., 200 USD per contact). This fact and the requirements and circumstances described above led to the installation of the first antenna at Ny-Ålesund on Spitsbergen in 2001 which was operated for frequent download contacts with CHAMP as an indispensable prerequisite for the near real-time GPS-RO processing activities.

3.2.2 BIRD

The German satellite BIRD (Bispectral Infra-Red Detection, (Figure 5: DLR, CC-BY 3.0) was operated by DLR and carried optical instruments for the detection of fires on the Earth. It was launched from India on 22 October 2001 (altitude: 566 km, inclination: 97.9°) and received support from the NYA-1 antenna between 2002 and 2006. The antenna collected housekeeping data, which was used to prepare BIRD for scheduled imaging campaigns. The corresponding configuration commands were transmitted during following contacts with German ground stations, e.g., in parallel with the downlink of payload data. The receiving activities for BIRD at NYA were ceased when the on-site BIRD-receiver hardware was broken.

Figure 5: Satellite BIRD (© DLR)

3.2.3 GRACE

The US-German GRACE (Gravity Recovery And Climate Experiment) mission engages two identical satellites (Figure 6) which were launched simultaneously into a circular orbit with an altitude of 500 km and an inclination of 89° from Plesetzk (Russia) on 17 March 2002. The satellites follow each other with a nominal distance of 220 km, principally in the same orbit (time offset). The design of the GRACE satellites is very similar to the design of CHAMP and includes special GPS-equipment (POD and GPS-RO), star-sensors (attitude determination) and accelerometers for the measurement of non-gravitational forces, but no magnetometers and instrument boom and no instruments for electric field measurements. Irregularities in the Earth's gravity field affect the orbits of the satellites, one after the other, and thus also the distance between the satellites.

Figure 6: GRACE satellites (© Astrium / GFZ)

A not preceded high accuracy of gravity determination from space is supported by an onboard K-band microwave ranging instrument (in combination with POD) which measures the inter satellite distance and distance rate very precisely (better than 1 µm and 0.1 µm/s). These very precise gravity-related measurements are the basis to derive routinely monthly solutions (with 60 days delay) within the GRACE Science Data System. Additionally, near real-time daily solutions (with 1-2 days delay) have been derived in the EU funded project EGSIEM (European Gravity Service for Improved Emergency Management, (Gouweleeuw, et al. 2018)).

The secondary target of the GRACE mission, as for CHAMP, is global atmospheric sounding based on GPS-RO measurements. The satellites fly in a face to face formation and thus the GPS-RO antenna of the leading GRACE satellite points in flight direction, while the GPS-RO antenna of the tailing GRACE satellite points to the anti-flight direction. The onboard GPS-receivers software does not allow the tracking of rising GPS-satellites (appearing in flight direction) and so in praxis only one of the two GRACE satellites can perform GPS-RO

measurements at a time. The regular frequent provision of GPS-RO data from the GRACE satellite actually flying in the tail position through downlink contacts with NYA began on May 22th 2006 right before ECMWF started the assimilation of RO data into their weather prediction models (Wickert et al. 2009 b).

The designed satellites lifetime of 5 years has been exceeded meanwhile by 10 years and the onboard batteries suffered from aging, similar as experienced with CHAMP. The thus required more intensive monitoring of both GRACE satellites health was supported by NYA through frequent contacts, from that time also including the second GRACE satellite which did not perform GPS-RO measurements, if required. Some measures were undertaken to maintain as much science instrument operation time as possible under these increasing adverse conditions, e.g., by applying special battery management strategies (Herman, et al. 2012). The mission was officially ended in October 2017 (Cole und Buis 2017).

3.2.4 SAC-C

The SAC-C satellite (Figure 7, credit: Juandedeboca (https://commons.wikimedia.org/wiki/File:Maqt2SACC.JPG), https://creativecommons.org/licenses/by-sa/4.0/legalcode) was launched from USA on 21. November 2000 into a circular polar orbit (altitude: 705 km, inclination: 98.2º) to collect data for research connected to the dynamics of the Earth's surface, the atmosphere, the ionosphere and the geomagnetic field. Main project contributors are the institutions CONAE (Argentina) and NASA (USA), while more partners from other countries participate with provided instruments etc. The instrument setup is similar to CHAMP, e.g., including basically the same vector magnetometer and GPS-RO instrumentation.

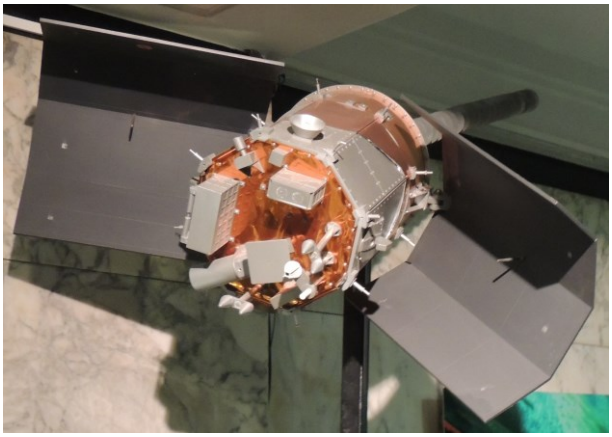

Figure 7: Model of SAC-C (© Wiki Commons)

First tests to receive SAC-C at NYA were made in 2009. The transmitted satellite data had a complex structure (e.g., Viterbi-coded) which could not be decoded by the receivers at NYA. GFZ developed some software for the decoding of SAC-C data and finally the tests were successful. SAC-C was received at NYA over a time of one year with several passes per day since November 2010, allowing an operational NRT-use of the satellite GPS-RO data.

3.2.5 TerraSAR-X

The German TerraSAR-X mission was realised in a public-private partnership between DLR and EADS Astrium GmbH (now Airbus Defence & Space). The satellite (Figure 8: © DLR, CC-BY 3.0) was launched from Baikonur (Kazakhstan) into a circular orbit with an altitude of 515 km and an inclination of 97.44° on 15 June 2007. The main target of the mission is in the field of SAR-measurements (Synthetic Aperture Radar) to map the Earth's surface. After some years in the orbit the satellite was operated in a twin formation with the satellite Tandem-X (3.2.6), to increase the aperture of the SAR antennas, which were then operated in a combined mode.

Figure 8: TerraSAR-X satellite (© EADS-Astrium)

The secondary payload, the TOR instrumentation (Tracking, Occultation and Ranging) with a special two frequency GPS receiver called "IGOR" (Figure 9) and GPS-antennas, was provided by GFZ and allows, beside the tracking of GPS satellites for POD, also GPS-RO measurements for the sounding of atmospheric and ionospheric parameters (Zus, et al. 2014). The TOR instrument uses a GPS signal tracking mechanism ("open loop tracking") that required a new data processing chain on ground, different to the already existing chains for CHAMP and GRACE. The regular frequent downlink of GPS-RO data over NYA started in 2010.

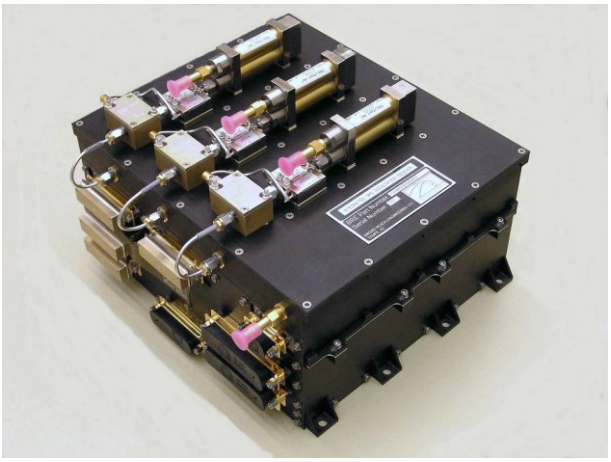

Figure 9: IGOR GPS-receiver (© GFZ)

3.2.6 TanDEM-X

The German TanDEM-X (TerraSAR-X add-on for Digital Elevation Measurement) satellite was launched from Baikonur (Kazakhstan) on 21 June 2010. As indicated by the satellite's name it was projected to improve the mapping of the Earth's surface together with

TerraSAR-X in a close flight formation. The orbit parameters of TanDEM-X are nearly the same as of TerraSAR-X, because the satellites maintain a nominal inter satellite distance of 200 m only (Figure 10: © DLR, CC-BY 3.0).

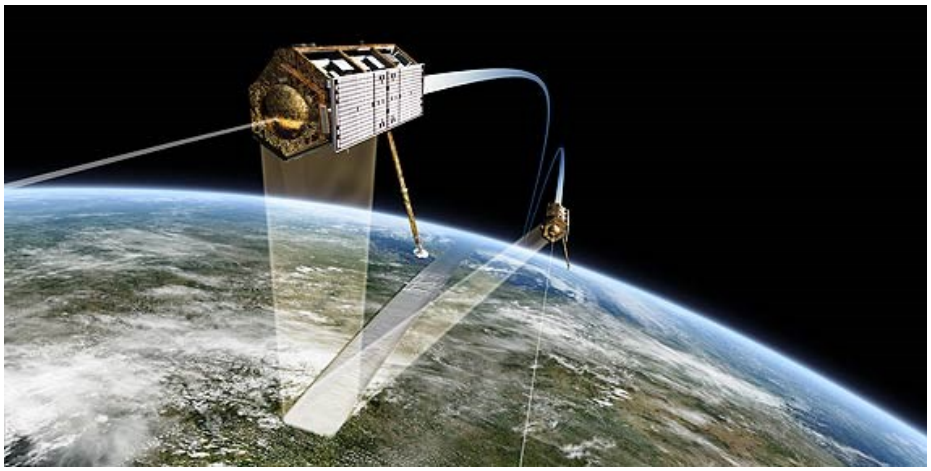

Figure 10: TanDEM-X and TerraSAR-X in tandem flight constellation (© DLR)

TanDEM-X was built as a twin of TerraSAR-X and also has a TOR instrument on-board, which was provided again by GFZ. GFZ was contracted by DLR to calculate the baseline (distance vector) between the two satellites precisely once per day. This is an important input for the processing of SAR data from the combined operation of the SAR antennas on both satellites and mainly based on the TOR POD data from TerraSAR-X and TanDEM-X, both downloaded via NYA.

The very similar, virtually identical orbits of TerraSAR-X and TanDEM-X cause that always the same descending GPS satellites are in the fields of view of both satellites, which allowed the verification of GPS-RO measurements with these satellites (Zus, et al. 2014). However, the GPS-RO data is redundant and there was no benefit from frequent TanDEM-X GPS-RO data downlink contacts over NYA in the first time. The situation changed in 2014 when a software update for TOR on TanDEM-X enabled the GPS-RO tracking of rising GPS-satellites also. TanDEM-X started GPS-RO measurements with GPS-satellites ascending in flight direction, while TerraSAR-X continued GPS-RO measurements with descending GPS-satellites in anti-flight direction. Both satellites receive frequent support from NYA since then.

3.3 Benefits for satellite operation from NYA support

Some benefits for the satellite projects with NYA support are already mentioned in the previous sections. The following sections give explicit examples and proofs for the benefits that were derived from the frequent “add on” satellite contacts with the NYA station

additional to ”nominal” contacts with other ground stations (e.g., in Germany). It can be stated that the frequent satellite contacts with NYA help to maximize on-board data collection by reduction of satellite or instrument outage times and through a positive impact on the satellite life time. The frequent NYA contacts are in praxis also a mandatory precondition for the fast provision of data for near real-time processing chains (currently GPS-RO). The low station operation costs make NYA contacts affordable, even for universities with low budget satellite projects.

3.3.1 Routine satellite operation

The operation of satellites includes several routine tasks. Some tasks require certain manual action and supervision, e.g., the regular transmission of commands to a satellite. Other tasks may be highly automated, e.g., the monitoring of satellite housekeeping parameters to support optimal operation conditions for the payload. Most tasks are realized as combinations of automated processes and human control. The monitoring of battery-parameters on CHAMP, as one example, was an important task, especially in the final years of the mission, when problems with the onboard battery system affected the satellite and instruments operations.

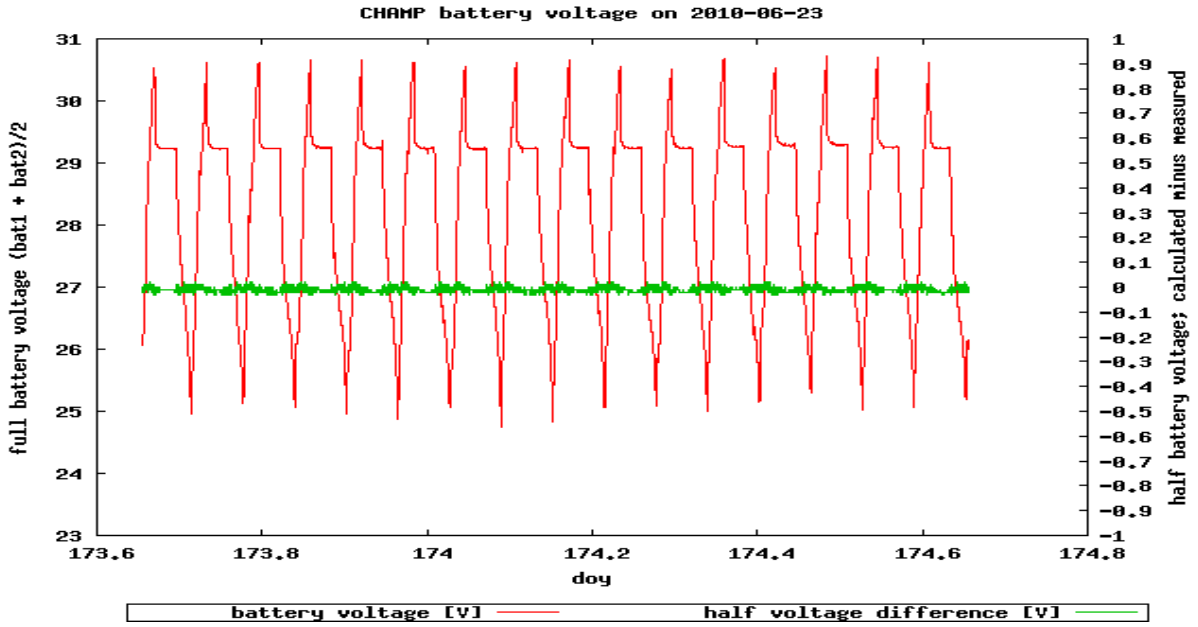

Figure 11: Graph for routine CHAMP battery monitoring (both vertical scales: Volts)

Figure 11 is an example of a graph type that was produced regularly for the monitoring of the battery on CHAMP. It shows the total voltage of the CHAMP battery system (red curve, mean value from 2 sensors), which was physically a pack of several battery cells, and a green curve

that represents the difference between half of the battery voltage as calculated from the total voltage, and half of the battery voltage as measured by a sensor in the middle of the battery cell pack. A perfectly equal behavior of the upper portion and the lower portion in the battery pack during charging and discharging periods would result in a half voltage difference of zero. Small amplitudes in the difference voltage curve may correspond to small technical differences (e.g., internal resistance) between individual cells in the stack, while greater amplitudes were considered to be a good alert indicator for degraded cells or other battery problems, which are not necessarily evident from other parameters, e.g., the total battery voltage.

Graphs like in Figure 11 were generated automatically at GFZ and sent to related CHAMP staff daily before office hours and on demand instantly at any time. The actuality of these plots and corresponding analysis depended of course on the actuality of housekeeping data, which was provided continuously through the frequent contacts between CHAMP and NYA. Similar services with similar objectives (including battery monitoring) are still running for the GRACE mission, which is also supported with frequent NYA contacts.

3.3.2 Special satellite operation

Special and sometimes unforeseeable satellite operation tasks may come up during a satellite mission. This was the case for CHAMP and GRACE and the NYA station supported these tasks with frequent contacts, to allow a low latency monitoring and thus a low reaction time for satellite operators in the special operation conditions. Examples are the position changing maneuvers of the both GRACE satellites, which are performed regularly since some years. The both GRACE satellites fly in an along track formation and from time to time the leading satellite is maneuvered to the rear position, while the formerly rear flying satellite gets in the leading position. The flight direction of both satellites is changed at the same time (180° turns around their yaw axes). These maneuvers are required when the sun travels from one side to the other (from the viewpoint of the satellites) and make sure that the better of the two star cameras on one of the GRACE satellites is not blinded by the sun. Examples from the CHAMP mission are maneuvers for the calibration of onboard instruments, when the satellite was turned by 90-degrees around the yaw axis. Moreover, there were orbit rise maneuvers with CHAMP, which were required to maintain and to extend the originally planned mission time.

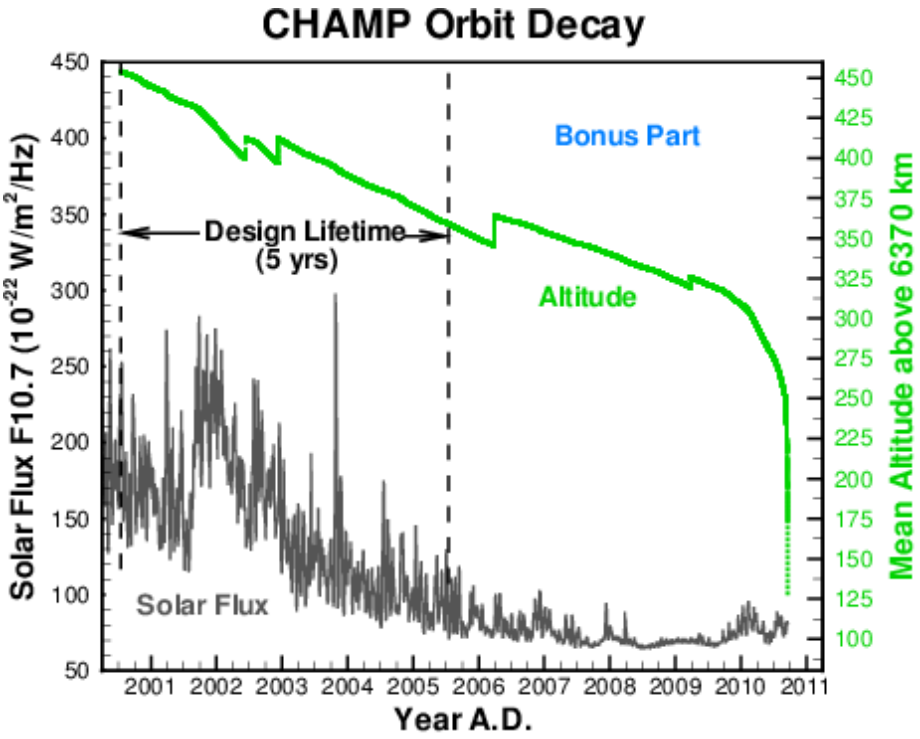

Figure 12: CHAMP orbit altitude and solar flux (Massmann 2011)

Four orbit rise maneuvers were performed with CHAMP between 2002 and 2009 to compensate the unwanted fast orbit decay from an unexpected high solar activity as well as to extend the planned mission life time (Figure 12). The orbit thrusters on CHAMP were operated during dedicated intervals in a series of successive orbits, based on the assumption that they delivered constant thrusts over their operation times. The result of the orbit maneuver depended on the accurate operation timing and nominal thrust of the orbit thrusters. Inaccuracies of thruster operations, which could not be monitored directly, could have affected the maneuver goal or even debased the orbit eccentricity. A good indicator for the maneuver monitoring was found in the on-board scientific accelerometer instrument. Graphs as in Figure 13, which showed the effective performance of the thrusters in terms of acceleration over time (here for one thruster operation interval), could be generated with low latencies through NYA contacts and provided valuable information during the maneuvers. Thruster performance issues, e.g., appearing as deviations from a perfect square shaped graph, could be discussed with a short time delay and corrected early if required. Examples in Figure 13 are the short periods with lower values of measured acceleration, one at the start and one at the end of the shown thrust interval, which could be interpreted, e.g., as a less than nominal thrust at the interval start and a too late termination of activity by one of the two orbit thrusters at the interval end.

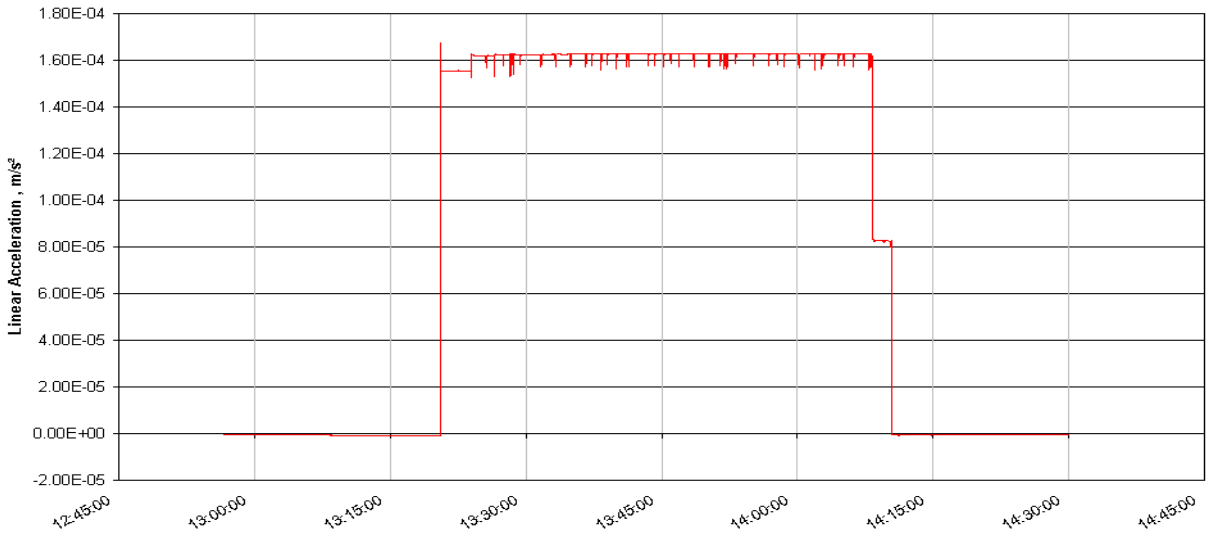

Figure 13: Graph of measured acceleration during orbit manoeuvre with CHAMP

3.3.3 Routine payload operation

An indirect but traceable benefit to the scientific outcome of satellite missions results from a provident care for onboard instruments and other satellite subsystems. Actual satellite and scientific instruments housekeeping data, which is the basis for a good care, is usually downloaded during all contacts. It is processed on ground automatically, together with science data, and checked regularly by satellite- and instrument-operators (e.g., GSOC and GFZ staff). Potential threats for a regular satellite operation, e.g., an approach to an instrument operation parameter limit, may be detected early. In consequence it is possible to adapt the settings of on-board instruments in time, which may prevent a reduced measurement availability of the satellite. The effectivity of the described process can be improved with decreasing data latency, which is reduced with an increased number of contacts between satellites and ground stations. Mission operation staff is well aware of this fact and the frequent contacts between satellites and NYA were exploited continuously in this sense.

An example is the operation of the Advanced Stellar Compass instrument (ASC) on CHAMP. This device provided precise satellite attitude data for other instruments, e.g., the vector magnetometers, and the satellite attitude control system. The ASC on CHAMP engaged 4 camera head units (CHU), which looked into space at different angles (Figure 3). The actual satellite attitude was determined by comparisons between the actual star pattern, as observed by the CHUs, and star pattern in an on-board catalogue.

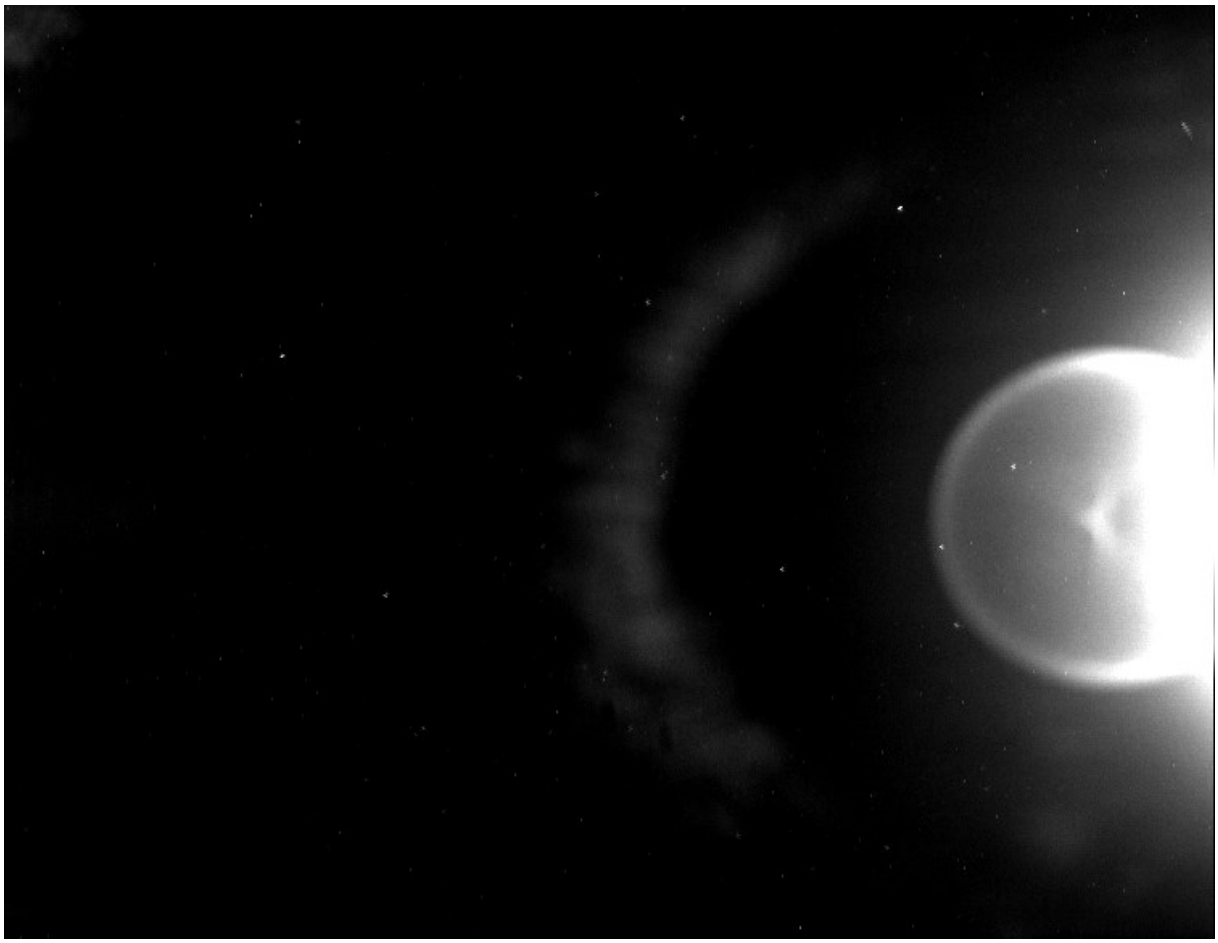

Figure 14: View of blinded camera of ASC on CHAMP

Figure 14 shows an example for the detected star pattern of a CHU when the moon is just entering the camera field of view (18.4° x 13.8°). The reflections in the camera lenses and baffle system cover some of the stars, which appear as small spots. They also cause an overload for the ASC processing unit during the corresponding time interval of every orbit, when the computable maximum of "detected stars" is exceeded. Figure 15 is an example for such a saturation effect with "luminous objects" from a similar blinding event. The overload led to bad and instable attitude information by the ASC and thus affected the accuracy or even the usability of scientific measurements, e.g., for the vector magnetometer data from CHAMP. Another consequence of an unstable attitude determination was an increased thruster activity to maintain the nominal satellite attitude. A high thruster activity was unwanted as it disturbed the accelerometer measurements. It also meant a significantly higher consumption of on-board propellant, which had a limited capacity and was thus a mission time limiting factor.

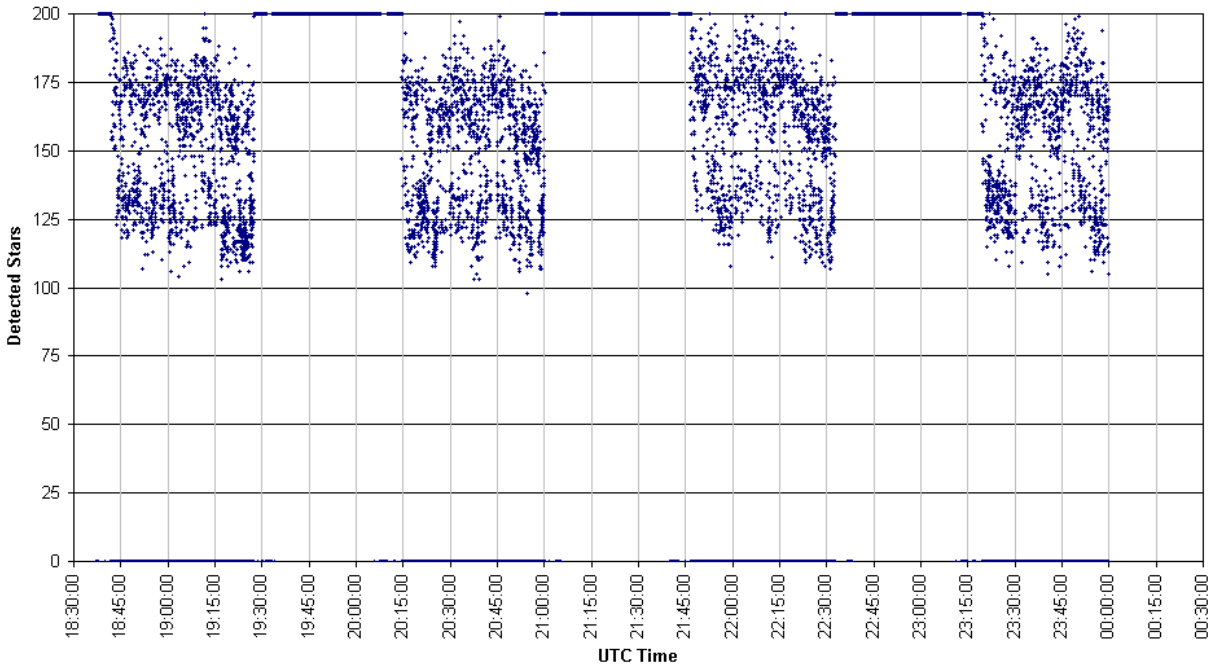

Figure 15: Number of detected stars as registered by a blinded CHU on CHAMP

The ASC function was not only affected by blinding through the moon and the sun, but also from other circumstances, e.g., instrument noise due to high operation temperatures, degradation of camera sensitivity and so called “hot spots”. These “hot spots” were permanently lightened pixels on the cameras CCD chips, which had to be excluded from onboard calculations by manual action (commands) from ground.

It was the task of GFZ to support the best possible ASC performance on CHAMP by the definition of situation-adopted settings. Corresponding commands were prepared by GFZ with low latencies, based on analysis of data from the frequent NYA contacts, which were (in general) earlier available than data from the NST or WHM stations. The shorter reaction times reduced the times of not nominal operation conditions with reduced data quality or no scientific data at all and the consumption of on-board propellant.

3.3.4 Satellite life time

An important task of GFZ for the CHAMP mission was the monitoring of satellite housekeeping data. High attention, as one example, was paid to the on-board battery systems with their crucial function for all active on-board systems, as they can suffer from extra-ordinary operation conditions but also from normal aging effects. This issue was addressed, e.g., by applying different battery charger settings, adapted to actual satellite operational

conditions and orbit phases with different actual power consumption, temperatures and availability of sun light for the satellites solar arrays.

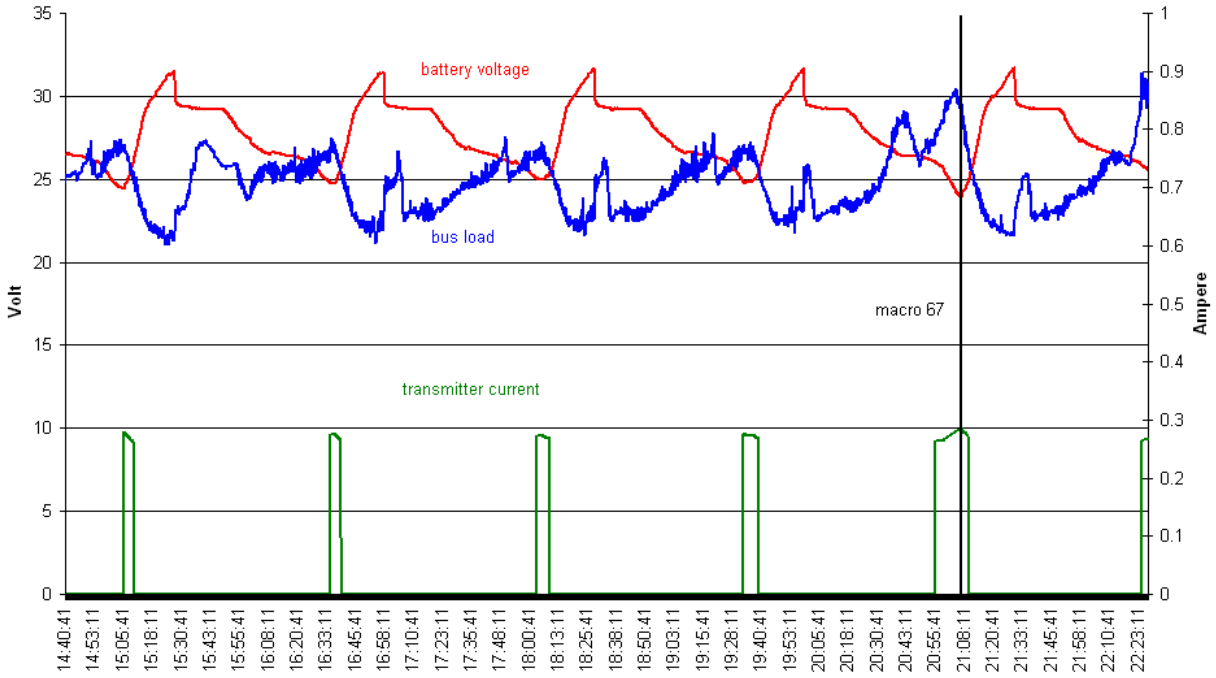

Figure 16: Analysis of a CHAMP "macro 67" automatic power problem recovery event

Figure 16 shows the battery voltage, the bus load (sum of currents drawn from all active on-board systems) and the telemetry transmitter current on CHAMP over a period of about 6 orbits at a time in 2010 when the battery performance was known to be precarious degraded. It was the task of the on-board function "macro 67" to prevent critical low power states automatically. Some less vital heaters were switched off in such cases, when the battery voltage dropped below 25 Volts for a certain time, which happened in this example about 21:08 UTC. Incidents like this were analyzed at the soonest as they were potential indicators for possible serious on-board problems. The main reason for the "macro 67" event in Figure 16 was found to be an undesirable coincidence of high power consumption (especially due to long transmitting time) with already previously low battery voltage, rather than a critical on-board problem or anomaly. In later steps such analyses were also often used to fine tune operational settings, e.g., of macro functions, allowing a better and thus potentially life extending battery power management

The beneficial role of NYA in the last phase of the CHAMP mission was generally recognized in the mission's final report (Massmann 2011). Details about critical situations on satellites and how they were solved are usually not spread more than absolutely required and published

very sparingly or not at all. However, at least three very critical situations for the satellite CHAMP, all of the same kind and with involvement of NYA, may be mentioned as they were documented at least to some extent (Keil and Altenburg 2003). Each time the satellite was found with the onboard computer electrically frozen, with no thermal control and flying with extreme not nominal attitude (e.g., upside down and rear side turned to flight direction). No scientific measurements could be made in that times of course, but really critical was the decreasing battery power as no or very little sun light was falling on the solar arrays. CHAMP could not recover by automatic on-board functions and needed help from the ground before the lack of power prevented the operation of the on-board telemetry command receiver. Satellites can also cool down below minimal system operation or survival temperatures when they are not electrically heated and may not start up normally again, even when a nominal power status is restored. Fortunately the operators at GSOC were alerted early enough because none of the contacts scheduled for NYA was received due to the described satellite state. Helpful commands for CHAMP were prepared and sent in time and solved the problem, which could be confirmed with low latency by following NYA contacts. A later detection of the described problems during NST or WHM contacts, which were scheduled the same days but several hours after the missing NYA contacts, could have resulted in a hardly controllable situation and, in principal, even in the loss of CHAMP.

3.3.5 Near real-time provision of GNSS-RO based products

The payload on CHAMP, and later on GRACE, TerraSAR-X, TanDEM-X and other satellites, included, respectively include, an innovative GPS radio occultation (GPS-RO) instrument for microwave-based sounding of atmospheric properties with GPS-signals (Wickert et al. 2009 a). The applied method (Melbourne, et al. 1994) uses regular GNSS-signals, which propagation paths and amplitudes are influenced by the passed media (atmosphere and ionosphere, Figure 4). The requirement for low latency data availability (weather forecasts) is briefly explained in section 3.2.1.

Figure 17 is an example of a probability density function (PDF) statistic for the total availability delay of GPS-RO data from the satellite GRACE-B as delivered by GFZ over a time interval of 28 days. The total delays are the sum of all delays after on-board measurements, including the times for data reception by a ground station, processing of satellite orbits and RO-products (e.g., temperature profiles) and all kind of data transfers between involved infrastructures. The blue scale and the blue dashed line indicate the

accumulated PDF. The graph shows that almost all of the delivered data (99%) was available within 3 hours after on-board measurement, which is the due time for assimilation by meteorological weather forecast services (indicated by vertical dashed grey line). Most of the data was available even earlier, with less than 2 hours delay.

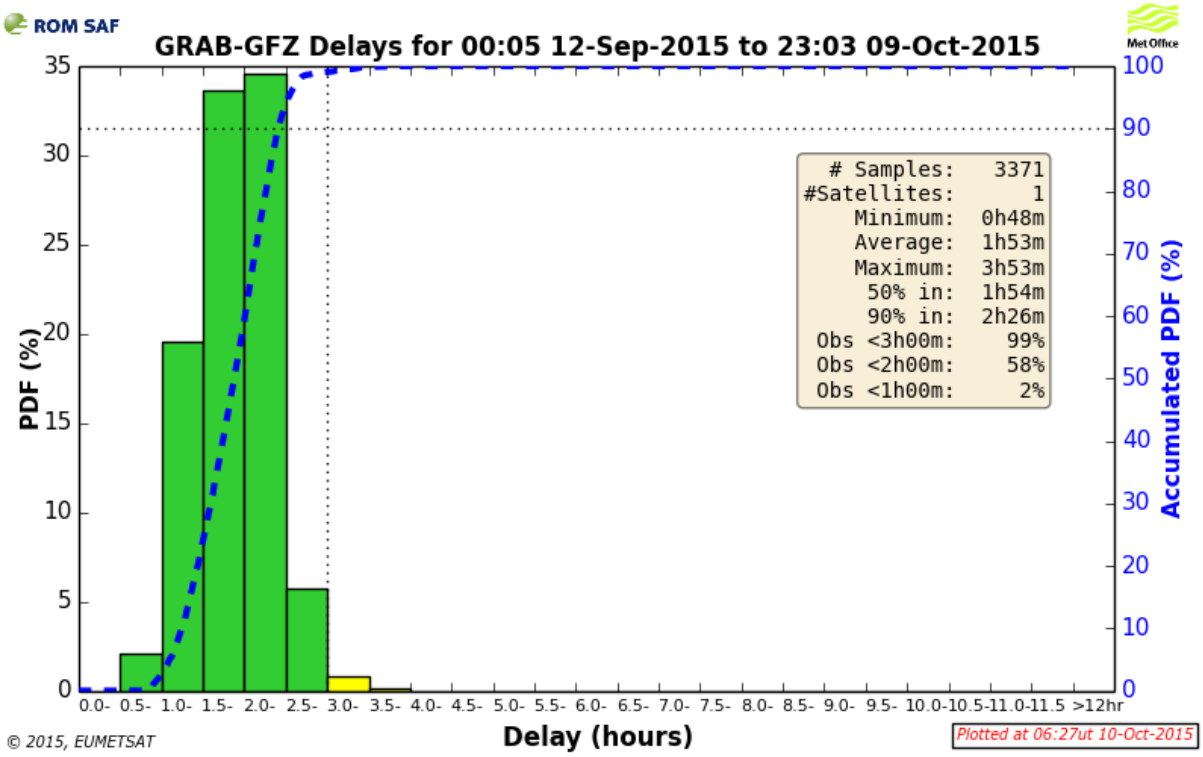

Figure 17: Availability delays of GPS-RO products from GFZ (© 2015 EUMETSAT)

This and many other statistics for several satellites with GNSS-RO instruments are published on dedicated websites (Danish Meteorological Institute 2015) of the EUMETSAT Radio Occultation Meteorology Satellite Application Facility (ROM SAF). Taking into account that one orbit of a GRACE satellite takes more than 90 minutes and that some procedural delays are unavoidable, it becomes clear that at least every second orbit of the satellite must be used for a downlink contact to a ground station. Otherwise the data would be too old to be used for weather forecast tasks. The high data provision efficiency, as visualized in Figure 17, can only be achieved if data downlink contacts are made almost every orbit, which is realized by the NYA station.

3.3.6 Low cost satellite missions

Low cost satellite missions, e.g., as most projects based on the Cubesat concept and other small satellite projects, e.g., of universities, usually cannot afford to operate costly

infrastructures. A common setup for the operation of such satellites typically includes a low cost VHF- or UHF-band (Very/Ultra High Frequency) ground station, which allows an uplink and a downlink, but both with narrow bandwidths only, e.g., for commanding and downloads of essential on-board house-keeping data. An additional S-band downlink system is operated on many small satellites to send scientific data to the Earth, as most scientific instruments generate higher data volumes, which in praxis cannot be transferred in the limited bandwidths of the VHF/UHF radio bands.

The counterpart for S-band transmissions from satellites is an S-band antenna on ground, e.g., a parabolic antenna, which is considerable more expensive than, e.g., VHF or UHF Yagi-antennas. The operation of S-band antennas, including tracking of satellites, also requires a higher accuracy due to their usually smaller antenna beam widths. This implies potential problems for the download of valuable scientific data from the satellites. Data that is not downloaded from the satellites in time gets lost forever as soon as the on-board memory is overwritten with data from newer measurements. The scientific output of such projects can thus depend directly on the availability of an effective satellite-receiving station that can offer downlink services at low costs.

GFZ offered such low cost S-band downlink services with the NYA-station to the German "Flying Laptop" mission (see section 3.4.2) and the Spanish (Catalonian) "^{3}CAT-2" mission (see section 3.4.1).

3.3.7 Miscellaneous

Receiving-problems at the ground stations NST and WHM during scheduled contacts with CHAMP and GRACE were occasionally compensated (filling of data gaps) by provision of data received at Ny-Ålesund. NYA thus contributed to the corresponding reception statistics of these stations, although this was apparently never published or acknowledged.

3.4 Recent and upcoming satellite projects with NYA support

Some upcoming satellite projects are already confirmed to get support from the NYA station. This section gives a short description of the corresponding missions and the involvement of NYA.

3.4.1 ^{3}CAT-2

The ^{3}CAT-2 satellite structure (Figure 18) was built with modules according to the Cubesat standards (California Polytechnic State University 2016). A GNSS-reflectometry experiment was foreseen, e.g., to determine sea level from reflected GNSS-signals. The basic principles of GNSS-reflectometry were described many years ago (Martin-Neira 1993) but were rarely exploited from space. Some background of the method can be found in 3.5.1, the experimental details of the ^{3}CAT-2 mission are described in corresponding project publications (Carreno-Luengo, et al. IEEE, 2013). The satellite was launched on August 15th 2016 and was operated through a ground station at Barcelona (VHF- and UHF-band communication). NYA was foreseen to support the mission with regular (daily) S-band downlink contacts, but the satellite failed to achieve the required functionality.

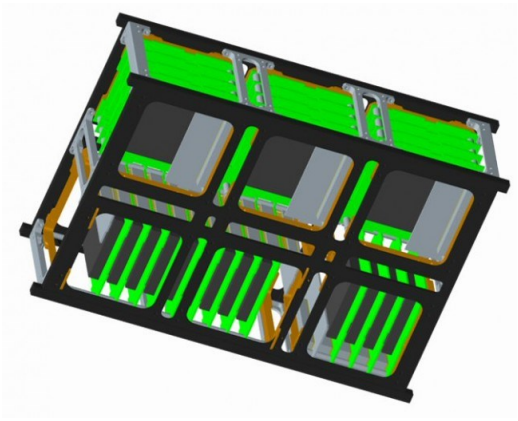

Figure 18: 3D-model of the 3CAT-2 satellite (Carreno-Luengo, et al. IEEE, 2013)

3.4.2 Flying Laptop

The satellite Flying Laptop (Figure 19, credit: Jonas Keim, IRS, University of Stuttgart) was developed and built by students at the IRS Stuttgart (Institut für Raumfahrtsysteme Stuttgart). It was launched into a polar orbit with an altitude of about 600 km on 17 July 2017. Various payload instruments are on-board of which some were provided by partner institutions and companies. Among them are a Multi-Spectral Imaging Camera System (MICS), which is the main payload, a panoramic camera for Earth observation, an experiment for optical communication (satellite to Earth) and three GPS sensors for POD and attitude determination.

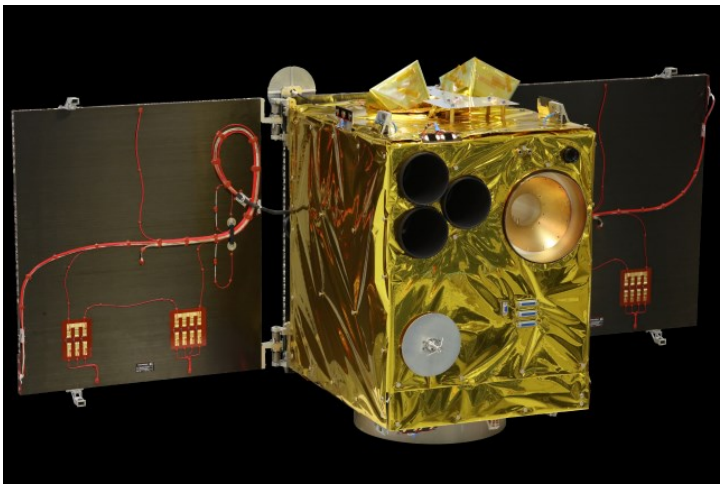

Figure 19: Flying Laptop satellite (© IRS Stuttgart)

Another instrument receives Automatic Identification System (AIS) signals from ships. One of the mission aims is the in-orbit validation of new developed technology.

Flying Laptop is denoted a small satellite with a size of 60 x 70 x 87 cm^3 and a weight of 110 Kg. It is operated by IRS with its own satellite ground station, which utilises a 2.5 m parabolic antenna for the up- and downlink in the commercial S-band and an additional downlink in the amateur radio S-band (for MICS-data). Both downlinks are supported by the NYA station (2 contacts per day) as part of an institutional partnership between IRS and GFZ.

3.4.3 GRACE-FO

The US-German GRACE-FO mission (GRACE Follow On) is the successor of the GRACE mission (3.2.3) and scheduled for a launch with a FALCON-9 rocket in March 2018. It will continue the current measurements of the GRACE satellites (gravity determination and GPS-RO) and uses basically the same mission designs, e.g., two satellites (Figure 20: credit: AEI/Daniel Schütze; background credit: NASA/NOAA/GSFC/SuomiNPP/VIIRS/Norman Kuring) with inter-satellite ranging, accelerometers and special GPS-equipment. The most significant difference to GRACE will be a new LRI Laser Ranging Interferometer (Sheard, et al. 2012), which is a supplement to the microwave ranging instrument. The LRI potentially provides higher measurement accuracy (Flechtner, et al. 2016), compared to the microwave based ranging, but is declared to be a demonstrator for Next Generation Gravity Missions, rather than as part of the scientific instrumentation baseline.

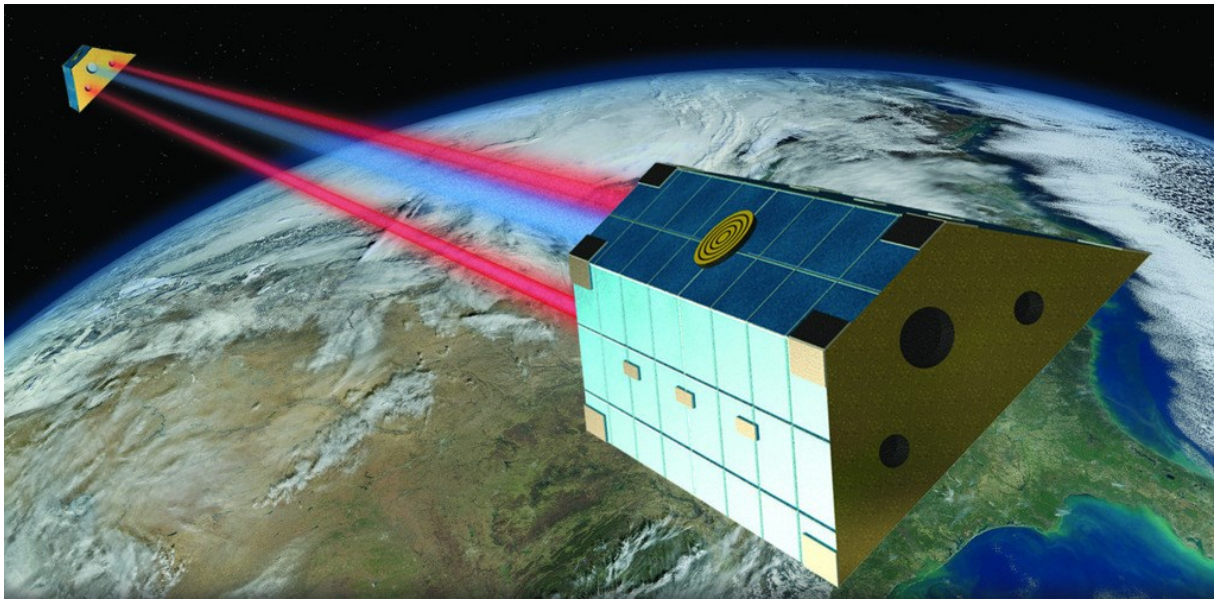

Figure 20: Artist view on GRACE-FO (© Earth: NASA, © satellites: Schütze/AEI)

GRACE-FO is the most important upcoming satellite project from the viewpoint of NYA, as NYA will serve this mission as the primary ground station for data downlinks. GFZ has the task (among others) to manage the Mission Operation System (MOS) for GRACE-FO. Analysis showed that the data volume from the GRACE-FO satellites will be too high to be received completely by the German ground stations at Weilheim (WHM) and Neustrelitz (NST), due to the relative low number of possible contacts per day for stations at lower latitudes (explained in section 3.1.1). The higher total contact time for the NYA station, resulting from the high latitude location and the polar orbit of GRACE-FO, was found to be more than fully sufficient to download all mission data. The high number of NYA contacts with the resulting low latency of data availability is also beneficial for the regular satellite health monitoring and even required for the NRT GNSS-RO processing chains, as explained in section 3.3.5.

The role of NYA as the primary downlink station for GRACE-FO implies a much higher demand to the station operation reliability than before, when the station was operated on a best effort basis only, and was the main driving factor for this work. The WHM and NST ground stations (both operated by DLR) will serve as secondary downlink stations for GRACE-FO and provide redundancies for data downlinks that could not be received by NYA for any reasons. They are also used for the uplink, which cannot be realised at NYA (see comments in section 5.1).

3.5 Outlook on future projects

More projects and trends for future satellite missions are on the horizon. This section gives some outlook, which suggests that support from NYA will be appreciated, furthermore, even beyond the recent and near future operation as described in 3.4.

3.5.1 Small satellites for GNSS-RO and GNSS-R

The function and usefulness of GNSS-RO measurements, e.g., for weather forecasts and climate-related research, was demonstrated with CHAMP and other satellites. GNSS-reflectometry (GNSS-R) is another method that uses GNSS-signals (Martin-Neira 1993) and has a high potential for scientific and social benefit. Special GNSS-reflectometry instrument setups receive the direct signals from GNSS-satellites (as usual) and the same signals after reflection from the Earth’s surface. The time delay between reception of direct signals and reception of reflected signals can be used to determine sea level and wave heights including

tsunami waves. A simulation study (Stosius, et al. 2011) showed that the detection of a tsunami like the Sumatra 2004 event could be detected reliably by a constellation of 18 GNSS-R satellites within 17 minutes. The detection time, which is crucial for early warning, could be reduced even to 6 minutes if 81 satellites were used.

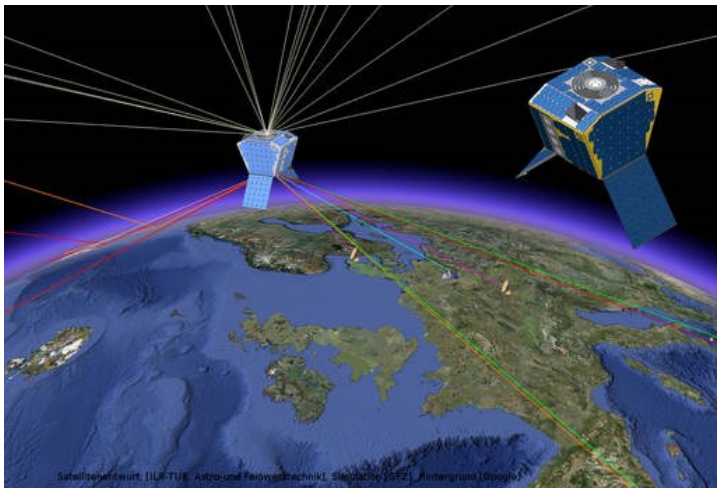

Figure 21: MicroGEM satellites (© ILR-TUB, Astrofein, GFZ, Google)

GNSS-R data from small satellites are currently already provided from the missions TechDemoSat-1 (TDS-1) and CYGNSS ((Unwin, et al. 2016), (Ruf, et al. 2013)) launched in 2014 and 2016 respectively. In addition ESA had plans to install an altimetric GNSS-R experiment aboard the International Space Station (ISS), called "GNSS rEflectometry, Radio Occultation and Scatterometry on board the ISS" (GEROS-ISS). The mission successfully passed two independent Phase-A studies (Wickert et al., 2016), but financial issues hold the mission to proceed to further phases of development.

It is expected that the availability of spaceborne GNSS-R data will be improved further by the engagement of very small and cost effective satellites with special GNSS-instrumentation in the near future. Several studies were performed to investigate the feasibility of such low cost satellites missions. Examples for the combination of GNSS-RO and GNSS-R instrumentation (together with other geodetic instruments) are the project studies for MicroGEM (Briess et al. 2009), with a satellite mass of 130 kg ((Figure 21, © satellite: ILR-TUB, Astro- und Feinwerktechnik GmbH, © simulation: GFZ, © background: Google)), NanoGEM (Wickert et al. 2011), and Nano-X (Buhl et al. 2013), each with a mass of about 50 Kg. Such small satellite missions will require frequent and also parallel downlinks from various satellites and NYA could continue to serve in this respect for pathfinding projects as well as for later operational GNSS-RO/R satellite constellation, possibly including early warning tasks.

3.5.2 New gravity missions and services

Great progress for the determination of the Earth's gravity field was made in the last 15 years with CHAMP and GRACE. However, CHAMP decayed in 2010 and the days of GRACE are numbered due to the very long operation time. New gravity missions with again better performance than the preceding gravity missions were discussed since many years. This already influenced the upcoming GRACE-FO mission, but the discussions and investigations for future gravity missions continue. Several studies, e.g., for a "Next Generation Gravity Mission" (NGGM) were performed to evaluate the necessary trade-offs between science, instrumentation and costs for new gravity missions with improved characteristics. An industrial-scientific study conducted for ESA (Thales Alenia Space 2010) states that "*An improvement in our understanding of continental water transport as hydrological processes*… [may arise from data (inserted by author)] …*on hourly to weekly time scales*". Other studies (Baldesarra, et al. 2014) showed that a temporal resolution of one week can be obtained from a two satellite constellation as well as an improved spatial resolution with novel instrumentation (e.g., LRI, as flown first on GRACE-FO). It is evident that future multi satellite constellations could increase the spatial and temporal resolutions significantly.

Also new services to exploit the data from gravity missions for more applications are formed. An example is the EGSIEM project (European Gravity Service for improved Emergency Management) that started officially in January 2015 and runs for 3 years. EGSIEM aims mainly on the provision of higher-level gravity data products with a temporal resolution of one day and a latency of 5 days (Jaeggi, et al. 2015). Such services could be very valuable in the future, e.g., for a monitoring, early warning and forecasting of extreme hydrological events, such as floods and droughts.

It cannot be foreseen if or how soon new "NGGM-type" gravity missions will come, but it seems to be sure that future gravity missions will be designed for increased resolutions. This will increase the data volume to be received on Earth and, analogue to the increased temporal resolution, maybe also the demand to provide this data with lower latencies. It is expectable therefore that future gravity missions benefit from frequent data downlink contacts to ground stations, such as available from NYA, most probably even more than GRACE in these days.

4 Backgrounds and theory

The following sections give some information about properties of ground stations with emphasis on antenna system parameter and antenna measurement methods, as far as applied in this work or otherwise relevant for the NYA-station. Some formulas are supplemented with example calculations. These refer in general to the S-band frequencies as currently used at NYA, but sometimes also to X-band frequencies, which might be used in the future, too.

4.1 General characteristics of ground stations

Satellite ground stations provide terminals for the communication with satellites. Most stations support the transmission of data to and the reception of data from satellites, while some stations, e.g., the satellite-receiving station at Ny-Ålesund, allow only one communication direction. The so-called uplink includes all transmissions to the satellite from ground, e.g., commands to change operational or instrumental setups and operation schedules. The so called downlink includes all data sent from the satellite to ground, e.g., housekeeping data of the satellite platform and instruments as well as scientific data of instruments. Some ground stations support an orbit tracking of satellites, which requires extra equipment, e.g., for automatic satellite direction tracking and ranging functions. Satellite orbit tracking delivers time series of satellite directions and distances from the viewpoint of the ground station. Effectively the method has a limited accuracy, but it can be used for course orbit determination tasks.

Just two numbers usually describe the main RF- (radio frequency-) related properties of a station, the *EIRP* (equivalent isotropic radiated power) for the uplink and the *G/T* (antenna gain to system noise ratio, pronounced “G over T”, explained in 4.4 and 4.5) for the downlink. These numbers, together with corresponding satellite parameters and orbit information, are sufficient to calculate link budgets for ground to satellite and satellite to ground links, but do not include all of the relevant ground station properties. More technical capabilities of a ground station are defined by the available communication directions (uplink and/or downlink), the useable radio frequency bands (e.g., S-band, X-band, K-band), the radio signal data rates (e.g., 1 Mb/s) and modulation types (e.g., BPSK = Binary Phase Shift Keying). Other important parameters are the capabilities to handle different polarisations of radio signals (e.g., linear, RHCP / LHCP = Right / Left Hand Circular Polarization), the antenna beamwidth and the manoeuvrability of antenna positioning systems, such as the angular

velocities of positioning system axes and masked or eventually otherwise problematic direction zones. The ability for telemetry data coding and decoding (e.g., forward error correction, Viterbi decoding) may be available at a ground station, but could also be implemented at other locations, such as a satellite control or data processing facility. In any case a ground station must have a reliable gateway for data transfers and, in some cases, for remote monitoring and control. The data connectivity of a station depends, beside data bandwidth, also on the layout of available interfaces.

The local environment of a station can have an influence on the operation conditions and station performance. An example is local, mostly man-made RF noise, which is emitted from electronic equipment (e.g., radar stations, microwave oven or WLAN) and which may disturb the sensitive receiving equipment. Radio transmissions from a ground station, which are necessary to provide an uplink function, are usually regularised by national laws or local regulations and can be restricted or even prohibited. This can also be the case for the receiving of satellite signals, even when this is not connected with any emissions from the ground station. The operation reliability of a ground station depends, beside the reliability of system components, principally also on the development of local infrastructure (e.g., for electric power), the availability of technical support, the accessibility of the location (travel and transportation) and redundancy concepts (e.g., for antennas and receivers). The versatility and operations costs of a ground station certainly depend on the degree of automation and engaged operation staff.

An ideal satellite ground station would be able to operate at optimal high numbers of EIRP, *G/T* and data rates, on all satellite communication frequencies and at all applicable polarisation and modulation types. The station would be installed at a geographical advantageous place (according to orbits of satellites to be tracked) with fully developed infrastructure (e.g., for power supply), transportation and high-speed data access without local RF-noise. It could be operated with low effort (highly automated) and high redundancy at low costs. Most probably no such ideal station exists, but it makes sense to consider all listed aspects to assess the benefit and effectivity of individual satellite ground stations.

4.2 Parabolic antennas

Antennas with parabolic reflectors are used at satellite ground stations most commonly. A parabolic shaped reflector “collects” radio signals and reflects them from all points on the

concave reflector surface to a focal point (Figure 22). All the reflected radio energy arrives here in phase, and thus with constructive interference, and is picked up by a feed antenna which is installed right at the focal point.

A well-adapted antenna feed illuminates a reflector (or secondary reflector, see below) as complete as possible, but limited to the surface of the reflector. The area outside the reflector rim should not be in the feed's field of view, as that area does not contribute to the wanted signal, but to the received noise power (e.g. thermal noise from the background). The aperture angle of a suitable feed must thus match to the reflector shape, w.r.t. curvature and diameter, which is technically commonly addressed by the ratio of the focal length to the diameter of the reflector, *F/D*.

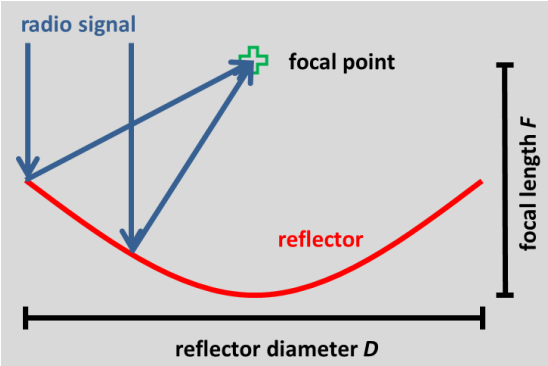

Figure 22: Main geometrical properties of a simple parabolic reflector antenna

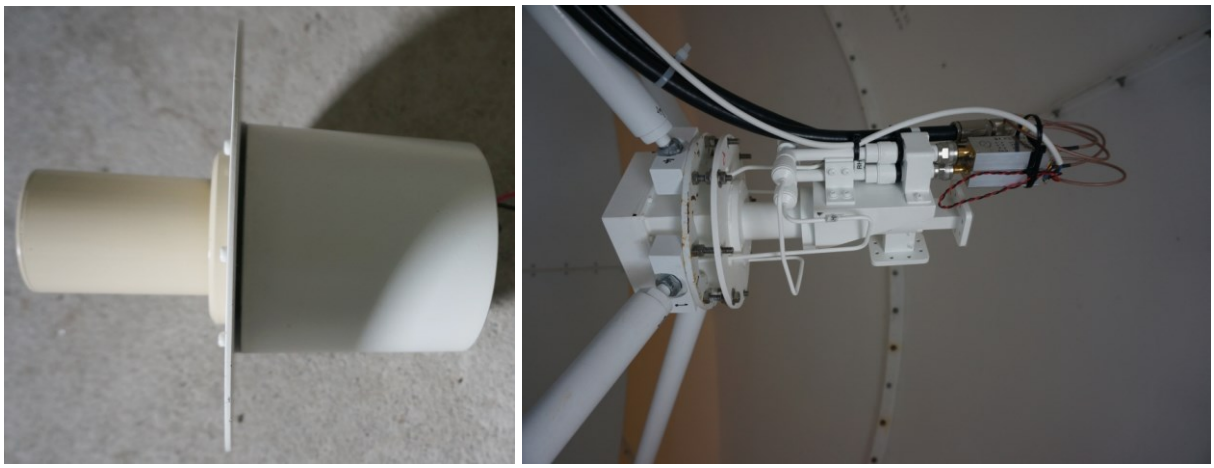

Figure 23: S-band antenna feed and X/S-band dual polarisation antenna feed

The mechanical structure of parabolic antennas is more robust than those of most other antenna types (e.g., Yagi-antennas[1]), which can provide the same typically required operation performance w.r.t. frequencies, polarisations and gain in many cases. Another advantage of parabolic antennas against many other antenna designs is their aptitude to provide a very high useable frequency range and even the possibility for multi-band operation. The antenna reflector efficiency generally shows only a small dependency from the operation frequency,

[1] Antenna was named after one of its inventors and is commonly known from terrestrial television.

provided that the reflector has a low surface roughness. Thus the antenna system operation frequency is mainly determined by the antenna feed, which is actually a small directional antenna itself, realised, e.g., as a helix or (crossed) dipoles construction. Feed antennas can be designed (optimised) to operate in one frequency range, but also to operate in several different frequency bands simultaneously. Figure 23 shows a single band antenna feed (left side, currently used for NYA-1) and a mounted antenna feed for RHCP and LHCP operation in the S-band and X-band with attached S-band LNAs (right side, currently used for NYA-2).

Several types of parabolic antennas with different constructional characteristics exist (Figure 24, © Wikipedia Commons). Some have a rotation symmetrically reflector with a central feed, other have a reflector with an offset feed, e.g., most of the antennas for TV-satellite reception at private homes. Antennas that illuminate the reflector directly are called prime focus systems. An advantage of the offset feed antennas is that the feed and the feed support construction do not obstruct the signal path, which could otherwise block the signals. More complex designs are found with the Cassegrain and Gregorian antennas, which use convex and concave secondary reflectors. Convex secondary reflectors are mounted between primary reflectors and their focal points, e.g., at large antennas with lower curvature primary reflectors and reduce the total size of the antenna (in beam direction). Concave secondary reflectors may be even more effective than convex reflectors and are mounted behind the focal points of antennas with higher curvature primary reflectors.

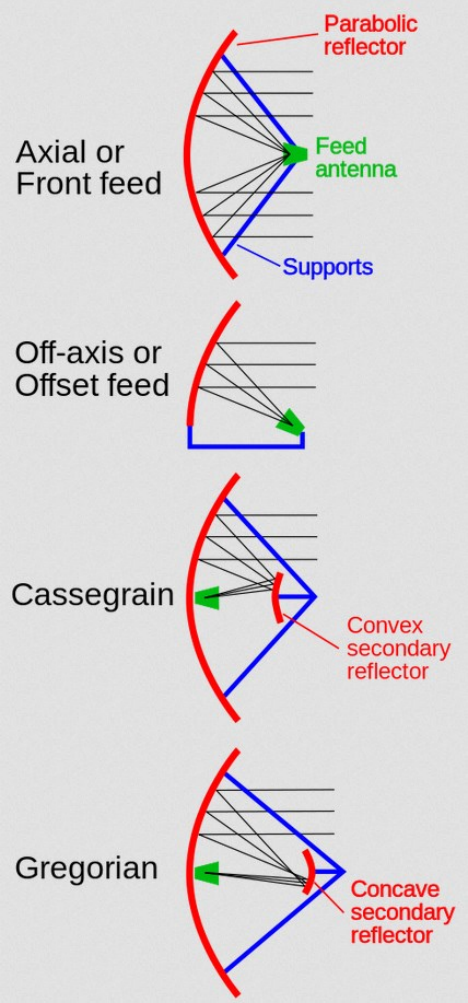

Figure 24: Commonly used types of parabolic reflector antennas

One advantage of antennas with secondary reflectors is that the main antenna reflector can be illuminated more precisely by carefully designed secondary reflectors, e.g., including the area of the primary reflector rim, but excluding the area behind it. Another advantage is that the feed beam is directed to the same direction as the antenna main beam, which is usually the

cold sky (e.g. behind a tracked satellite). The feed thus receives less thermal noise from the environment (ground), even if the feed beam pattern is not perfectly adapted to the secondary reflector shape. Both designs, Cassegrain and Gregorian, are also beneficial if an antenna is used for an uplink. Transmitter equipment, which is usually somehow bulky, can then be placed at the backside of the primary reflector, close to or directly at the feed. This avoids long transmission lines (e.g., coaxial cable or waveguides) with corresponding signal power losses.

A disadvantage of the secondary reflector designs is that the secondary reflectors block the central areas of the primary reflectors, at least of the commonly used prime focus systems, which results in a reduction of antenna gain. This effect becomes more and more acceptable with increasing size of the primary reflector. It must also be considered that a reflector needs a certain minimum size with respect to the wavelength of the radio signals (literature states no fixed value but a reflector size of "several wavelengths"). Otherwise a reflector will not reflect the signals in the wanted way, but more diffuse, resulting from diffractions at the reflector. This unwanted effect could be found with primary reflectors also, but it is more probably to arise with the smaller secondary reflectors. A favourable ratio of advantages against disadvantages of secondary reflector antenna systems may be met with large antennas and high operation frequencies and if the antennas are to be used for transmitting.

4.3 Antenna directional characteristics

The main characteristics of directional antennas are the gain and half power beam width (HPBW) of the main lobe direction, as sketched in Figure 25. The antenna gain decreases with increasing angular offsets to the antenna boresight and increases again in the directions of side lobes and back lobes, but stay below the boresight level. The antenna half power beam width Θ is defined by the angle where the antenna main lobe maximum gain is reduced by 3 dB (equivalent to half power). The angle Θ can be measured, calculated (modelled) or

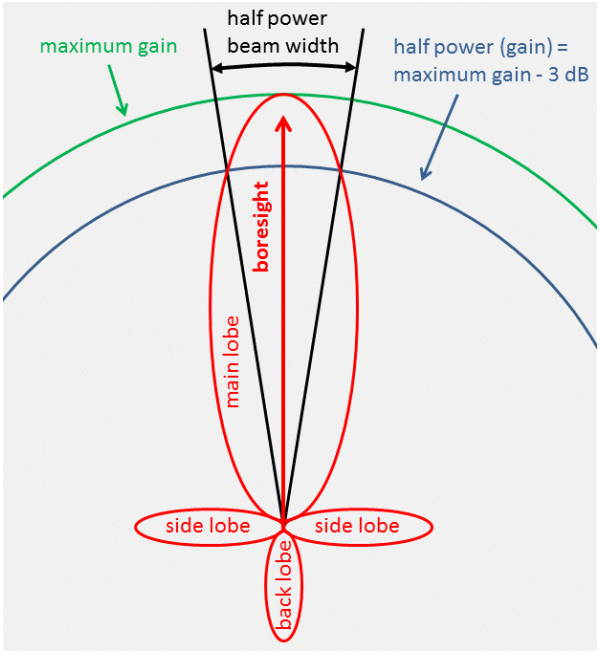

Figure 25: Half power beam width of main lobe

estimated by adopted “rule of thumb” formulas. In case of parabolic prime focus antennas with central feeds (both NYA-antennas) Θ can be assessed with equation (1), resulting in 2.33° for NYA-1 (4 m reflector) and 2.22° for NYA-2 (4.2 m reflector) at an exemplary frequency of 2250 MHz.

$$\Theta = \frac{21}{f_{[GHz]} \cdot D} \tag{1}$$

where

Θ = half power beamwidth [°]

D = diameter of antenna reflector [m]

$f_{[GHz]}$ = frequency [GHz]

The loss of antenna gain L_{pr} (in dB) in the region of the half power width, e.g., due to pointing errors e_r (in °), relative to the antenna main lobe direction, can be calculated with equation (2). Figure 26 shows corresponding graphs for typical S- and X-band frequencies and an antenna diameter of 4m (as NYA-1).

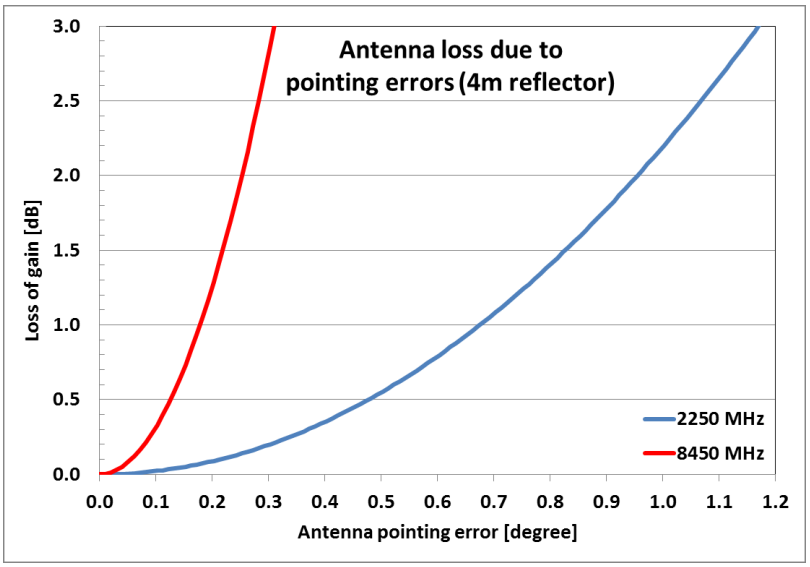

Figure 26: Loss of antenna gain due to antenna-pointing errors

Only very small, not to say, nearly negligible losses must be expected in the S-band for pointing errors below 0.1° (precise numeric examples in section 6.2, Table 6). Higher errors result from pointing errors when the antenna is operated at higher frequencies (not practiced at NYA).

$$L_{pr} = -12\left(e_r / \Theta\right)^2 \tag{2}$$

where

L_{pr} = loss of gain from antenna-pointing error [dB]

e_r = antenna-pointing error [°]

Comprehensive antenna specifications include directional characteristics as graphics, according to measured antenna gain, in sectional or 3-dimensional views. Most common are views for the horizontal and vertical planes, which are different for most antenna types (e.g., dipoles or Yagi-antennas). The diagrams also show the directions and relevance (beamwidth, gain) of side lobes and back lobes. These lobes are generally unwanted, because they increase the amount of noise that is received by an antenna, e.g., from sky and local environment, which leads to a performance reduction in terms of *G/T* (see section 4.5). It is also possible that unwanted signals are received from side lobe directions, e.g., from other satellites or the sun, which can disturb the reception of the wanted signal. Figure 27-a (complemented graphic from www.radartutorial.eu, © CC-BY-SA 3.0) shows a polar diagram of a parabolic reflector antenna directional characteristic. The strongest side lobes in this example appear in a 30° wide sector around the main lobe and at higher offset angles of about 80°.

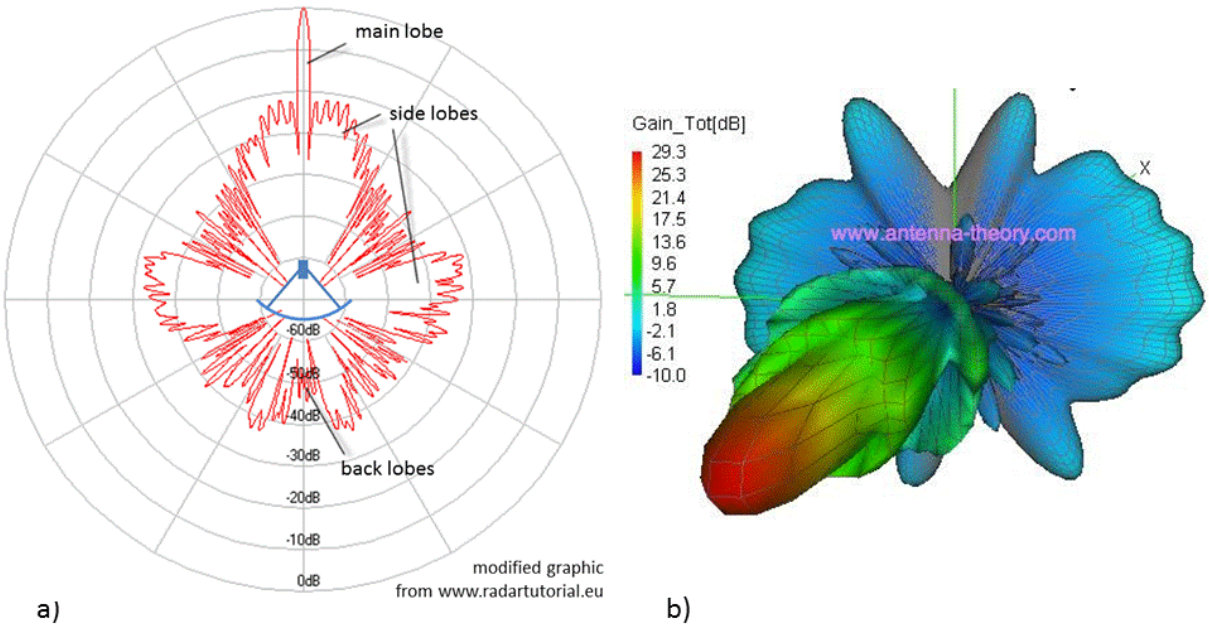

Figure 27: Examples of parabolic antenna radiation pattern

Figure 27-b is a 3-dimensional directivity graphic (from www.antenna-theory.com, © CC-BY-SA 3.0) for a parabolic reflector antenna (*F/D* ratio = 0.5) and shows that the distribution of side lobes can be complex and that it is not necessarily axially symmetric. Graphics as in Figure 27-b, with the corresponding data sets behind, allow a full characterisation of antenna gain. Sectional views as in Figure 27-a are also helpful, but cannot be extrapolated unconditionally to 3-dimensional information.

Antennas with rotationally symmetric parabolic reflectors and a central feed, such as the two antennas at the satellite-receiving station Ny-Ålesund, are in principle expected to have a rotationally symmetric directional characteristic around the antenna boresight axis. The antenna main lobe, which is the direction of maximum antenna gain (RF-boresight), is expected to coincide with the normal direction of the reflector midpoint towards the feed installation point (geometrical boresight). A possible deviation between the RF-boresight and the geometrical boresight is, as well as a not axially symmetrical directional characteristic, a typical evidence for a not optimal antenna performance. Such boresight errors and imperfect directional pattern (bad symmetries) can result from feed position biases with respect to the reflector normal direction and antenna reflector deformations. Boresight errors must be known to be considered (compensated) during antenna positioning, respectively to track satellites with maximum antenna gain

4.4 Link budgets

The link quality of a radio telemetry connection between a satellite and a satellite ground station depends on several factors. These factors are addressed in dedicated link budget calculations, which can help for several communication engineering tasks. Most of the following theory is based on equations from “Communication Architecture” (Dietrich and Davies 1999), but it is described here with some focus on the receiving side and supplemented with corresponding derivations and explanations.

Adequate data reception requires a certain minimum signal to noise ratio level at the receiver, depending on the used modulation technique and the acceptable bit error rate (BER). A minimum BER, which must be accepted at a certain signal to noise ratio even when using an imaginary ideal telemetry receiver, results from theory (error probability in presence of additive white Gaussian noise) and can be described by formulas that address the different modulation techniques (Proakis and Salehi 2007). Equation (3) applies for common PSK-type modulations (PSK = Phase Shift Keying), as used with CHAMP (BPSK = Binary PSK), GRACE-FO (O-QPSK = Offset Quadrature PSK) and other satellites, and shows that a minimum theoretical BER can be calculated from the ratio between the energy per bit E_b and the noise power spectral density N_0. The complimentary Gaussian error function *erfc* in equation (3) has the mathematical form of equation (4). It requires a numerical solution, which can be obtained in praxis, e.g. with dedicated programming recipes (series expansion),

as available for several programming languages, or a corresponding Windows EXCEL function, as used in this work.

$$BER = \frac{1}{2} erfc \sqrt{\frac{E_b}{N_0}} \tag{3}$$

where

erfc = complementary Gaussian error function [ ]

E_b = energy per bit [Ws] (in this context often applied in the equivalent unit W/Hz)

N_0 = noise power spectral density [Ws] (usually measured in the equivalent unit W/Hz)

$$erfc_{(x)} = \frac{2}{\sqrt{\pi}} \int_x^{\infty} e^{-r^2}\, dr \tag{4}$$

The BER performance of a real world telemetry receiver system is worse than described by theory. It corresponds to the degree of technical imperfection and must be determined experimentally, e.g., by a bitwise comparison between transmitted and received data at different signal to noise ratios (SNR). Figure 28 shows the measured BER performance of a tested telemetry system over a certain SNR-range, expressed in terms of E_b / N_0, which is the ratio (dimensionless) of received energy per data bit to the noise power spectral density.

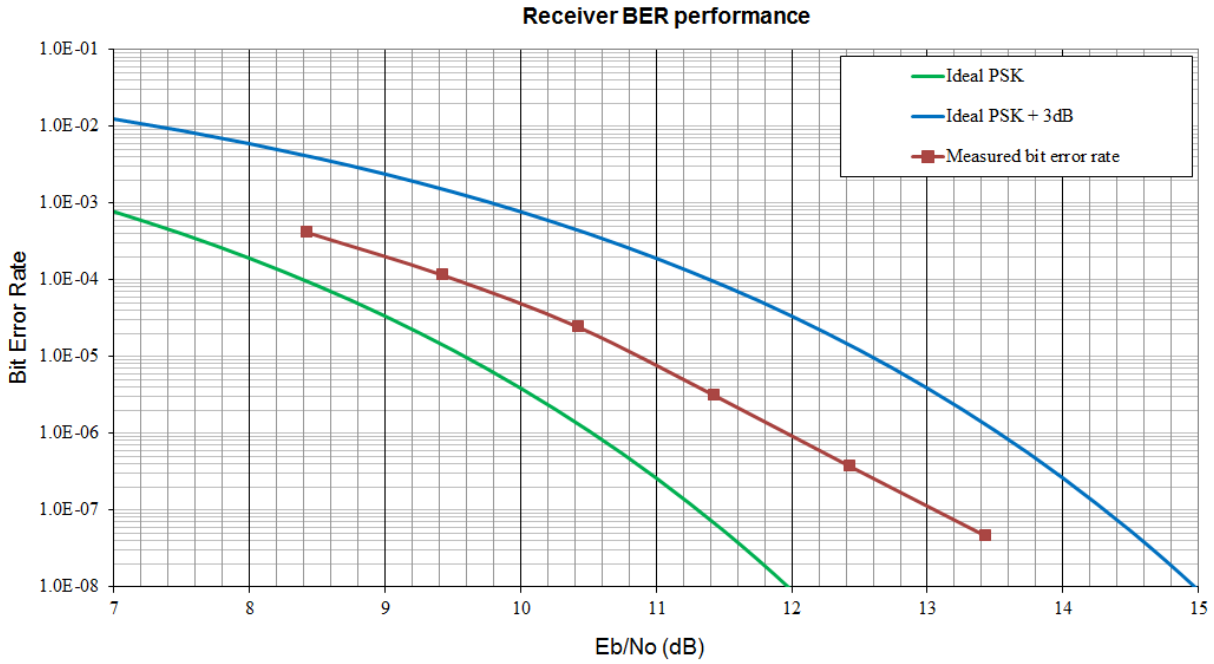

Figure 28: Example for a BER performance test result

The green curve for ideal PSK in Figure 28 corresponds to equation (3), the red line to the measurements (dots) and the blue curve to the green curve plus 3 dB, indicating the limit of tolerated telemetry system implementation loss (transmitter and receiver, e.g., from mission requirements). The graphic allows to determine, e.g., that the receiver requires an E_b / N_0 of about 12 dB to achieve a BER of 10^{-6} (1 bit-error per 1 million received bits), when operated with the transmitter as used in the test setup.

In praxis of telemetry reception one bit error affects the corresponding byte that includes the wrong (flipped) bit and thus also the next higher data units (e.g., packets). CRC (cyclic redundancy check) checksums of transmitted data packets are calculated on the transmitter side and included in telemetry data frames before transmission to ground. It is thus possible to detect even single bit errors by comparison of received CRC checksums in telemetry frames with correspondingly calculated checksums of received data. The detected CRC-errors cannot point on the false bits but may be correctable if the transmission technique includes a forward error correction mechanism (FEC, e.g., Viterbi or Reed Solomon). Otherwise affected data packets are unusable, either because they cannot be decoded or because they are not trustworthy.

Equation (5) is a formula for a link budget, solved for E_b / N_0, e.g. to calculate the expectable signal to noise ratio on the receiver side according to a certain link configuration. The parameters related to the signal power are found above the fraction bar of the right term, those that affect the system noise below it. The parameters in equation (5) refer to the spacecraft transmitting system (P, L_l, and G_t), losses on the link path (L_s and L_a), the receiving antenna gain G_r, the receiving system noise temperature T_S (G_r and T_S explained in section 4.5), the data rate R and Boltzmann's constant k, to calculate noise power from noise temperature.

$$E_b / N_0 = \frac{P L_l G_t L_s L_a G_r}{k T_s R} \tag{5}$$

where
E_b = energy per bit [Ws]
N_0 = noise power spectral density [Ws] (usually measured in the equivalent unit W/Hz)
P = power of satellite transmitter [W]
L_l = factor of losses between satellite transmitter and satellite antenna [ ]

G_t = gain factor of the satellite transmitter antenna [ ]
G_r = gain factor of receiving antenna (ground station) [ ]
T_s = system noise temperature (ground station) [K]
L_s = free space signal propagation loss factor [ ]
L_a = atmospheric loss factor [ ]
k = Boltzmann's constant (1.381×10^{-23} J/K respectively Ws/K)
R = data rate [bps = bit per second]

A more advantageous link budget notation for engineering calculations, which works with addition and subtraction of small grouped values in the "decibel domain", rather than with the multiplication and division of large factors, can be achieved with some transformations of equation (5). Equation (6) is the basic relation to transfer numbers, respectively factors or ratios, to their equivalents in dB-units. The ratio term E_b / N_0 in equation (5) can thus be transferred to a representation in the unit dB as in equation (7).

$$parameter_{[dB]} = 10 \log(parameter)\ dB \tag{6}$$

$$E_b / N_{0\,[dB]} = 10\ log\left(E_b / N_0 \right)\ dB \tag{7}$$

The application of equation (6) on both sides of equation (5) derives equation (8).

$$E_b / N_{0\,[dB]} = 10\ log\left(\frac{PL_l G_t L_s L_a G_r}{k T_s R} \right) dB \tag{8}$$

The application of the calculation rule in equation (9) on the numerator term of equation (8), except of G_r, and the application of the calculation rule in equation (10) on the denominator term, except of T_s, delivers equation (11).

$$log(xy) = \log x + \log y \tag{9}$$

$$log \frac{1}{x} = -logx \tag{10}$$

$$E_b / N_{0\,[dB]} = 10\ log(P) + \cdots + 10 \log\left(L_a \right) - 10 \log k - 10 \log R + 10\ log\left(\frac{G_r}{T_s} \right) dB \tag{11}$$

The terms on the right hand side of equation (11) can now be replaced with equation (6) by equivalent terms in dB-notation, resulting in equation (12).

$$E_b / N_{0\,[dB]} = P_{[dB]} + \cdots + L_{a[dB]} - k_{[dB]} - R_{[dB]} + \left(\frac{G_r}{T_s}\right)_{dB} \; dB \tag{12}$$

The emitted power from the satellite in the direction to the receiving antenna is usually represented by a value of *EIRP*, which is the Effective Isotropic Radiated Power as defined in equation (13).

$$EIRP_{[dBW]} = P_{[dBW]} + \; L_{l\,[dB]} + G_{t\,[dB]} \tag{13}$$

The term $k_{[dB]}$ in equation (12) can be replaced by its numerical value, as calculated in equation (14).

$$k_{[dB]} = 10\; log\; k = -228.6 \tag{14}$$

Insertion of equations (13) and (14) into equation (12) delivers equation (15), which allows link budget calculations in a more convenient way than with equation (5). The RF-related performance of the receiving system $G_r \,/\, T_s$, which is the relation between the receiving antenna gain G_r and the receiving system noise temperature T_s, appears in equation (15) independently from other parameters. This term is also known as the so-called "figure of merit of the receiving system" and it must be known to design satellite radio telemetry links or to assess if a certain satellite can be received with a particular receiving system.

$$E_b / N_{0\,[dB]} = EIRP_{[dB]} + L_{s\,[dB]} \; + L_{a[dB]} + 228.6 + \left(\frac{G_r}{T_s}\right)_{dB} - R_{[dB]}\; dB \tag{15}$$

The practical application of equation (15) requires a determination of the atmospheric loss L_a and the free space signal propagation loss L_s. The atmospheric loss L_a is usually assessed with models as provided by the ITU (ITU Radiocommunication Assembly 2013). The free space signal propagation loss L_s can be derived from equation (16) and has by far the highest impact on link budgets as it usually results in large numbers. For the use in equation (15) it is also necessary to transfer equation (16) to the "dB domain", applying the calculation rules of equations (9) and (10) and further simplifications, as shown in equation (17).

$$L_s = \left(\frac{c}{4\pi s f} \right)^2 \tag{16}$$

where

L_s = free space signal propagation loss factor [ ]

s = distance (slant range) between satellite and ground station [m]

c = speed of light [299 792 458 m/s]

f = frequency of radio link [Hz]

$$L_{s[dB]} = 20\log\left(3 \cdot 10^8\right) - 20\log(4\pi) - 20\log s - 20\log f = 147{,}55 - 20\log s - 20\log f \tag{17}$$

where

$L_{s\,[dB]}$ = free space signal propagation loss [dB]

Equation (18) can be used to calculate the distance (slant range) between a location on the Earth's surface (ground station) and a satellite.

$$s = \sqrt{(R_E \sin\alpha)^2 + 2R_E H + H^2} - R_E \sin\varphi \tag{18}$$

where

s = distance (slant range) between satellite and ground station [km]

R_E = Earth's radius [6371 km]

H = satellite altitude [km]

φ = elevation angle of satellite from viewpoint on the Earth's surface [°]

Figure 29 shows graphs for the free space propagation loss at typical S- and X-band downlink frequencies as a function of the link distance. The maximum telemetry link distance s to a satellite occurs at a ground station elevational viewing angle of 0°. For a satellite in a circular orbit of 500 km this would result in a distance s of about 2573 km. The corresponding free space signal propagation loss L_s for a S-band frequency of 2250 MHz would then be about 153 dB with the satellite in zenith (distance = orbit altitude) and about 168 dB when the satellite is at the horizon (blue graph). The losses in the X-band (at 8450 MHz) are about ~11.5 dB higher (at these frequency examples) than in S- band for all distances (red graph).

The stability or link reserve of a communication link can be assessed by calculation of a link margin LM (equation (19)) which is the difference between the available E_b / N_0 (e.g., from equation (15)) and the required signal to noise ratio $(E_b/N_0)_r$, e.g., as determined by BER measurements (Figure 28). Usually such calculations also consider a system implementation loss L_i, as in equation (19), e.g., to provide a more resilient basis for the generation of system requirements in a satellite mission design phase.

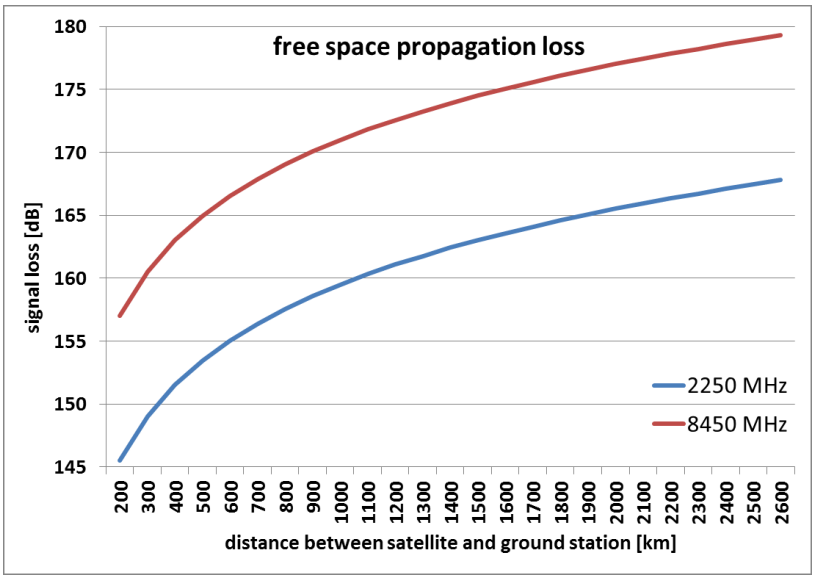

Figure 29: Free space propagation loss in S-band and X-band

$$LM = E_b / N_0 - (E_b / N_0)_r - L_i \tag{19}$$

where

LM = link margin [dB]

E_b / N_0 = available signal to noise ratio [dB]

$(E_b/N_0)_r$ = required signal to noise ratio [dB]

L_i = system implementation loss [dB]

The equations in this section, especially equation (15), can be used to derive requirements for individual communication system components to establish a stable communication link. Such dedicated requirements are subjects of mission requirement documents and typically concern the $EIRP$, to be provided by a satellite, and a minimal G_r / T_s, to be provided by ground stations.

4.5 Receiving system performance

The effective RF-related performance of a receiving system, also sometimes denoted as "antenna sensitivity" or "figure of merit", is usually specified in numbers of G_r / T_s (or simply

G/T), which is the ratio of the receiving antenna gain to the receiving system noise temperature. A *G/T* number can also be regarded to quote the useable gain of an antenna system. Numbers for the antenna gain *G* are often presented in the unit dB or dBi (dBi = gain on logarithmic scale, relative to isotropic radiating antenna), which is equivalent in this case, while the system noise is often specified in Kelvin (not yet on logarithmic scale). For the use with equation (15) it is thus required to calculate the G_r / T_s as shown in equation (20). G_r / T_s and *G/T* are used synonymous in this work and both according to equation (20) as it is common praxis in most literature as well.

$$G_r / T_s = G_r - 10 \log T_s \tag{20}$$

where

G_r / T_s = receiving system performance [dB/K]

G_r = gain of receiving antenna [dB]

T_s = noise temperature of receiving system [K]

The theoretical gain of an antenna is mostly defined by the antenna design, the antenna size and material properties. For antennas with parabolic reflectors (applies for NYA-1 and NYA-2) the antenna gain G_r, relative to an (imaginary) isotropic radiating antenna, can be calculated according to equation (21). The parameter η summarizes several efficiency parameters regarding, e.g., the reflector illumination spill-over, the aperture taper, the reflector surface (reflectivity, errors, roughness) or the radiation efficiency, cross polarisation and blockage.

$$G_r = 10 \log \left(\eta \cdot \pi^2 \left(\frac{D}{\lambda} \right)^2 \right) \tag{21}$$

where

G_r = antenna gain [dB]

η = Efficiency of antenna (typical value: 55%)

D = Diameter of parabolic antenna reflector (e.g., 4 m for NYA-1 antenna)

λ = Wavelength of received radio signal (e.g., 0.1333 m for frequency of 2250 MHz)

The wavelength λ of radio waves in space and on Earth can be calculated from the frequency *f* and the signal propagation speed, which is approximately the speed of light in vacuum *c* as in equation (22).

$$\lambda = \frac{c}{f} \tag{22}$$

where

c = speed of light in vacuum = 299 792 458 ms^{-1}

Figure 30 shows the theoretical antenna gain, based on equation (21), for different antenna reflector sizes, typical S-band and X-band downlink frequencies and a typical antenna efficiency of 55%. The antenna gain increases with the antenna reflector diameter.

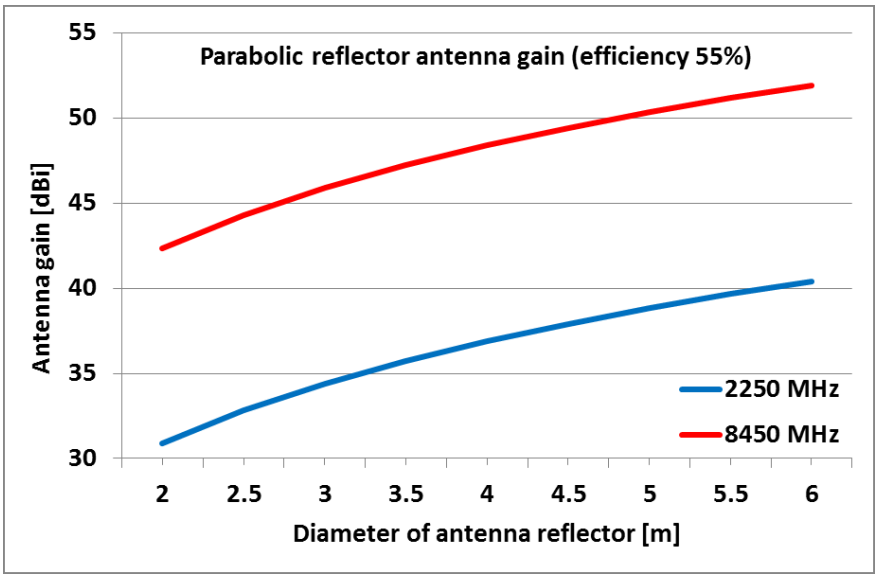

Figure 30: Antenna gain in S-band and X-band w.r.t. antenna size

The gain also increases from S-band to X-band, which implies that higher frequencies might be generally favourable for satellite communication. This is somehow true from the perspective of an antenna or for other reasons (e.g., increase of useable signal bandwidths at higher frequencies), but it must be considered that the increase of antenna gain with frequency is just the same (here about 11.5 dB) as the increase of free space propagation loss (Figure 29). Technical problems usually also increase with higher frequencies, e.g., w.r.t. reflector roughness (affects η), pointing loss (from smaller Θ) and LNA performance figures (gain versus noise). Another point is that in general the components costs increase with frequency.

The expectable theoretically gain G for NYA-1 at a frequency of 2250 MHz is = 36.9 dBi (equation (21)). A reduction of antenna gain must be considered if the antenna is installed under a radome. The amount of such losses depends on material properties of the radome and increases if the radome is covered with precipitation, especially with water, e.g., from rainfall. Radomes thus usually have a special hydrophobic coating on the outside. However, the effect of rain, ice, snow and dust directly on an antenna reflector or feed can have a by far more

negative impact on antenna performance than losses from a radome. Another reduction of the antenna gain (if not yet included in η) may arise from the obstruction of the effective antenna area (aperture) by constructional elements in the signal path. This can be, e.g., the support bars for feed installations or secondary reflectors (see section 4.2). The resulting antenna gain reduction is proportional to the blocked aperture area.

The radio signal power, as received by an antenna, cannot be transferred completely from the signal pickup point (e.g., the feed antenna port) to the subsequent signal path, which usually continues with a RF-filter or a LNA. The signal power is reduced during the transfer, especially at physical connections (e.g., RF-plugs), due to ohmic losses and losses from impedance mismatches. Ohmic losses may be treated as constants (not frequency dependent) and should be denoted in manufacturer specifications. Low loss coaxial connections, e.g., such as N-type connectors, provide connectivity with an ohmic loss corresponding to about 0.05 dB, additional to an impedance mismatch loss. The impedance mismatches are expressed in values of SWR (standing wave ratio), which are usually a function of frequency and should be available from corresponding manufacturer data sheets as well. A connection impedance mismatch causes some portion of the power to be reflected from the connection (e.g., back to the feed) according to equation (23). The resulting loss follows from equation (24).

$$r_p = \left(\frac{SWR - 1}{SWR + 1}\right)^2 \tag{23}$$

$$SWR_{loss} = 10 \cdot LOG(1 - r_P^{\,2}) \text{ [dB]} \tag{24}$$

where
r_p = reflected power (factor) [ ]
SWR = standing wave ratio [ ]
SWR_{loss} = signal loss due to SWR mismatch [dB]

The term noise temperature quantifies the thermal noise due to the movement of charge carriers, such as ions and electrons. Thermal noise has a very broad or even white frequency spectrum (up to ~100 GHz) and reduces the sensitivity of electronic devices as an increase of the noise floor reduces the SNR of wanted signals. The noise temperature T_s of a receiving system results from many noise sources with different characteristics, which are sorted by two

groups, the antenna noise temperature $T_{antenna}$ and the receiver noise temperature $T_{receiver}$ (equation (25)).

$$T_s = T_{antenna} + T_{receiver} \tag{25}$$

The assignment of ground station system components (basic configuration of station with up- and downlink) to the grouping of noise is shown in Figure 31.

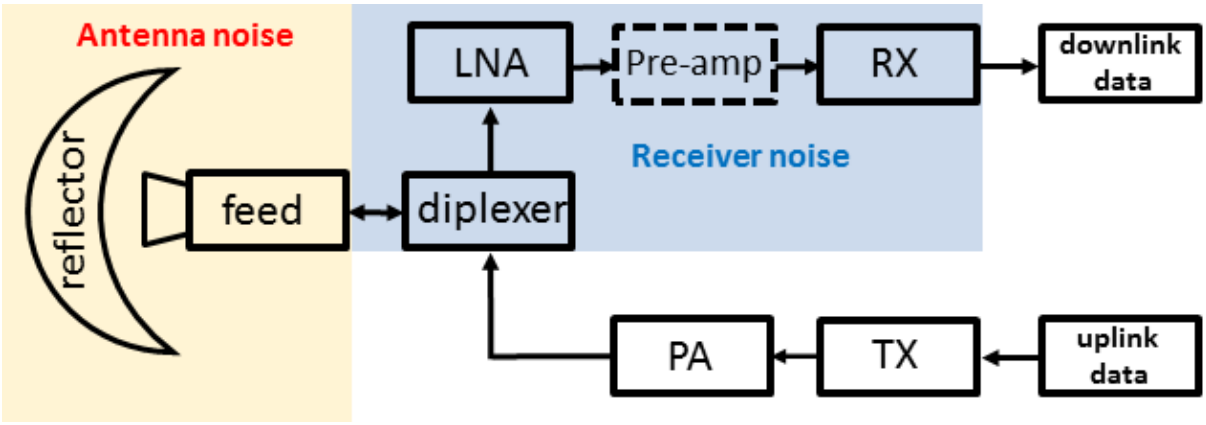

Figure 31: Categories of system noise w.r.t basic signal paths at ground station

Not only dedicated system components themselves contribute to the system noise, but also the connections between them, which can be waveguides, cables or direct connections (e.g., plugs or adapters). The uplink path (TX = transmitter, PA = Power Amplifier) has no direct relevance for the noise temperature of the receiving system in principle, except when it requires the use of a diplexer (direction selective element), which is the normal case for stations with an uplink. These topics are discussed further below in this section and in section 5.3 (calculation of *G/T*). The antenna noise with antenna noise temperature $T_{antenna}$ is the sum of all noise contributions from far distance (e.g. galactic noise) to the output port of the antenna feed system. Equation (26) shows some examples, but does not consider all possible contributions.

$$T_{antenna} = T_{sky} + T_{local} + T_{radome} + T_{ground} + \ldots \tag{26}$$

where

T_{sky} = noise temperature of sky [K]

T_{local} = noise temperature of local environment [K]

T_{radome} = noise temperature of radome [K]

T_{ground} = noise temperature of ground [K]

The values of some terms in equation (26) can be obtained from component specifications (e.g., T_{radome}), which are usually based on measurement data, e.g., from the particular manufacturers. Other terms (e.g., T_{local}) may be estimated or calculated by formulas, which follow certain models or exemplary measurements. The contribution of sky noise (oxygen and water vapour) is elevation-dependent (Table 4, section 5.3), with the minimum at 90° elevation (zenith) and the maximum at 0° elevation, corresponding to the length of the signal path through the atmosphere. Thus, also the *G/T* performance in total is a function of elevation. Some noise is picked up from the ground through antenna side and back lobes. The magnitude of received ground noise can be assessed from the relation between the solid angle of the ground Ω_{ground} (e.g., 180° x 180°) to the solid angle of the antenna main lobe $\Omega_{main\ lobe}$ ($=\Theta^2$), the relation of the antenna gains in these directions and the physical temperature of the ground T_0 (e.g., 290 K) as in equation (27). The parameter $G_{side\ lobe\ mean}$ in equation (27) is the mean antenna gain for all side lobes and back lobes in directions to the ground, relative to the main beam gain.

$$T_{ground} = T_0 \frac{\Omega_{ground}}{\Omega_{main\ lobe}} G_{side\ lobe\ mean} \tag{27}$$

where

T_{ground} = noise temperature of noise that is received from the ground [K]
T_0 = physical temperature of the ground [K]
Ω_{ground} = solid angle of the ground, as seen from the antenna [sr]
$\Omega_{main\ lobe}$ = solid angle of the antenna main lobe [sr]
$G_{side\ lobe\ mean}$ = gain factor of side lobes, relative to main lobe gain [ ]

The receiver noise temperature $T_{receiver}$ results from noise contributions of components on the downlink signal path beyond the antenna feed output port. These components are arranged in a chain, and the gains and losses of all components affect the noise contribution, respectively the noise effect of successive components.

The resulting total receiver noise temperature can be calculated with Friis' formula in the notation as shown in equation (28), with all values in absolute numbers (factors), not in their quantities of dB. A calculation for a typical signal chain, beginning behind an antenna feed, would require to consider at least the noise temperature and gain of the LNA (T_1, G_1), the noise temperature and loss of the cable and RF signal distribution devices (T_2, G_2) and the noise temperature of the telemetry receiver (T_3).

$$T_{receiver} = T_1 + \frac{T_2}{G_1} + \frac{T_3}{G_1 G_2} + \ldots + \frac{T_n}{\prod_{N=1}^{n-1} G_N} \tag{28}$$

The crucial impact of the LNA noise (T_1) and LNA gain (G_1) on the total system noise becomes clear, and also that there is no alternative to a high performance LNA at a preferably early point in the signal chain. An additional amplifier at a later stage of the signal chain might be useful for other reasons (e.g., to equalize high cable losses), but amplifies both, the wanted signal and the noise from previous stages, while adding another amount of noise (e.g., from the amplifier electronics and connections) to the total noise budget.

Specifications of antenna and receiver components are not always unique with respect to quoted parameter units and definitions, apparently especially when addressing noise related properties. Commonly used values are the noise factor F as defined in equation (29), the noise figure NF, also denoted F_{dB} as in equation (30) and the system noise temperature T_S.

$$F = 1 + \frac{T_S}{T_0} \tag{29}$$

$$F_{dB} = 10 \log\left(1 + \frac{T_S}{T_0}\right) \tag{30}$$

where

F = noise factor [ ]

F_{dB} = noise figure NF [dB]

T_S = System noise temperature [K]

T_0 = Physical device temperature (usually assumed to be 290°) [K]

Sometimes it is required or at least more convenient to calculate with the system noise temperature, rather than with noise factors or noise figures, e.g., to work with Friis' formula in the notation of equation (28). The equations (29) and (30) may thus be rewritten for the noise temperature, as shown with equations (31) and (32). The same applies for gain values, which are required as factors to be used with equation (28). Gain values can be converted from db-quantities to factors with equation (33).

$$T_S = (F - 1) \cdot T_0 \tag{31}$$

$$T_S = \left(10^{F_{dB}/10} - 1\right) \cdot T_0 \tag{32}$$

$$G = 10^{\left(\frac{G_{[dB]}}{10}\right)} \tag{33}$$

where
G = gain factor [ ]
$G_{[db]}$ = gain [dB]

The equations in this section can be used to assess the RF-related performance of a receiving system, based on component specifications, models and assumptions, which are of course afflicted with uncertainties. In praxis it is thus preferable to determine a receiving system *G/T* by measurements (see section 9.2). The theoretical performance parameters can then be used to assess the measurement results and the quality of system implementation.

4.6 Antenna tracking systems

A satellite tracking system for ground stations must be able to direct an antenna to a satellite, which can be in general any direction in the hemisphere above the station. This task requires a mechanical system with at least two axes and with sufficiently high maximum angular velocities to follow the satellites to be tracked. Most common are "elevation over azimuth" systems as in Figure 32 a (used with NYA-1) and "X over Y" systems as in Figure 32 b (used with NYA-2). "Elevation over azimuth" systems can address antenna directions (in principle) directly in the horizontal coordinate system of the antenna, which is also easier ascertainable for humans. The azimuth is usually counted clockwise from North (nautical convention) and the local horizon corresponds to 0° elevation for all azimuths.

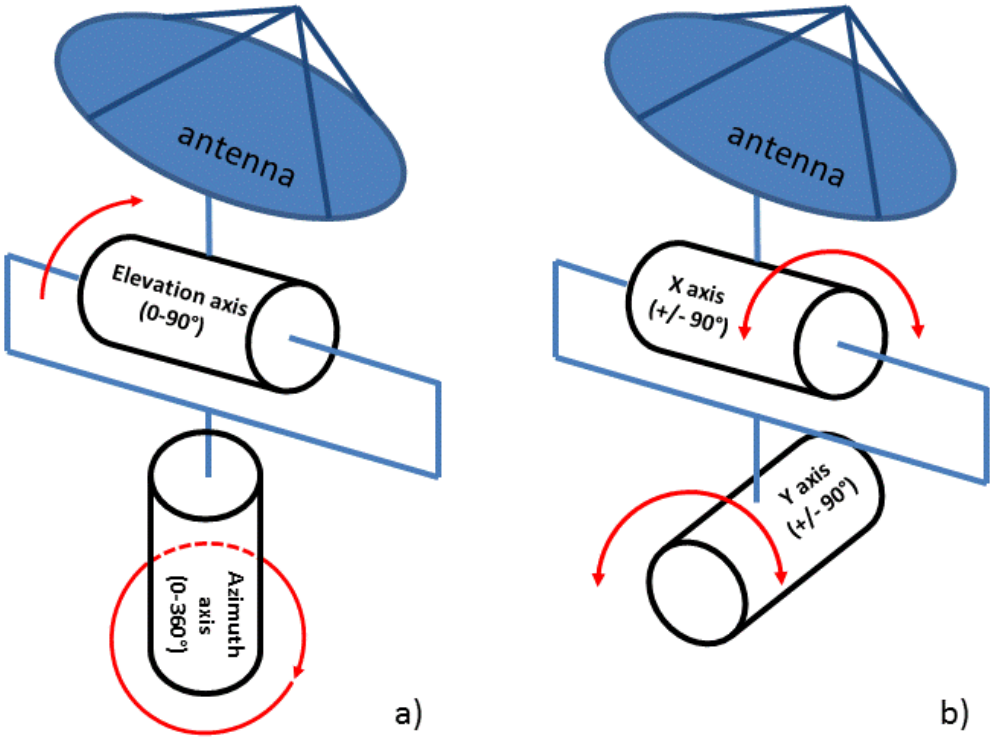

Figure 32: Layout of elevation/azimuth and X/Y antenna positioning systems

Zenith is equal to 90° elevation and Nadir is zenith minus 180°. The arrangement of the axes in an "elevation over azimuth" system can cause some technical problems in praxis. If the ascending part of a satellite pass (from viewpoint of ground station) is tracked up to high elevations, e.g., close to 90°, then the azimuth axis has to turn around by nearly 180° very fast, to continue the tracking on the descending part of the satellite pass, from close to 90° downwards. Such high elevation satellite passes are known as "keyhole passes". If not considered in the satellite contact scheduling, they can cause loss of data, due to signal losses, or complete signal outages from temporary wrong antenna-pointing. Therefore, some ′"elevation over azimuth" systems use a third axis and some other have an elevation axis range of 0-180°, which provides sufficient or at least more agility to cope the problems of keyhole passes. Another problem can arise if the azimuth axis has a range limitation, which is the normal case. The azimuthal limits might be shortly beyond a nominal useable range of 360°, e.g., to avoid problems with the cable guiding to the antenna (winding). Axes limits must thus be considered for antenna tracking in advance.

An "X over Y" axes system has two perpendicularly arranged horizontally oriented axes (Figure 32 b), e.g. with the lower one aligned to the East-West direction and the upper one

aligned to North-South direction. Such systems have the advantage that there are no mechanical limitations for antenna movements close to elevations of 90°. Thus there are no problems with "keyhole passes". Another advantage is that the "X over Y" system can make an infinite number of antenna movements around the vertical axis (no azimuthal limits) without problems due to wound up cables etc. A potential disadvantage of the "X over Y" system is limited system agility when directions with low elevations are tracked in the direction of the lower axis. Both axes are close to their mechanical limits (+/- 90°) in these cases and azimuthal position changes according to directions behind the approached upper axis limit are hindered. It is no problem for the system to point to any direction of the hemisphere in principle, but the continuation of azimuthal tracking in the described situation requires a large turn of the lower axis first (up to 180° at 0° elevation). Such large movements take some time, depending on the systems axes rates, and can thus cause positioning errors if commanded directions are achieved too late or skipped. These limitations are similar to the problems of "elevation over azimuth" systems with "keyhole passes", but should have no significance if very low elevations are avoided (Rolinski, Carlson and Coates 1962), which is the satellite tracking standard procedure for other reasons anyway (e.g., to avoid high slant distances and higher ground noise).

The effective angular velocity of an antenna tracking system (e.g., vector sum of involved axes velocities) must be at least as high as the angular velocity of the satellite to be tracked, which depends on the satellite orbit velocity and the distance to the ground station. The velocity of a satellite in a circular orbit can be approximated with equation (34).

$$v = \sqrt{\frac{G\,M}{r}} \tag{34}$$

where

v = velocity of the satellite [ms^{-1}]

G = gravitational constant of the Earth (6.67408×10^{-11} m^3 kg^{-1} s^{-2})

M = Earth mass ($5{,}972 \times 10^{24}$ kg)

r = distance between gravitational centre of Earth and satellite [m]

The highest angular velocity appears during the culmination of the satellite pass (point with highest elevation). During culmination (from the viewpoint of the ground station) there is no radial velocity component and the angular velocity can be approximated with equation (35). A satellite in an altitude of 350 km, for example, has an orbit velocity of 7.7 km/s. It passes a ground station with about 1.26 °/s in zenith (slant range s = 350 km) and with about 0.2 °/s at 5° elevation (s = 2211 km, equation (18)).

$$\omega = \sin^{-1}\frac{v}{s}\ ^\circ \tag{35}$$

where

ω = angular velocity of satellite (in cases without radial velocity component) [° s^{-1}]

s = distance between satellite and ground station [m]

The task to maintain a stable radio link between a satellite and a ground station requires a certain accuracy of antenna-pointing, as any pointing error leads to signal losses (4.3). The main factors that can affect the accuracy of satellite tracking are sketched in Figure 33. Nominal directions to a satellite to be tracked are calculated from satellite orbit predictions. The real directions to a satellite during time of tracking differ from the predicted directions to some extent in praxis. The corresponding prediction errors Δ-predictions usually increase with the age of the predictions (example in section 4.7). Also not foreseeable changes of solar activity or of other parameters to be considered for orbit predictions may increase prediction errors. Some errors (not addressed in Figure 33) can result from coordinate transformation errors of satellite positions to directional values (e.g., celestial to horizontal coordinates). A good alignment of the principal axes of an antenna tracking system to a

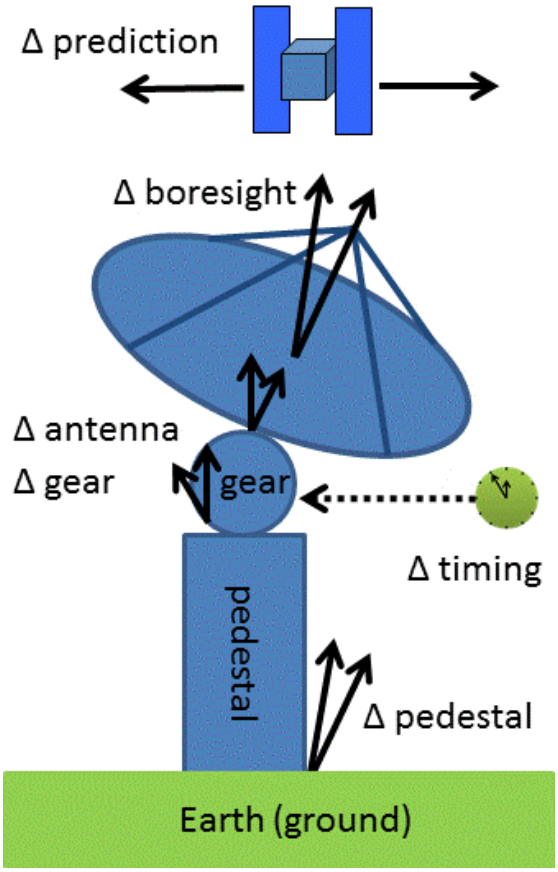

Figure 33: Origins of satellite tracking errors

geographic coordinate system, usually the zenith and north directions of the local horizontal coordinate system, is sought during the installation of a tracking system. However, the pedestal of a tracking system can hardly be installed without a certain Δ-pedestal bias. A Δ-gear error, e.g., due to lose movements in the gear mechanisms, may be added by the mechanical systems that perform the antenna positioning. The mechanism to move the tracking system axes must be operated also timely precise. Any Δ-timing errors, such as a delayed execution of tracking commands, cause a certain directional error. The nominal antenna beam direction may not be in perfect alignment with the normal direction of the tracking system's antenna mounting flange, resulting in a Δ-antenna bias. It can also happen that the nominal antenna beam direction has an angular offset to the real, RF-related, effective antenna boresight, resulting in a Δ-boresight bias.

The sum of all biases could be compensated during satellite tracking by a correction value in principle, so that the nominal directions are adjustable with sufficient low misalignment, despite of all system biases, provided that the sum of all biases is known. A correction value (one value per axis) has the same amplitude as the sum of all biases to be compensated, but the opposite sign, as in equation (36). It can be used to generate the right commands for antenna movements and to correct the antenna system directional feedback (readings from direction sensors) according to equation (37) and equation (38). These corrective tasks, forward (commands) and backward (readings), can be addressed by dedicated functions of the antenna tracking system, either as part of the interface system (antenna control unit) or the operation software.

$$\begin{aligned} \Delta\, correction &= -1\,(\Delta\, sum\ of\ biases) \\ &= -1\,(\Delta\, pedestal + \Delta\, antenna + \Delta\, boresight + \cdots) \end{aligned} \tag{36}$$

$$direction\ command = nominal\ direction + \Delta\, correction \tag{37}$$

$$real\ antenna\ direction = direction\ sensor\ reading - \Delta\, correction \tag{38}$$

where

Δ correction = correction value to compensate sum of known biases

The correction of antenna misalignment during satellite tracking in the basic approach is limited to quasi-static biases, such as Δ-pedestal, Δ-antenna, Δ-boresight and Δ-timing. All

other biases are either very small (Δ-gear), difficult to assess (non-static components of biases) or even unknown or unforeseeable (Δ-prediction), but the corresponding antenna-pointing errors could be corrected dynamically during satellite reception. Dynamic corrective input for an antenna tracking system can be obtained in real-time from special devices (e.g., mono pulse feed systems, if installed), which sense the offset of the real satellite direction to the antenna-pointing direction and support an auto tracking functionality by this.

A simple way to assess antenna-pointing errors is to look at the differences between the azimuth and elevation values of a tracking antenna and the corresponding true satellite directions. This approach may be used to investigate the performance of individual axes. However, that way is not applicable to calculate the loss of antenna gain due to pointing errors, which is a function of the angular distance e_r (total error) between the antenna-pointing vector *a* and the vector to the satellite *s*. It can be calculated with equation (39) if the coordinates of both vectors are transformed from the local horizontal coordinate system to the local Cartesian coordinate system first.

$$e_r = arccos\left(\frac{a \cdot s}{|a||s|}\right) \tag{39}$$

where

e_r = angle between antenna direction and satellite direction [°]

a = antenna direction vector in Cartesian coordinates

s = satellite direction vector in Cartesian coordinates

4.7 Satellite tracking with twoline elements

The accurate direction of an antenna to a satellite requires good knowledge about the satellite's position at the time of tracking. Actual positions of satellites can be calculated from orbital elements, which describe the satellites orbit parameters. Satellite orbits follow Kepler's laws in principle but are not stable, because they are influenced by several forces, e.g., from the gravitation of the moon, solar wind, radiation pressure, gravitational irregularities (Earth) and (rest) molecules along the orbit track (atmospheric drag). The twoline elements (TLE) format (CelesTrak 2004) is commonly used to provide satellite orbit information for tasks, where satellite positions need to be predicted, such as for satellite tracking with directive antennas. The parameter values in TLEs (examples in Appendix) are calculated from orbit

observation data (e.g., from SLR, on-board GNSS or RADAR) and referenced to an epoch. This is a certain point of time, which is not necessarily included in the observation interval. The actual quality of TLEs depends on the data quality and timely coverage of used observations, the program for orbit calculation and (in general) the distance between observations and prediction epoch. The accuracy of TLE-based predictions also decreases with the age of used TLEs.

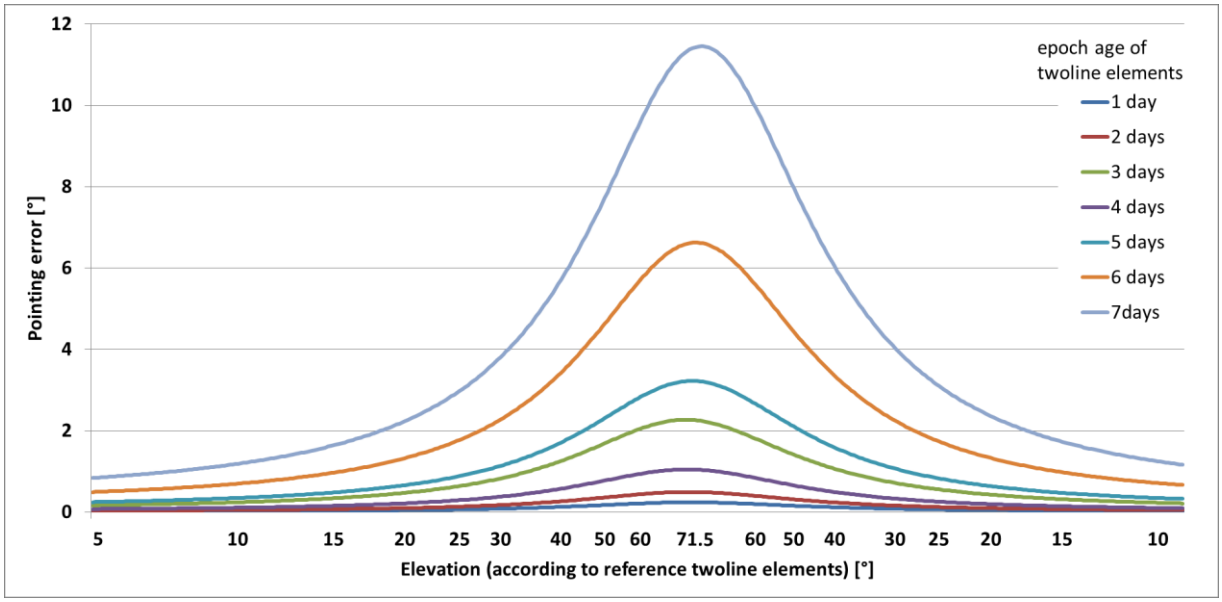

Figure 34: Example for antenna-pointing errors versus age of twoline elements epoch

Figure 34 shows antenna-pointing errors for a test scenario where an antenna uses increasingly outdated twoline elements for the calculation (prediction) of directions to a satellite. Eight twoline elements with epochs according to 8 consecutive days (source: GSOC) were used to calculate antenna-pointing directions for the same GRACE-1 pass (culmination 71.5°), from the viewpoint of the NYA-station. The pointing directions from the most recent of the 8 twoline elements (epoch 14th November 2016) served as a reference to calculate pointing errors (with equation (39)) from directions as calculated with the other 7 twoline elements, which were thus effectively out-dated by 1 to 7 days. All directions were calculated with the same "Spacetrack report #3" program routines (6.7.4), which are also used with the new NYA-Sattrack antenna operation program (introduced in section 6). The graphs may be regarded as rough examples for the pointing error effect of out-dated TLEs.

Figure 34 shows that pointing errors occur, in this example, even with twoline elements which are only 1-day old. Maximum pointing errors are observed at the culminations of the passing satellite and the errors increase rapidly with an increasing age of the twoline elements. The

error maxima are about 0.24° after one day, followed by 0.49°, 2.26°, 1.05°, 3.2°, 6.6° and 11.4° after 7 days. Surprisingly the pointing errors with 4-days old twoline elements are smaller than the errors with 3-days old elements. Such discontinuity is not the regular case, but it may be regarded as an example for the changing quality or other problems in the TLE generation procedures. However, the TLE-based satellite tracking is a proven and widely used method. It allows sufficient tracking accuracies in most cases, provided that the used TLEs are based on accurate orbit determination / prediction, and not too old. The frequency for TLE updates at a tracking station may be adapted to the rate of expectable orbit variations. These depend, e.g., on the orbit altitude and solar activity, which was low for all days in the shown example scenario (solar flux $F < 81$ SFU @ 10.7 cm wavelength)[2].

4.8 Antenna measurements with the sun

Section 4.3 discusses the importance to know about possible antenna boresight errors, imperfections of the beam pattern and, if possible, about the direction and effect (gain) of side lobes. Section 4.4 highlights the relevance of the receiving system *G/T*, which is mainly determined by antenna properties and must be known to calculate link budgets. All these points can be investigated by measurements that involve the sun as a signal source.

The sun is emitting electromagnetic waves in a wide spectrum, partly as visible light, but also as microwaves in the frequency bands, which are used for communication with satellites. It is possible to receive these radio signals from the sun with high and medium gain antennas, such as used at satellite ground stations. It is also possible to calculate the actual direction from a local horizontal coordinate system (viewpoint of a ground station) to the sun very precisely. These two factors make the sun a good reference target, e.g., to calibrate the directional controls of antenna tracking systems and to provide a reference signal.

The total antenna misalignment, as it results from different installation misalignments and boresight errors, can be determined by a simple procedure. A receiver or spectrum analyser is connected to the antenna under test and measures the radio noise signal power as received from the sun. The antenna is directed to the sun with some deliberately introduced deviations from the nominal sun direction. The best alignment of the effective antenna boresight (corresponding to the main lobe gain maximum) with the true sun direction is achieved when

[2] SFU = solar flux unit, more details are explained in sections 4.8 and 9.2

maximum signal strength is detected. Care must be taken that the signal strength maximum was really found, e.g., by repeated systematic variation of the antenna direction around the direction of the signal maximum. The difference between the calculated (theoretical) sun direction and the observed direction as indicated by the antenna tracking system provides the calibration (correction) value to correct the actual total antenna misalignment.

Also the antenna performance in terms of *G/T* can be determined with the sun as a radio signal source. The method is described and recommended by ITU publications, although the corresponding documents (ITU Radiocommunication Assembly 1992-1993-2000) refer to more distant radio stars than the sun. However, there are several examples of successful *G/T*-measurements with the sun (Cakaj, Keim and Malaric 2005) all assuming that no significant sun flux fluctuations occur at the measurement time. The method requires only two measurements. The first one determines the system noise power at the nominal antenna operation frequency, e.g., with a spectrum analyser, when the antenna is pointed to clear, RF-related cold sky, where no signal should be received. The second measurement determines the received power at the same frequency when the antenna is directed to the sun. This measurement provides the test signal, which also has a noise character (as the system noise), but a determinable signal source power (from solar flux measurements). The ratio of noise power received from the sun to the system noise power is the so called "*Y*-factor":

$$Y = \frac{P_{sun}}{P_{cold\ sky}} \tag{40}$$

where

Y = "*Y*-factor" [ ]

P_{sun} = received (signal) power when antenna is directed to the sun [W]

$P_{cold\ sky}$ = system noise power when antenna is directed to cold sky [W]

The *G/T* value then follows from equation (41).

$$\frac{G_r}{T_s} = \frac{(Y-1)\ 8\ \pi\ k\ L}{(F * \lambda^2)} \tag{41}$$

where

L = antenna beam correction factor (~1 for small antennas as at Ny-Ålesund) [ ]

λ = wavelength (according to antenna operation frequency) [m]

F = solar flux at antenna operation frequency (in solar flux units of 10^{-22} Wm^{-2} Hz^{-1}) [SFU]

Equation (41) requires the knowledge of the actual solar radio flux density F during the G/T measurements at the antenna operation frequency. The corresponding value is not required to be measured on-site and at the experiment frequency, but can be derived from an interpolation of solar flux measurements at nearby frequencies, as they are available from observatories with special solar flux monitoring instrumentation. The described procedure delivers reliable in situ values of the G/T performance, provided that the monitored solar flux shows no irregularities for the time of measurements (e.g., no sun flares). Another advantage of the method is that it does not require any consideration of individual system properties, such as component gains and noise temperatures (see section 4.5).

The sun may also be used as a radio signal source to detect the directions and to measure the gain of antenna side and back lobes, in principal with the same method as for the main lobe. However, the success of such measurements depends on the signal power density of the radio signals from the sun in the investigated radio bands and the antenna G/T characteristic in the probed directions. More details are given in section 9.

5 NYA, the satellite-receiving station at Ny-Ålesund

5.1 Location and local infrastructure

The satellite-receiving station at Ny-Ålesund, Spitsbergen (Figure 35), is installed about 1 km away from the village at 78° 55´ North, 11° 56´ East, between the local airstrip (length 808 m) and the Kings Bay fjord. The closer environment is shown in Figure 36 with the NYA station in the middle of the photo, near to the upright looking antenna of the local VLBI-station (Very Long Baseline Interferometry). The local horizon allows a good visibility for the antennas in general (distance to glaciers in background of Figure 36 is about 15 km), but with some masking, e.g., by three mountains. Figure 37 shows the two closest and most sight limiting mountains, which is the Zeppelin Mountain (distance of summit: 2.4 km, Az: 183°, El: 12.6°) and the Schetelig Mountain (distance of summit: 3.5 km, Az: 270°, El: 11.0°). It also shows the position of the local VLBI station and a DORIS beacon (Doppler Orbitography and Radiopositioning Integrated by Satellite), which is another instrument for space geodesy.

Figure 35: Satellite-receiving station Ny-Ålesund

Despite being located close to the North Pole (distance only about 1230 km), Ny-Ålesund is reachable through regular travel connections (aircrafts from Longyearbyen and ships). Practically all kind of local infrastructure and services (airport, harbour, road system, energy, board and lodging etc.) is provided and operated by the Norwegian Kings Bay Company on a commercial basis. The receiving station gets electric power from the nearby (~ 1 km) power plant of Ny-Ålesund which uses 3 diesel-powered generator blocks of 630 KVA each. The power plant is maintained on a high level as it also provides warm water to the central heating system of the village, which is essential for life in Ny-Ålesund. Regularly only one block is in

active operation, delivering sufficient power for all consumers in and around the village of Ny-Ålesund, while the other two blocks are kept on standby.

Figure 36: Site of the NYA satellite-receiving station

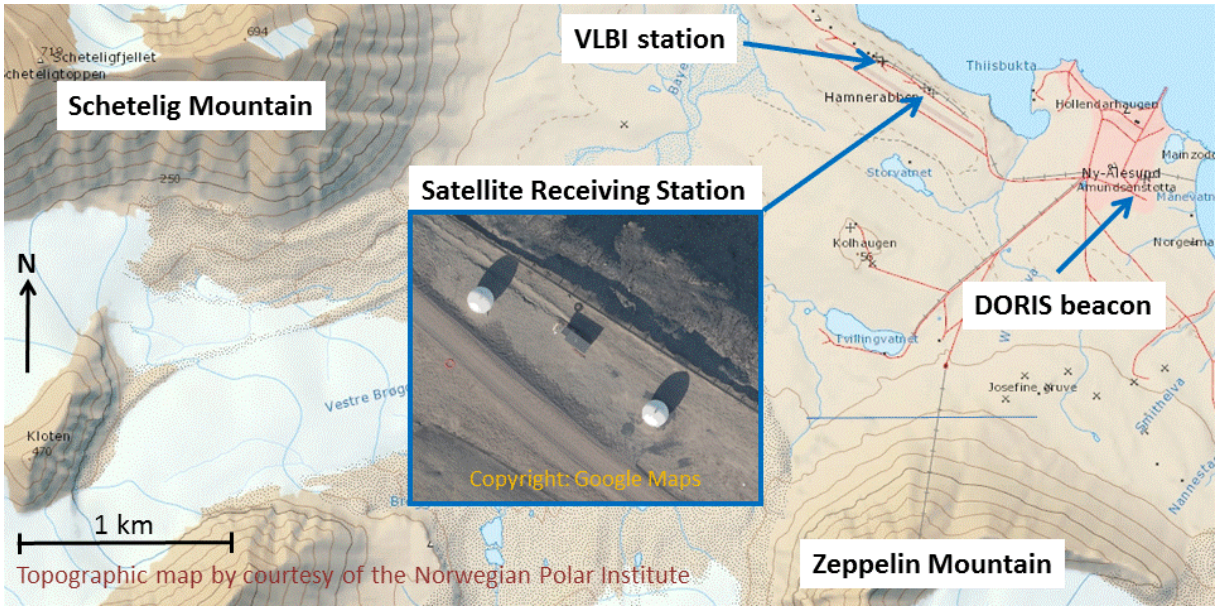

Figure 37: Locations of the NYA-station, closest mountains and space geodesy instruments

The area of Ny-Ålesund (20 km radius around village) is defined as a radio silent area, in order to avoid any radio signal disturbances to the local VLBI-station. In principle all kind of local radio transmissions are tried to be kept at a minimum, but there are several exceptions in frequency bands that are not used for VLBI signal receptions (e.g., VHF-band for voice

communication). The frequency range from 2 to 32 GHz, which includes the S-band for communication between satellites and groundstations, enjoys special protection, even outside the currently used VLBI-frequencies. An exception is the local DORIS beacon, which transmits shortly above 2 GHz. The restrictions for radio signal emissions are an advantage for the receiving activities at the NYA satellite-receiving station, as it reduces the probability of disturbing signals, but it also prevents the use of the station for transmitting activities (no satellite uplink).

5.2 Station equipment (hardware)

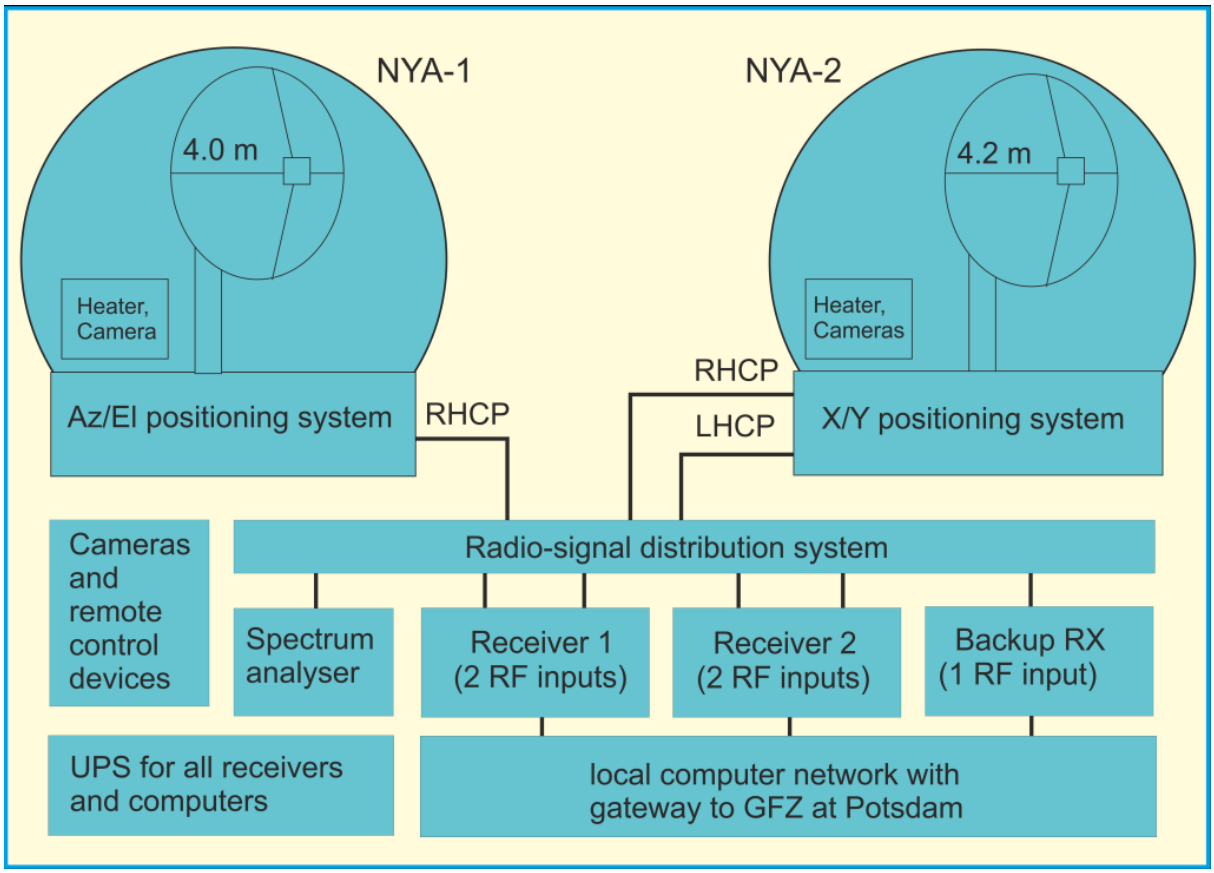

Figure 38: Components of the NYA station

Figure 38 is a sketch of the basic station layout. The ground station has two antenna systems, which are sheltered against the rough climate conditions on Spitsbergen by heatable radomes. All receivers and devices for antenna operation are installed in a small operation cabin between the radomes (Figure 35, Figure 39). The main properties of the antennas are listed in Table 1, a more detailed description is given in 5.2.2 and 5.2.3.

	NYA-1	NYA-2
Antenna Diameter	4.0 m	4.2 m
Frequency	S-band	S-band
F/D ratio	0.42	0.375
Reflector surface tolerance	0.02 inch rms	0.025 inch rms
Calculated gain at 2250 MHz (equation (21))	36.9 dBi	37.3 dBi
Calculated half power beam width at 2250 MHz (equation (1))	2.33º	2.22 º
Polarization	RHCP	RHCP and LHCP
Positioning system	Elevation / Azimuth	X / Y
Manoeuvrability	Azimuth: 720º Elevation: 0º - 90º	no Azimuth limit Elevation: 0º - 90º (180º) X-axis: Zenith +90º / -90º Y-axis: Zenith +90º / -90º
Maximum tracking speed	20º / sec	4° / sec
Pointing accuracy, (manufacturer specifications)	Lost motion: not specified Backlash: 0°	Lost motion: 0.035° Overall backlash: 0.0125°

Table 1: Main properties of the antennas at the satellite-receiving station Ny-Ålesund

Figure 39: View on desk and racks in operation cabin

Most of the devices at the station are installed at least twice and operated in parallel (hot redundant). Thus the failure of one device does not necessarily cause an interruption of reception. The ground station is connected to GFZ at Potsdam via Internet. Until October 2015 the routing of all Internet data from Ny-Ålesund included a microwave repeater link. This microwave link was somehow instable on occasion and was thus replaced by two fibre-optic cables. IT-security is established through special soft- and hardware, such as VPN-devices (Virtual Private Network). All Internet traffic from the ground station is encrypted and routed to GFZ at Potsdam. The minimum available bandwidth for data traffic from the station to GFZ was 1 Mb/s at times with the microwave link, which proved to be already fully sufficient for data transfers, remote monitoring and remote control activities, and increased to several Mb/s (up to ~10 Mb/s) with the fibre optic cable.

Remote monitoring and control is carried out with special software and hardware. Among these devices are sensors for temperature and electric power, remote computer management cards, KVM- (Keyboard Video Mouse) and Ethernet-switches with remote control, remotely controlled mains power and RF-signal distribution switches, and 8 cameras, which provide visual control. Devices with essential functions for satellite reception get their mains power from UPS-devices (UPS = Uninterruptable Power Supply), which ensure stable voltage conditions and provide power for some time (depending on battery status) in case of mains power outages.

5.2.1 Receiver systems

The ground station uses two CORTEX-RTR receiver systems (IN-SNEC 2006) with S-band frontends as main receivers, manufactured by IN-SNEC (a branch of Zodiac Aerospace, France). The receivers were installed in 2006 and 2007 and replaced older equipment[3]. Each of the two receivers (Figure 40) has the functionality of two independent telemetry receivers, with two radio signal input ports and two independent, yet combinable, demodulation chains. Usually each of the two internal receivers is connected with one of the antennas, which allows receiving of two satellites with same or different transmission parameters simultaneously. It also supports the reception of one satellite with two antennas in a combined mode or a diversity mode. The combined mode can improve the signal to noise ratio as two antennas, in principle, pick up more transmission energy than one antenna. However, a constructive signal combination (summation) requires a compensation of the continuously changing phasing between the two antenna signals, which can fail in some cases (error probability increases, e.g., with increasing phasing and data rates). The diversity mode also uses two antenna signals for the reception of one satellite. In this mode the receiver compares the quality of both received signals and takes the better for demodulation and data output. The two signals to be compared can be provided by two antennas (antenna diversity) or by a special feed at one antenna, e.g., one RHCP- and one LHCP-signal (polarisation diversity).

Figure 40: Front panel of CORTEX RTR receiver at NYA

[3] A third CORTEX-RTR was installed as backup in summer 2017.

Both CORTEX-RTR main receivers are operated in parallel, so that in total 4 independent receiver chains are operated hot redundant. Two PC-servers are also operated in parallel and care for the setting of the receiver operation parameters (according to the tracking schedules in jobfiles, see section 5.5) and the local storage of the receiver's data output (satellite data). Communication between the CORTEX-RTR receivers and the control PCs is established via Ethernet.

Another S-band receiver (manufactured by STT GmbH, Munich) and a spectrum analyser can be used for occasional testing or independent monitoring activities. Different signal routings between the antennas, receivers and devices for testing are user-selectable through a dedicated RF signal distribution system, which can be controlled locally or remotely through a web-interface or by a program.

5.2.2 Antenna 1 (NYA-1)

The first antenna at Ny-Ålesund (Figure 41) was purchased in the early 1990s from a company in the USA (Scientific Atlanta 1996 b). Previously to the installation at Ny-Ålesund in 2001 the antenna was used for the reception of SAR-data in the X-band, as the so-called "DLR-GFZ Mobile Antenna Unit". Later, after installation of a second antenna system at Ny-Ålesund, it was named NYA-1.

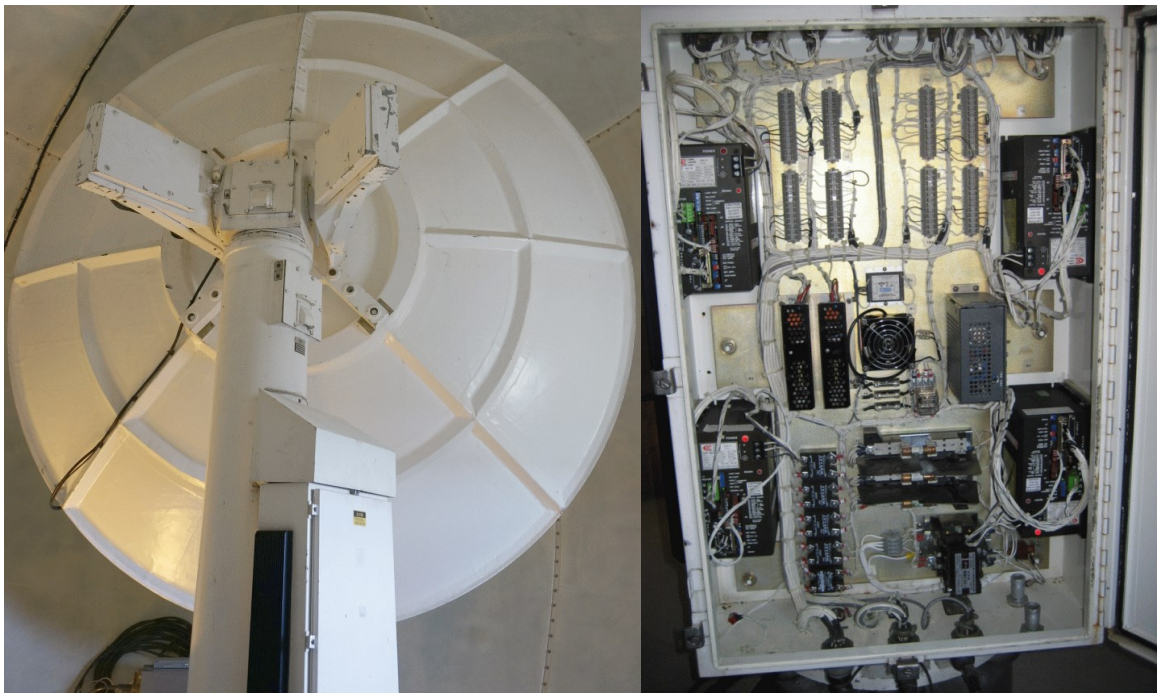

Figure 41: NYA-1 antenna system and drive electronics cabinet

The X-band specific antenna feed and LNA of the antenna system were exchanged by DLR against corresponding parts for the S-band, because CHAMP, the first satellite to be received at the station, was using an S-band communication system. The X-band related parts and other devices of the former Mobile Antenna Unit (e.g., receiver, synchroniser, tape recorder and archive etc.) remained at DLR (Oberpfaffenhofen) and the modified antenna system was sent to Spitsbergen. The new S-band feed (for RHCP only) was selected carefully by DLR for an adequate illumination of the antenna reflector. The LNA in this initial configuration was taken from a damaged and discarded ground station antenna as used in the PRARE project (Falck, Flechtner, et al. 2013). A second LNA (initially also “type PRARE”) was used as an intermediate preamplifier (Figure 31, dashed line box in signal path). It was placed at the antenna pedestal, connected to the LNA (at the feed) with a coaxial cable (5-6 m long), and provided a higher signal level to equalize subsequent losses in the long coaxial cable to the operation cabin (about 35 m) and further equipment such as power dividers and relays. The PRARE-LNAs had a rather high noise figure and were replaced by newer LNAs two times later. The intermediate preamplifier was removed completely in November 2016 when it was identified to be connected with receiving problems (section 9.4), while the increased gain of the new first LNA made it obsolete also.

NYA-1 has an elevation over azimuth positioning system, which means that an axis for elevation positioning is installed above an axis for azimuth positioning. The nominal range for antenna movements is limited to 720° on the azimuth axis (addressed as two sectors [0, 1] of 360° each) and 0-90° on the elevation axis. The mechanical limits of the axes are some degrees outside the nominal ranges and protected by electrical switches, which provide a stop signal when the antenna movement exceeds the nominal range by some degrees. The stop signals for the azimuth axis are triggered when the nominal 720° range is exceeded by approximately 15°. The maximum antenna system axes speeds are high (up to 20°/s), but this can still be too slow for a continuous tracking of very high elevation satellite passes due to the arrangement of the axes (explained in section 4.6).

Control access to the NYA-1 antenna must be established through an ACU (Antenna Control Unit). The ACU is an interface that mediates between user commands, which are either received from a connected computer or the built in keyboard, and the antenna drive electronics. Positions are adjusted with an ACU-internal loop procedure by comparison of actual (feedback from resolvers) and desired positions (commands).

Figure 42: Antenna control unit (ACU) for NYA-1 antenna system

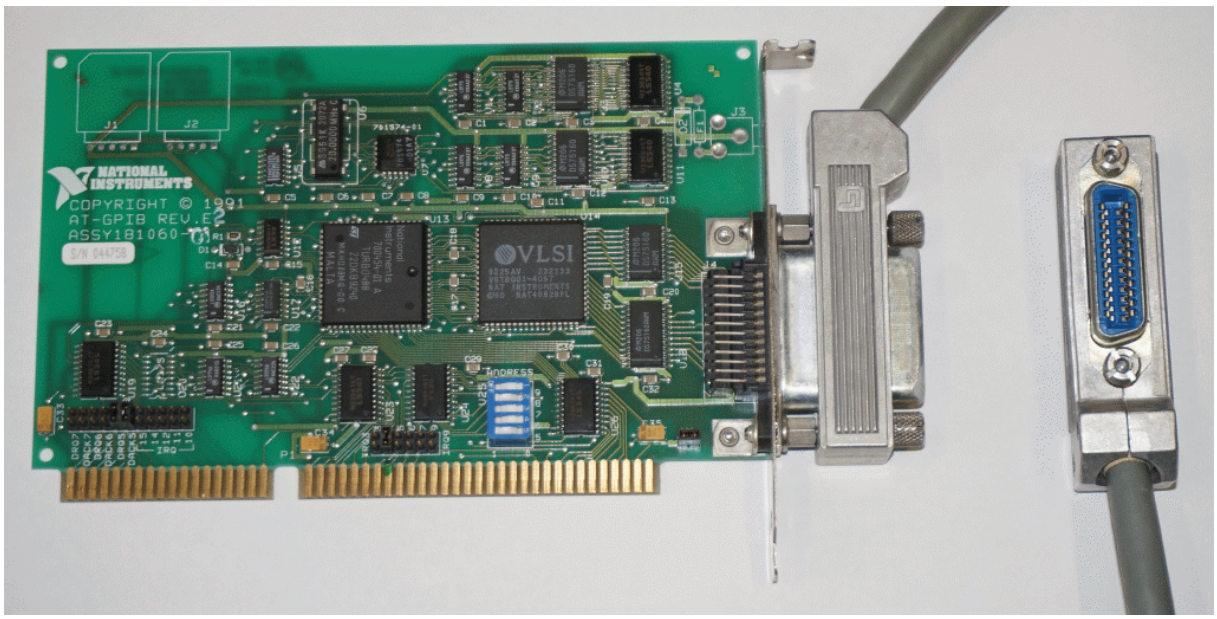

Figure 43: IEEE-488 board for PC ISA-slot with interface cable

The ACU for NYA-1 is a Scientific Atlanta Series 3860 Digital Controller (Scientific Atlanta 1996 a) as shown in Figure 42, which connects to computers via an IEEE-488 standard interface. This standard is also known as GPIB (General Purpose Interface Bus) or HP-IB (Hewlett-Packard Interface Bus) and has been used widely and for decades in connection with scientific instruments. An IEEE-488 computer interface board (Figure 43), which is not a standard component in common computer layouts, must thus be operated by an appropriate antenna operation computer. The ACU is designed for operation in a warm and dry place and

was thus installed in the station operation cabin. A number of cables connect the ACU with the antenna drive electronics cabinet at the antenna pedestal (Figure 41) over a distance of about 35 m.

The antenna boresight offset of NYA-1 was determined at the time of installation. However, the determination process was not witnessed by or reported to GFZ and thus the quality of the resulting calibration could not be assessed.

5.2.3 Antenna 2 (NYA-2)

In 2005 GFZ installed a second antenna system at Ny-Ålesund (Figure 44), together with the antenna manufacturer (CGC Technology Ltd, England). The antenna has an "X over Y" positioning system and was named NYA-2. It is equipped with a dual polarisation (RHCP and LHCP), dual frequency feed (S- and X-band) and protected by a radome. The two LNAs at the antenna feed (at time of initial installation), as well as two intermediate preamplifiers (Figure 31, dashed line box in signal path) were ordered by GFZ from another supplier. The intermediate preamplifiers were removed in November 2016 as they were identified to be connected with receiving problems (section 9.4), while the higher gain of the new first LNAs made them obsolete anyway.

The NYA-2 antenna system does not use a dedicated external ACU comparable to the ACU as for NYA-1 operation. A so-called motion controller of the type "Baldor NextMove BX" is used instead as an interface between antenna motor electronics and an antenna operation computer. The motion controller is integrated in the servo control cabinet, located directly at the antenna pedestal, and does not allow direct operator interactions as it has neither manual controls nor a display. It is connected to the antenna operation computer in the station's operation cabin via a 35 m long RS-422 standard serial communication cable with interface converters to the RS-232 standard at both cable ends. Apparently there are no resolvers on the axes to provide position feedback to the motion controller. Actual directions are thus, most probably, calculated internally from feedback of the pedestal motors. A somehow advantageous feature of NYA-2 (e.g., over NYA-1) is an electronic clinometer, which is installed at the antenna mount mechanical interface. It is used for the determination of the antenna (mount) zenith direction with high precision (resolution 0.002°, repeatability 0.01°). The motion controller can be commanded to direct the antenna to zenith, controlled by the

clinometer, and to calibrate the axes zero points accordingly, which eliminates the effect of a possible tilted pedestal, e.g., from an imperfect installation.

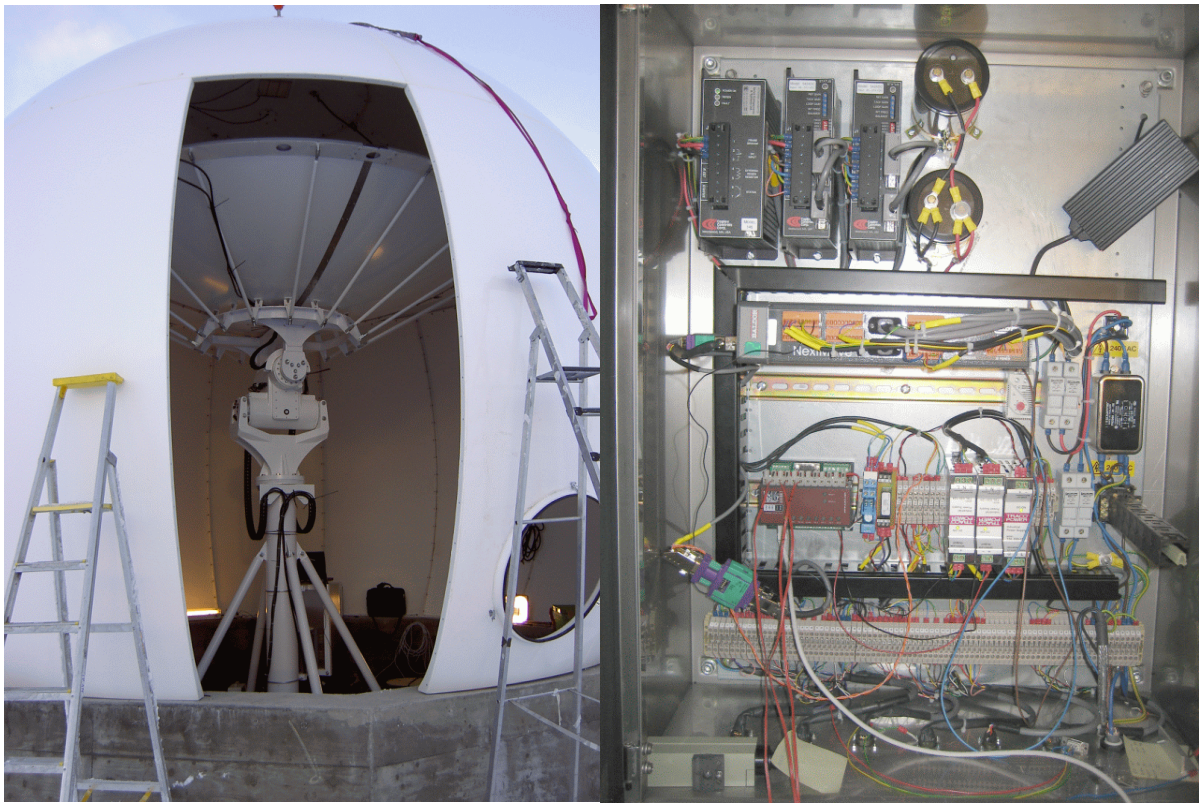

Figure 44: NYA-2 antenna system and servo control cabinet

Before installation at Ny-Ålesund the complete antenna system was tested at the manufacturer's facilities (factory acceptance test). Some technical problems occurred during these tests and also in the first months after installation at Ny-Ålesund. These problems caused at least two serious mechanical crashes between the antenna reflector and the antenna pedestal. The reasons for these accidents were identified and removed by the manufacturer. Questions about the degree of remaining antenna reflector damages (deformations) were discussed, but not answered with final certainty. Consequently it was not unlikely that the antenna reflector performance and thus the total system performance could be reduced.

The experimental determination of NYA-2 boresight offsets by the antenna manufacturer was observed by the author at the time of installation and some doubts about the accuracy arose. The antenna was pointed to the sun and the shadow of the antenna feed on the antenna reflector was observed. The antenna feed was checked to be mounted exactly in the normal direction of the antenna reflector midpoint and the degree of coincidence between the feed's

shadow and the midpoint of the antenna reflector was used as an indicator for the antenna system pointing error. The measurements with NYA-2 were performed in October 2005 with diffuse sunlight (fog and clouds) at small elevation angles to the sun, which was only slightly above the local horizon. These were considerably adverse conditions for the experiment and in consequence the shadow of the feed on the antenna reflector was more a subject to make a guess than a clear and reliable indicator. The experiments were made just before the radome installation was finished, so that the antenna was optically screened afterwards.

5.3 Calculation of receiving system *G/T* performance

G/T measurements are the best way to determine the RF-related performance of antenna systems, which is a mandatory input for reliable calculations of link budgets (see section 4.4). The upcoming GRACE-FO mission required a minimum *G/T* performance from ground stations of 17 dB/K at 5° elevation and it was not clear if or how the NYA station could fulfil that requirement. An Excel-sheet was developed to calculate the theoretical and thus expectable performance of the antennas at Ny-Ålesund. It addresses all relevant parameters as discussed in section 4.5 and can thus be regarded as a kind of antenna model. The parameters are sorted to groups and provide a direct indication of intermediate and final results according to the changeable input parameters.

Antenna Gain [dB]				
	Input	**Comment**	**Intermediate**	**Result**
Antenna diameter [m]	4,0	NYA-1		
Antenna reflector efficiency [%]	55	typical value		
Operating frequency [MHz]	2250	typical, S-band		
Theoretical antenna gain [dB]		equation (21)	36,89	
Antenna 3dB beam width [degree]		equation (1)	2,33	
Antenna-pointing accuracy [degree]	0,1	estimated		
Antenna-pointing loss [dB]		equation (2)	0,02	
Radome loss dry [dB]	0,3	specification		
Radome loss wet (additional to dry) [dB]	0,15	spec. for 25 mm/hr		
Radom loss total [dB]		sum dry + wet loss	0,45	
Feed loss (connection to LNA) [dB]	0,05	direct, no cable		
Feed SWR [ ] 1:	1,2	specification		
Feed SWR loss (mismatch to LNA) [dB]		equation (24)	0,04	
Effective antenna gain G [dB]		theor. gain - losses		36,33

Table 2: Excel sheet for calculation of antenna gain

Table 2 lists several parameters, which have an effect on the antenna gain up to the input port of a connected LNA. All parameter effects are given in dB directly or converted to dB, which eases calculations. The headline “Antenna gain” corresponds not only to the gain of the antenna, but also to certain losses, which reduce it to an “effective antenna gain”. The given numbers refer to the NYA-1 antenna with a reflector diameter of 4 m at an operation frequency of 2250 MHz, which is the approximate mean value for the downlink frequencies of the satellites that are currently received at NYA.

The NYA-1 antenna reflector efficiency was not known and thus a typical mean value of 55% (Dietrich and Davies 1999) was used. The theoretical antenna gain and the antenna half power beam width were calculated with equation (21) and equation (1). The specification of the Scientific Atlanta antenna lists a half power beam width of 0.6° for an operation frequency of 8.4 GHz, which was the antenna’s nominal operation frequency before it was modified for the S-band. A calculation of the half power beam width with equation (1) at a frequency of 8.4 GHz results in 0.625°. This is in good agreement with the manufacturer’s number and thus confirms that this “rule of thumb” equation is applicable with the antenna as done here for the S-band. The pointing loss was estimated with equation (2), based on an assumed pointing inaccuracy of 0.1° and the calculated antenna half power beam width (equation (1)).

Additional losses to be considered arise from the radome as it attenuates RF-signals, even more when it is wet, which was addressed also. Corresponding values for the losses were found in the radome specification. The loss due to the coaxial connection between the antenna feed and a LNA is derived from the ohmic loss and the impedance mismatch (SWR), both according to component specifications. Additional loss from a possible feed spill-over or otherwise imperfect reflector illumination was not considered. Information about the beam pattern of the feed was not available, but according to personal communication with DLR-staff it was assumed that the used feed was selected very carefully at the time of antenna system conversion to S-band operation (5.2.2). This might justifies the neglecting of corresponding losses.

Receiving system performance in terms of G/T is affected by the antenna gain (Table 2) and the system noise, which results from noise contributions of several sources (4.5). The RF signals received by an antenna must be fed to the receiver and some noise is added on that path. The total receiver noise according to all considered components as listed in Table 3 was calculated with Friis formula (equation (28)).

Receiver noise [K]				
	Input	Comment	Intermediate	Result
LNA noise figure [dB]	0,39	spec. maximum		
LNA noise contribution (T_1) at 290 K [K]		equation (32)	27,25	
LNA gain [dB]	58	spec.: 60 +/- 2		
LNA gain factor (G_1) [ ]		equation (33)	630957	
Loss of cables and connectors behind LNA [dB]	20	specs., incl. splitter		
Gain factor cables + con. behind LNA loss [ ]		equation (33)	0,01	
Noise temp. cab. + con. b. LNA (T_2) at 290 K [K]		equation (32)	28710	
Noise contribution of cab. + con. b. LNA [K]		T_2/G_1	0,05	
Receiver noise figure [dB]	8	spec. CORTEX RTR		
Noise temperature of receiver (T_3) at 290 K [K]		equation (32)	1540	
Noise contribution of receiver [K]		T_3/G_1*G_2	0,244	
Sum of noise contributions behind LNA [K]		cab. + conn. + rec.	0,29	
Receiver noise total [K]		sum contributions equation (28)		27,54

Table 3: Calculation of receiver noise

The parameter input values in Table 3 were taken from specifications (e.g., data sheets) of components used with NYA-1 and reflect the status since November 2016, after the removal of the previously used intermediate preamplifier, which was identified to contribute to receiving problems (section 9.4). It is evident that the total receiver noise is mainly determined by the properties of the LNA, which should have a low noise figure (noise generated by the LNA). But not only the LNA noise figure is of high importance, also the LNA gain helps to keep the system noise low. A high LNA gain maintains a high initial signal to noise level and partly compensates the losses of subsequent components in the signal chain, e.g., from coax cables, power splitters for signal distribution and the telemetry receiver.

More contributions to the system noise are shown in Table 4. These have different origins, but are summarised as antenna noise components, because they are received or even generated by the antenna. All antenna noise sources, except of the sky noise, are treated as independent from antenna elevations. This might not be fully correct for all sources, e.g., for man-made noise, which is usually expected to have an origin on the ground, e.g., in the village of Ny-Ålesund. However, this worst-case approach seems to be common praxis and was considered the same way in related ITU recommendations (ITU Radiocommunication Assembly 2015 a), which were also used to assess the effect of the other noise sources in Table 4.

Antenna noise				
Not elevation dependant	**Input**	**Comment**	**Intermediate**	**Result**
Radome noise temperature [K]	7	specification		
Man made noise [K]	5	radio silent area		
Galactic noise [K]	0	ITU		
Cosmic noise (black body) [K]	2.7	ITU		
Rain noise [K]	2	ITU: 50mm/hr 5km		
Atmospheric noise [K]	0	n.a. @2250 MHz		
loss connection antenna to LNA [dB]	0.05	spec., direct, no cable		
noise connection antenna to LNA [K]		equation (32)	3.36	
Mean effective side lobes level [dB]	-50	estimated		
Ground noise (antenna side lobes) [K]		equation (27)	17.26	
Sum (non elevation dependant) [K]			37.32	
elevation dependant		add non el. dep. to el. dep.		
Sky noise @ 0 degree elevation [K]	80		117.32	115.97
Sky noise @ 5 degree elevation [K]	20		57.32	56.66
Sky noise @ 10 degree elevation [K]	12	ITU recommendation	49.32	48.75
Sky noise @ 20 degree elevation [K]	6	(ITU-R P.372-8)	43.32	42.82
Sky noise @ 30 degree elevation [K]	4	at f=2250 MHz	41.32	40.84
Sky noise @ 60 degree elevation [K]	2.5		39.82	39.36
Sky noise @ 90 degree elevation [K]	2		39.32	38.87
			apply loss	
			factor	
loss factor conn. antenna to LNA [ ]		equation (33), loss = 0.05 dB	0.9886	

Table 4: Calculation of antenna noise

The value of man-made noise was chosen lower (5 K) than recommended for a "*median business area*" (~ 15 K by ITU). This seems to be reasonable, because Ny-Ålesund is a very secluded village with small population and declared as a radio silent region (20 km radius around village). Diagrams for the directivity of both antennas at NYA, especially about the effect of side lobes, were not available. The effect of noise that is received through antenna side lobes (-50 dB) was estimated on basis of published directivity diagrams, such as Figure 27 a, and equation (27). This is the weakest point of the antenna model as an also thinkable mean side lobe gain level of, e.g., -45 dB would result in a significant higher noise contribution of 54.57 K (instead of 17.26 K at -50 dB).

Another significant contribution to the antenna noise is the sky noise, which is elevation-dependant as it depends mainly on atmospheric parameters. The used sky noise temperatures

for different elevations in Table 4 were picked from a graphic of "*sky brightness temperatures*" in a corresponding ITU publication, related to radio noise (ITU Radiocommunication Assembly 2015 a). The values are based, according to the document, on calculations with a "*…radiative transfer program…*" for *"…an average atmosphere (7.5 g surface water vapour density, surface temperature of 288 K, and a scale height of 2 km for water vapour…)*", the "*…1976 United States Standard Atmosphere… for the dry atmosphere…*" and "*…a typical water vapour contribution…above the tropopause*". The model description lists many assessed parameters and thus implies a certain degree of model uncertainty, but is generally accepted as the standard model for this type of radio noise. The connection between the antenna and the LNA has a certain loss, which has a notable effect, even if the loss is very small. It reduces the antenna noise on the way to the input port of the LNA (application of a corresponding loss factor), which could be considered to be a positive effect. On the other hand it is a component with own noise contribution (3.36 K).

Table 5 shows the final calculations to derive the modelled, respectively expectable *G/T* performance of the NYA-1 antenna. The system noise (sum of receiver and antenna noise) is listed for different elevations in the unit Kelvin and in the unit dB (conversion with equation (42)), to allow the calculation of *G/T* (usually specified for El=5°) according to equation (20).

$$T_{system\ noise\ [dB]} = 10\log(T_{system\ noise\ [K]}) \tag{42}$$

G/T at particular elevations [dB/K]				
	elevation	System noise		G/T @ elevation
	[deg]	[K]	[dB]	[dB/K]
System noise = Antenna noise + Receiver noise	0	146,87	21,67	14,66
	5	84,20	19,25	**17,08**
Conversion $T_{[K]}$ => $T_{[dB]}$ with equation (42)	10	76,29	18,82	17,51
	20	70,36	18,47	17,86
G/T = Antenna gain [dB] - System noise [dB]	30	68,38	18,35	17,98
(Antenna gain = 36,33 dB)	60	66,90	18,25	18,08
	90	66,40	18,22	18,11

Table 5: Calculation of antenna G/T

The discussions and calculations above show that the *G/T* is mainly determined by the antenna gain (size) and the noise temperature (noise figure) and gain of the LNA. Other system components have either only small impacts or cannot be influenced by engineering measures (e.g., sky noise). For a given antenna system, especially when it is installed under an

antenna-size-limiting radome, it is only the LNA parameters that give room for a significant improvement of the *G/T*. This conclusion is true if the connection between antenna and LNA already has a very low loss, e.g., due to a direct connection (no cable), which is the case at NYA. A significant reduction of the *G/T* performance can result from additional losses between the antenna and the LNA, even if the absolute numbers of these losses appear to be still low. Such additional losses can be caused by a cable or waveguide or, which is the case at most satellite ground stations, a bandpass filter and / or a diplexer, such as shown in Figure 31. The latter are often used to reduce disturbing effects on the reception from signals, which are close to the antenna receiving frequencies (e.g., 2.4 GHz WLAN), and to feed an uplink signal into the antenna (from a local transmitter) with a diplexer, which is a special frequency- or direction-selective device (e.g., network of bandpass filters and / or circulator). The replacement of the low connection loss of 0.05 dB in Table 2 and Table 4 by a hypothetical value of 0.5 dB, according to a realistic level of insertion loss for filters or diplexers, just as an example, would reduce the system performance of the NYA-1 antenna at 5° elevation and 2250 MHz from 17.08 *dB/K* to 15.58 *dB/K*. However, filters are not required at NYA and an uplink is not installed, both due to the local radio silence regulations. This explains the relatively high *G/T* performance numbers of the antennas at NYA with reflector sizes of 4 m and 4.2 m only. A comparable *G/T* performance (~17 *dB/K* for S-band) at an installation with uplink capacities usually requires larger reflectors, e.g., such as used with the 7.3 m S-band antennas at the ground station Neustrelitz.

The first S-band LNA of the NYA-1 antenna, which was installed at the NYA-1 antenna by DLR had a noise figure of 1.7 dB, equivalent to 138 K. That LNA was a reused part from a former PRARE antenna with a design and semi-conductors from the mid 80's, which explains the now outdated high noise figure. Later GFZ replaced the PRARE-LNA by a LNA with a noise figure of 0.6 dB, equivalent to 43 K, which was a significant system improvement. The reason was that the same up to date type LNA (at that time) was purchased for the new installed antenna NYA-2, rather than demands to fulfill certain requirements. Both antennas were using this LNA type since 2005.

It was the proposed use of NYA as primary downlink station for the GRACE-FO mission that required the careful assessment of *G/T* values as done in this work. One of the mission's requirements for ground stations of the GRACE-FO ground segment was to provide a *G/T* performance of 17 *dB/K* at 5° elevation. Calculations as described in section 4.5 and executed

as shown above revealed that the expectable *G/T* performance of the both NYA antennas with the currently (before August 2014) used LNAs (*NF* = 0.6 dB) was clearly below 16 *dB/K* at 5° elevation. It was also concluded that a sufficient performance was reachable with a LNA noise figure of 0.4 dB (or less) and a LNA gain of more than 50 dB. This was an important result of this work at an early point and new LNAs with sufficient performance figures were purchased and installed by the author at Ny-Ålesund in August 2014.

5.4 Time keeping at the station

The positioning of antennas for the tracking of LEO satellites requires a certain timing accuracy as positioning timing errors affect the satellite tracking accuracy (4.6, 6.2). Positioning commands for the antennas at NYA are generated and issued by antenna operation software that runs on regular computer systems. The antenna operation software timing relies on the computers system time, which is a software function of the computer operating system. The system time is synchronised with a computer-internal so-called real-time clock (hardware function), e.g., at system boot time, which is thus the basic time reference for all executed processes (programs). The short-term accuracy of the system time (and real-time clocks) within some minutes is usually sufficient for the positioning of satellite tracking antennas. However, system time and real-time clock errors can accumulate up to several seconds per day. Thus, for the operation of antenna operation software, it is necessary to control the system time frequently and to correct it as soon as too high deviations are detected. This task requires an external time reference with a higher accuracy than the system time.

There is no atomic or other high performance time reference on-site at the satellite-receiving station Ny-Ålesund that could be used to control the computers and other system clocks. The accuracy of time information from remote NTP-servers (Network Time Protocol) is certainly better than one second in general, but it was observed that there can be unacceptable high variations in the sub-second range (some tenths of a second). Time maintenance by remote NTP-servers also requires stabile Internet connections, which might be not given at all times, either due to local or remote technical problems. Appropriate sources for time information are GPS-receivers, which were already in use since the installation of the first antenna at NYA. Even low cost models usually provide an accuracy of better than 1 ms, which is fully sufficient for the correction of real-time clocks in antenna steering computers (discussion in section 6.2).

A first GPS-based time keeping system was operated in the antenna steering computer for NYA-1 as an integrated device (ISA-standard extension-board). The hard- and software components were parts of a commercial product from the company “hopf”. The antenna steering computer for NYA-2 was delivered with an own GPS-controlled time synchronisation system. The package contained a regular GPS receiver from the company GARMIN and software from the antenna manufacturer CGC. All other devices at the station with internal clocks are synchronised with a locally installed NTP time server. It is connected with a third GPS receiver and can serve also as a backup time reference for the antenna operation systems, but with lower accuracy than the PC-internal GPS-based time systems.

5.5 Routine station operation

The routine operation of the satellite-receiving station at Ny-Ålesund is based on automatic procedures and conducted unmanned respectively without local supervision. It is controlled and monitored remotely by GFZ using special remote monitoring and control devices, such as cameras and remote management computer cards. Staff from the local German-French AWIPEV polar research station and the local Kings Bay Company occasionally gives support in case of problems that cannot be solved from remote.

All satellite passes to be tracked at NYA are scheduled by GFZ staff in Oberpfaffenhofen, Germany. The DLR-site Oberpfaffenhofen hosts several facilities such as the German Space Operation Center (GSOC) with several satellite operation control rooms, and a subsidiary of GFZ (currently about 18 staff members). The presence of GFZ in Oberpfaffenhofen supports a close procedural relationship to the executing satellite operators for GRACE, TerraSAR-X and TanDEM-X (formerly also CHAMP), as these missions are operated by GSOC. The satellite transmissions are time tagged and must be synchronised to the NYA receiving times schedules. One so called “jobfile”, which is the GFZ term for a NYA satellite-receiving schedule, is prepared for each of the two antennas[4]. Also the receiver systems at NYA are configured automatically (e.g., setting of frequencies) according to the jobfile entries.

The practically available time for an individual satellite contact results from the satellite orbit parameter and the local horizon mask and is about 5 minutes for the GRACE satellites. Usually many (up to 15) contacts per day are scheduled for each of the received satellites and

[4] A changeover to only one jobfile for both antennas is foreseen for late summer 2017.

the total contact time per day and satellite is higher than the required contact time for the download of all on-board data. Advantage is taken from this fact by a preferred allocation of contact times to time intervals with high elevations, respectively smaller distances to the satellites, and thus potentially higher signal levels, due to less free space propagation loss.

The jobfiles are usually generated 3 days before becoming valid and cover an operation period of one week. After generation by GFZ in Oberpfaffenhofen the jobfiles are sent to GFZ at Potsdam from where they are forwarded to the ground station at Ny-Ålesund automatically. A similar procedure applies for twoline elements, which are used at the station for the prediction of satellite directions. The twoline elements are generated from satellite orbit determinations and predictions, usually either by GFZ or DLR (GSOC). They are sent to the station between 2 and 4 times per day and in one file for all satellites to be tracked. However, not all twoline elements in the file are necessarily updated with the same frequency. Data received at the station is automatically sent to GFZ at Potsdam, where it is processed and / or distributed to other users.

All receiving activities at the station must be logged and the logfiles must be stored for at least 2 years, not only for statistics or troubleshooting, but also to fulfil the obligations of the receiving licences. The station logfiles and the compliance with all related regulations, especially the non-military use of the station, is controlled on-site twice per year by representatives of the Spitsbergen government, the Norwegian military and the Norwegian telecommunication regulation authorities.

5.6 Previously used antenna operation software

The software described in the two sections below was not developed by the author and not by GFZ, except of some small add-on programs for the operation of NYA-2 (automatic system updates with jobfiles and management of twoline element files). The described software packets were used for the two antennas at the satellite-receiving station Ny-Ålesund until summer 2014, when they were replaced by the new developed NYA-Sattrack software.

The descriptions of software designs, software properties and software operation performance are given for reference only and not to advertise or bad-mouth any developments of other parties. Details are thus limited to points that contributed to the lessons learned and that explain the motivation to develop a new software. It should also kept in mind that the

software described here (sections 5.6.1 and 5.6.2) was developed with partly different development backgrounds and 10 to 15 years earlier than NYA-Sattrack.

5.6.1 DLR-software for NYA-1 operation

The software for the operation of Antenna 1 was developed by DLR around the year 2000. It was a modification of software that was formerly used with the so called “Mobile Antenna Unit”, which was jointly owned and operated by GFZ and DLR for the reception of SAR-data from satellites like ERS-2. The antenna operation software was a package of several binaries (not human readable) and DOS scripts (human readable) to manage the interaction of the binaries.

Figure 45: GUI of DLR software for operation of NYA-1 antenna

The GUI of the DLR-software was realised as a DOS-like terminal window (Figure 45) and provided some essential information, e.g., about the next satellite contact, but only a few functions for antenna operations. GUI-selectable functions (to be accessed via keyboard function keys) were mainly residues from the time of SAR-data reception, e.g., for operation of data record tapes, and of no use for the antenna operation at Ny-Ålesund. In fact, it was not even possible to point the antenna manually to a certain direction. More drawbacks of the program were regular software crashes during turns of the year and that year numbers were

not included into logfile-names for tracked satellite passes, not even in a “two year digits” format. This regularly required manual action, e.g., renaming of files, to avoid ambiguities. The program did not generate a general program activity logfile, e.g., to list error messages, operation parameters or filenames according to actually used twoline elements or jobfile updates, which could have supported the frequently required troubleshooting and reestablishment of system operation a lot.

The program’s orbit prediction algorithm used twoline elements and apparently worked well in principle, but it was suspected that the program generated antenna direction files for all passes only once a week after receiving a jobfile, without updating them when new twoline elements were provided. One strong indication was good NYA-1 tracking performance (strong and stable satellite signals) at the beginning of a week and continuously decreasing performance towards the end of a week, while the NYA-2 antenna, operated with the same twoline elements but a different antenna operation software, showed a regular performance during all days of a week. Another indication was the timestamps and contents of the files with antenna direction commands, which remained unmodified through an operation week. For GFZ it was hardly possible to control or determine, which twoline element file from a number of files in a directory was actually used. No documentation or references for the implemented orbit prediction algorithm and the internal program logic were available, at least not for GFZ.

From time to time (mean period about 2 weeks) the NYA-1 antenna triggered one of the azimuth axis limit protection switches. The antenna movement stopped automatically to protect the mechanical limits (function of ACU) and the actual satellite pass and also subsequent satellite passes were either not tracked completely or not at all, resulting in loss of data. The antenna had to be moved back into the regular azimuth axis range, but there was no program function for that or any function for “manual” antenna movements at all. In the beginning (2001) the antenna was moved back by hand on interaction of staff from local partners (AWIPEV) and later by a procedure[5], involving several manual file edits and multiple program restarts. The program did not show whether the left or right limit switch was hit and not even the event itself, although all information was displayed by the ACU (LCD screen and LEDs in Figure 42). Thus, the detection of limit switch events and the

[5] The procedure had to be performed by DLR for several years, as its details were not disclosed to GFZ.

corresponding directions was only possible through an Internet camera, which was installed in front of the ACU.

A software patch by DLR reduced the number of accidental stop events, compared to the first years of operation, but did not solve the problem completely. The software patch strategy was apparently (author interpretation from observed antenna movements) to move the antenna back to the start position of a finished pass and then to the mid of the total azimuth axis range (+/- 360°), before moving it to the start position of the next pass. This “limit switch avoidance patch” was a small improvement on the one hand, but increased the system wear and reduced the available operation time due to the extra movements on the other hand. Unfortunately the patch did also not work in all cases and so the antenna still had to be moved away from the azimuth axis limits manually many times. The reason for this system behaviour was not identified. However, main power outages during satellite tracking times had a high probability to induce this kind of malfunction, most probably when these hindered the execution of the movements as foreseen by the “limit switch avoidance patch”.

The DLR-software used a special device driver for the IEEE-488 interface board, which was necessary to communicate with the NYA-1 ACU. The driver was also a DLR or third party development and its function calls unknown to GFZ. Nonetheless the author tried to run the original DLR antenna operation software with the original driver software (binary) and the same type of interface board on a newer computer model, to solve at least the problem of the overaged hardware. These attempts did not succeed and thus the DLR-software, with all described handicaps, had to be operated on the original hardware (“Pentium 1” PC with IEEE-488 board in an ISA-slot) and Windows 98, until it was replaced by NYA-Sattrack and a modern computer (Core 2 Duo, Windows 7, USB to IEEE-488 converter).

5.6.2 CGC-software for NYA-2 operation

The CGC-software for the operation of Antenna 2 was installed on a PC running Windows XP and part of the manufacturer’s deliveries, when the antenna system was installed in 2005. The program packet was delivered to GFZ as executable binaries with some readable DOS scripts and included a good documentation (CGC Technology Ltd 2005). It had a lot of features that were accessible through a number of GUI views, which had a clear structure. The CGC-software was designed for a fully automatic antenna operation, including an automatic multi satellite contact scheduling function. Tracking schedules generated by the program were

stored in a file using a manufacturer defined, but simple and user-readable format (ASCII). The automatic antenna operation followed a tracking schedule until it expired after the last scheduled satellite contact. A new schedule could be generated automatically, if desired (configurable).

The automatic tracking schedule generation was an advanced feature but not compatible with the frequently changing demands from multi satellite operations in praxis. Especially the resolving of scheduling conflicts (two or more satellites appearing at the same time) usually requires several trade-offs or even discussions with other parties (e.g., satellite owner or operation agencies) and thus the automatic scheduling function of the CGC-program was never used. An alternative way of program steering was established through some small extra programs (programmed by the author). These generated a schedule file in the manufacturer format, based on the actual GFZ-jobfile information, and cared for the automatic update of twoline element files. This approach was discussed and tested with the manufacturer before purchasing the antenna system and proved to be stable in practice.

A good point of the CGC-software was seen in the logging features, which were very helpful for occasional troubleshooting. Separate logfiles for each satellite contact and 4 types of operation logfiles were generated. One logfile was for the scheduled tasks (e.g., program start times), one for “real-time” events (e.g., error messages), one for the automatic computer system time synchronisation with GPS (part of software package) and one for the automatic deletion of entries in all logfiles after a configurable time. A minor shortage was the logfile-format for tracked satellite passes. It contained several fields that were probably tailored to needs of other customers. These were not useable at NYA, but logged as comma separated empty entries anyway.

After installation at Ny-Ålesund the CGC-software had some problems in the first months, e.g., no correct detection and / or processing of axes limit protection switches and wrong readings from the system clinometer, which fulfilled an essential system function in connection with the CGC-software (detection of home position). These problems were solved and the system then showed a well and stabile performance over many years. However, the software license was limited to one computer only and guarded by an USB-dongle key. Thus a backup antenna operation computer for NYA-2 could not be prepared up to a fully operational state and would have required at least some local action to be activated. A

migration to newer computer operation environments appeared to be problematic (e.g., dongle software).

The regular antenna operation sequence for tracking of satellites, as defined through the manufacturer's software, included a stowing of the antenna in the home direction (zenith) after each finished satellite tracking. This is probably a good strategy to protect an antenna against strong winds. However, the CGC-antenna at Ny-Ålesund is installed under a radome and never exposed to winds. The frequent movements to the stowing position were thus considered to be not only unnecessary but also even unfavourable, as they cause additional load to the antenna-pointing system (motors, gear boxes). The movements also created extra waiting time before a next satellite could be tracked. The software had no user selectable option to omit the stow-positioning procedure and so the home-turns were running until 2014 (installation of NYA-Sattrack).

Another drawback was seen in the program GUI. The main GUI was well designed and informative (not shown here), but it could not be used in connection with the operation mode as described above (external generation of CGC-format schedule files). In consequence there was no GUI window displayed at all, except during the times of active satellite tracking. Thus there was no information on the screen about satellite passes to be tracked and not even a direct indication if the program was running properly.

Only a small GUI window (Figure 46) with basic information popped up during an actual satellite tracking and disappeared right after the contact. This point was discussed with the manufacturer as well as the not fully adequate pass logfile format and other small software issues. It turned out that the operation software was not an in-house development of the antenna manufacturer. Consequently, these issues could not be solved.

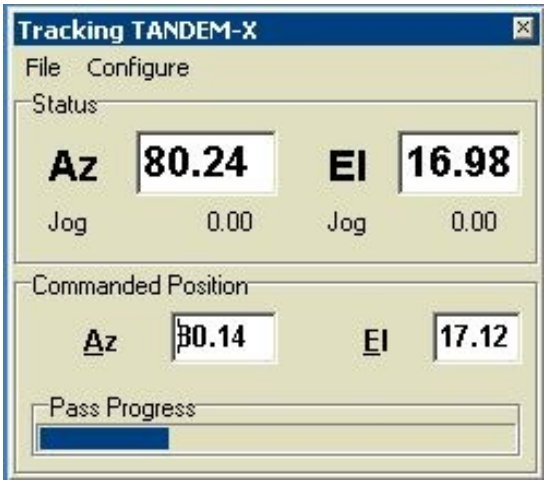

Figure 46: CGC-software "Tracking" window

5.7 Antenna performance before introduction of NYA-Sattrack

The performance of the NYA-1 antenna was tracked by DLR, mainly as a record of DLR's dedication to the NYA-1 operation and troubleshooting, from the time of antenna installation at Ny-Ålesund until October 2005. Figure 47 shows a graph of availability figures ("Verfügbarkeit" = availability) for the reception of the satellite CHAMP in terms of received contacts against scheduled contacts (more than 25000).

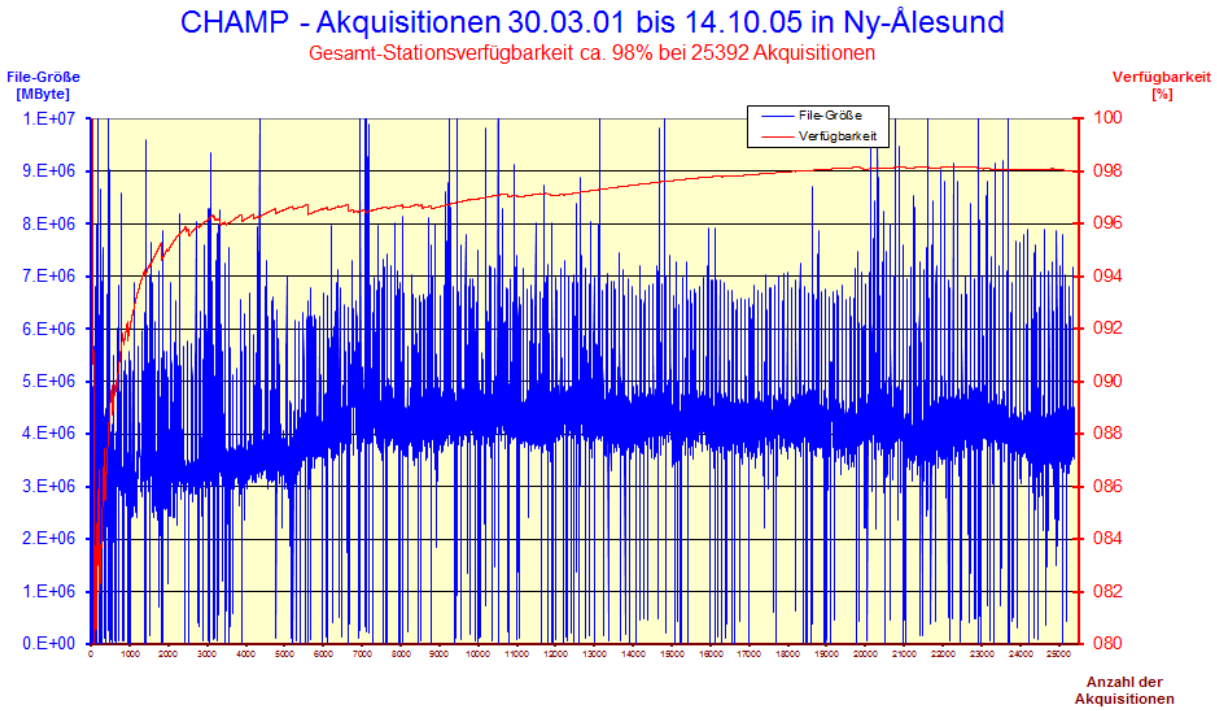

Figure 47: NYA-1 reliability between 2001 and 2005, as reported by DLR

Tracking statistics were calculated regularly and graphs like in Figure 47 were provided by DLR, e.g., for the regular GFZ-reports to the Ny-Ålesund Science Manager Committee (NYSMAC). The performance of NYA-1 increased, according to the graph, from an availability of 96% in 2001 to a more or less stabile level of 98% in 2005 (slightly decreasing at end of record). It is unknown to the author how the statistics considered incomplete contacts, e.g., due to axis stop events (5.6.1) or such that suffered from many crc-errors (partly data losses). As suggested by the figure's title the statistics were restricted to CHAMP only, which joined the highest attention and scheduling priority at that time. The values of the red graph were integrated over the time series and cover also the very first time of operation. Thus all numbers for later operation times suffered from initial operation problems, which are not really representative for the routine antenna operation reliability. Anyway, Figure 47 can

serve as a good estimation of the NYA-1 system reliability, also for other satellites and the following years, as the relevant system configuration and operation procedures were not changed until 2014 (installation of NYA-Sattrack). The main reasons for outages of NYA-1 were connected with the operation software and the described axis limit stop events. Other problems resulted from defects of the ACU. The gearing systems and cables never failed.

The performance of the NYA-2 antenna before 2014 has never been subject of dedicated statistics. There were initial operation problems similar to that with NYA-1, but then the performance was very good in general. Later comprehensive analyses were prevented from the loss of several logfiles due to PC hardware crashes. Especially the first years of operation could not be recovered anymore. However, the total system availability can be estimated to have been 99 %, at least in the last years before 2014 (before installation of NYA-Sattrack). Analysed problems were, with few exceptions only, not related to the manufacturer's antenna operation software, which thus might had a performance better than 99.5 %. Some problems were connected with power outages and communication failures between the antenna operation PC and the antenna ACU. These problems could often be verified by the software's logging functions, which was a big advantage for troubleshooting compared with NYA-1. Several times there were problems with the guiding of coaxial cables (e.g., damaged shielding) and at least one longer outage was due to some badly soldered connections in cable plugs. Most of these problems occurred in the first years of NYA-2 operation.

Both antenna systems, NYA-1 and NYA-2, suffered occasionally from wrong PC system clocks, which caused inaccurate antenna tracking with low signal to noise ratios and high numbers of crc errors.

6 Development of the new antenna operation software "NYA-Sattrack"

6.1 Design objectives for the new antenna operation software

The initial and main motivation for this work was to solve the problems encountered with the operation of the NYA-1 antenna system. Less urgent but also important, especially to increase the sustainability of the station, was the consideration of NYA-2 operation. Primary development targets thus were to increase the antenna operation reliability, particularly through analysis of monitored problems, to develop an informative GUI, to improve the logging capability of system activities (antenna and software) and to provide some advanced operation options, all with full control over the software code for both antennas. The new software also had to be compliant with previously used station operation interfaces and procedures as described in section 5.5 (e.g., jobfile concept). Some possibilities for extra program features were recognised and defined as additional objectives during the time of program development. Among them were the skyplot display (visualisation of satellite tracks etc.) and special tracking functions (sun-tracking, square-, stripe- and horizon-scans).

A program-internal remote control interface, e.g., through a web-interface, was not foreseen. All computers at the receiving station provide access through different kinds of remote desktop functions (software and hardware solutions), so that an informative but not overloaded program GUI with keyboard and mouse interface (buttons) was assessed to support remote monitoring and control sufficiently. The following chapters show the manifold aspects related to program functions, accuracies, program flow and constraints, which were considered for the software development.

6.2 Discussion of antenna-pointing accuracy

Beside software functional design and operation demands it was also considered to which extend antenna-pointing accuracy must be maintained within the antenna operation software. Software induced uncertainties can result from numerical effects, such as known from trigonometric functions, or due to limited resolution of used variables and deliberately implemented truncations. Another critical point is the punctual execution of antenna-pointing commands. Either the computer system time or the program flow or even both can be timely imprecise. Also the related hardware (e.g., interfaces) may introduce command execution delays to be considered and compensated by the operation software.

An arbitrary high accuracy could be demanded from antenna operation software in principle. However, in praxis this could not become effective without substantial effort, e.g., by engagement of a real-time computer operation system and an atomic clock, while both may not be required. It thus makes sense to apply a reasonable scale for software requirements, e.g., such that is based on technical qualities and typical tracking requirements.

There seems to be no real standard or natural derivation for a requirement regarding the angular and timely precision of antenna operation software. A hint to a kind of standard for the total pointing accuracy of tracking systems is given in an engineering handbook (Williams 2013), where it is stated for Earth station antenna tracking systems that the *"Tracking error is usually specified to be less than 0.1 of the HPBW"* (10 % of half power beam width). The HPBW Θ of a 4 m antenna (NYA-1) at 2250 MHz is about 2.33° (equation (1)) and thus a corresponding total antenna-related tracking error of 0.233° might be acceptable for that antenna.

The precision of antenna operation software is only one factor that contributes to the total antenna system accuracy and must thus be small against it. On the other side it can be assumed that the contributions of all other antenna-related error sources are also small. The highest error contributions must be expected from boresight errors and pedestal installation errors, even when these were determined (9.1). The remaining errors of these sources after correction or compensation are difficult to assess, but should be not higher than 0.05° in total. More but minor contributions result from lost motion in the antenna drive gear and the resolution of pointing commands. The maximum values for theses parameters, according to the system specifications, are 0° and 0.00549° for NYA-1 and 0.035° and 0.00004° for NYA-2. Thus, it appears reasonable that the not software-related errors are smaller than 0.09° (NYA-1: 0.05° + 0° + 0.00549° = 0.05549°; NYA-2: 0.05° + 0.035° + 0.00004° = 0.08504°) for both NYA-antennas. In consequence this allows a software-related error (sum of numerical and timing errors) of about 0.14°, without violation of the *"0.1 of the HPBW"* criterion (0.233° > 0.09° + 0.14°).

Table 6 compares the antenna gain reduction that results from antenna-pointing errors with the effects of other sources for antenna performance reduction. It also gives some examples for the effects of timing errors, which were converted to equivalent pointing errors first (equation (35)). The losses from pointing errors were calculated with equation (2) for Θ=2.33°.

Source of loss or attenuation			Equivalent loss of gain [dB]
Attenuation from dry radome (NYA-1 radome specification): 0.3 dB			0.3
Additional attenuation from water on radome (NYA-1 radome specification): 0.15 dB			0.15
Direct RF-connection between antenna feed and LNA (no cable, according to specification of high-grade N-type connectors): 0.05 dB			0.05
Impedance mismatch between antenna feed and LNA (equation (24) with SWR = 1:1.2)			0.036
Inaccuracy of twoline elements (depending, e.g., on its age and the orbit prediction quality) resulting in antenna-pointing errors: 1° and more			2.21 for the first degree
Antenna-pointing error from lost motion in antenna drive gear boxes, according to NYA-1 specification: 0.0°			0.0
Antenna-pointing error from lost motion in antenna drive gear boxes, according to NYA-2 specification: 0.035°			0.0027
Resolution of antenna-pointing commands, smallest bit NYA-1, smallest step NYA-2		0.00549° (NYA-1)	0.000066
		0.00004° (NYA-2)	0.0000000035
Antenna-pointing error (e.g., induced by antenna operation program through uncertainties in calculations, value truncations etc.)		0.5°	0.5526
		0.2°	0.0884
		0.1°	0.0221
		0.01°	0.000221
Timing errors, e.g., caused by PC system-time clock, program or antenna system; corresponding pointing errors assessed with equation (35), resulting losses assessed with equation (2)	satellite in 350 km altitude passes the antenna in zenith (distance = 350 km)	1 s => 1.26 °	3.5
		0.1 s => 0.126 °	0.035
		0.05 s => 0.063 °	0.00877
		0.01 s => 0.0126 °	0.00035
		0.001 s => 0.00126 °	0.0000035
	satellite in 350 km altitude passes antenna with culmination of 5° (distance = 2211 km)	1 s => 0.2 °	0.0884
		0.1 s => 0.02 °	0.00084
		0.05 s => 0.01 °	0.000221
		0.01 s => 0.002 °	0.00000884
		0.001 s => 0.0002 °	0.0000000884

Table 6: Some sources of losses and attenuation

The allowed total software-related uncertainty of 0.14° was distributed to a direct pointing accuracy of 0.1° and a timing precision of 0.05 s. The latter translates to a pointing error of 0.01° for a satellite at 5° elevation and 0.063° for a satellite in zenith (350 km altitude, Table 6). The total pointing error would then be between 0.11° at 5° elevation and 0.163° at zenith, which is 0.023° higher (at zenith) than 0.14°, as required to fulfil the *"0.1 of HPBW"* criterion. However, this was accepted because the corresponding antenna gain reduction is very small (effect of 0.02° error = 0.0884 dB) and more than compensated by the reduction of free propagation loss due to the smaller distance to the satellite at high elevations (Figure 29, equation (17)). The total effect of gain reduction from 0.1° pointing error and 0.05 s timing error is 0.0221 dB + 0.00877 dB = 0.03087 dB (Table 6). This is about 1% of typical minimum link margins (3 dB), which can serve here as a reference with respect to commonly found mission requirements.

The calculations above considered worst cases, respectively the simultaneous occurrence of maximum errors for all individual parameter. This approach appears to be justified to derive engineering design targets, but the mean in praxis errors are smaller of course. An estimation of the practically met mean errors can be derived with equation (44), assuming that all error contributors are independent from each other (Gaussian theory of errors). This approach suggests mean errors of 0.128° for NYA-1 and 0.133° for NYA-2, when using the maximum possible Δ_{timing} which occurs in zenith, and even smaller values for lower elevations.

$$\Delta_{mean} = \sqrt{\Delta^2_{compensation} + \Delta^2_{lost\ motion} + \Delta^2_{resolution} + \Delta^2_{pointing} + \Delta^2_{timing}} \qquad (43)$$

Noticeable in Table 6 are also the other listed sources of antenna performance reduction. Very high reductions of system performance can result from aged or incorrect twoline elements and an inaccurate computer system time. The connection between the antenna feed and the LNA causes a small but not negligible total loss of gain (about 0.086 dB), even if very high quality connectors with low SWR- and low ohmic-losses (0.036 and 0.05 dB) are assumed. It is evident that losses of 0.03 dB from software-related uncertainties (corresponding to the design target, inclusive timing) would still be small against the smallest hardware related sources of gain reduction, such as the impedance mismatch of the connection between a feed and a LNA (0.036 dB).

The developed design target for the antenna operation software accuracy (0.1° and 0.05 s) might still appear to have a somehow arbitrary character, despite of the discussion above. This cannot be denied completely, but it was shown that the resulting maximum loss of antenna performance (0.03 dB) is small against all other kinds of antenna related losses and that it does not cause a significant reduction of typical link margins. It was also shown that it is in general agreement with the only found reference in literature (*"0.1 of HPBW"* criterion), although it does not point explicitly on software accuracy. Higher software accuracies may be desirable in principle, but it was shown here that these, at the discussed accuracy level, would not result in significant improvements of the antenna system performance.

6.3 Preparative and accompanying works

The program development started with the assessment of requirements and a couple of ideas to fulfil them. First concepts were sketched and changed occasionally due to new ideas or findings from detected problems or performance analysis. The main initial problems during the programming work were related to the communication with antenna interfaces; later most problems were related to the timing concept and the graphical display function. The following sections 6.3.2 to 6.3.3 describe works that were necessary or useful to support the program development.

6.3.1 Determination of local horizons (antenna masking)

In 2011 the author determined the local masking of the antenna sight by the environment at Ny-Ålesund. Measurements for both antennas were made with a theodolite from WILD Heerbrugg (Switzerland), model "T2" (Figure 48). The antenna pedestals, which would have provided the best measurement basis points, could not be used because the optical sight from those points was blocked by the radomes. Instead, the measurements were made from some positions on a close circle around the radomes. The azimuthal

Figure 48: Theodolite used for determination of local antenna horizon masking

measurement interval was variable, according to elevation variations in the environment. Intervals between discrete measurements (about 90 per antenna) were interpolated as straight lines (Figure 49). The measurements are valuable for satellite contact scheduling (no contact times corresponding to masked directions) and are used for the local horizon graph in the NYA-Sattrack skyplot display (explained in section 6.11.2).

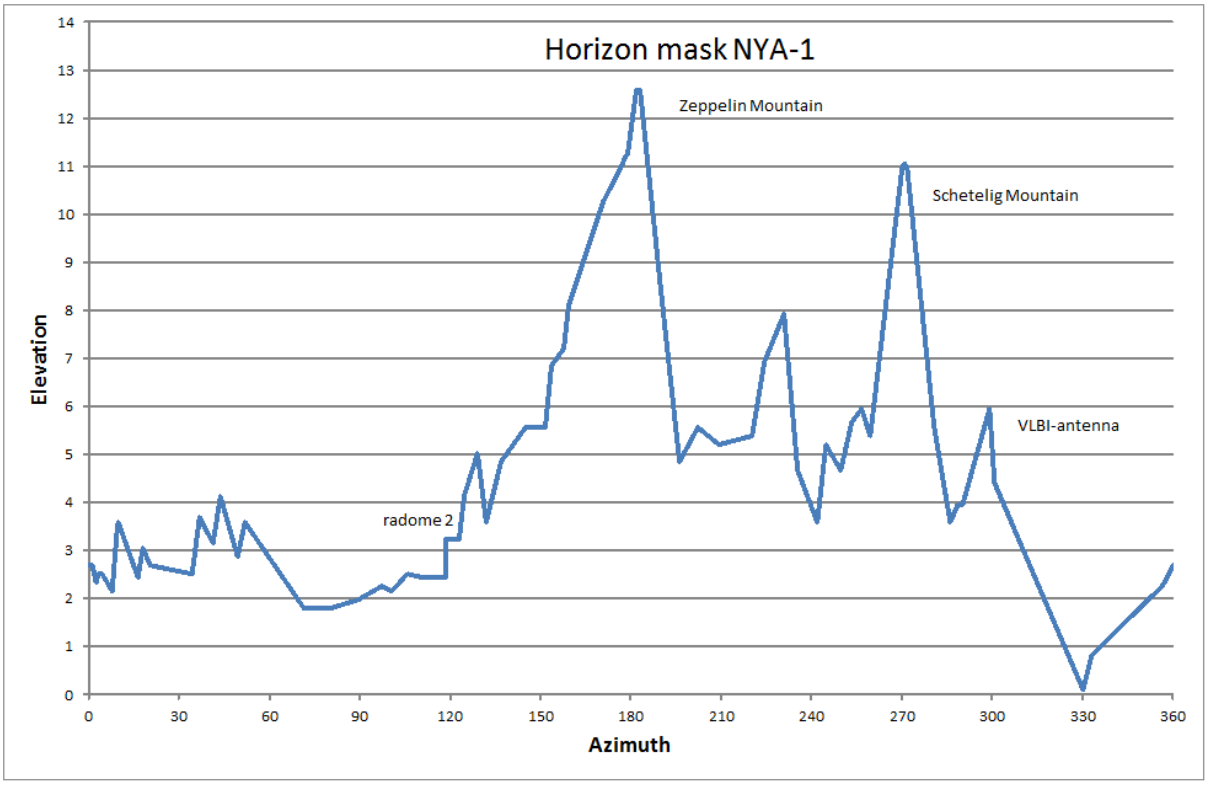

Figure 49: NYA-1 antenna horizon mask

6.3.2 Interfaces and communication protocols

The planned implementation of new communication interfaces between NYA-Sattrack and the connected antennas and ACUs required some investigations about the communication line protocols and command syntax. Most information for communication with the antenna systems was found in the antenna systems documentation. However, the documentation was limited at some points and left many questions unanswered. Missing information was thus obtained through dedicated experiments and tests.

The IEEE-488 interface properties and the Scientific Atlanta (manufacturer) antenna control syntax for communication with the NYA-1 antenna (in fact with the NYA-1 ACU) were explored and tested with the "Measurement & Automation Explorer" software (Version

5.1.0f0) from National Instruments. These activities took place at Potsdam using a spare ACU device (Figure 42). Many issues could not be cleared at Potsdam, because there was no feedback from an antenna system behind the ACU, but the basic communication principles were understood. It was also found that the ACU-documentation was incorrect in some points (e.g., flipped data fields). Later the communication and some first experimental software routines were tested at Ny-Ålesund with involvement of NYA-1 (2 weeks each in 2012 and 2013). These tests were necessary to learn about the real antenna system behaviour and could not be done from remote to prevent eventual antenna system damage.

The documentation for the NYA-2 antenna provided almost all necessary information to develop new antenna operation software. Listed commands were tested and confirmed with first experimental own software routines. The experiment findings were supplemented by observation of the communication traffic between the antenna operation computer and the antenna system, when operated with CGC-software. This traffic was monitored, respectively "tapped" at the RS-232 interface with the software "Free Serial Port Monitor" (Version 3.31), built by the company "HDD-software".

6.3.3 New software for GNSS-based PC system time keeping

One reason for the development of NYA-Sattrack was the planned replacement of outdated computer hardware with outdated computer operation systems, such as found with the previously used antenna steering computer for NYA-1 (Pentium 2, WINDOWS 98). This computer, as well as the antenna steering computer for NYA-2, was running special, manufacturer-made software for the time keeping of the computer system clock, which is an important precondition for accurate antenna-pointing operations (6.2). The time keeping software on the NYA-1 computer was part of a "HOPF" (company) GPS time system, which could operate only one special GPS receiver on a computer card from the same company. This card was still in working order, but required an ISA-standard extension slot, which is not found on regular modern computers anymore. There was also no driver and software available to operate the computer card, other than for the meanwhile outdated WINDOWS 98 computer operation system. The time keeping system of the NYA-2 computer was also based on the reception of GPS-time information. It could be used with more modern computers but only up to WINDOWS-XP computer operation systems and with one type of GPS receiver, which restricted the sustainability.

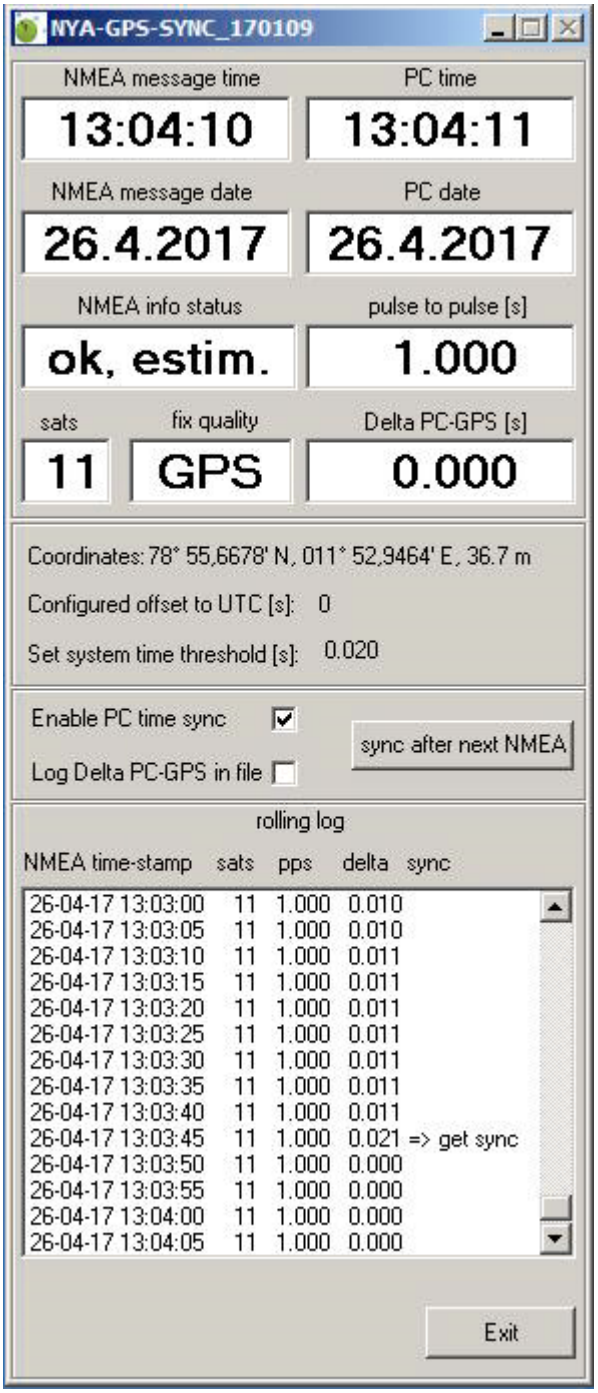

Figure 50: Screenshot from new program for GNSS-based time-keeping

An alternative way for the PC time keeping had to be found, most urgently to allow the operation of a modern computer for the steering of NYA-1 and, with lower priority, to support a sustainable operation of NYA-2. A commercial system could have been used for the time-keeping task again, but it was decided to develop new software that can work with many different types of GNSS-receivers, as this avoids dependencies from a company or specific hardware. The new developed time keeping software "NYA-GPS-SYNC" is a separate program, rather than an integral part of NYA-Sattrack, to allow the usage with computers that do not run NYA-Sattrack. The control and monitor window of the time keeping program (Figure 50) was designed in an upright format with a vertical length identical to the vertical length of the NYA-Sattrack main GUI window, in order to allow a unique and place saving arrangement of the GUIs on the computer desktop. The GNSS time keeping software was programmed in the same environment as NYA-Sattrack (see 6.4) and some of the time related routines and methods, e.g., the "ss2000 domain", are used by both programs (described in sections 6.6.1 to 6.6.4).

Time information is obtained from a GNSS-receiver, which must provide NMEA-183 standard messages (National Marine Electronics Association 1983) with date and time stamps (resolution of 1 second) and a pps-signal (pulse per second). The GNSS-receiver has to be connected to a RS-232 serial interface of the hosting computer. Both types of information (NMEA, pps) can be received through only one serial port, because the GNSS-receiver's

pps-signal is fed in through an otherwise unused signal line of the computer's RS-232 interface (DSR-line). This solution spares additional interfaces and other auxiliary hardware.

A dedicated strategy was developed for the software controlled time monitoring and synchronisation. All timely critical processes are clocked by a program loop that runs at a nominal frequency of 1 KHz, which is slightly reduced (shortly interrupted) for the processing of NMEA messages. The timing-related loop is realised in a separate program thread to make it independent to the greatest possible extent from other program tasks (e.g., update of GUI), which are allocated to another program thread. The computer RS-232 port is checked for the arrival of pps-pulses from the connected GNNS-receiver every 1 ms, according to the loop repetition frequency of 1 KHz. The length of the square shaped pps-signal to be detected is not standardised for all types of GNSS-receivers. It is usually also user configurable (GPS receiver setup) and thus the program detects both, the rising and the falling edge of the pulse. This allows the calculation of the pulse length (uptime, e.g., 100 ms), which is used to stabilise the program flow, inclusive the process for the pps-signal detection. Any signal change of the pps, which is either 0 or 1, triggers the program to instantly read the PC system time clock information with the highest possible resolution and to assign a "pps time stamp" in the range from 0 to 0.999 seconds (PowerBASIC TIMER-function).

The program checks the RS-232 port also for new NMEA-messages each time when a pps-signal is detected. The NMEA-messages are sent less often by the GNSS-receiver, e.g., at a nominal rate of 1/5 Hz. If new data is received, then it is filtered for messages of the types "GPMRC" (Recommended Minimum Sentence) and "GPGGA" (Global Positioning System Fix Data) as defined by the NMEA-0183 standard (National Marine Electronics Association 1983) and checked for consistency and correct crc-checksums. The messages contain time stamps with 1 second resolution and information about the number of tracked satellites, the so called GNSS fix quality (parameter for precision) and the local coordinates etc. The NMEA time stamps are compared with the PC system time, provided that the data quality complies with a minimum standard (e.g., at least 3 GNSS satellites tracked, no errors detected). The total difference between the PC system time and the GNSS-time is determined from the difference "PC time minus GPS-NMEA" (resolution 1 second) plus the "pps time stamp" (numerical resolution 1 ms) as determined at pps-detection. If the calculated difference is higher than a user-defined threshold, e.g., to maintain the accuracy requirement of the antenna tracking system, then the program synchronises the PC system time.

The synchronisation of the system time to GPS-time does not take place immediately, e.g., not right after calculation of the time-offset, and the system time is not set with time stamps that contain smaller units than one second (e.g., milliseconds). Such procedures were tried, but delivered an unstable performance. Instead, the system time is set to the last received NMEA message time plus one second, right on detection of the next pps-pulse (rising edge). This strategy allows high synchronisation accuracy as it provides a considerably long time (about 1 second minus pps-length and minus NMEA processing time) for the described processes, including the preparation of the "NMEA time plus one second" string for the synchronisation command. All these processes are thus finished well before the arrival of the next, synchronisation-triggering pps-signal, so that the timing loop is operated at 1 KHz again at that time. In consequence the accuracy of the synchronisation is about 1 ms.

The total accuracy of the computer clock with respect to GPS-time after synchronisation depends in principle also on the accuracy of the processed GPS-time information. The specification of the used GPS receiver (GARMIN International, Inc. 2005) lists a typical pps-accuracy of 1 µs. It can thus be assumed that it has no significant influence on the total accuracy.

The program threshold level to trigger the synchronisation of the computer system time is user selectable and currently adjusted to 20 ms. A maximum total timing error of 40 ms can result for antenna commands with this setting (analysis in section 6.13.2), but the aspired timing accuracy of 50 ms (design accuracy goal, section 6.2) is still preserved in any case.

6.4 Computer environment for software development and operation

The NYA-Sattrack software was developed for windows operation systems. The source code was generated in the programming language PowerBASIC and compiled with the PowerBASIC compiler version 10.4 (PowerBASIC, Inc. 2012). The software PowerBASIC Forms (PowerBASIC, Inc, 2010) supports the generation of code for program windows (templates in Windows-style) and was used in the version 2.0 for the development of the program GUI. The main reason for choosing the PowerBASIC programming environment were good personal experiences with this programming language from former, although admittedly smaller, software projects. PowerBASIC internal computations use the variable type "EXTENDED" with 18 digit precision and the compiler was known to generate highly effective, small and fast program executables. It was also assessed to be competitive,

regarding accuracy and speed, with programming languages like C or PASCAL and superior, with respect to efficiency and speed, to Visual BASIC and other BASIC-dialects and compilers.

The external program module for the twoline-elements based orbit prediction is based on code from an external source (6.7.4) and was edited and compiled with the "Lahey ED for Windows" FORTRAN developer environment (version 3.80).

6.5 Main program

Static program parameter are defined and set in the main program. The main program opens the main GUI window (section 6.11), starts three threads and cares for a proper termination of the second and third threads (main timing loop and tracking loop threads) at program end. The first thread is started for the program initialisation only and reads static information, e.g., some of the settings in the program configuration file and the local horizon mask (6.3.1). This thread is terminated when these one-time tasks are finished, shortly after program initialisation. The second program thread contains the main timing loop (6.6.5) while the third thread is for the tracking module loops (6.8).

The concept to run two program threads (after program configuration) was chosen, to decouple processes with timing tasks for antenna tracking from other program functions. Both threads run in parallel, but influence each other by exchange of information through global program variables. It was not tested if this concept really has a significant advantage over a single thread design. However, the timing performance of the program is assessed to be very accurate and the chosen concept certainly supports a clearer program structure too.

NYA-Sattrack reads all externally provided numbers according to their original resolution and assigns them for internal calculations to variable types with at least corresponding or even greater numerical resolutions. The resolution of antenna direction commands (output to antenna systems) was limited to 3 decimals and the GUI displays to 2 decimals.

6.6 Program timing

NYA-Sattrack has to manage many timing tasks, which require calculations in the time domain, e.g., to trigger a task that should be started with a certain offset to another point in time. An example is the system initialisation phase, which starts 5 seconds before AOS time.

The computer system time and the times that trigger the main program actions (e.g., start and stop of satellite tracking) are read by the program in civilian time format. The civilian time format is convenient for humans, but not easily handled by a computer program. A special time scale (6.6.1) was thus developed for NYA-Sattrack. It allows timing and time calculations with a coarse resolution of 1 second in an easy way.

Some tasks require a higher precision than 1 second, e.g., the sending of tracking commands to an antenna. Therefore, a fine time scale (6.6.4) was used for these tasks. Both time scales, coarse and fine, are used in a nested system of timing loops with different loop frequencies, corresponding to the different program phases and actually executed program tasks.

6.6.1 Program coarse time scale “ss2000” (seconds since 2000)

A program internal time scale was created and used for calculations in the time domain and all timing-related internal processes with accuracy demands not higher than 1 second. The time scale refers to the 1.1.2000 at 00:00:00 h as reference (ss2000 = 0) and counts full seconds since then. Civilian date and time statements that are converted to their ss2000 equivalents (6.6.2) can be compared (earlier, due, later) very conveniently on that time scale. Also the subtraction or addition of offsets to civilian times is very easy when using the ss2000 environment in an intermediate step. The addition of one minute to a civilian time, for example, is obtained by simply adding 60 seconds to the ss2000 equivalent and transforming the result back to the corresponding civilian time. Eventual simultaneous changes of hours, days, months and years due to the added minute are respected by the back-transformation routines (6.6.3).

The selection of a variable zero point for this type of time scale (instead of 1.1.2000), e.g., such as the beginning of the last year relative to the current system date, would omit the calculations for years previous to the variable zero point. This would increase the routine calculation speed. However, the routines to transform between civilian date and ss2000 are very fast so that the choice of the time scale’s zero point has no significant effect on the program performance. A variable zero point was not used because it was assessed to have disadvantages with respect to clear static conditions for all routines, while the benefit of processing speed would be small and not required at all.

6.6.2 Module “toss2000”

This module calculates the number of seconds (output) elapsed since January, 1st 2000 (00:00:00 hours) until a given civilian time (input). The method is to build the sum of seconds elapsed in full years before the current year (considering also switch years), the elapsed seconds in months before the current month, and so on, with the seconds in the civilian time string as last term. An extract from the source code for this function is listed in the appendix.

6.6.3 Module “fromss2000”

This module is the counterpart of “toss2000” and calculates the civilian date and time (output) from ss2000 values (seconds since 2000, input). The method is to “fill” ss2000-seconds into civilian time units, beginning with years, until there are not enough ss2000-seconds left to “fill” another full unit. Then the routine steps to the next smaller civilian time unit (e.g., from years to months) and “fills” them again until there are not enough ss2000-seconds left to “fill” another full unit. The counted number of fully filled time units then refers, e.g., to the month, day etc. As the number of seconds in a year and a month are not constant (switch years, days in month = 28 to 31), these values are selected from corresponding DATA lines in the code. An extract from the source code for this function is listed in the appendix.

6.6.4 Internal fine time scale

A fine time scale was found with the PowerBASIC Compiler “TIMER” function. The function counts seconds since midnight of the current day with a numerical resolution of 1 ms and an accuracy (real resolution) of 10 ms according to the compiler documentation (PowerBASIC, Inc. 2012). Both was considered to be suitable and sufficient even for the program tasks with relative high timing accuracy demands, such as found in the main tracking loop. A precaution-mechanism was implemented to handle counter overflows at midnight.

6.6.5 Main timing loop

The main timing loop (Figure 51) is one of the two continuously running program threads and controls many important program tasks directly. It has a loop frequency of slightly less than 10 Hz, which supports a low program-caused CPU load, while a fully sufficient timing accuracy for the loop tasks is still maintained. An example is the update of the program GUI (6.11), which includes the display of the system time. There is virtually no visible delay with respect to the system time display of the Windows OS, despite the low loop frequency.

The basic operation principle of the loop is to read the actual system time with one second resolution and to compare it to the due times of tasks to be triggered. All time checks are performed on the ss2000 time scale. The triggered tasks are, e.g., the next satellite tracking (defined by jobfile) and the next checks for a new jobfile or twoline-elements file (update intervals defined in program configuration file). Inside the loop there are also several checks for changed values to be displayed in the numerical GUI and the loop also continuously monitors if the system time changed in an abnormal way, e.g., if it changed into the past or by more than one second into future. This can happen by mistake (user interaction) or by a process, e.g., such for the synchronisation with an external reference time like NYA-GPS-Sync. An entry into the program logfile is generated in these cases, including the old and the new system time. If the system time has changed behind the LOS time of the currently expected next satellite contact, then a reread of the jobfile is initiated to determine which scheduled satellite contact has to be served next.

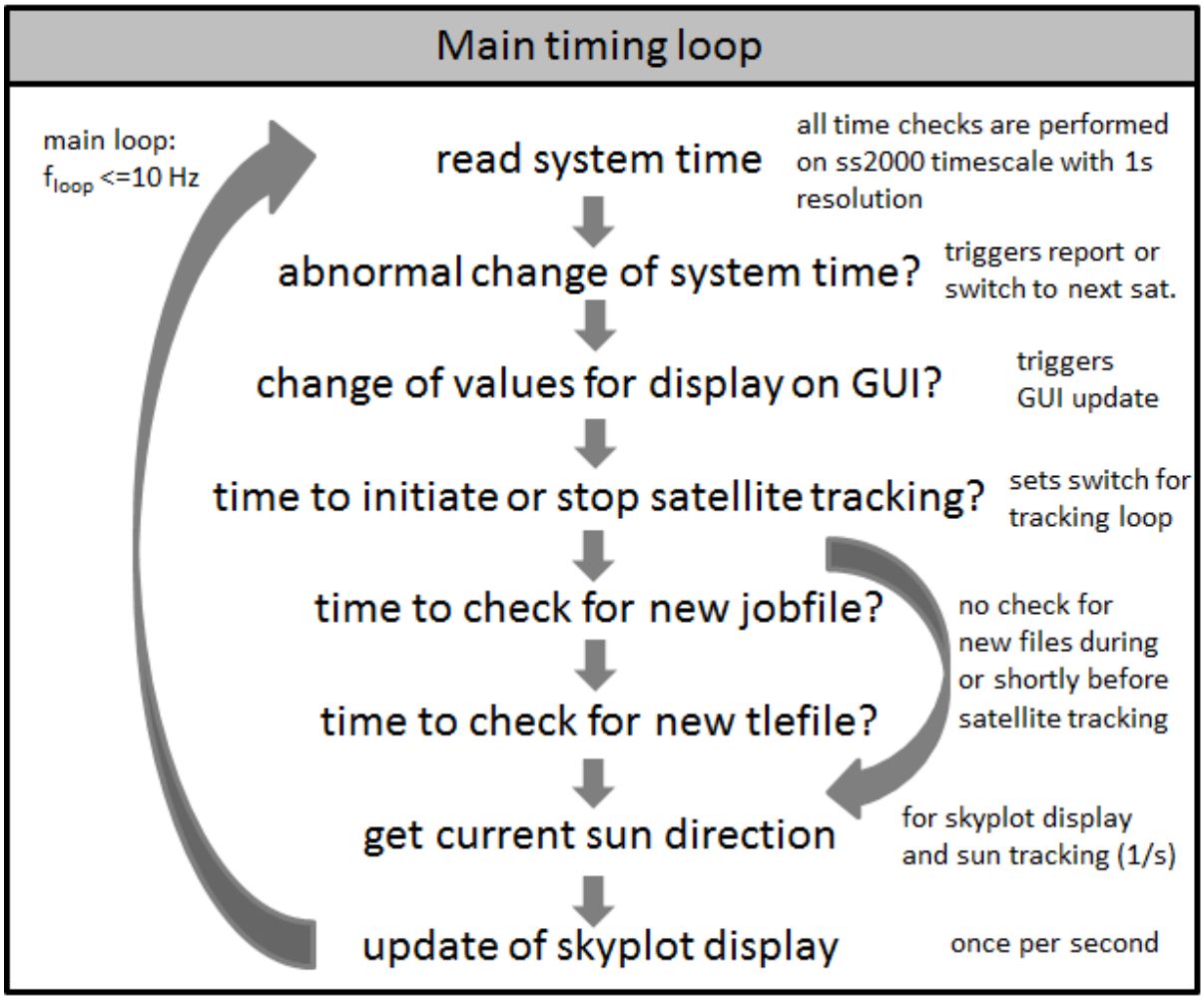

Figure 51: Layout of the main timing loop

Some of the loop steps are suppressed during satellite tracking, e.g., the search for new twoline-elements. A frequent test of the communication line between the antenna operation computer and the antenna (ACU) was implemented and tested, but disabled at a later time. These verifications of connectivity worked fine on the program side but prevented the antennas to enter dedicated rest modes, where some antenna components are powered down automatically outside the active satellite tracking intervals (antenna features).

The most important timing target of the loop is the “tracking-switch”. This switch is set to the “track now” position 5 seconds before the computer system time has reached the time to track the next satellite (AOS time). It controls the main tracking loop (the second program thread function), which cares for the more precise timing of antenna commanding. The actually too early setting of the tracking switch provides a short system initialisation phase. In this phase the connected ACU and antenna systems are waked up by NYA-Sattrack (e.g., release of electromagnetically driven pedestal brakes) before first antenna positioning commands are issued. The program also checks the antenna status prior to satellite tracking and triggers the execution of an external program (e.g., to set RF-relays) if this was configured in the NYA-Sattrack configuration file. The tracking switch is set back to “no tracking” by the main timing loop as soon as the LOS-time has been reached.

6.6.6 Other time-related modules

Some routines are implemented to calculate the calendar week of the year (woy) and the day of the year (doy) according to the actual system time. The routines consider leap years and the rules for the differentiation between a calendar week 1 and a calendar week 53, as defined with ISO 8601 (International Organization for Standardization 1988). The woy and doy numbers are calculated for the comparison with week number information in jobfile names, but they have no meaning for the program flow.

6.7 Scheduled satellite tracking

NYA-Sattrack operates in a semi-automatic mode. The program performs automatic processing of satellite tracking schedules (jobfiles) and automatic consideration of updated or new jobfiles and twoline elements, which are searched for in a dedicated “incoming directory” (configurable). The generation of satellite tracking schedules and the provision of the corresponding files however, must be carried out by external functions. For Ny-Ålesund these tasks are carried out by GFZ staff (see section 5.5).

6.7.1 Processing of jobfiles (satellite tracking schedules)

Jobfiles contain tracking information about the satellites to be received and are used to configure the automatic processes which operate antennas and receivers at NYA. The file format is simple (example in Appendix) and was once specified for the operation of the first antenna at Ny-Ålesund. The jobfile-lines beginning with the keyword for acquisition ("Acqn") hold start and stop times of satellite data transmissions (transmitter is on, but not necessarily sending data yet) and trigger the continuous antenna positioning. The jobfile lines beginning with the keyword for data-dumps ("Dump") indicate the time interval in which a satellite is expected to send data. Satellite transmitter frequencies are found in lines beginning with "Frequency". They are used for the operation of the receivers and are displayed by NYA-Sattrack for operator information, although they have no meaning for the antenna steering. The most actual jobfile format has some more keywords to address more parameter (example in Appendix), but these also have no relevance for NYA-Sattrack.

A jobfile is read each time when it was selected for operation, either automatically by the program or by an operator. It is also reread after each finished satellite tracking (see 6.8.1). This allows an update of the actually used jobfile at any time, e.g., by manual editing of particular entries or by the complete replacement of a currently used jobfile with a new one. An updated jobfile can be sent by an operator, e.g., when a certain satellite needs more contacts than previously scheduled, which might be required to support a better monitoring of on-board parameters, such as the battery voltage. The program checks a new jobfile line by line for AOS-times and selects the most due AOS-time according to the actual system time. The satellite name acronym (e.g., GR1 for GRACE-1), which is found in the line preceding the selected AOS-time, is used to select the corresponding set of twoline elements from the actually used twoline elements file. Finally the calculation of antenna directions for the upcoming satellite pass is initiated through the interface to the external pass prediction program (see 6.7.5) and the antenna is moved to the first direction to be tracked according to AOS-time.

If no AOS-time past the actual system time was found, then the program checks if another jobfile ("job_next.txt") is waiting for execution (see 6.7.2) and continues regular operation with that file. If no next jobfile was found or if all AOS-times in the next jobfile are outdated, then the program waits for the arrival of a new jobfile without tracking satellites in the

meantime. The program GUI shows “waiting for job” and “no sat to track” with red background in these cases.

6.7.2 Updating of jobfiles

Jobfiles for each antenna of the satellite-receiving station Ny-Ålesund are currently sent manually by a planning-operator (GFZ-staff) once per week, but could also be sent more frequently or in inhomogeneous intervals. A new jobfile may seamless continue the previous tracking schedule in the previous jobfile, but could also overlap the previous jobfile in time. It could even address exactly the same operation intervals and contacts as the previous jobfile. Dedicated program routines make sure that the right jobfile is chosen for operation and that it contains no fatal inconsistencies. Some basic information about the properties of the currently active jobfile is determined and displayed on the program GUI. This allows an operator to get a direct confirmation that the right jobfile is used, not only according to the filename, but also according to the number of scheduled satellite contacts, the jobfile timestamp (time of generation) and jobfile size (bytes).

The jobfile routines are called by the main timing loop with a configurable frequency (default: 1 minute), but can also be called directly by an operator through the test and maintenance GUI (manual selection of jobfile). When a new jobfile has arrived in the dedicated incoming directory or when a jobfile was selected manually by an operator, it is checked for a correct jobfile naming and if the file size is sufficient to schedule at least one contact. Jobfiles that arrived in the incoming directory are also archived in any case. If a new jobfile was found in UNIX format, then it is converted to the DOS-format (basically by adding of linefeed characters at end of lines). The DOS formatted jobfile is then checked line by line for issues related to scheduled times. Detected inconsistencies are cases where the AOS time in the current line is earlier than the AOS time in the previous line (e.g., wrong contact order), if the AOS time in the current line is earlier than the LOS time in the previous line (time overlapping of scheduled contacts) and if the AOS time in a line is later than the LOS time in the same line (stop before start).

If a new jobfile has passed all consistency checks successfully then it is determined if it has to be used immediately or in the future. If the first AOS time in the new jobfile is earlier than the last LOS time in the currently used jobfile, then the new jobfile is activated immediately. Otherwise it is kept in the program working directory with the filename “job_next.txt”

(indicating that it is the next jobfile to be used) and activated automatically when the current jobfile expired.

All jobfile update functions are blocked during satellite tracking.

6.7.3 Updating of twoline elements

The prediction of satellite orbits, respectively the calculation of timetables with satellite directions for precise antenna-pointing through NYA-Sattrack, is currently based on twoline elements (example in appendix). Good antenna-pointing system accuracy must be maintained by regular updates of twoline elements, e.g., about three times per day for the tracking of LEO-satellites (current practise for station at Ny-Ålesund). The continuously updated twoline elements are used with the first prediction program (displayed on GUI as "prediction 1"), which is the standard prediction configuration for routine operations. Twoline elements to be used with the second prediction program must be selected manually by an operator, as this is an alternative configuration for special cases. The second prediction program and the second twoline elements could be identical to their pendants in the primary configuration. However, during satellite manoeuvres and LEOP it might be a combination of twoline elements from NORAD and a differently configured prediction program (concept explained in section 6.7.4).

The program update procedures of twoline elements for the "prediction 1" configuration are similar to the jobfile update procedures. The main timing loop calls the routines for twoline elements updates at a configurable frequency (default: 1/minute), but not at the same time when the program processes a new jobfile. An operator can also select a twoline elements file manually through a corresponding GUI function. If a new twoline elements file is found by the automatic routines or selected by an operator, then it will be converted automatically from UNIX- to DOS-format first (if applicable). The file length is checked to have at least as many bytes as needed for one set of twoline elements (according to one satellite). As by format specification (see "ADCOM/DO Form 12" in (Hoots and Roehrich 1980), example in appendix) there is a modulo-10 checksum in the last digit of each data line in a twoline elements file. These checksums were generated at the source of twoline elements (e.g., GFZ, DLR or NORAD) and are compared with the data line checksums as calculated by NYA-Sattrack. If the individual checksums are not equal for all lines, e.g., due to errors during file transfers, then the file will not be used for satellite orbit predictions. NYA-Sattrack then continues to use older twoline elements until arrival and positive validation of a new file.

Some information about the currently active twoline elements file, as used in the currently active prediction configuration, is displayed on the program GUI. This includes the file name, the file time stamp and the file size [bytes]. Also the actually used twoline elements for the upcoming satellite pass are displayed in a dedicated GUI data field, which makes sense, because files with twoline elements usually contain data for all satellites to be tracked at the station. At any time this gives an operator a direct and unquestionable confirmation that the right twoline elements are in use. This can be important especially during special satellite orbit manoeuvres with rapidly changing orbit parameter and accordingly updated twoline elements, as experienced with the CHAMP mission.

All twoline elements update functions are blocked during satellite tracking.

6.7.4 External orbit prediction programs

The tracking of a satellite with an antenna requires time-position information for the satellite pass interval to be tracked. NYA-Sattrack has no own program-internal routines for the calculation of satellite directions and was designed to interact with an external program or two external programs for orbit prediction. A useable external program must be able to provide calculations without user interaction and in a file. A number of programs from commercial and non-commercial vendors fulfil these requirements with the functionality of a command line mode. NYA-Sattrack works with simple ASCII-format files that contain timetables for satellite directions (azimuth and elevation) according to the next satellite pass to be tracked, preferably with a resolution of 1 second. These timetables must be provided by the external orbit prediction program. NYA-Sattrack triggers the execution of the external pass prediction program and provides it with local station coordinates, the start and stop and command interval times for the next satellite contact and the corresponding satellite twoline elements (6.7.5).

For the interaction with NYA-Sattrack it was decided to use freely available software source code with excellent reputation. F. Hoots and R. Roehrich published it first in a FORTRAN version along with the “Spacetrack report #3” (Hoots and Roehrich 1980). The program uses twoline elements and an implemented SGP4 propagator (Simplified General Perturbations) for orbits with a revolution time of up to 225 minutes, corresponding to satellite altitudes (semi-major axis) up to about 5883 km, which is the case for all satellites that are received at NYA. Many revised or slightly modified versions of this code were published later in different

programming languages, referred here as the “Spacetrack-code” family. The FORTRAN code as used explicitly for the orbit predictions in this work, respectively as called by NYA-Sattrack, is described in the paper “Revisiting Spacetrack Report #3” (Vallado, Crawford, et al. 2006 a) and was downloaded from the official Celestrak-Website (Vallado, Crawford, et al. 2012). This software version is open to the public, was referenced in many related publications and regarded to have a very well performance for LEO satellites orbit predictions from twoline elements. It was also identified to be the basis for other software developments such as the free program WXtrack and, as mentioned in a dedicated paper (Vallado, Crawford, et al., Implementing the Revised SGP 4 in STK 2006 b), even STK (Satellite Tool Kit) from Analytical Graphics, Inc. (AGI), which is most probably the leading vendor for professional satellite orbit-related software. The current version of STK is 11.0 and the help text of this version states: “*By default, STK utilizes the CSSI* (CSSI = Center for Space Standards and Innovation) *SGP4 routine, Version 2008-11-03*”. This code version is also freely available from the CSSI website and nearly identical to the code version as used for this work. The differences between the versions as used with NYA-Sattrack and STK are that the latter, according to the corresponding author’s release notes (Vallado, Crawford, et al. 2012), lacks two software updates. The first update (30.8. 2010) concerned different calculation methods of some parameters (release note: “*The change produces a minor effect (cm-level) on the SGP4 results”*) and the second update (30.12. 2011) was no change of source code, but a release note reply to user comments about parameters that were observed to always be set to “0”.

By default the “Spacetrack-code” generates output (e.g., satellite positions) in the Cartesian TEME coordinate system (True Equator Mean Equinox), which is also used for the generation of twoline elements at NORAD. Some transformation is required to derive azimuth / elevation directions to the satellite as they are needed for practical antenna tracking. Helpful subroutines were found in a code package, which was published by one of the Spacetrack-code authors in the book “Fundamentals of Astrodynamics and Applications” (D. Vallado 2007). Some appropriate routines of that code package were implemented in the Spacetrack-code to provide the desired satellite direction output, relative to the location of a ground station (local horizontal coordinate system).

The implemented sequence of additional routines is repeatedly executed for each individual point of time of satellite tracking (defined by jobfile schedule and tracking command time

interval) and starts with the calculation of the corresponding Julian day (JD). The JD info is the input for the next step, the calculation of the Greenwich Mean Sidereal Time (GMST). The GMST is then used, together with the local station longitude, to calculate the local sidereal time GMST(λ). This allows the transformation of the satellite coordinates in the TEME frame to the ECEF (Earth-Centered, Earth-Fixed) frame, where the direction between the ground station and the satellite is calculated as the final output (local horizontal coordinate system).

Apparently all published "Spacetrack-code" versions use an interactive function to get user input through a terminal window, e.g., asking to provide local coordinates, twoline elements, a time interval, the prediction time increment and a datum (e.g., WGS84). This interactive terminal function was replaced for the use with NYA-Sattrack by a non-interactive, file-based input function. The modified "Spacetrack-code" receives all necessary information through a small file with 3 lines. The first two lines are unmodified twoline elements for the next satellite to be tracked (see section 6.7.5) and the third line provides the additionally needed information, except which datum is to be used, as this topic was addressed in a different way.

The authors of the Spacetrack-code made comments in their paper and the related code "*Operation Notes*" that WGS84 may be taken as the standard datum, but that their software might delivers higher precision with the WGS72 datum, provided that the used twoline elements have been generated by NORAD. Two different executables from the modified "Spacetrack-code" have been compiled for NYA-Sattrack. One uses internally the WGS84 datum and the other the WGS72 datum. NYA-Sattrack supports to use two different satellite directions tables ("prediction 1" and "prediction 2") that can be generated with these or other external prediction programs (executables) and different twoline elements (see 6.8). This allows an operator to switch between the two correspondingly different prediction tables during satellite tracking at any time and as often as desired, e.g., between a prediction from the WGS84 executable with twoline elements generated by GFZ and a prediction from the WGS72 executable with twoline elements generated by NORAD. A benefit from this feature could arise shortly after a satellite launch, e.g., after satellite separation, when first twoline elements are obtained from radar-observations, as usually provided by NORAD. Such radar based twoline elements have a limited accuracy and it is thus desirable to replace them by more accurate twoline elements, e.g., such based on on-board GNSS-measurements or SLR-observations. Right after a satellite separation phase it is usually also unclear, which twoline

elements from NORAD belong to a certain object. NORAD usually issues more than one set of twoline elements after a launch, corresponding to all tracked objects, which may include all launched satellites and the last rocket stage. In these cases NYA-Sattrack could be configured to use the WGS72-based executable for both user-selectable prediction tables, but with two different twoline elements from NORAD. This might help to identify the right twoline elements for the satellite to be tracked and to establish sooner stable contacts with the ground station.

6.7.5 Interface to external pass prediction programs

The jobfile processing routines (6.7.1) check which satellite is to be tracked next and select the corresponding twoline elements (two lines of data) from the twoline elements file. The selected twoline elements are then passed to an external pass prediction program, together with additionally required information (e.g., local coordinates and tracking interval). The satellite orbit number at the next satellite contact is calculated according to the scheduled AOS time (from jobfile) and values in the selected twoline elements (epoch year, epoch, mean motion, revolution number at epoch). The calculated orbit number is displayed on the GUI and used as one component for the naming of logfiles as this is mandatory (Norwegian regulations) for the logging of satellite reception activities on Spitsbergen[6].

NYA-Sattrack currently uses a modified FORTRAN executable of the Spacetrack-Code (6.7.4), but any other external pass prediction program could be used in principle as well. In fact, NYA-Sattrack can call two external pass prediction programs that may use the same or different twoline elements and receives antenna direction tables for the next satellite pass from both (“prediction 1”, “prediction 2”). These tables with timestamps and directions (azimuth and elevation values) for the satellite to be tracked are sent back from the external programs to NYA-Sattrack as files but are immediately sorted into dedicated arrays (program memory).

The two pass prediction arrays are supplemented with more “columns” holding the same direction data, but transformed to be directly displayable in the Cartesian coordinate system of the skyplot display function (three projection types, see 6.11.2). This is a measure to reduce CPU load during an actual satellite tracking as the transformed directions can be displayed

[6] This feature was implemented after NYA-Sattrack installation in 2014 as it was not mandatory before.

directly and simultaneously with the tracking process, without any mapping transformations to be performed at the same time.

Each of the two pass prediction arrays then holds antenna direction information and skyplot mapping coordinates for the same satellite pass. These directions are not necessarily identical to each other as the external pass prediction programs may use different methods or parameter for the predictions (see 6.7.4) and / or different twoline elements. Holding the antenna direction tables in program memory allows very fast data access during the satellite tracking process and an operator could switch even frequently between the two direction tables during satellite tracking, without causing detectable delays in the program execution. This feature is not foreseen for regular automatic program operation, but to support satellite tracking at special occasions or to compare the “in praxis quality” of different satellite predictions during tracking in real-time.

A third array is prepared in the pass preparation phase to store the sun directions for the time interval of satellite tracking, again to be used directly by the skyplot display function. The sun directions are already transformed to mapping coordinates for all three implemented display projection types (6.11.2), which omits a corresponding CPU load at tracking times.

6.8 Antenna positioning modules

A system of antenna positioning modules prepares the commands that guide the antenna movement according to the different operation tasks. The main tracking module (6.8.1) cares for the preparation and precise timing of positioning commands for satellite tracking (regular operation) and sun-tracking (maintenance tasks).

A square scan function (6.8.2) and a stripe scan function (6.8.3) are used for special tasks only, e.g., in combination with the sun-tracking function (6.8.5), to determine antenna boresight offsets (9.1) and antenna directional characteristics (4.3, 9.3). The sun-tracking function can be used to support a determination of the main antenna RF-performance parameter (G/T, 9.2), provided that all antenna boresight offsets are known and compensated.

6.8.1 Main tracking module

The main tracking module is structured as a nesting of timed loops (Figure 52). It is realised in a separate program thread, which provides a smooth program flow with respect to the

execution speed and, to the greatest possible extent, from program steps in the main program loop, such as the continuous update of the NYA-Sattrack GUI.

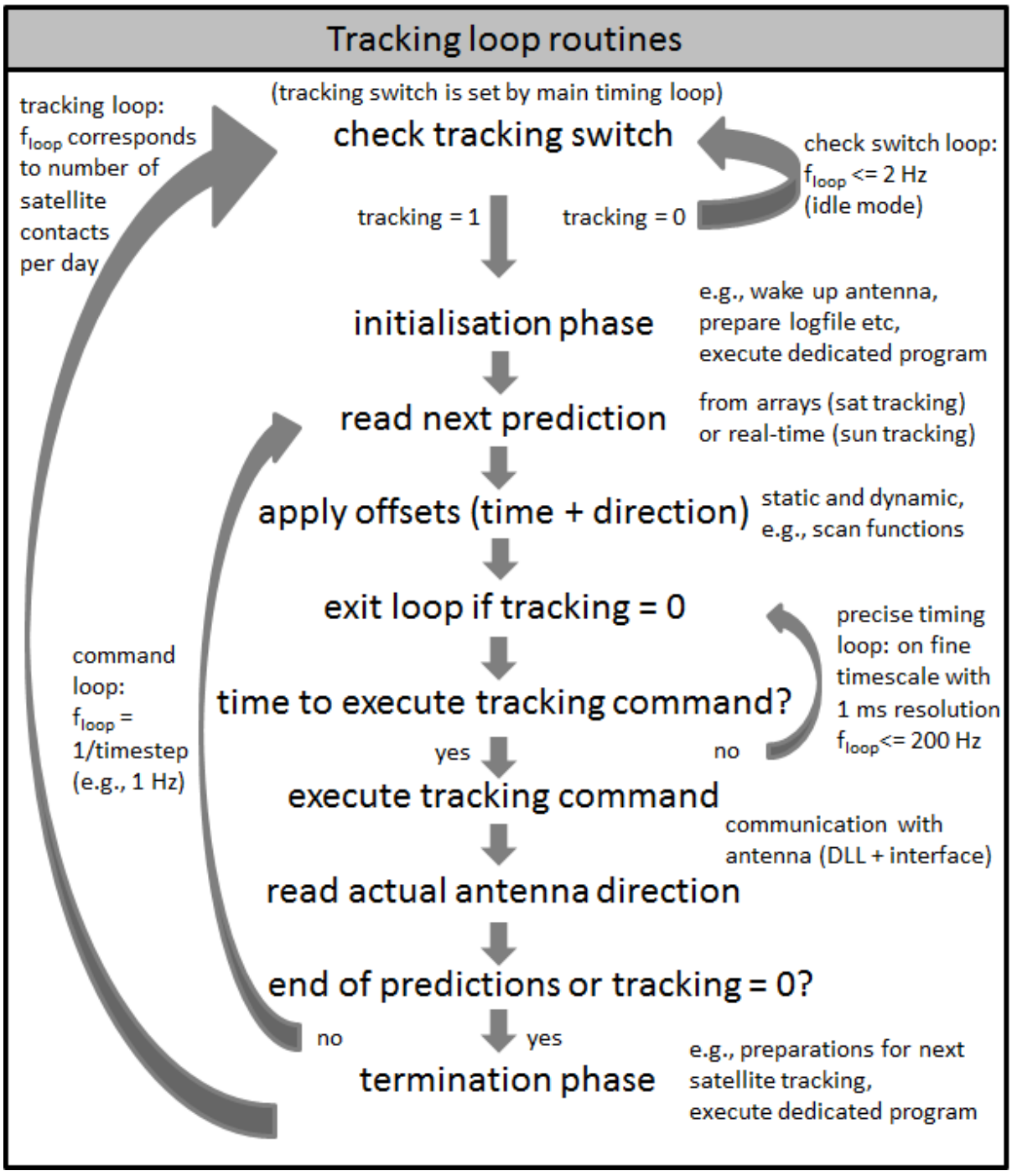

Figure 52: Layout of the tracking loop system

The first loop ("check switch loop") is running at a low frequency of 2 Hz and checks the global "tracking switch" variable (0 = not tracking, 1 = tracking), while all other loops of the main tracking module remain passive. The "tracking switch" is controlled automatically by

the main timing loop (6.6.5) based on the actual tracking schedule (jobfile). Five seconds before due time for a satellite tracking it is set to “1”, to allow a program initialisation phase.

The initialisation phase can be used to execute a predefined external program or command (entry in configuration file), before the command loop is started. This might be used to configure the signal paths between antennas and receivers (switching of relays) or to request a photo or video from a camera. The initialisation phase may also be needed to establish the communication with the connected antenna, which may be found in an idle mode (power saving), requiring some seconds before it can accept antenna positioning commands.

The command loop reads times and directions to the tracking target, either a satellite or the sun. In fact, it reads two sets of directions and times for each tracking step. One set according to the direction that is achieved at the end of the currently running tracking step (= last tracking command) and the second set according to the next tracking step. The required data for satellite tracking is found in precalculated tables (6.7.4). For sun-tracking it is provided through repeated calls of the sun-tracking module (6.10.3), first using the actual system time and then using the actual system time plus one second. This approach allows the calculation of antenna movement rates for individual tracking steps in the antenna software modules as used for the ACU-operation (currently NYA-2 only). The command loop frequency is 1 Hz for the sun-tracking (constant) or according to the timely resolution of precalculated satellite directions (usually 1 second, respectively 1 Hz). A next step in the command loop compensates known static antenna system offsets (boresight and delays) and considers dynamic offsets as coming from an operator (GUI function) or through another interface, e.g., from a future autotracking function (not implemented yet). Also the actually required offsets according to special scan patterns for maintenance tasks (squares and stripes, explained in 6.8.2 and 6.8.3) are taken into account at this point.

The preparation of an individual antenna command as described above does not affect the command timing accuracy as the program must wait anyway until the command is due to be sent to an antenna, according to the command frequency (usually 1 Hz). The command dissemination at the right time is triggered by a precise loop function, which checks the system time at a rate of 200 Hz. A time offset (range +/- 10 s) can be applied to the command due time, either temporary by manual selection (test and maintenance menu, resolution 10 ms), or to be considered permanently (configuration file, resolution 1 ms). This function can

be used to detect and compensate time offsets, e.g., from a delayed dissemination or execution of antenna positioning commands.

The command loop reads back the actual antenna direction from the antenna system right after dissemination of an individual antenna positioning command. Reported antenna directions are displayed on the GUI, stored in a logfile and used also to monitor the proper system function. Antenna positioning commands must be sent to an antenna only as long as the antenna acknowledges commands with corresponding actual position reports and as long as the commanded direction and the actual direction do not differ too much. The satellite tracking procedure is terminated with an error flag as soon as one of these conditions is not met. This function was implemented for safety reasons to avoid abrupt and very fast antenna movements after any temporary connection problem between antenna, ACU and steering computer. Another reason is to prevent system damage that could result from related mechanical problems (e.g., physical obstruction), which are a probable source of such anomalies. The antenna direction feedback is also stored in a dedicated antenna direction program memory array. This array is used by the skyplot function to display a track of the antenna movements, which should coincide with the also displayed track of predicted satellite directions. The file-based logging of antenna directions appends one line per tracking command to a dedicated log file. This approach supports a continuous and complete logging over the full tracking time, no matter if it is terminated regularly or due to a serious system problem, such as a main power outage.

The precise command loop (200 Hz) is terminated when there are no more satellite directions in the prediction table to be tracked or if the user stops the tracking process, e.g., a tracking of the sun. A following termination phase allows an eventually desired automatic execution of external programs (entry in configuration file) according to the tracking success. One external program can be defined for the normal termination of satellite tracking, e.g., for an automatic ftp-transfer of the last logfile. A second external program can be defined for cases when a too early termination of satellite tracking was detected (error flag), e.g., to send a warning-mail to remote operators. A reread of the jobfile to find information for the next satellite tracking is triggered in any case. Finally the main tracking module returns to the entry point of the low frequency loop, which is the low frequency check of the “tracking switch” condition.

6.8.2 Square scan function

This function causes an automated antenna movement, according to a scheme that is built by squares with increasing sizes (Figure 53 a). The result is a raster of accessed directions as sketched in Figure 53 c, which can be used for systematic scans of antenna properties in different directions. The midpoint of the sketch refers to the nominal antenna boresight direction without offsets from the scan function. The order and directions of movements are indicated in Figure 53 a by arrows and indices. The antenna is moved from the mid direction to the first square at "1". It follows the first square, turns to the next larger square at "10" which is tracked also and ends at "n". One point on each square is scanned twice, at the beginning and at the end of the movements on the square. A user has to select the maximum offset to the nominal antenna boresight direction (equal to half length of largest square sides) and the movement step size (equivalent to raster interval) through the program's test and maintenance menu (section 7.2 => Antenna maintenance scan functions). The square scan function can be used standalone or while tracking a satellite or the sun as done in this work (9.3).

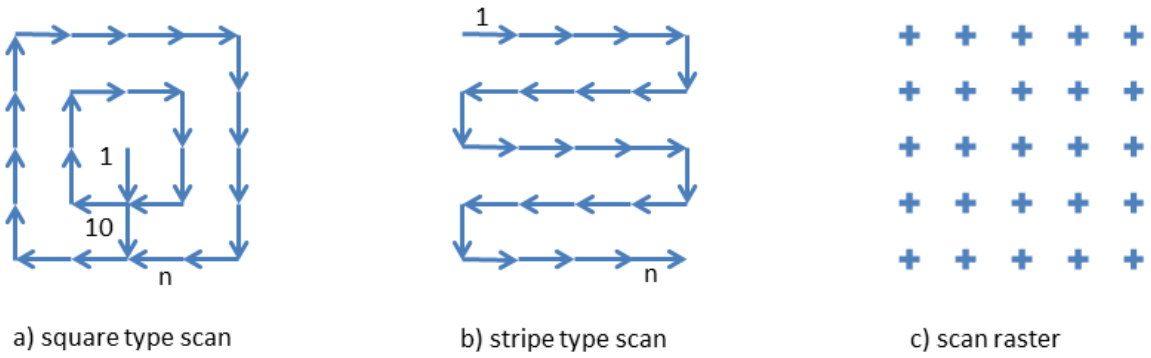

Figure 53: Movement schemes and raster of scan functions

6.8.3 Stripe scan function

The stripe scan function was implemented to provide another scheme of automatic antenna movements, different to the square type scheme. The obtained scan raster is the same as with the square type scan, but systematic problems of an antenna positioning system may show up in a different way with this scheme, due to the different movement pattern. The antenna movements (Figure 53 b) begin at the upper left corner of the rectangular movement range at "1" (first step) and end in the lower right corner at "n" (last step). The scan raster is the same

(Figure 53 c) as for the square scan function (6.8.2), but no direction is accessed more than one time. The maximum scan offset, which has to be defined by an operator as well as the step size (test and maintenance menu, section 7.2 => Antenna maintenance scan functions), refers to the nominal zero offset direction of the nominal antenna boresight and is equal to half of the stripes length. The stripe scan function can be used standalone or while tracking a satellite or the sun as done in this work (9.3).

6.8.4 Horizon scan function

A function to scan the horizon over selectable ranges of azimuth and elevation and with selectable step-sizes was implemented in NYA-Sattrack. This was a late amendment to NYA-Sattrack and it is still provisional as the code was placed in the main program (instead of the antenna DLLs), although there are differences in the function application between the two NYA antennas. The function is also not yet properly supported by the GUIs. The horizon scan uses the stripe type scan scheme (Figure 53b) and cannot be combined with any other scan function. The application of the horizon scan is described in section 9.4.

6.8.5 Sun-tracking function

This function supports a continuous antenna tracking of the sun and must be called by an operator via the test and maintenance menu. A “track the sun” flag is set in the program, which causes other routines to execute special routine parts according to the sun-tracking mode. The antenna is moved to the current sun direction as calculated by the sun direction module (6.10.3). All following sun-tracking steps are calculated continuously by the same module at a rate of 1 Hz, but for times that are 1 second ahead of the actual time (using the ss2000-routines 6.6.2 and 6.6.3), which is a similar approach as for satellite tracking. The main tracking module (6.8.1) cares for the timely precise dissemination of the positioning commands and the logging of directions in special sun-tracking logfiles (example in appendix). Process details are displayed by the main GUI. A satellite tracking cannot be triggered during the sun-tracking.

The sun-tracking function can be combined with either the square scan function (6.8.2) or the stripe scan function (6.8.3). The angular offsets of the scan movements are then executed relative to the actual sun direction.

6.9 Software interfaces to antennas

The communication interfaces of antenna systems can have very different properties regarding interface-hardware, interface-protocols and antenna operation commands (e.g., proprietary formats). Also the antenna positioning systems can be very different (e.g., number and orientation of axes), which requires different parameter to be communicated with the antenna operation program. The two antennas at the satellite-receiving station Ny-Ålesund are good examples for two very different systems. An addressing of too many different properties in one program is difficult and a later modification for another antenna type even more. It was thus decided to allocate antenna specific program code to dedicated antenna-DLL files. In consequence this strategy avoids the inclusion of code into the main program that is not needed for the operation of all (both) antennas and supports a future adaptation of NYA-Sattrack for the operation of any other antenna systems with different operation properties.

The antenna interface modules (DLLs) have a unique software interface that allows NYA-Sattrack to operate them with the same set of commands or calls. The unique commands from NYA-Sattrack are received by the DLL and it then calls the corresponding DLL-subroutines, which address the related antenna-specific functions.

6.9.1 Software interface to NYA-1 antenna

The IEEE-488 interface standard, as being used for communication between the NYA-1 antenna ACU and an antenna operation computer, may be regarded as a relative old standard, but it is still supported by some manufacturers. The currently leading company in this sector is probably National Instruments (NI). It still provides interface-hardware, software and even adapters from standard USB computer interfaces to IEEE-488 (Figure 54). These USB-

Figure 54: USB to GPIB (IEEE-488) adapter from National Instruments

adapters do not longer need a special interface board in a computer, because all interface electronics are integrated in the IEEE-488 plug case. It was thus decided to use NI-technology for the computer interface, implying also the use of a NI software driver.

A variety of software drivers for their hardware interfaces is provided by NI. The use of these drivers requires a high number of declarations for variables, constants and functions in the calling program. NI provides example files with declarations and small functions for several programming languages, to be used directly in user source code, e.g., through an INCLUDE statement. No such file was available for PowerBASIC directly, but the files “niglobal.bas” and “vbib-32.bas” were identified to apparently fit best to the syntax of PowerBASIC. They contain code for declarations and functions, addressing routines in the NI-provided driver “gpib-32.dll. The parts of “niglobal.bas” and “vbib-32.bas” which are required for the communication between NYA-Sattrack and IEEE-488 boards were modified according to PowerBASIC syntax and properties (e.g., different variable type definitions) and included in the source code of the NYA-Sattrack software interface for NYA-1 antenna operation. The resulting “NYA-1 antenna-DLL” proved to work with NI IEEE-488 interface boards inside a computer (former setup at Ny-Ålesund) and NI USB-IEEE-488 adapters (actual setup).

The NYA-Sattrack software interface module (antenna DLL) for NYA-1 reads the primary and secondary IEEE-488 interface address of the antenna system from the NYA-Sattrack configuration file. This address information is required for ACU communication because IEEE-488 is a bus-interface standard and thus there could be more than one listening device with a connection to the same communication line. The IEEE-488 interface device of the antenna operation computer must be configured as the master device. The corresponding parameter must be set by the user (once only). The NYA-Sattrack interface module handles IEEE-488 interface messages (driver protocol), such as detected interface hard- and software errors, and “translates” messages from and to the ACU, respectively the antenna. The message structure for ACU communication was available from manufacturer manuals. An example for message translation (transformation) is the exchange of antenna positioning information (azimuth, elevation). In communication with the ACU these values are sent and received as 16 bit hexadecimal numbers in a scaled binary coded angle format (engineering units, e.g., 0001H = 0.00549°), rather than degrees in the common decimal format as used by NYA-Sattrack. Another example is the antenna system status with 32 independent status bits, e.g., for the actual states of all limit switches and the azimuth sector information, which is received

by the NYA-Sattrack antenna-DLL from the ACU as 2 hex-bytes and then evaluated and translated to clear text messages for the program GUI and logging.

One main target for the new software was to prevent antenna positioning system stops of NYA-1 due to movements to the azimuth axis limits as they occurred with the formerly used software. The developed strategy is to position the antenna prior to each pass in that azimuth sector (sector 0 = 0° - 360°, sector 1 = 360° - 720°) that provides maximum freedom for the antenna movement, according to the AOS azimuth of a next satellite pass. The antenna always takes the shortest way to a commanded direction as observable and noted in the manual (Scientific Atlanta 1996 b), and so a single position command might not move the antenna to the desired azimuth sector. There are no dedicated ACU-commands to force the positioning to a preferred sector or to dictate a turn direction. A way out was found with a guiding of the desired antenna movement by a number of positioning commands, starting with a position close to the current direction (Az_now) at the corresponding turn side and ending at the finally desired direction. The best sector to start a next satellite pass tracking and the turn direction to the start direction is chosen by the NYA-1 interface module according to Table 7.

AOS azimuth of next pass	Starting sector providing at least +/-180° freedom for next pass tracking	Detected current antenna direction Az_now = azimuth reading 0-360° Sector 0 = 0 - 360° Sector 1 = 360 - 720°	Mandatory azimuth turn direction towards next pass AOS direction
< 180°	1	Sector 0, any Az_now	Clockwise
		Sector 1, Az_now < AOS next pass	Clockwise
		Sector 1, Az_now > AOS next pass	Counter-clockwise
> 180°	0	Sector 1, any Az_now	Counter-clockwise
		Sector 0, Az_now < AOS next pass	Clockwise
		Sector 0, Az_now > AOS next pass	Counter-clockwise

Table 7: Decision logic for best starting sector and antenna turn direction

Experiments showed that this concept worked in general, but that smooth antenna movements could not be achieved by commanding antenna directions at low rates, e.g., once per second only. The NYA-1 antenna then moved fast to the desired direction, rested there for a short time and moved to the next desired direction rapidly again, which resulted in a somehow sufficiently continuous but jerky tracking. A smooth antenna movement was obtained with higher command rates and an additional function to support this operation mode was implemented in the software interface for NYA-1. The function splits movements according to incoming tracking commands (from main tracking module, usually at 1 Hz) into a series of small tracking steps. The series of intermediate tracking commands is then sent to the NYA-1 ACU with a corresponding timely spacing, resulting in a higher internal command rate. The command rate, respectively the split factor to be applied by this function, can be configured in the program configuration file (parameter “interpoint”). Good results were observed with a command rate of 5 Hz, which is now the standard setting for NYA-1 routine operations.

The ACU was initially expected to support an antenna-tracking mode that is based on commands of desired directions paired with corresponding axes movement rates. This is the regular tracking mode for NYA-2. However, the author did not succeed to implement this mode during the on-site installation in summer 2014, although the ACU manual describes a dedicated rate mode. In 2016 it was possible to move NYA-1 with NYA-Sattrack (experimental extension of antenna DLL) in the ACU’s rate mode, but without a possibility to command desired positions at the same time. It was concluded that either one of the both modes can be used, but not a combination of them. An antenna operation in the exclusive rate mode appeared to be more risky than in the already practised exclusive position mode, as a loss of connection between NYA-Sattrack and the ACU (e.g., due to computer problems) would not stop the movement, which would finally end at the systems axes limits. It was thus decided to continue the positioning of NYA-1 with the commanding of individual direction series as described above.

6.9.2 Software interface to NYA-2 antenna

The NYA-2 antenna communicates with a connected computer (antenna operation PC) using a proprietary format of the antenna manufacturer. The task of the NYA-Sattrack software interface (DLL module) for the NYA-2 antenna is the handling of the communication between the main program and the antenna. It must thus consider the corresponding format, syntax and procedural issues. The communication is established via a regular RS-232 serial computer

interface. Windows computer operation systems provide a standard driver for such interfaces so that (different to NYA-1) no complex interface protocol handling or extra software drivers were required on the side of the connecting computer and NYA-Sattrack. Many details of the syntax and the format for communication with the antenna are described in the manufacturer manual (CGC Technology Ltd 2005) and some more were found by experiments. Most required program structures were implemented in the interface module in a straightforward manner. Some more effort was required to address the properties of the "X over Y" axes positioning system.

The NYA-Sattrack main program handles directions (azimuth and elevation) in the local horizontal coordinate system. This kind of directional information cannot be used directly with the NYA-2 antenna as the antenna's ACU works with values according to the "X over Y" axes positioning system. A suitable transformation method from the azimuth / elevation system to the "X over Y" system (commanding of directions) is described in the manufacturer manual and was taken as a guideline for the generation of corresponding software interface code. The reverse transformation, from "X over Y" (feedback from antenna) to azimuth and elevation (needed, e.g., for logfiles), was not described, but could be realised similarly, basically in two main steps, as shown with equations (44) and (45). The NYA-2 antenna manual uses the terms "upper axis" and "lower axis" (instead of "X and Y"), which are used here also.

Step 1: Calculation of Cartesian direction vector

$$\begin{aligned} X_{Satellite} &= \sin\,(upper\ axis) \\ Y_{Satellite} &= \cos\,(upper\ axis) * \sin\,(lower\ axis) \\ Z_{Satellite} &= \cos\,(upper\ axis) * \cos\,(lower\ axis) \end{aligned} \tag{44}$$

Step 2: Calculation of elevation and azimuth angles from Cartesian direction vector

$$\begin{aligned} Elevation_{Satellite} &= \arcsin\,(Z_{Satellite}) \\ Azimuth_{Satellite} &= \arccos\,\frac{Y_{Satellite}}{\cos\,(Elevation_{Satellite})} \end{aligned} \tag{45}$$

The PowerBASIC compiler does neither provide an arc sine function nor an arc cosine function. These functions were thus replaced in the program code by corresponding functions of the arc tangent as defined for an angle α by equations (46).

$$\arcsin(\alpha) = \arctan\left(\frac{\alpha}{\sqrt{1-\alpha^2}}\right)$$
$$\arccos(\alpha) = \frac{\pi}{2} - \arctan\left(\frac{\alpha}{\sqrt{1-\alpha^2}}\right) \quad (46)$$

Commands for the movement of the NYA-2 antenna must provide the direction to be reached at the end of the positioning step (e.g., now plus one second) and the corresponding axes movement rates. These rates are calculated in the software interface module from two pairs of azimuth and elevation values, one for the actual time and one for the actual time plus 1 second, as received from the main tracking module (section 6.8.1).

The performance of the transformation routine program implementation was investigated and found to be good in general (error < 10^{-11} °). However, some additional program code was required to handle special constellations of the X-Y axes system. The tests and the resulting supplementary code for the software interface module are described in section 6.13.1.

6.10 Other functions and modules

6.10.1 Test mode function

NYA-Sattrack can be started without a connection to an antenna system, but under regular operation conditions the program does not continue a satellite tracking sequence if it detects the missing connection to an antenna at AOS-time. For testing purposes it can be useful to simulate a connected antenna system, at least partly. A dedicated test mode can be selected by an operator through the test and maintenance menu or by a corresponding entry in the program configuration file (causes automatic start in test mode). When operated in test mode the program ignores failure messages due to the missing antenna link and feeds back the commanded directions as detected directions. This allows the generation of skyplots and logfiles without a connected antenna and supported many tests during program development, e.g., the program stress test as described in section 6.13.3. The selection of the test mode changes the station info GUI field background colour to red and adds the entry “test mode” to the same field, the logfiles and the GUI skyplot graphic.

6.10.2 Program configuration

A configuration routine reads the program configuration file, checks the integrity of important definitions in the file, sets related program parameters accordingly and displays some information on the main GUI immediately. The routine is called automatically at program

start (program start thread), but can also be called by an operator though the test and maintenance GUI. The routine checks the defined paths in the program configuration file, e.g., the incoming directory for jobfiles, and creates them if they do not exist yet. Detected inconsistencies are sent to the program logfile as error messages.

6.10.3 Sun direction module

The position of the sun is calculated by a routine in a dedicated "sun direction module". The routine inputs are a civilian time and local geographic coordinates and the output is the corresponding direction to the sun's azimuth and elevation values. The implemented routine algorithms were mainly developed from formulas, constants and explanations as found in the Internet (livioflores-ga 2006) and a NOAA publication (National Oceanic and Atmospheric Administration 1997), which included FORTRAN source code. These were cross-checked, as far as applicable, with an astronomical almanac (United States Naval Observatory 2014). Later the performance of the implemented NYA-Sattrack code (PowerBASIC) was assessed (compared) with the published accuracy of another routine (Andreas 2008-2011), which is described in section 6.13.1.

6.10.4 Interface to spectrum analyser

The application of the scan and sun-tracking functions (6.8.2 to 6.8.5) for the measurements in this work, e.g., for the determination of antenna directivity (section 9.3), require a simultaneous logging of received signal levels and antenna directions. The antenna directions are logged by NYA-Sattrack in logfiles that are either dedicated to satellite tracking or tracking of the sun. The strength of received signals as received during experiments with the antennas was initially (experiments in 2015) recorded from the output of a telemetry receiver. This approach turned out to be problematic due to an imperfect synchronisation between receiver measurements and direction readings, especially when the data was logged on two computers.

A software interface was developed that allows communication with a spectrum analyser FSP-13 (Rohde & Schwarz), a well suited instrument for many types of radio signal measurements, via a regular RS-232 standard serial interface. The corresponding interface parameters must specified in the NYA-Sattrack program configuration file and an operator can check the connection to the analyser with a test button (test and maintenance menu) prior to the start of an experiment. The data from the analyser is received and logged in an

additional column of the logfiles if the operator selected this. NYA-Sattrack requests the analyser to send readings from an automatic noise power peak marker function (FSP-13 firmware). The corresponding command is issued from the precise timing loop (200 Hz) within the tracking loop (Figure 52) right after the commanding of antenna directions, which delivers also the actual antenna directions in response.

The analyser interface function was used first in 2016 and proved to be very useful (e.g., for measurements of antenna directivity, described in 9.3.3). It was also used for certain timing tests as described in section 6.13.2.

6.10.5 Logging functions

NYA-Sattrack writes major activity details, preceded by time stamps (resolution 1 s), as short messages in a program logfile. The program logfile contains messages from the program start (e.g., program version), start and stop of satellite tracking, updates of jobfiles and twoline element files, user initiated actions (e.g., changes made through test and maintenance menu) and detected problems (e.g., tracking abortion before LOS). Even a user selected program termination is logged, to allow a differentiation to eventual program crashes or operation stops due to main power outages. Log messages are generated directly by the program routines that initiated or detected the events.

Separate logfiles are generated for each tracking of a satellite or the sun (examples in appendix). The filenames are built from tracked objects acronyms, orbit numbers, AOS-times and an antenna acronym (e.g., GRACE_1_74039_20150601_170814_NYA1.trk). An additional innovative way of logging was realised with the automatic storage of skyplot displays at LOS times (user selectable), as described in section 6.11.2.

6.11 Display of relevant program data

It was desired to build a Graphical User Interface (GUI) for NYA-Sattrack that displays all important system and antenna operation information to a user in a direct way. Some information should be displayed in a map-style graphic. Graphics might be generated best with dedicated or more modern programming languages (e.g., JAVA), but this was not required for the basically simple contents to be displayed for satellite tracking. It was thus decided to develop the GUI as a standard program window with graphic means that were available through PowerBASIC functions.

The developed program GUI has some fields to display static information (e.g., the station name) and several to display non-static information (e.g., the actual system time). The static information fields are filled once during program start or when an operator initiated a reread of the program configuration file. Non-static information types that are not influenced by the program itself (e.g., the system time) are checked for changes frequently and updated by a dedicated display update function. Display updates according to parameter changes induced by program routines are managed by theses routines directly (e.g., commanded antenna movements). Also the antenna DLLs can modify entries in the GUI fields directly.

6.11.1 Alphanumerical displays

Most of the relevant program operation information is displayed by NYA-Sattrack with alphanumerical displays. The majority of the corresponding display fields need only low information update rates, e.g., one refresh after some minutes (e.g., data related to next satellite pass), some hold static information (e.g., the station name). These fields are filled with information by the routines that read or manage the information, e.g., the routine to read the station configuration file.

Information with frequent changes is, e.g., such with a direct relation to the actual time, like the system time or the “time to AOS”. The function for the update of these time-related display fields is called frequently by the main timing loop at a rate of about 10 Hz (see section 6.6.5). The contents to be displayed are not refreshed at that high rate, as this would result in unnecessary high system (CPU) load. The function for the update of time-related display fields thus checks first which contents (program variables) to be displayed have changed since the last update. Then only the corresponding fields are updated while all other fields are not addressed by any action. This strategy was found to reduce the CPU load significantly, most probably because a simple matching of strings (performed by program) produces by far less calculation effort than calls for graphical functions, which are performed by the computer operation system (Windows). The display fields related to antenna directions require frequent updates during tracking activities and are handled by the tracking module directly, right at the times when the corresponding values have changed. The described approach, namely frequent checks for changed contents to be displayed with selected and consequently less frequent and less comprehensive display updates, produces only little processing load, while still allowing a low response time to changed values.

6.11.2 Graphical display (skyplot function)

A function to plot direction-related information in a graphical display has been developed and implemented into NYA-Sattrack. The main task of the function is to show the local horizon mask, satellite pass tracking directions and sun directions, all from the perspective of the satellite-receiving station, quasi as a skyplot.

PowerBASIC graphical functions work with a 2-dimensional Cartesian coordinates system. The NYA-Sattrack skyplot display was defined as a map with horizontal and vertical extensions *h* and *v* (Figure 55). The skyplot display uses so called dialog units, which are provided by the Windows OS and offered by the compiler, as they adapt more flexible to different computer screen resolutions and font sizes than pixels. The actual number of generated pixels, e.g., for the smallest possible graphical element in this unit system with a size of 1 x 1 dialog units, thus depends on the actual screen resolution and font size. However, the smallest dialog unit generates a minimum of one pixel in any case.

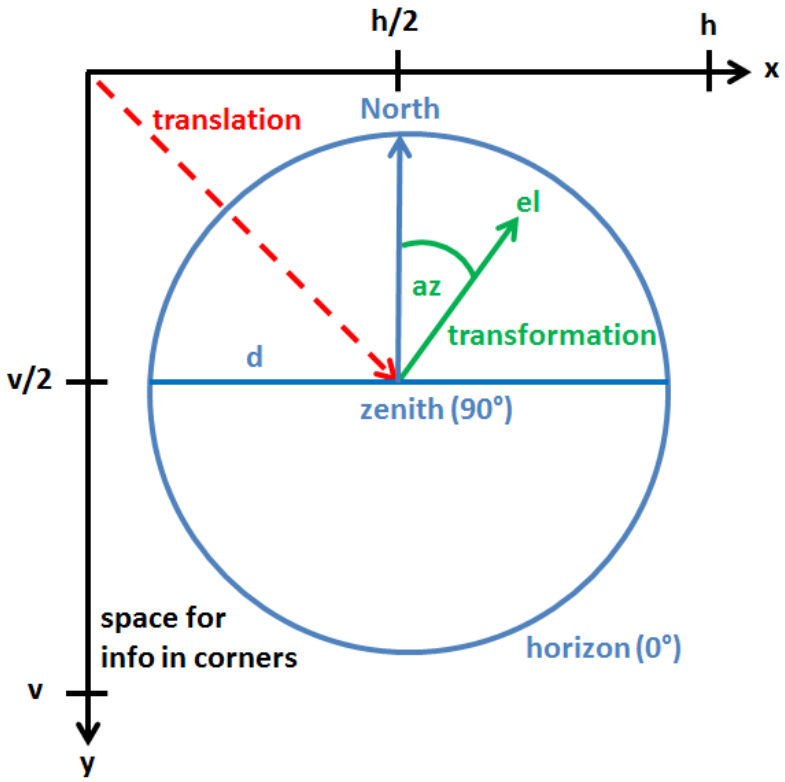

Figure 55: Construction scheme of NYA-Sattrack skyplot display

All directional data in the skyplot display is plotted inside a circle with the diameter *d*. The circle represents the horizon, respectively the 0° elevation line, while the centre of the plot corresponds to the zenith (90° elevation). The positions of graphical elements to be displayed, e.g., the end of the green vector in Figure 55, must be passed to the PowerBASIC graphical function as pairs of *x*- and *y*-values (Cartesian), but directional data is available as values of elevation and azimuth only, corresponding to the local horizontal coordinate system. It was thus necessary to apply a transformation for this data. A translation must be applied also, due to the different origins of the two coordinate systems. The offset between the origin of the

map coordinate system (upper left corner of map) and the origin of the horizontal coordinate system (centre of map) is $h/2$ and $v/2$ respectively. The combination of a regular transformation (horizontal coordinates to two-dimensional Cartesian coordinates) and a translation is shown with equations (47). The calculation of a z-coordinate is not required, as it is not mapped (z-axis orthogonal to x-y mapping plane).

$$x = \frac{h}{2} + \frac{d}{2} \sin az \cos el$$
$$y = \frac{v}{2} - \frac{d}{2} \cos az \cos el \tag{47}$$

where

x, y = Cartesian coordinates for skyplot map [dialog units]

h, v = horizontal and vertical size of skyplot map [dialog units]

az, el = coordinates of object to be plotted on map (horizontal coordinate system) [°]

d = diameter of 0° circle (horizon) [dialog units]

Figure 56 shows an example of the skyplot display, when directional data is transformed with equation (47). The directions to the satellite to be tracked are displayed as a blue bow, which spans from AOS- to LOS-directions. The satellite transmitter is operated in the corresponding time interval and two shades of blue indicate the times, respectively directions, with data transmission (dark blue) and without data transmissions (bright blue), based on information from the currently used jobfile. The actual antenna direction is displayed by a bright green circle with a certain extension to indicate that the antenna has a considerable beam width (symbol not up to scale).

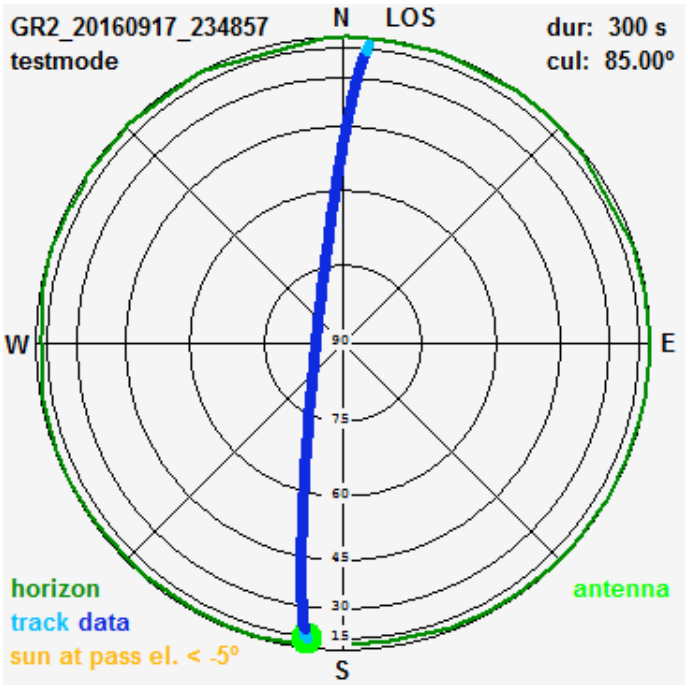

Figure 56: Skyplot display with "zoom" on zenith zone

Some additional information is positioned in the corners of the skyplot, e.g., the pass duration, the pass culmination, and a plot name (built from the satellite acronym and the AOS time) to tag it according to the currently running, the just finished or the next satellite tracking, depending on the actual program phase. The message "testmode" indicates that NYA-Sattrack was in the program testmode when the plot was generated. The local horizon (antenna view mask) is plotted in a dark green colour. Input is read from a dedicated file (6.3.1) and stored in a program memory array at program start, to be available for fast access by the skyplot routines. The shape of the local horizon is hardly visible in Figure 56, because the mapping with equation (47) results in a kind of "zoom" on the zenith zone, at the price of a low resolution for low elevations.

An opposite effect, namely a "zoom" on the horizon with a suppression of the zenith area, was achieved with equations (48).

$$x = \frac{h}{2} + \frac{d}{2} - \frac{d}{2}\sin az \cos el$$
$$y = \frac{v}{2} - \frac{d}{2} - \frac{d}{2}\cos az \cos el \qquad (48)$$

Figure 57 shows an example of the skyplot display with a "zoom" on the horizon area, which is thus displayed in more detail (different satellite pass, but same horizon data as in Figure 56). The track of the very short satellite contact at low elevations (duration 90 s, culmination ~16°) is at least resolvable, which would not be possible with the mapping algorithm for Figure 56 (equations (47)). The actual direction to the sun (according to system time) is displayed as a single spot (legend entry "sun now"). This allows a fast analysis if possible reception problems could be caused by the sun, which is most probably the case when it is

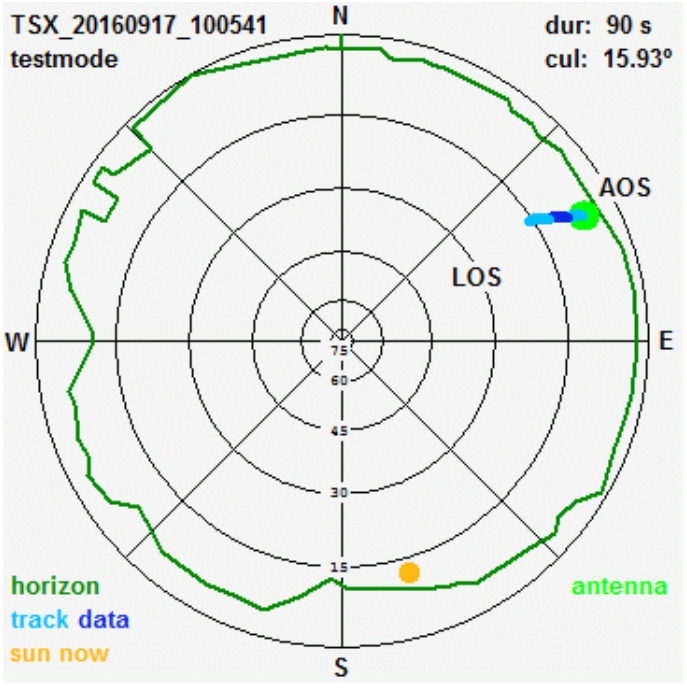

Figure 57: Skyplot display with "zoom" on horizon

found on or nearby the antenna directions track. The both "zoom types" according to Figure 56 and Figure 57 allow a closer view on the potentially critical zones, which is the zenith zone during keyhole passes and the (masked) horizon when tracking with low elevations. However, the probably most "natural" mapping from the viewpoint of an observer at a ground station is obtained with a linear (proportional) elevation scale, which was achieved with equations (49).

$$x = \frac{h}{2} + \left(\frac{d}{2} - el * C\right) \sin az$$

$$y = \frac{v}{2} - \left(\frac{d}{2} - el * C\right) \cos az \tag{49}$$

where

C = elevation mapping scale factor [dialog units/°]

(Number of dialog units along $\frac{d}{2}$ divided by 90°)

Figure 58 shows a screenshot of the skyplot display with a linear elevation scale. It was taken at a time when a satellite was tracked (simulated in testmode), shortly before LOS. The bright green antenna symbol coincides with the satellite symbol (red dot), which is an indication for an actually correct antenna-pointing. A trace of earlier antenna directions during the satellite pass is displayed also (bright green), based on antenna system feedback data, as collected and stored by the main tracking module in a dedicated program memory array (see section 6.8.1).

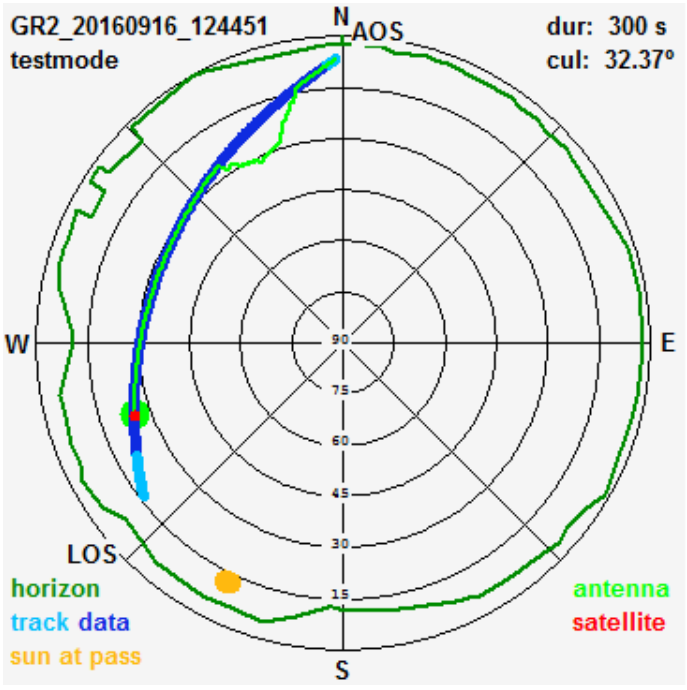

Figure 58: Skyplot display with linear elevation scale

The antenna trace must be expected to be in perfect alignment with the pre-calculated satellite track (blue colours). A temporary wrong antenna positioning in the azimuth interval between

325° and 350° (close to AOS) was commanded here deliberately to demonstrate how such system malfunction would be displayed on the skyplot. A malfunction like this could be caused by several sources in principle, e.g., a wrong dissemination (program) or reception of positioning commands (defective communication lines) or hardware problems (antenna drive and position feedback systems). The sun directions for the time interval of the pass (legend entry adapted to “sun at pass”) are plotted as a short trace. This function is user selectable (compare Figure 57), but no sun direction is shown if it is too far below the horizon (Figure 56, no sun symbol, legend entry “sun at pass el. < -5°”).

A user can switch between the three described projections at any time without causing significant processing load for the computer (CPU) because the mapping coordinates for the directions to the satellite, the horizon mask and the sun (for the satellite tracking interval) are calculated and stored for all projection types in memory arrays during the pass preparation process (6.7.5). This measure prevents high processing loads for the automatic update of the skyplot display or a desired change of projection (by user). The mapping of the actual directions of the antenna, the satellite and the sun (if user selected “sun now” function) must be calculated by the program in real-time, but don’t generate noticeable processing load neither. An operator can save the full skyplot graphic to a file (bitmap format, ~390 KB / file) by pressing the “save skyplot” GUI button at any time. A skyplot graphic is also archived automatically (by default) as a “bitmap-logfile” at the end of each tracked satellite pass, when it shows the complete tracking process (example in Figure 68).

None of the displayed lines and numbers of the skyplot function, including the grid of elevation isolines, the line tags and acronyms for capital direction, is loaded from a static source, such as a bitmap. All these elements with their map positions are defined by source code and drawn again and again with each automatic update of the skyplot display (1 Hz). This approach keeps the skyplot function open for changes and additions, e.g., to include more information or other types of maps and projections.

The skyplot logging function has proven to support fast and efficient checks and troubleshooting, especially when the generated graphical logs are displayed with the skyplot viewer (7.3.2, Figure 68), which is a related tool of NYA-Sattrack. Anyway, the function can be de-selected, e.g., to save hard disc space.

6.12 Program installation

The installation process for NYA-Sattrack is simple. The program binaries (main program and antenna DLL) are placed in the desired software operation directory (e.g., C:\NYA-Sattrack). The program configuration template file must be edited by an operator according to the operation conditions. Among other settings it is required to declare which antenna DLL file is to be used (depends on antenna type) and which directory has to be scanned by NYA-Sattrack for incoming jobfiles and twoline elements files. Mandatory entries in the configuration file are checked by NYA-Sattrack at program start. Missing or clearly wrong entries, e.g., not existing directories, are reported to the program logfile. Default program directories, as those for archiving of logfiles, are generated by NYA-Sattrack automatically, in case that they were not found at program start.

A jobfile and twoline elements are needed to start regular satellite tracking operations. Copies of the jobfile in use, the previously used and the next jobfile to be used (e.g., addressing operations of the subsequent week) are stored in the program's working directory.

6.13 Test activities

Most of the individual functions and routines of NYA-Sattrack were tested and validated during the programming works. Simple program functions were regarded to be implemented in a sufficient way when the functions showed reasonable results and did not cause malfunctions or significant CPU-load. Some more effort was driven to evaluate and validate the proper function of program elements that affect the antenna-pointing accuracy. One example is the transformation between the horizontal (azimuth and elevation) and the X/Y coordinate systems (NYA-2 system axes angles). Another one is the precise timing of antenna movement commands.

6.13.1 Test of program calculation accuracy

NYA-Sattrack has no internal module for satellite orbit predictions and relies in this point on the accuracy of external programs. It uses an adapted version of the "Spacetrack Code" (6.7.4), which is known to be the basis for the calculations of the commercial program package STK as well. As a first test it was confirmed that the output (directions to satellite) of both programs (executable for NYA-Sattrack and STK version 11.0) is basically the same. The satellite directions for several contacts with the NYA-station were computed for different

dates and times of a day. It was found that the maximum differences were 0.002° for the azimuth and 0.001° for the elevation. The output resolution of both programs was 0.001° and so it can be concluded that the maximum deviation between the tested programs is smaller than 0.003° for the azimuth and smaller than 0.002° for the elevation

Predicted directions are in general not subject of calculations in NYA-Sattrack, beside the antenna boresight compensation, which is a not further tested simple summation (equation (36)). An exception is the operation of the NYA-2 antenna, which requires some transformations of directions including several trigonometric operations (6.9.2). Different series of azimuth and elevation values (range azimuth 0-360°, range elevation 0-90°, step-size 0.0001°) were generated by NYA-Sattrack (temporarily implemented function) and transformed to the X-Y domain. The resulting data was then transferred back to the azimuth-elevation domain and the total error (forward-error plus backward-error) was determined as the difference between the output and the input of the two transformations. It was confirmed that the transformations delivered high accuracies of better than 10^{-11} ° in general, e.g., for almost all azimuth values when the elevation was between 0° and ~89.9°. Exceptions with extreme high errors (up to ~180°), were noticed when the input data azimuth was very close to 0°, 90°, 180° or 270°, independent from the elevation (if < ~89.9°), and at an input data elevation very close to 90°, independent from the actual azimuth. These cases correlate clearly with very small angels for the X-axis, the Y-axis or both and corresponding numerical errors of the trigonometric functions as used in the X-Y to azimuth-elevation transformation routines (6.9.2).

A practical solution of the problem was found with the definition of special cases in the X-Y to azimuth-elevation back-transformation routine. X and Y input angles between 0 and 0.000001 rad (PowerBASIC calculates with rad, rather than degree), are replaced by static values of 0.000001 rad (~0.0000573°) with preserved signs, but otherwise independent from their exact original values. This measure eliminates the high transformation errors, even for the worst case azimuths of exactly 0°, 90°, 180° or 270°, at least in the elevation range between 0 and 89.994°. The maximum errors for these extreme cases are better than 0.01° for the azimuth and better than 10^{-11} ° for the elevation (error maximum at 89.994° elevation). Especially the azimuthal error increases rapidly with higher elevations up to a climax at 90° elevation, where an azimuth is not defined. A program mechanism was implemented to limit transformation errors to 0.01° in the delicate elevation range above 89.994°. A “best azimuth”

with values of either 0°, 90°, 180° or 270° replaces the regular program calculation results as soon as the azimuthal error of the regular routine calculation becomes larger than 0.01°. This was found to occur if either the X- or Y- axis angle is 0.000001 rad (or smaller before assignment of static value), while the other axis angle is smaller than 0.0058 rad.

The implemented program code for the described special cases aims on the reverse transformation routine (X-Y to azimuth-elevation), which is used to display and log reported antenna directions, and results in maximum error of 0.01° at 89.994° elevation. The accuracy of the forward transformation (azimuth-elevation to X-Y), which is the only relevant for the antenna-pointing accuracy was equal or better than 10^{-11} ° in all cases.

The sun direction module of NYA-Sattrack (6.10.3) is used for routine operation to place a sun symbol or a sun track on the GUI skyplot display. This display function has no relevance for the antenna-pointing accuracy, but was tested to be in accordance with the calculated values for the sun directions. The sun direction module is also used by NYA-Sattrack as a central function for antenna system calibration tasks to determine the antenna boresight offset (9.1), the antenna (main lobe) directional characteristics (9.3) and the G/T performance (9.2), all requiring a high accuracy of sun direction computations. The accuracy of the sun direction module computations was cross-checked with computations from external sources. The apparently best reference was found at the website of the US “National Renewable Energy Laboratory” (Andreas 2008-2011), which provides an online tool and corresponding program code for the calculation of sun directions. Both are based on published algorithms (Reda and Andreas 2004). The authors of the paper claim that their methods and published code provide angular certainties of +/- 0.0003° (for the years -2000 to 6000). A comparison with the sun directions as calculated by NYA-Sattrack for the times of the measurements (section 9) showed deviations of up to 0.01° for the azimuth and up to 0.02° for the elevation. It was concluded that the currently implemented routine for the calculation of sun directions in NYA-Sattrack might be less accurate than possible and that the measurements in section 9 might profit from corresponding corrections, but this point was not investigated any further in this work.

Some calculations are made in the program to support the display of azimuth-elevation values on the GUI skyplot graphic. The accuracy of these transformations has no relevance for the antenna-pointing accuracy and so the tests for these routines were limited to the visual confirmation of reasonable displays on the skyplot graphic.

6.13.2 Test of program timing performance

Most of the program loops have no relevance for the antenna-pointing accuracy and were thus not tested intensively with respect to precision, even when they use the NYA-Sattrack program-specific ss2000 time scale (6.6.1) or the fine time scale (6.6.4). They were all confirmed to work as planned and considered to be proofed by the flawless program flow. Some more attention was paid to the accuracy of the computer system clock and the performance of the tracking loop (6.8.1) as both is relevant for the antenna-pointing accuracy.

The program internal timing accuracy during satellite tracking was assessed in a first approach by registration of system time stamps with 1 ms resolution (PowerBASIC TIMER-function), which were logged right at the moments when positioning commands were sent to an antenna (function temporarily implemented in NYA-Sattrack). The logged data showed none or very small variations in the 1 ms domain (e.g., +/- 1 ms) over the typical time intervals of a satellite contact (e.g., 5 minutes), but occasionally some "jumps" of 10 ms. This behaviour could not be explained from analysis of program code and it was suspected that it was related to an unstable PC system time or the performance of the used PowerBASIC TIMER-function. Some clarifications were obtained by analysis of the computer system time evaluation relative to GPS-time, as monitored by the new time keeping program NYA-GPS-Sync (6.3.3). The PC system time of a computer at NYA was compared by the program with the NMEA-messages and pps-signals from a local GPS-receiver at a rate of 1/5 Hz.

Figure 59 shows the recorded data according to a monitoring period of 24 hours. The total time-offset (PC-GPS) accumulates to more than 0.9 second in that time with an apparently linear mean drift rate of about 38.3 ms/h. This result was not surprising, but anyway confirmed that a PC system clock must be controlled by a more accurate clock to execute precise timing tasks.

The time offset evaluates with a constant mean rate (drift), but apparently in a step-like manner with a step size of 10 ms, rather than continuously. The observed step-size character is interpreted as a quantisation error due to the limited resolution of the PowerBASIC TIMER-function, as it is used in the NYA-GPS-Sync program. Program calls of the TIMER-function return the system time with a numerical resolution of 1 ms, but the compiler documentation states for the function that *"The resolution is about 1/100 of a second on NT-based platforms, or 1/18th of a second on earlier platforms"* (PowerBASIC, Inc. 2012). It was concluded that

the numerical resolution of 1 ms, which is factual available for programmers, is most probably achieved (compiler method) with unreliably measures, e.g., such as interpolations. The TIMER-function thus may be useable with a 1 ms resolution in program code to access the 1 ms domain in a tentative way, while it must be accepted that the real timing accuracy is not better than 10 ms.

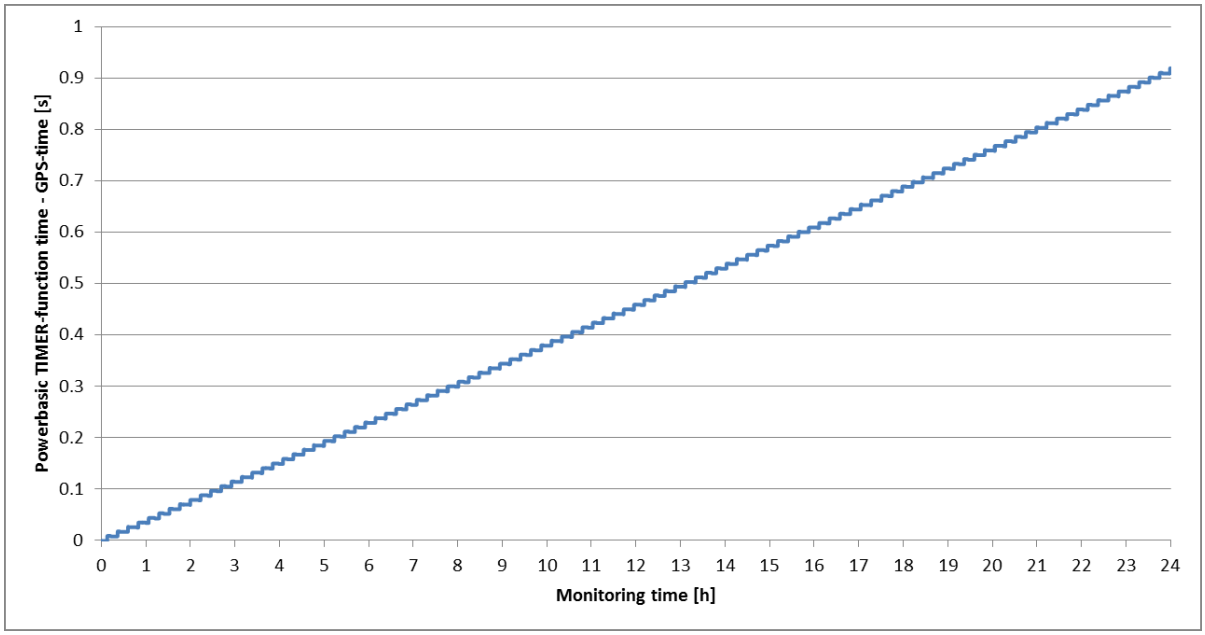

Figure 59: System time drift of a PC as determined with program "NYA-GPS-Sync"

A closer look into the time series of the experiment reveals some systematic 1 ms steps (Figure 60), which were analysed, although their accuracy was doubtful anyway, as explained above. The period $T_{1\ ms\ steps}$ (about 12 minutes) of these steps is slightly shorter than the period $T_{10\ ms\ steps}$ (about 14 minutes)

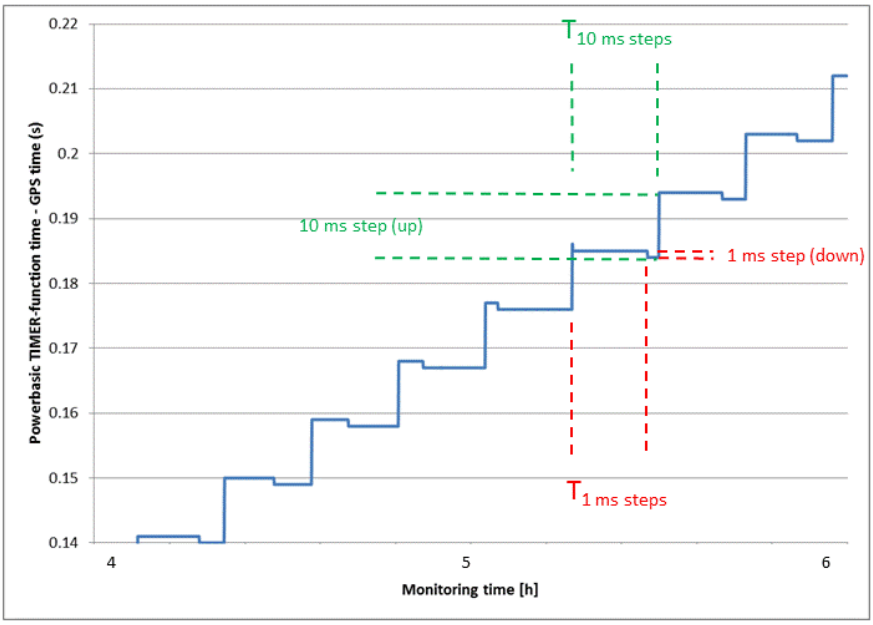

Figure 60: Closer view on PC system time drift

of the 10 ms jumps. Thus up to two 1 ms steps can appear, in this example, during the period of one 10 ms step. A 1 ms step at the end of a 10 ms step interval is marked in Figure 60, while another occurs at the beginning of the same 10 ms jump. The observed 1 ms steps are suspected to result from the program code in NYA-GPS-Sync. The execution speed, respectively the repetition rate of the program loops, is mainly determined by the used timing functions, which are the TIMER-function and the SLEEP-function. The SLEEP-function causes a program pause of the corresponding program thread for a certain time. The resolution of the SLEEP-function is 1 ms, but the total time for 1000 SLEEP-commands of 1 ms can be different to 1 second as measured with the TIMER-function. The system time logging in NYA-GPS-Sync is based on output of the TIMER-function, but the time-readings of that function are triggered by a loop that uses the SLEEP-function. The timing difference between these two functions might be very small, but it accumulates over longer times until it becomes detectable, e.g., in this case after about 12 minutes.

Another experiment with an extended setup (Figure 61) was conducted at Potsdam to determine the absolute delay of issued antenna operation commands with respect to GPS-time. Some additional program code was inserted temporarily into the DLL for antenna operation. It had the task to set the DTR line of a RS-232 computer interface to “High” and back to “Low” (after 100 ms) each time right after the last character of a direction command was sent to the antenna interface. The generated pulses thus corresponded to the program status “antenna commanding ready”.

The “antenna commanding ready” pulses were used as stop signals for time interval measurements, which were started continuously with a nominal frequency of 1 Hz by the pps pulses of a GARMIN-17 GPS receiver (GARMIN International, Inc. 2005). The measurement data of the connected time interval counter (TIC), model SR-620, was received via another RS-232 interface and logged with an interface function in the tracking loop of NYA-Sattrack (6.10.4), which was otherwise used for measurements with a spectrum analyser[7]. The TIC had a stable internal time base and the measurements were not affected by any relevant quantisation errors. The maximum instrument error could be expected to be < 1 ns after execution of the self-calibration procedure as described in the manual of the TIC (Stanford Research Systems 2006). NYA-Sattrack was operated in the sun-tracking mode (6.8.5) to generate antenna-positioning commands and “antenna commanding ready” pulses

[7] The interface was adapted to the TIC command syntax by small modifications in the code.

continuously at 1 Hz over several hours. The computer in the experiment was the same model with the same configuration as used at NYA for antenna operation (local engineering model).

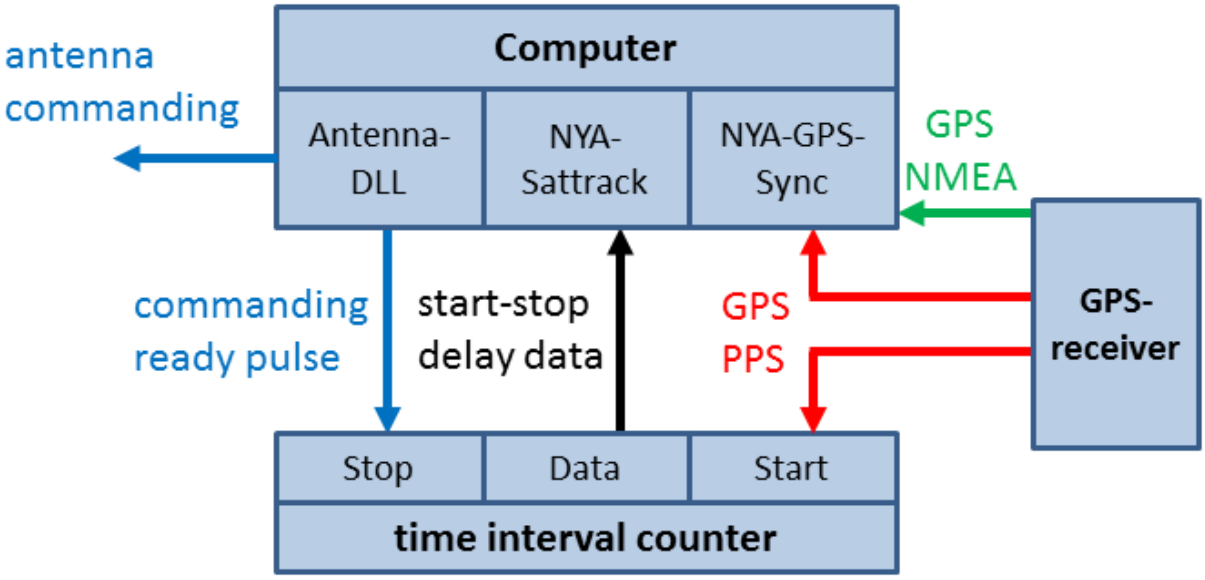

Figure 61: Setup for the experimental determination of antenna commanding delays

The pps and NMEA signals of the GPS receiver were also provided to the computer directly, as input for the NYA-GPS-Sync program (6.3.3), which was configured to synchronise the PC-clock when the offset between PC- and GPS- time exceeded 20 ms. The GPS-receiver (antenna) had a limited view to the sky as it was installed at the wall of a building at GFZ. Thus, only relative few GPS-satellites were tracked during the experiment, as shown in Figure 62, sometimes even less than 3, which was the required minimum for NYA-GPS-Sync to synchronise the PC-clock. The experiment setup was considered representative for a normal program operation, but at less than optimal or even critical GPS-signal receiving conditions.

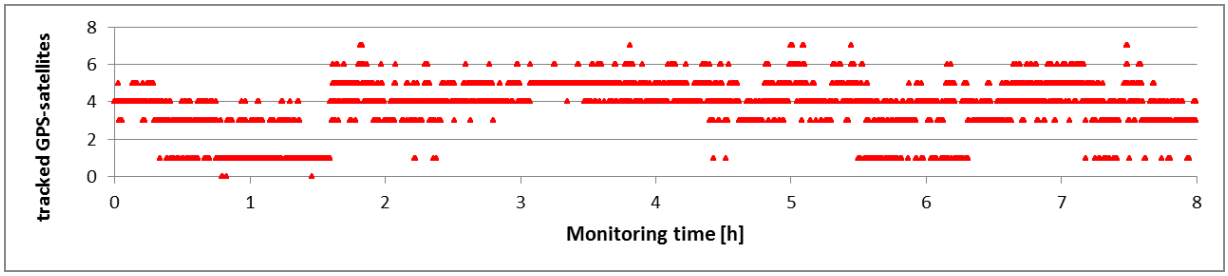

Figure 62: Number of tracked GPS-satellites during timing experiment

The blue graph in Figure 63 shows the times when antenna commanding was accomplished, relative to GPS-time, as measured by the time interval counter. All deviations from zero are thus the result of time errors. Possible sources for timing errors are the computer (system

clock) and the NYA-Sattrack program (timing of commands), but also NYA-GPS-Sync, as it controls the computer system clock.

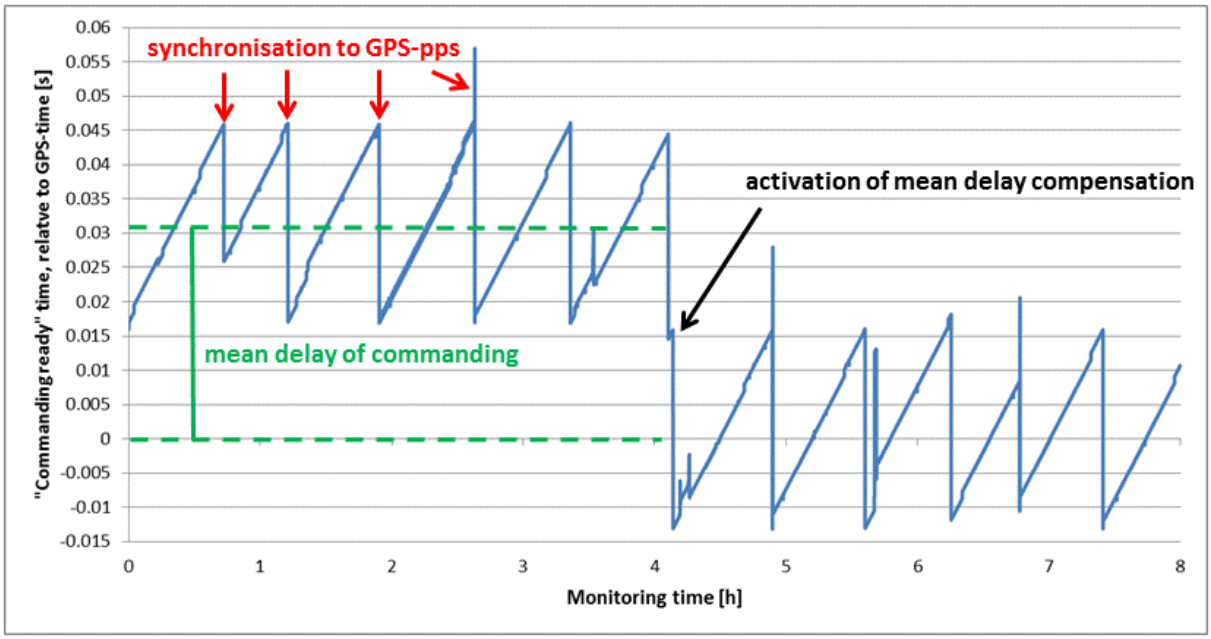

Figure 63: Timing accuracy of antenna commanding

The slowly ascending slopes in the graph (about 38 ms/h) are due to the drift of the computer clock, which caused a correspondingly delayed dissemination and completion of antenna-pointing commands. The rapidly falling flanks of the graph correspond to the times when NYA-GPS-Sync synchronised the computer clock to GPS-time. Sometimes the synchronisations are triggered by a 10 ms step (up), which occur due to the effectively limited resolution (10 ms) of the TIMER-function in NYA-GPS-Sync, as discussed above.

Some smaller anomalies with amplitudes up to 5 ms are visible, e.g., after monitoring times of 3.5 hours and 4.2 hours, sometimes as “add on” on 10 ms steps, e.g., at about 4.9 hours. These are assumed to result from the design of the precise timing loop (part of tracking loop, described in 6.8.1). That loop runs at a nominal frequency of 200 Hz and compares the system time (TIMER-function) with the due time of the tracking command in intervals of 5 ms (SLEEP function). This construction works fine in general but may become “unlocked” temporarily, e.g., when the loop is delayed due to high CPU load from other processes on the computer or a synchronisation to GPS-time. Visual correlations between the blue graph in Figure 63 and the number of tracked GPS-satellites (Figure 62) were not found.

A minimum commanding delay of about 16 ms remains in the left part of the graph, even at the time of clock synchronisation. The reason for this offset was found to be the transmission time of antenna positioning commands. The RS-232 transmissions to the antenna were configured to a data rate of 19200 bits per second, according to the regular NYA-2 antenna system parameters. Each bit thus required 1/19200 s, which are about 5.2×10^{-5} s or 0.052 ms to be transferred. A data byte has 8 bits and is embedded by1 start bit and 1 stop bit, which are 10 transmitted bits per byte in total, equivalent to a transfer time of 0.52 ms per byte. Tracking commands for the NYA-2 antenna are 31 bytes long and thus the theoretical total command transmission delay is ~16.12 ms. Commands cannot be executed by an antenna unless they are received completely. The experimental detection of "commanding ready" pulses right after the sending of the last command byte is thus considered to deliver a very realistic assessment of the delay on program- and computer-side and it explains the observed minimum offsets very well. Corresponding tests with the IEEE-488 interface, as used for NYA-1, showed no detectable command delay, most probably as the data transfer rates of that parallel interface are much higher.

The right part of the graph in Figure 63 shows the effect of a delay-compensation. It was realised by a commanding that was ahead in time with respect to the nominal commanding time. The compensation time shift was equal to the mean delay as indicated in Figure 63 and thus included the transfer time of commands and half of the computer clock drift between synchronisation steps, which sums up, based on the measurement data in this example, to about 32 ms. The effect of this measure was that the timing error was confined to about +/- 15 ms, with some outliers, but none that exceeded 30 ms.

The theoretical maximum total timing uncertainty (coincidence of all errors) after application of the described delay compensation can be calculated as the sum of all individual timing errors. It includes half of the 20 ms GPS-synchronisation threshold (the other 10 ms are part of the compensation), the resolutions of the TIMER-function (10 ms) and the SLEEP function (1 ms) in the NYA-GPS-Sync timing loop and the resolutions of the TIMER-function (10 ms) and the SLEEP function (5 ms) in the NYA-Sattrack timing loop, which results into 36 ms. Some milliseconds for a possibly imperfect delay command delay compensation might be added to that number, but it can be expected that the maximum timing error does not exceed 40 ms.

The total timing error could be reduced by a smaller threshold level of the NYA-GPS-Sync program, but this would force more frequent adjustments of the computer system time. It was not investigated if this could have a negative impact on any program- or computer-functions, while it was considered to be not required to achieve the projected antenna operation accuracy (discussed in section 6.2). The developed measurement setup (Figure 61) could in principle be used as a feedback system to compensate timing errors, based on continuous measurements during regular antenna tracking. Such dynamic timing error compensation is also considered to be not required, at least not as long as the errors (delays) are small and well characterised, as shown above.

6.13.3 Program operation stress test

Some code was implemented into NYA-Sattrack temporarily to test the program performance in a simulated long-term operation. The code caused a change of the PC system time to a point that was 5 seconds before the AOS-time of the next scheduled satellite contact (beginning of initialisation phase), just 5 seconds after each finished satellite tracking (end of termination phase). By this measure the program was operated with all program phases, but without waiting times between satellite contacts. The test was made without connection to an antenna in the program's test mode. A batch of jobfiles according to an antenna operation time of one year, including a turn of the year, was placed in the incoming-directory for jobfiles. All jobfiles and simulated satellite tracking operations were processed in the right order and all types of logfiles were generated completely and in the right way. This confirmed the long-term operation stability of NYA-Sattrack in principle (under the given test conditions) and suggested that it was stable enough to be operated with the antennas at Ny-Ålesund.

Information on the performance of the two tracking systems at Ny-Ålesund in the practical routine operation setup of antennas, ACUs and antenna operation PCs with NYA-Sattrack, is provided in sections 9 and 10.

7 NYA-Sattrack GUI (Graphical User Interface)

7.1 Main GUI

The main task of the main GUI (Figure 64) is to show all essential information according to the actual system status and scheduled antenna operations. This includes information that might appear to be not much important or even trivial, e.g., the timestamps and sizes of the actually used job- and TLE-file. However, it provides maximum certainty to an operator that a dedicated file has arrived at Ny-Ålesund in the correct version and that it is really used for the actual antenna tracking, which turned out to be important in the past, e.g., during satellite orbit manoeuvres.

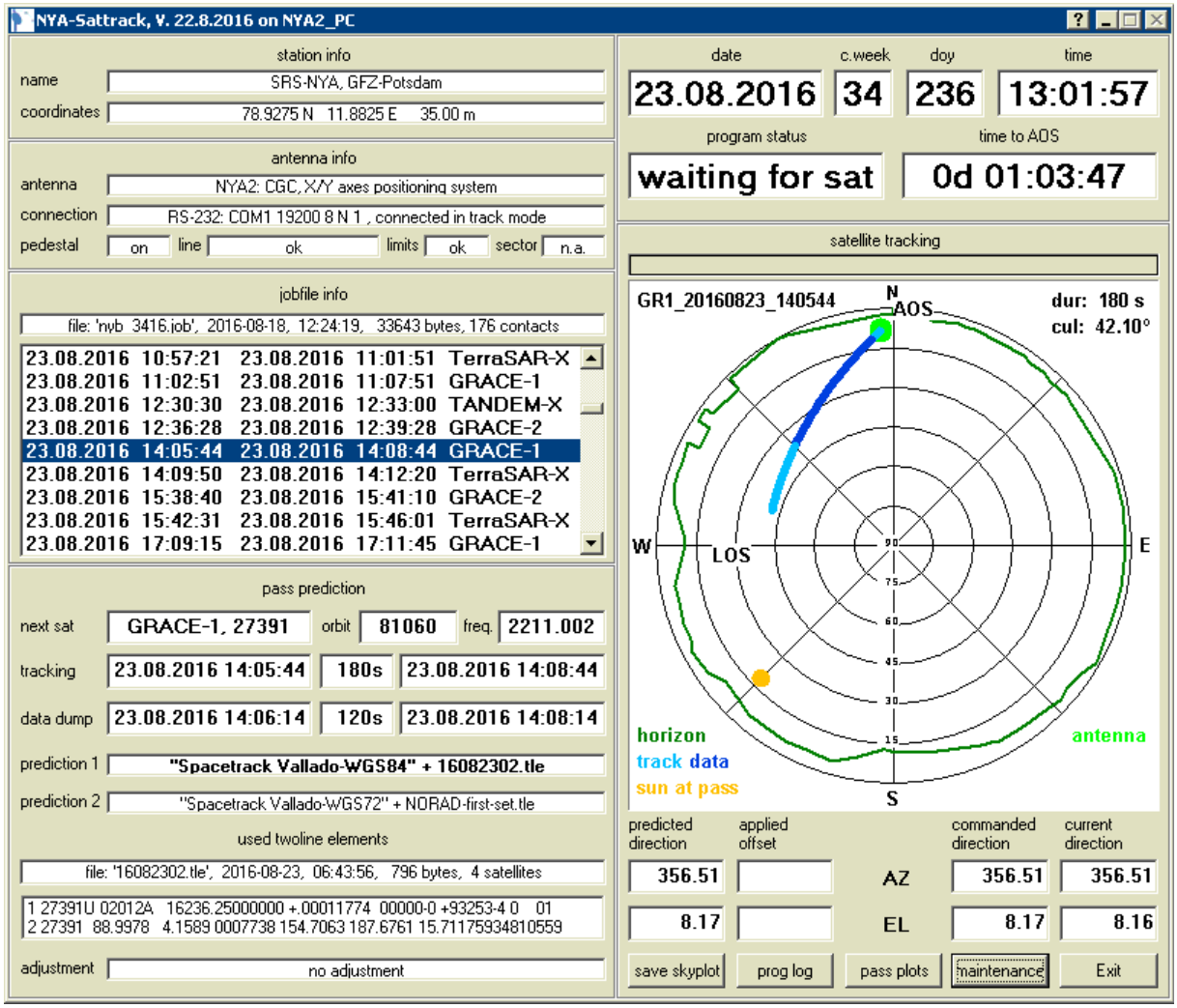

Figure 64: Main window of NYA-Sattrack GUI

On the other hand the main GUI does not provide any buttons that could interrupt or hinder the automatic program operation through a single accidental or careless operator mouse click. Even the "close window symbol" (cross in upper right corner of program window) is disabled and a click on the program's "Exit" button does not immediately terminate the program. A new window with a warning message is opened instead (Figure 65), requesting a confirmation to finish the program (applies also for the program NYA-GPS-SYNC). Changes to the program configuration or special operation modes can only be selected with the "test and maintenance" menu. The GUI windows title contains information on the program release date and the detected name of the hosting computer. A brief description of the main GUI contents and functions is given below.

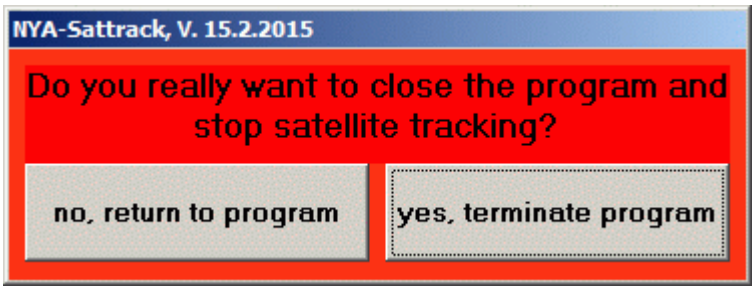

Figure 65: "Exit" button warning window

Station info

- Name and coordinates of the station (according to entries in station configuration file)

Antenna info

- The information about the antenna type is "hard coded" in the antenna DLL-file and reported to the main program. The antenna identifier (e.g., NYA-1) and the interface configuration info ("connection" and "line") correspond to the currently applied parameters, according to the entries in the station configuration file and the actual status of the connection. The status of the connection, the pedestal, the limit switches and, if applicable, the current azimuth sector (for operation with NYA-1), are displayed in corresponding fields also.

Jobfile info

- Name, timestamp, size and number of listed contacts in jobfile. The user-scrollable list shows AOS- and LOS-times for all scheduled contacts in a jobfile. The next or actually tracked satellite pass is always highlighted and shown in the middle of the list (automatic focus).

Pass prediction

- *Next sat* = name and NORAD ID (equivalent with SCN = Satellite Catalog Number) of next satellite to be tracked
- *Orbit:* Satellite orbit number (since satellite start) of next pass to be tracked

- *Frequency* = transmitter (downlink) frequency of next satellite to be tracked
- *Tracking* = start and stop times and duration [s] of next satellite tracking
- *Data dump* = start and stop times and duration [s] of next satellite data transmission
- *Prediction 1, Prediction 2* = Prediction programs and tle-files as used for satellite orbit predictions. The active prediction configuration (program + twolines) is user selectable (through test and maintenance menu) and highlighted by bold letters.

Prediction elements

- Name, timestamp and size of the actually used twoline element file and number of sets of twoline elements (number of satellites) in the file. The actually "active" twoline elements (according to next satellite contact and selected prediction) are shown also.
- *Adjustment* = information about eventually applied adjustments to predicted satellite directions, e.g., with corrective data from an auto-tracking device or corrections due to radio signal path bending from atmospheric and ionospheric properties (low elevation angles). The corresponding functions are not implemented yet.

Date, c.week, doy, time

- Actual system date, calendar week of the year, day of the year and system time

Program status: Actual program status according to

- current program activity, displayed with white background, e.g., "waiting for job", "waiting for sat", "prepare pass", "goto AOS pos", "job update", "tle update", "user move", or with yellow background , "initialisation", "tracking sat", "tracking sun",
- detected problems, displayed with red background, such as "no config", "wrong input", "passfile error", "satid-tle error", "no tlefile", "tlefile error", "calcpass error", "abort tracking".

Time to next tracking

- Display of difference between actual system time and AOS-time of next or actually tracked satellite contact (the field label changes accordingly from "time to AOS" to "time since AOS" during tracking).

Satellite tracking

- Bargraph = time proportional linear display of tracking progress
- Skyplot = shows direction angels to the local antenna horizon (mask), to the satellite to be tracked and the sun. "dur" = pass duration, "cul" = pass culmination (highest elevation). A detailed description is given in section 6.11.2.
- *Predicted direction* = actual direction to tracked object as calculated, "applied offset" = direction offset to predicted direction (e.g., from manual offset selection or square type scan function), "commanded direction" = sum of predicted direction and applied offset, "current direction" = detected direction (antenna feedback)

Buttons in right bottom area of GUI

- *Save skyplot* = Saves the actual skyplot display, inclusive legends to a bitmap file with a filename according to the tracked object and system time (e.g., "GR1_20150211_160704.bmp").
- *Prog log*: Opens an additional program window (Figure 67:) to display the program activity log. A description is given in section 7.3.1.
- *Pass plots*: Opens the viewer window (Figure 68) to display logs (text-based and bitmaps simultaneously) for tracked satellite contacts. A description is given in section 7.3.2.
- *Maintenance*: Opens an additional program window with test and maintenance functions, description in section 7.2.

7.2 Test and Maintenance menu

The options for an interactive change of program settings and some less important operation information is given to program operators exclusively through a dedicated "test and maintenance menu" window (Figure 66). This window opens after clicking the corresponding button on the main GUI. None of the applied changes to program settings are stored permanently. They are lost as soon as the program is terminated. If permanent changes are desired, then they have to be made in the program configuration file. A brief description of the information types and functions is given below.

Info

- Name of the actually used program binaries (program.exe, antenna.dll) and disk usage information for the program start disk volume (HDD)

Main Settings

- *Test mode*: Checkbox to switch between normal program operation and test mode
- *Use autotracking*: Meant to receive and apply directive correction input (e.g., from an autotracking device) for the calculated tracking target directions (function prepared but not fully implemented yet)
- *Job auto update*: Enable or disable the automatic lookup and processing of jobfiles
- *Tle auto update*: Enable or disable the automatic lookup and processing of twoline elements files
- *Skyplot logging*: Enable or disable the function for an automatic storage of skyplot displays right after LOS
- *Reread job and tle1*: Forces a reread of the jobfile and the first twoline elements file and a new calculation of satellite tracking directions.

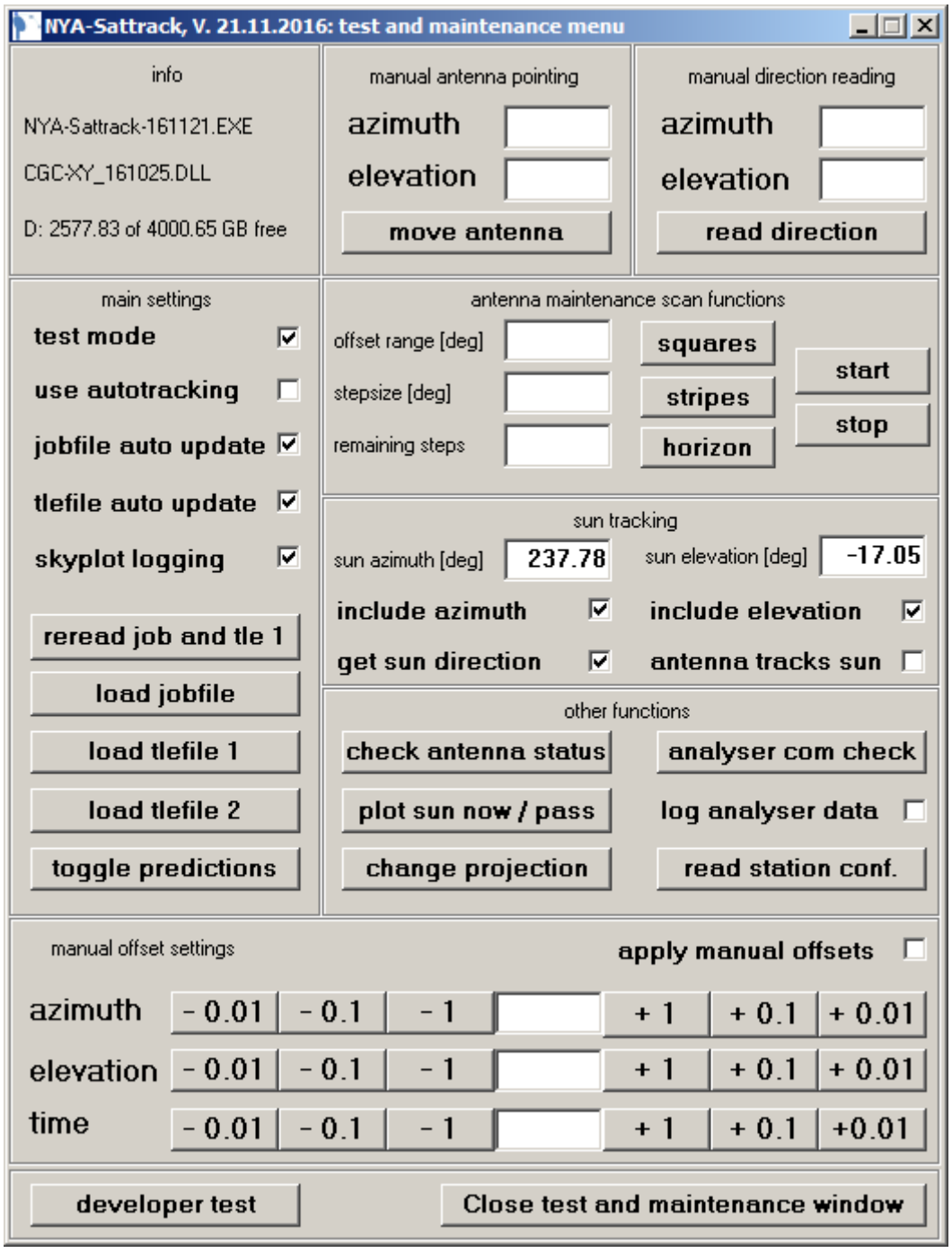

Figure 66: Test and maintenance GUI of NYA-Sattrack

- *Load jobfile*: Opens menu for manual selection of jobfiles. Forces a new calculation of satellite tracking directions if a new valid jobfile was selected.
- *Load tlefile 1*: Opens menu for manual selection of the twoline elements file to be used with the first prediction program. Forces a new calculation of satellite tracking directions for the first predictions (if new twoline elements are valid).
- *Load tlefile 2*: Opens menu for manual selection of the twoline elements file to be used with the second prediction program. Forces a new calculation of satellite tracking directions for the second predictions table (if new twoline elements are valid).

- *Toggle predictions*: The button allows to select which of the both precalculated prediction tables for the next or actual satellite contact is used actively for antenna tracking (active prediction is highlighted by bold characters on main GUI).

Manual antenna-pointing and manual direction reading

- Function allows to move the antenna to a user defined direction and to request an actual direction feedback from the antenna.

Antenna maintenance scan functions

- *Offset range*: Value to be entered by an operator. It defines the maximum offset of the scan movements, relative to the antenna normal direction (squares and stripes scans). For horizon scans this value defines the highest elevation to be scanned.
- *Stepsize*: Defines the size of individual scan movements (resolution of scan).
- *Remaining steps*: Shows total number of movements (one per second) according to selected offset range, stepsize and movement type and the number of remaining movement steps (counting down) when a scan was started.
- *Squares*: Initiates the preparation of a movement schedule (raster) for a square type scan, but does not yet start the movement.
- *Stripes*: Initiates the preparation of a movement schedule (raster) for a stripe type scan, but does not yet start the movement.
- *Horizon*: Prepares a zigzag stripes (0° - 360° / 360° - 0°) movement raster schedule for scans of the horizon.
- *Start*: Immediately starts antenna scan movements according to selected parameter.
- *Stop*: Stops a currently running scan.

Sun-tracking

- *Sun azimuth and elevation*: Display of the current direction to the sun.
- *Include azimuth*: The azimuth axis can be disabled with this function during sun-tracking mode, while the elevation axis still follows the actual sun directions, e.g., to allow a very smooth horizontal transition of the sun through the antenna's angle of view.
- *Include elevation*: The elevation axis can be disabled with this function during sun-tracking mode, while the azimuth axis still follows the actual sun directions, e.g., to allow a very smooth vertical transition of the sun through the antenna's angle of view.
- *Get sun direction*: Enables the continuous display of the direction to the sun, even if it is below the horizon and thus not shown on the skyplot display.
- *Antenna tracks sun*: Initiates an immediate transition to the sun-tracking mode or back to the regular satellite tracking mode

Other functions

- *Check antenna status*: Sends request for antenna status feedback to the connected antenna. The antenna feedback varies with the connected antenna type and the corresponding functions in the dedicated antenna-DLL.

- *Plot sun now / pass*: Changes display of sun directions on the skyplot display. The skyplot function will either show a trace corresponding to the sun directions in the time interval between AOS and LOS of the next satellite contact or the actual sun direction.
- *Change projection*: Changes the skyplot mapping function between "normal" (linear elevation scale) and "zoom" (enhancement of either zenith or low elevation zones).
- *Analyser com check*: Opens window that displays actual detected signal level of a connected FSP 13 spectrum analyser, as a verification for a proper two way interface connection.
- *Log analyser data*: Enables logging of data from analyser (e.g., signal level) in an additional column of the tracking logfiles (satellite and sun-tracking).
- *Read station config*: Initiates a reread of the station configuration file, inclusive display updates of read parameters, but no further program action.

Manual offset settings

- *Apply manual offsets*: activates or deactivates the application of selected manual offsets to the current antenna tracking procedure.
- *Azimuth, elevation, time*: Allows the fast variation of offsets by an operator in predefined steps (+/- 0.01, 0.1, 1 [degree, seconds]).
- *Developer test:* Button triggers program functions that are under development.

7.3 Logging windows

NYA-Sattrack generates individual logfiles and graphical logs for each satellite tracking and a general program activity logfile. All logs are accessible in their dedicated archive directories, but also through the program GUI in a comfortable and time saving way.

7.3.1 Rolling Log

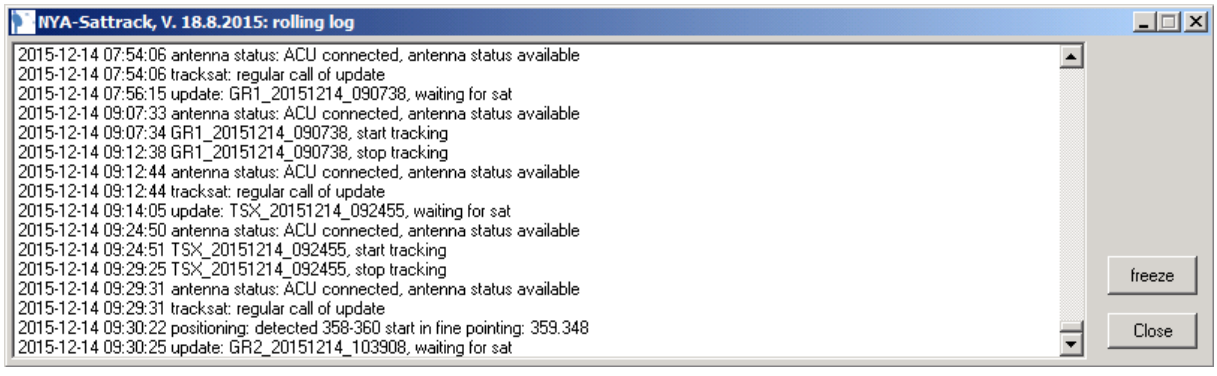

Figure 67: Rolling log program window

The rolling log window is opened with a button at the main GUI and displays the last 300 program activity messages in a separate program window (Figure 67). By default the display

is updated in real-time according to the program activity, but the display updates can also be paused with a “freeze / unfreeze” button, e.g., to search for certain messages.

7.3.2 Viewer for graphical logs

NYA-Sattrack generates conventional text-based logfiles and graphical logfiles (skyplots, 6.11.2). Both file-types are easily accessible at their dedicated directories, but NYA-Sattrack provides also an even more convenient way to check them simultaneously. A “passlog viewer” function, as shown in Figure 68, can be started with the “pass plots” button from the main GUI. A new program window is opened and displays the graphical log (bitmap format file) of the last satellite tracking, which was stored automatically at the end of the satellite contact, together with the corresponding regular satellite tracking logfile (ASCII-format). An operator can navigate through the local archive of stored logs with the buttons “previous” and “next”. The viewer then steps to the next or previous graphical logfile and automatically selects the corresponding ASCII-format pass logs. It is also possible to select logfiles from a list with the “load” button (example in Figure 69).

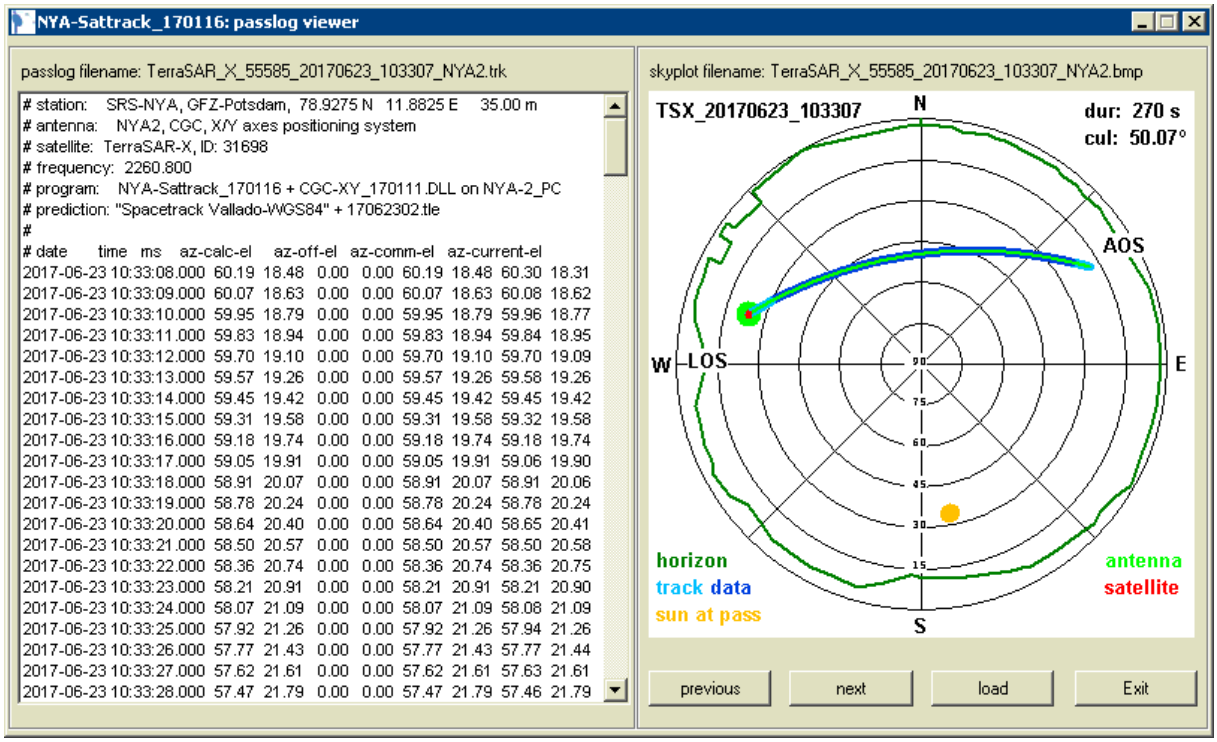

Figure 68: Window for display of text-based logfiles and logged skyplots

7.4 File selection GUIs

The GUIs for manual selection of files by an NYA-Sattrack-operator are based on the standard Windows dialog box type, as it is provided by the Windows computer operating system. This standard dialog box type was adopted for NYA-Sattrack, according to the file-types to be selected, by assignment of a corresponding dialog box name and preselection of a default directory and filename-mask. The design of these GUIs varies according to the general Windows computer settings, such as the default language. Figure 69 shows three examples for different styles of NYA-Sattrack dialog boxes (Windows XP classic style English, Windows XP style English, Windows 7 classic style German).

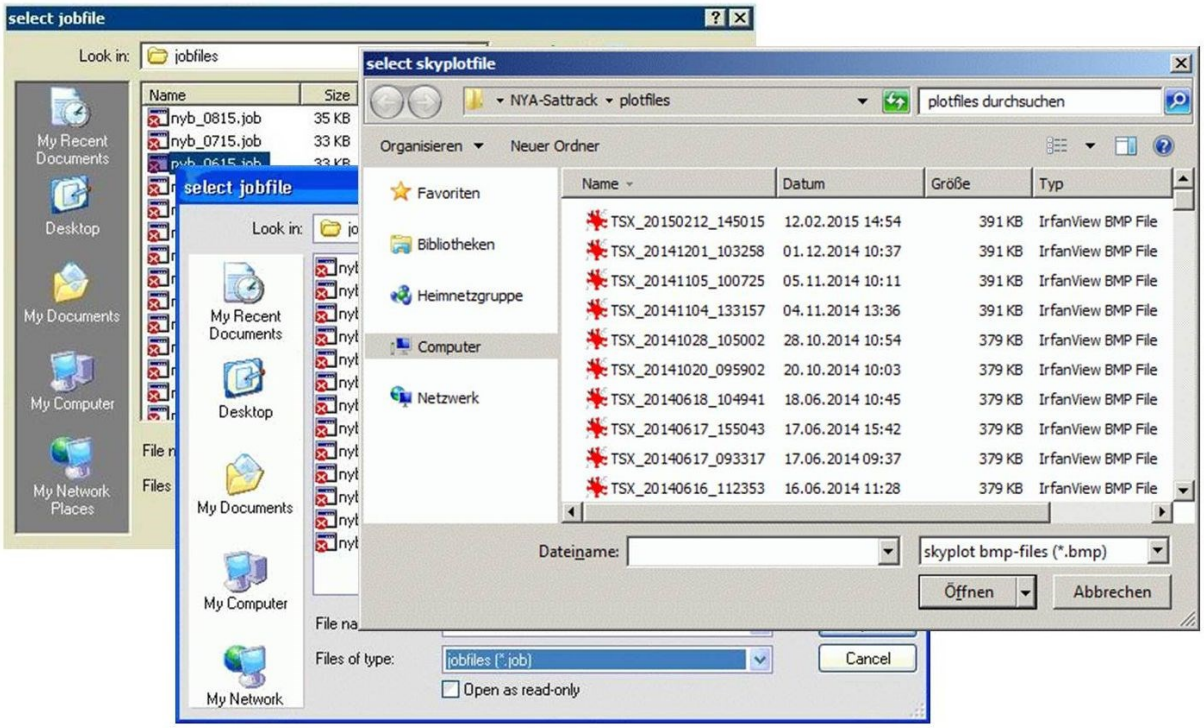

Figure 69: File selection dialog boxes with different display styles

8 Installation of NYA-Sattrack and bug-fixing

NYA-Sattrack was installed for the operation of both antennas at Ny-Ålesund mid of July 2014 and is used permanently since then. The new software worked flawlessly with NYA-2 from the beginning. A suspected bug of the NYA-2 software interface (DLL) concerned a problem with satellite tracking that start with an azimuth of exactly 0°, as one such pass failed in April 2016 with a suspicious logfile entry of 360°. The problem could not be confirmed by experiments but a prophylactic patch (360° => 0° conversion) was adopted anyway.

The operation of NYA-1 with the new software was fine at the beginning, but a first problem, which is described in section 8.2, appeared right when the author had left the satellite-receiving station after the installation in July 2014. The problem resulted in azimuth axis stops, although it was explicitly one objective of NYA-Sattrack to prevent such accidents. A second problem, concerning the software interface to NYA-1, was identified much later, as it appeared only two times in the first 6 month of operation. Both problems were fixed within some days or weeks after becoming visible. From that time on only small or even only "cosmetic" software changes were introduced, but no more bug-fixes with relevance for the antenna operation reliability or accuracy.

8.1 Installation of NYA-Sattrack at Ny-Ålesund

The NYA-Sattrack software was installed for the operation of NYA-1 on a PC with WINDOWS 7 and a built in IEEE interface card from National Instruments. The previously used PC for operation of NYA-1 (WINDOWS 98, antenna operation software from DLR) was disconnected from the antenna and removed later. The old PC as used previously for NYA-2 operation was initially also operated with NYA-Sattrack. In July 2015 the PC crashed (hardware failure) and was replaced by a backup system. Both PCs were operated with WINDOWS XP. New PCs for the antenna operation of NYA-1 (with a USB to IEEE-488 adapter) and NYA-2 were installed in 2016, both running WINDOWS 7. The installation of NYA-Sattrack was problem-free in all cases.

8.2 Initial problems with operation of NYA-1

After some days of regular program operation, unfortunately shortly after the author left the station, the NYA-1 antenna failed to track parts of satellite passes about once per day. The antenna operation log-files showed that these outages resulted from antenna movements to

one of the azimuth axis limit protection switches, which caused an antenna-pointing system stop. This was a surprising finding, because the prevention of these accidental events was an explicitly outlined and tested feature of the new software (see 6.9.1).

Intensive analysis revealed that the problem showed up only, but not always, when a previous satellite tracking finished with azimuth values between 358.5° and 360°. This was never the case during the days of software installation and also the on-site testing apparently never started in this range of azimuth. Experiments under remote control from Potsdam showed that the sector-information from the ACU, respectively the antenna, was not in logical agreement with the azimuth information in the ”critical range” between 358.5° and 360°. A sector information change from sector 0 (0° to 360°) to sector 1 (360° to 720°) should happen, just when the antenna is turned over 360°, but was observed to happen at 358.5°. It was concluded that most likely the sector information is detected at the antenna by a switch or a similar device and not by the azimuth angle synchro resolver, which provides the numerical feedback of the detected azimuth axis angle.

The NYA-Sattrack routine for antenna-pointing of NYA-1 (see 6.9.1), including the mechanism to determine a “safe” start direction for the next satellite tracking, was working correctly at any time. However, it was designed to rely on correct input from the azimuth direction sensor and the section sensor, which was not given in the “critical range”. A proper adjustment of the sector sensor would have solved the problem, but it was unclear if this was possible and, even if being successful, could be expected to persist over longer times. A sensor adjustment would have required another (expensive) visit at the station in any case.

A simple and effective software-based solution was conceived instead and implemented into NYA-Sattrack. The measure was to turn the antenna automatically “to the left” (decreasing azimuth) by 4° when the actual azimuth was found to be in the range between 358° and 360°, prior to a movement to the start direction of a next satellite tracking. The new direction is then, even more than actually required, outside the critical azimuth range. Sector information readings at the new and “safe” azimuth direction can be regarded to be reliable and in logical agreement with actual azimuth sensor readings. The program then determines the best starting sector for the next tracking process and the correct turn direction to reach that sector as described in section 6.9.1. This procedure works perfectly since implementation in NYA-Sattrack and no axis stop events at all occurred since then.

8.3 Later problems with operation of NYA-1

Some months after installation, it was noticed that the NYA-1 antenna stopped operation, although the ACU and NYA-Sattrack seemed to work normally. The events were logged automatically by NYA-Sattrack as communication problems (no replies to antenna positioning requests). Also manual attempts to initiate communication in this problematic state, e.g., to request antenna status parameter with the NYA-Sattrack test and maintenance functions, failed to get replies. A restart of NYA-Sattrack cured the problem for some time, but it appeared again and again, sporadically in different intervals, but always only after some weeks. Meanwhile no problems with NYA-Sattrack and the NYA-2 antenna were observed and consequently first suspicion was an NYA-1 ACU malfunction. Reboots of the NYA-1 ACU did not help and so it became more likely that the problems were induced by a not yet detected software bug, most probably localised in the specific code for NYA-1 operation, which is allocated in the corresponding antenna DLL (6.9.1).

It was found that the mean value of program working memory, as displayed by the Windows OS task manager, was increasing slowly with time, when NYA-Sattrack was operated in connection with NYA-1. The communication between NYA-Sattrack and the antenna ACU stopped as soon as the IEEE-488-interface buffer usage reached a certain critical value. The monitored traffic on the interface between the antenna operation PC and the ACU revealed that the remote IEEE-488-device ID-number was increasing by one with each tracked satellite pass. The reason was a program feature in the NYA-1 software interface (DLL), which repeatedly sent requests for IEEE-488-device initialisation before each tracking sequence. This feature was tested to be not necessary and was thus removed in the next, bug-fixed NYA-1 antenna DLL version. The described bug was discovered that late, because the program and the hosting computer were restarted frequently in the first months of operation, e.g., during trouble shooting (see section 8.2), so that the interface buffer usage never reached the critical level in that time.

9 Software aided determination of antenna system properties

Good knowledge about the main properties of a specific antenna is a mandatory precondition for an effective antenna operation and for a reliable assessment of antenna performance. Antenna boresight offsets must be known to be compensated correctly. Otherwise an antenna cannot be operated with maximum gain. The antenna G/T figure must be known for calculations with link budgets and to approve compliance with corresponding satellite mission requirements. Information on the antenna half power beamwidth and side lobes can help with the antenna operation, e.g., when being considered for exclusion of the sun, which could generate a high and performance-reducing noise level otherwise.

The planned operation of the satellite-receiving station at Ny-Ålesund as the primary downlink station for the upcoming GRACE-FO satellite mission required to determine the G/T figures of both NYA antennas, which required adequate boresight offset compensation first. These parameters, as well at the other discussed antenna characteristics, were so far unknown or uncertain and untested. A determination of antenna characteristics is supported by special functions of NYA-Sattrack. These functions were the basis for all corresponding measurements at the NYA station in August 2015 and June 2016 as described in sections 9.1 to 9.3 and measurements from remote (Potsdam) in autumn 2016 (9.4)

9.1 Determination of antenna system boresight offsets

The tracking of any targets with an antenna requires knowledge about the alignment of the antenna's principal axes (coordinate system), as determined by the true boresight of the antenna (maximum gain direction), to the coordinate system in which the target is observed. Both coordinate systems could be in perfect alignment in principle, but this case is usually not met in praxis. The main expectable biases result from hardly avoidable antenna system installation errors and a deviation between the main lobe direction to the nominal direction, e.g., as defined by the normal direction of the antenna reflector installation flange. In practice it is sufficient to consider the sum of all possibly contributing biases, rather than each of the individual biases as discussed in section 4.6.

The total bias of an antenna positioning system can be determined when it is directed to a point with known coordinates, respectively a known direction from the antenna site. The difference between the true direction and the direction reported by the positioning system

delivers the unknown total bias. The target with known coordinates can be a regular landmark. It can be observed through a telescope, which must be in alignment with the antenna's RF-related boresight. The accuracy of this method depends strongly on the accuracy of the alignment between the effective antenna boresight (for radio signals) and the optical boresight of the telescope. A perfect alignment might be difficult to be established and the method cannot be used if there is no optical view from the antenna location, e.g., because it is covered by a radome, which is the case for both antennas at Ny-Ålesund.

An alternative method is to use an artificial radio source (transmitter) as an observation target. The sum of all biases can be determined when the antenna is directed to the radio target (transmitter) and carefully aligned for the maximum of received signal strength. This is an indication that the centre of the antenna main lobe, and thus the effective antenna boresight direction, is best directed to the radio target. The difference between the true direction and the direction as displayed by the antenna-pointing system corresponds to the total antenna boresight bias. The advantage of this method is that it works also for an antenna under a radome. Problems could arise from radio signal reflections by the local environment in the vicinity of the transmitter, the receiving antenna or by the ground between these locations. At Ny-Ålesund this method cannot be used at all because it is not allowed to use any transmitter on S-band frequencies.

Another calibration target, not only as a source of light (observation with telescope), but also as a source of radio noise over a wide spectrum of frequencies, is the sun. The direction to the sun from any location on the Earth is of course not static, but can be calculated easily and precisely from known local coordinates and local time (section 6.10.3).

Repeated antenna calibration experiments for both antennas were performed with support from NYA-Sattrack in August 2015. In a preparative step it was confirmed by metering rule measurements that the feeds at both antennas were installed in the desired central position (equal distances to rim of antenna reflector, measured along feed support bars). Then the antennas were pointed to the sun using the sun-tracking mode of NYA-Sattrack. While maintaining a continuous sun-tracking over the full time of the measurement in principle, the antennas were misaligned with respect to the nominal sun direction by different angular offsets, which corresponded to the scheme of a stripe- or a square-shaped pattern (Figure 53a, Figure 53b). In consequence the scan raster virtually moved with the sun and the radio noise

signal of the sun was received from defined directions with defined offsets to the actual sun direction.

The received solar radio noise levels were measured with a telemetry receiver (CORTEX). The receiver delivered so-called RSSI readings (Radio Signal Strength Indicator) which were recorded by the receiver operation computer. The RSSI readings of the receiver were not calibrated but anyway considered to be suitable for qualitative measurements, which do not require a certain accuracy of absolute values or a high linearity. The actual sun directions, the applied offsets (raster positions), the commanded directions (absolute values) and the reported direction (feedback from antennas) were logged by NYA-Sattrack on the corresponding antenna operation computers (in sun-tracking logfiles). A small self-made program was used to merge RSSI readings and direction logs into one data set (correlation over time stamps), to eliminate outliers and to normalise the data. The described setup and procedures were used not only to determine the antenna boresight offsets, but basically also for experiments to determine the antenna directivity in the main lobe region (9.3).

Figure 70 shows the time series of the solar radio noise signal levels as recorded during the experiment to determine the boresight offset of NYA-1 with a squares-type scan pattern. Antenna positioning commands, each corresponding to one raster direction, were commanded by NYA-Sattrack at a frequency of 1 Hz and the detected radio signal strength was recorded for each of these steps. The step interval of the scan scheme was 0.1° and the elevational and azimuthal maximum offsets were +/- 3.0°. Effectively 3721 directions were probed, some more than once (6.8.2, Figure 53a), beginning with small offsets. The boresight offset value as determined by DLR during system installation at NYA was applied (by ACU). A perfectly aligned or calibrated antenna system with no boresight offsets would have delivered maximum signal levels at the beginning of the experiment, when azimuth and elevation offset angles were zero. The graph shows that the maximum was detected at a later time, corresponding to some angular offset, which corresponds to the true antenna system boresight.

The display of the solar noise signal levels as a time series, such as in Figure 70, allows the immediate detection of offsets, but the numerical values of the elevational and azimuthal offset angles cannot be determined directly. The experiment data set was sorted for signal levels (Microsoft Excel). The unknown antenna boresight offset angles were obtained from the differences between the calculated sun directions and the directions as reported by the

antenna positioning system at the time of maximum signal levels. The mean value of the offsets from four evaluated experiments with NYA-1 (square and stripe scans at different day times) was - 0.4° in azimuth (max. deviations + 0.2° / - 0.1°) and - 0.1° in elevation (max. deviations +/- 0.2°).

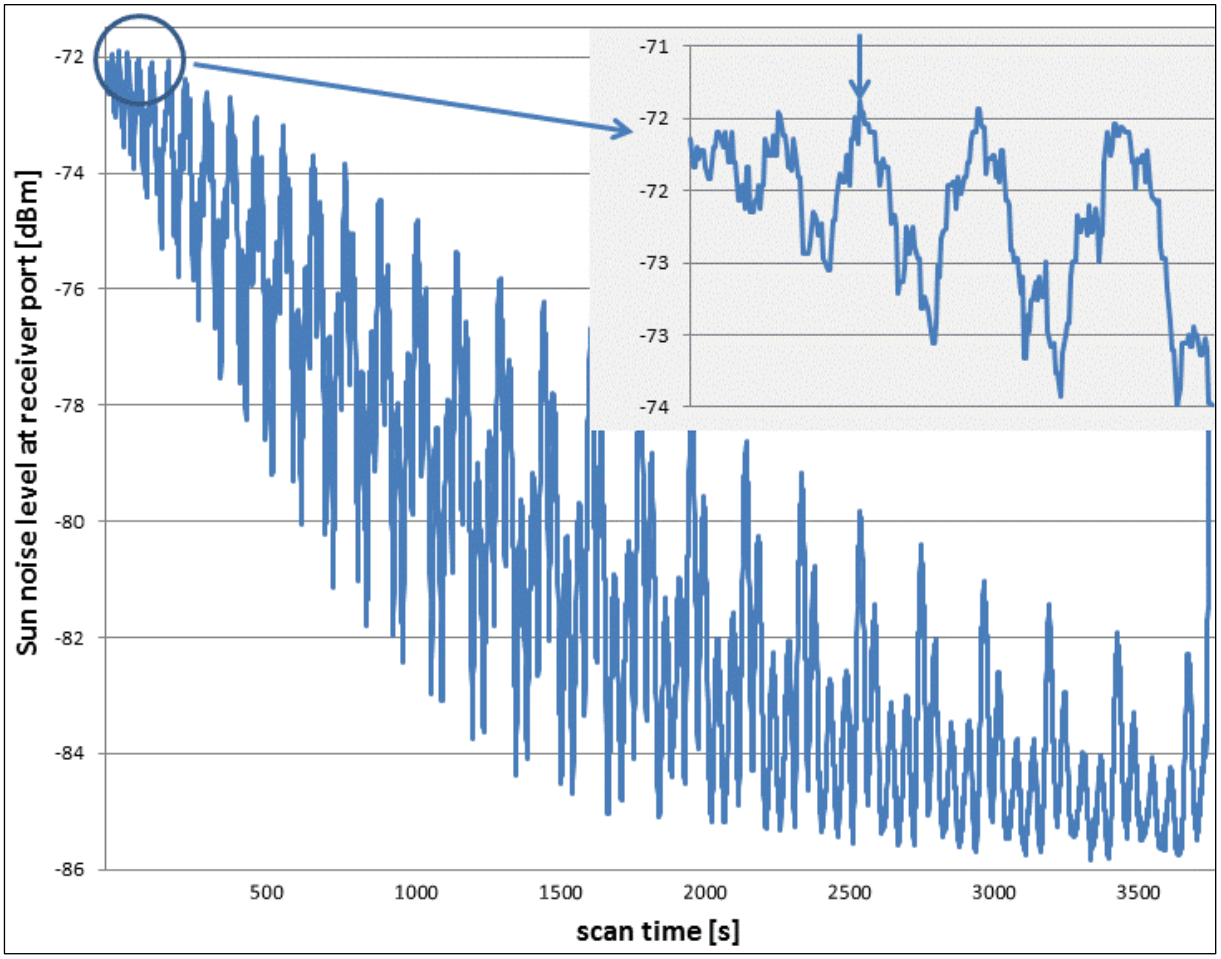

Figure 70: Sun noise during first experiment with NYA-1 (square-type scan)

Also the boresight offset angles of NYA-2 were determined by detection of solar radio noise signals during sun-tracking, superimposed with scan patterns. Both implemented types of scan patterns, the square-type and the stripe-type, were applied for NYA-2. The previously determined boresight offset from the time of system installation in 2005 was not applied, because it was not trusted (discussed in 5.2.3) and most probably also modified since then. Figure 71 shows the time series of the first experiment with NYA-2 and a stripe-type scan pattern. The step interval of the stripe scheme was 0.1° and the maximum offset was +/- 3.0° as for NYA-1. The maximum of radio noise signal levels in Figure 71 appears close to the midpoint of the time axis, but with a certain timely offset to the left. The corresponding

angular offset angles (calculated sun directions minus reported antenna directions at signal maximum) were determined from the data set, again after sorting it for radio signal levels first (Microsoft Excel). The mean values of the offsets from five evaluated experiments with NYA-2 (square and stripe scans at different day times) were - 1.4° (max. deviations + 0.2° / - 0.3°) in azimuth and - 0.15° (max. deviations +/- 0.15°) in elevation.

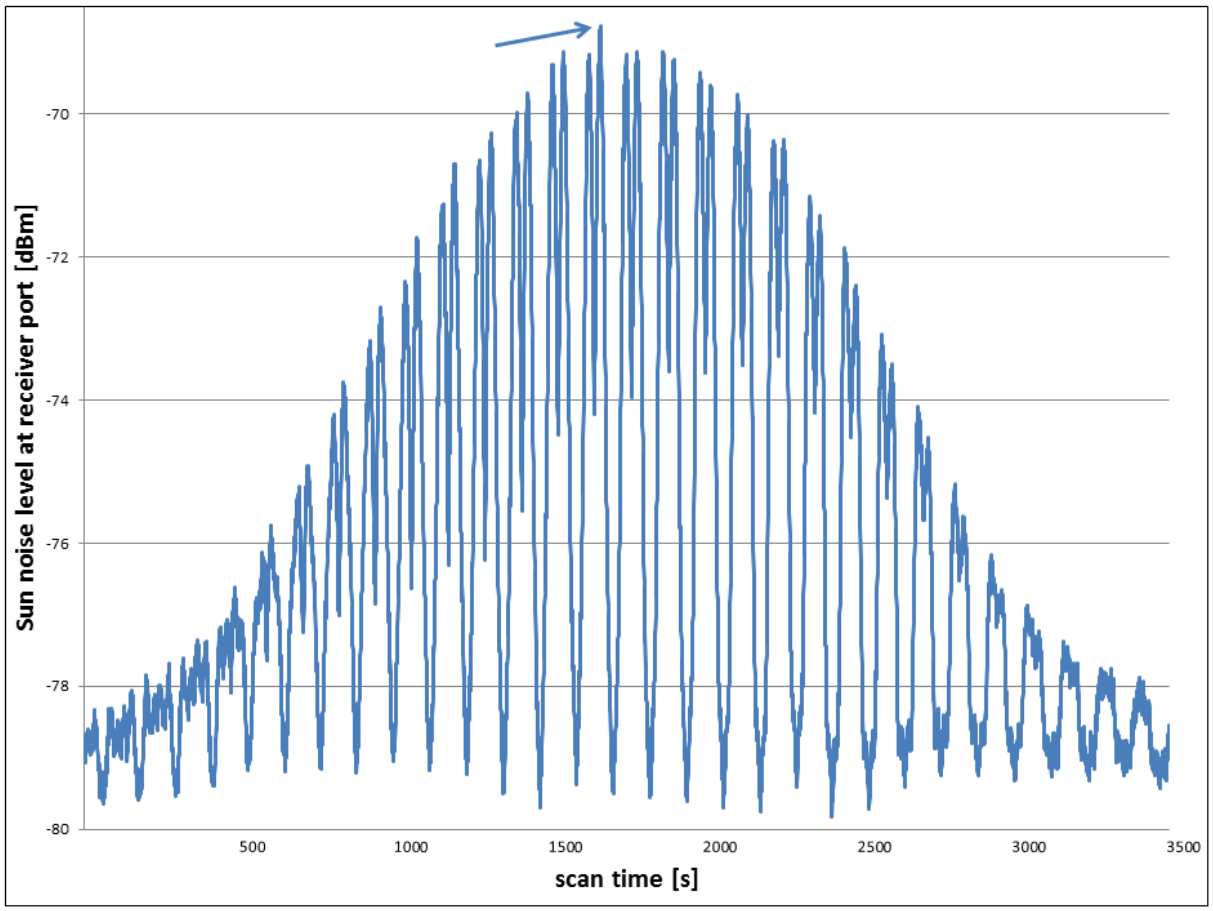

Figure 71: Sun noise during first experiment with NYA-2 (stripe-type scan)

The observed deviations from the mean values can be explained with natural short-term variations of the solar radio noise signal. These might cause a detection of highest signal levels in directions which are close but probably not exact the antenna boresight direction. An experimental recording of the solar radio noise level for an interval of one hour was obtained with NYA-1, when the antenna tracked the sun without additional scan movements. The related time series of measurement data in Figure 72 shows some very short-term variations of about 0.5 dB, which are represented by the thickness of the graph (noise). Larger variations of over 2.5 dB in total were detected at rates of up to about 2 dB within 10 minutes, equivalent to 0.2 dB per minute. The directional scans as described in this section used a

raster of 0.1° and a command rate of 1 Hz. A scan of the directional region around the antenna boresight with a range of +/- 0.3°, for example, thus takes 49 seconds, according to 49 individual directions. Consequently a not negligible variation of the natural solar radio signal, in this example of about 0.2 dB per minute, must be considered.

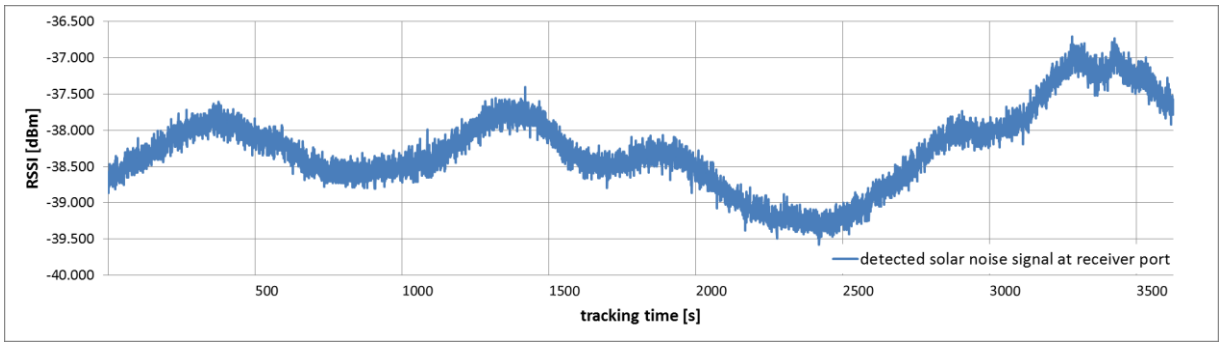

Figure 72: Variation of solar radio noise signal (S-band) from exemplary measurement

The determined antenna system boresight offsets of both antennas were stored in the NYA-Sattrack program configuration file and could be used for the boresight offset compensation thereafter. This measure was required to improve the antenna-pointing accuracy for satellites, but it was also a precondition for a correct antenna-pointing to the sun, which was required to determine the antenna's *G/T* performance, as described in section 9.2. The experimental determination of antenna directivities (section 9.3) used the same basic experimental concept (sun-tracking plus stripe- or square scans) as described in this section and some of the graphics in section 9.3 are somehow a visual verification for the correctness of the found antenna boresight offset values.

9.2 Determination of G_r / T_s

The G_r / T_s values for the antennas at Ny-Ålesund were assessed on basis of available components specifications, models and assumptions (5.3). These assessments provided a model for the NYA receiving system performance (less than 16 dB/K at 5° elevation, before 2014) and revealed that the NYA antennas needed LNAs with better performance figures (max. 0.4 dB noise, min. 50 dB gain) to fulfil the GRACE-FO requirements (17 dB/K at 5° elevation), as listed in the corresponding MOS (mission operation system) requirements document (Klein and Snopek 2015). A more reliable determination, to be considered as a proof of the upgraded system performance figures with new LNAs, could only be achieved with measurements. Measurement methods, which involve local radio emissions, e.g., to

provide a reference signal, were not an applicable option at Ny-Ålesund. Such methods are connected with an undesirable high effort (e.g., logistics and costs) and were not allowed, due to the general prohibition of transmissions at Ny-Ålesund in the S-band. Instead, it was decided to determine the desired *G/T* antenna performance figures with the method as described in section 4.8 (sun as source of reference signal). Corresponding ITU recommendations (ITU Radiocommunication Assembly 1992-1993-2000) recommended the reception of quasi-calibrated signals (well-known and stable) from distant radio stars but indicated also that the antennas at NYA were too small to receive them with sufficient signal levels. As it is common praxis to choose the sun as a more nearby and thus stronger radio signal source in such cases, it was also used for the measurements with the NYA antenna systems.

The required measurements were conducted with a FSP 13 spectrum analyser on August 25th 2015 around noon (UTC). A calibration of the analyser was carried out by the instrument manufacturer shortly ahead in time (June 2015) and documented in a calibration report (Rohde & Schwarz 2015), to support the reliability of the measurements. The task of the analyser was to provide figures for the noise power densities as received by the antenna systems when they were pointed to the cold sky, which can be any direction above the horizon with certain distance to the sun (and other signal and noise sources), and when they were pointed to the sun. Noise is a random process and the measurement of radio noise power density must address this nature by a suitable measurement setup. Some recommendations and a description of the corresponding analyser-internal measurement procedures were found in the chapter *"2.4.1 Measuring noise power density"* of the analyser operation manual (Rohde & Schwarz 2009). The instrument was set to a frequency of 2260.8 MHz because this is the highest downlink frequency of the GRACE-FO mission, which was used also for similar tests at other ground-stations (e.g., station WHM). Additional parameters were defined for the radio bandwidth (1 MHz), the Video bandwidth (10 MHz), the span (1 MHz) and the sweep time (500 ms). These settings cause a kind of integration over time (sweep time) and frequency (bandwidths) and thus support the generation of mean values for the detected signals with random noise character. The actual values of the system noise power (cold sky measurement) and the received sun noise power were detected by the analyser's "rms-detector" function. An additional averaging effect was obtained by the "trace average" function of the analyser and the finally resulting readout at the nominal centre frequency was provided by the analyser's "noise marker" function. A sufficient low reaction time of the

analyser, despite of all the averaging effects, was confirmed by a dedicated experiment during the directivity tests (section 9.3.3, Figure 85), which used the same analyser settings.

Some maintenance functions of NYA-Sattrack (test and maintenance menu: manual pointing and sun-tracking) were used to point the antennas to the cold sky and to the sun. First the antennas were pointed to a manually selected cold sky direction for some minutes until the analyser readout for the detected system noise power settled to a virtually stable value (fluctuation 0.1 dB or less). Best results with respect to the stability of the cold sky noise measurements were achieved at very high elevations (85°). The following measurement of the sun noise power could be made in a very similar way, owing to the NYA-Sattrack program function for a continuous tracking of the sun. It allowed the observation of the detected sun noise power level for several minutes and thus as long as required until a virtually stable value was reached. This helped to make sure that the readings were not affected by short-term signal fluctuations, e.g., due to noise signal bursts from sun flares, which would have corrupted the measurements. The measurement with continuous sun-tracking was regarded to be advantageous over the method as recommended by the ITU. That method recommends the antenna to be directed to a future (some minutes ahead in time) sun direction, so that the sun "travels" through the main lobe of the antenna. The maximum of the recorded sun noise signal power is then taken as the measurement result, but, at least as interpreted by the author, with less certainty about potential signal fluctuations.

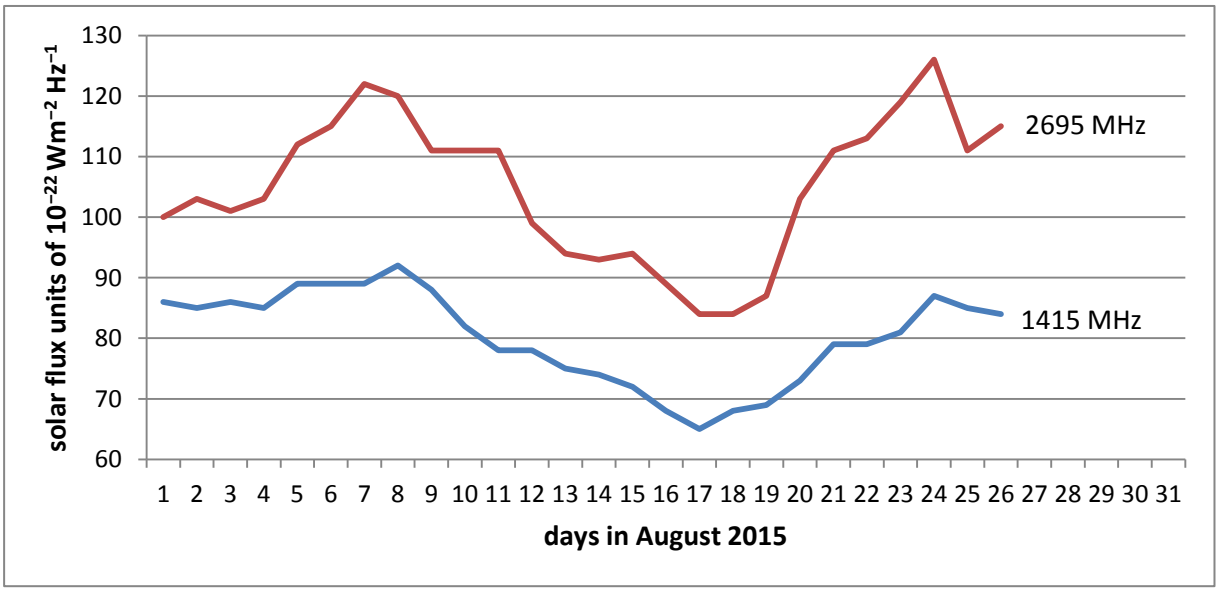

Figure 73: Solar flux measured at San Vito at frequencies nearest to NYA test frequency

The evaluation of the measurements with equation (41) requires knowledge of the solar flux at the measurement time and frequency. Corresponding sun flux observations were obtained from the San Vito observatory in Italy as its coordinates are the closest to NYA among all known observatories with public available data. Figure 73 shows sun flux measurement data from the San Vito observatory for the two closest observation frequencies, w.r.t. the test frequency used at NYA, in August 2016. The data series stops after the 26th of August, most probably due to problems at the observatory, but the date of measurements at NYA (25th of August) is covered by observation data. The graph shows that there was significant fluctuation of the solar flux in that month, even from day to day. The observations at San Vito were performed once per day at 12:00 h UTC timely close (less than 30 minutes difference), to the measurements at NYA which should provide a high data transferability for the measurements. The solar flux at the NYA test frequency of 2260.8 MHz in Table 8 was assessed from a cubic spline interpolation of data for all frequencies (1415, 2695, 4995, 8800, 15400 MHz, not all listed) that were observed at San Vito on 25th of August.

San Vito, 1415 MHz	San Vito, 2695 MHz	Interpolation to 2260.8 MHz (NYA)
85	111	104.6

Table 8: Solar flux during G/T measurements (25th Aug. 2015) in solar flux units (1 sfu = 10^{-22} Wm^{-2} Hz^{-1})

Table 9 shows the measurement data of the *G/T* determination at NYA (P_{sun}, $P_{cold\ sky}$), the *G/T* value at the measurement antenna elevation (~21.3°), calculated with the assessed solar flux (104.6 sfu at 2260.8 MHz) and equation (41), and extrapolated values for an antenna elevation of 5°, which is the finally relevant result (e.g., w.r.t. GRACE-FO requirements).

	NYA-1	NYA-2
P_{sun} [dBm Hz^{-1}]	103.47	103,68
$P_{cold\ sky}$ [dBm Hz^{-1}]	117.88	118.41
G/T at elevation during measurement (~21.3°) [dB K^{-1}]	17.22	17.56
***G/T* at 5 degree elevation** [dB K^{-1}]	**16.93**	**17.27**

Table 9: Measurement data and calculated *G/T* values of the antenna systems at NYA

The unit "dBm Hz^{-1}" is commonly used for measurements of the noise power density (analyser readout data) and corresponds to "dB relative to 1 mW per 1 Hz bandwidth". The extrapolation from 21.3° to 5° addresses the atmospheric attenuation effect that increases with decreasing elevation. A complex way for the extrapolation is described in the ITU recommendation ITU-R P.676 (ITU Radiocommunication Assembly 2013) and related graphs

and instructions were found in books, e.g., (Maral and Bousquet 1998) and (Dietrich and Davies 1999). The numbers in Table 9 were calculated with equation (50), which was adopted from a related document ("GRACE Follow On RF Compatibility Test Report") for the ground station at Weilheim (Wiedemann, K. 2014), to achieve project internal conformity.

$$G/T_{(5°)} = G/T_{\text{(measurement)}} + 0.034\ \text{dB/K} * (\ 1/\sin \text{Elevation}_{\text{(measurement)}} - 1/\sin(5°)) \quad (50)$$

The methods and results of the *G/T* performance measurements at NYA were described in a technical report (Falck 2015) and provided to the GRACE-FO project to document the compliancy with the corresponding requirement for the reception of GRACE-FO satellites (17 dB/K at 5° elevation). Compliancy was confirmed for the NYA-2 antenna and slightly dismissed by the NYA-1 antenna. The results of the measurements are in good agreement with the modelled, respectively expectable *G/T* performance, as calculated in section 5.3 (NYA-1: 17.08 dB at 5° elevation), which is interpreted as a confirmation for a proper system implementation.

Figure 74: Automatic webcam picture taken at NYA at the time of *G/T* measurements

The local weather conditions during the measurements (Figure 74) with deep clouds and sporadic rain precipitation (noticeable by partly wet concrete basement) can be regarded as somehow representative adverse conditions (e.g., due to water film on radome and noise from

clouds). Slightly better *G/T* figures might be obtainable at more favourable weather conditions.

9.3 Determination of antenna directivity

Information about the directional characteristics of the antennas at NYA was desirable, but no corresponding diagrams were available. Some experiments with support by the NYA-Sattrack sun-tracking and scan functions were made in 2015 and 2016 to investigate the beam pattern regions of the main lobe and the angular near field, which were considered to have the highest relevance for regular antenna operation. The experiments also led to some additional findings on the performance of the antenna positioning systems.

9.3.1 Setup of experiment and data processing strategy

The experiment setup was in principle the same as for the determination of boresight offsets (9.1). The antennas followed the direction of the sun and additionally the scheme of a square type scan (6.8.2) or a stripe type scan (6.8.3). A measurement of received signal power was performed and recorded for each of the scan raster directions, while the antennas moved continuously with a step frequency of 1 Hz. The obtained data sets (signal power over antenna direction) were processed to 3D heat maps (program gnuplot). The plot axes scales (azimuthal offset and elevational offset) are referred to the actual sun directions. Different scan raster definitions were applied, e.g., with maximum scan ranges of +/- 1.5°, +/- 3.0° and +/- 10° in 2015 and additionally with +/- 15° and +/- 30° in 2016, to focus on the main lobe sector or to include the area of suspected nearby side lobes. The scan resolution was adapted to the actual range of the measurement in a way that the measurement time for a full scan was in the range of 1 hour. The resulting scan step sizes were 1/60 of the selected scan range in most cases, which then generated a scan raster with 61 lines of 61 measurement points each (center lines plus 30 lines in each principal direction).

Each individual measurement of the obtained data sets was plotted as a single point. The plot size of the points was selected large enough to generate coherent patterns of the direction-gain distributions, but also small enough to distinguish between individual points. This allowed a mapping of the gain pattern and also a graphical analysis of the antenna system response to positioning commands. No filter or smoothing functions were applied to the measurement data sets or the graphics, except of Figure 86 and Figure 87, where data was interpolated to a regular grid. Only extreme outliers of RSSI readings were eliminated and are not displayed

(applies for 2015 measurements only, less than 1 % for each data set). The position of data points in the plots refers to the antenna positioning systems feedback. Data points with reported direction offsets greater than the nominal scan ranges were not displayed. An exception is Figure 75, where data points were plotted corresponding to commanded directions for reference (same data as for Figure 76). It shows that the distribution of RSSI reading outliers and data gaps (white points in the graph) has no systematic pattern with respect to certain directions, which applies for all measurements.

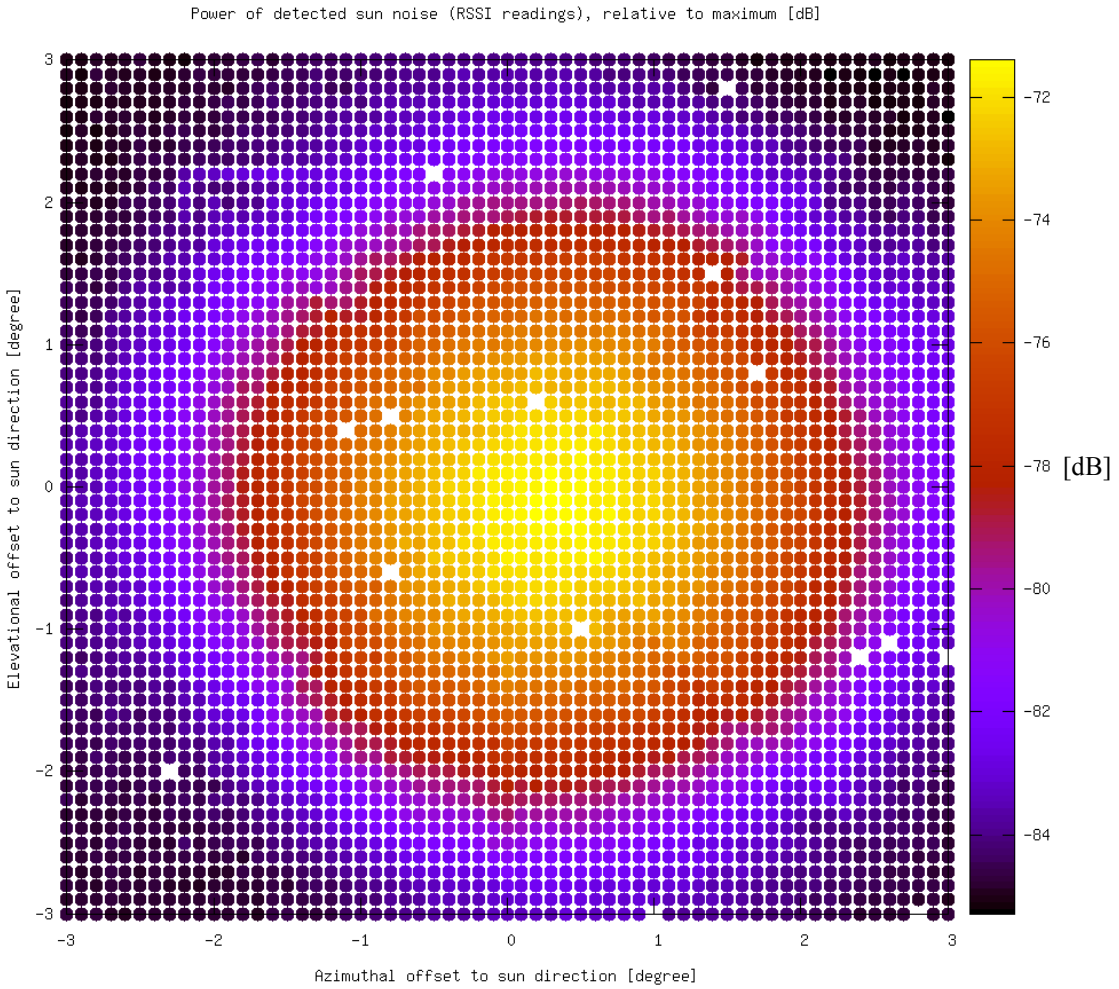

Figure 75: Distribution of data gaps and outliers (NYA-1, commanded directions)

All useable sun noise signal strength readings in each individual experiment data set were scaled (normalised) with respect to the maximum RSSI value in the same data set, which was set to “0”. The difference of the measurement values to “0” is thus the relative gain with respect to the maximum gain in the antenna main lobe direction. The normalised data points were plotted with colour scales. All colour scales use the same colour code and the maximum of all scales is “0”, but the lower end of the scales was either defined by the lowest

measurement values in the data sets or to a fixed value in some cases. The normalisation and scaling were preconditions for the comparability of the obtained results as the absolute values of received sun noise power varied from day to day (Figure 73) or even faster (Figure 72) and between the two antennas (different signal routing).

9.3.2 Antenna directivity measurements in 2015

The antenna directivity measurements in 2015 were performed as described above (9.3.1). The relevant received signal power levels and directions (sun and antenna) were obtained, recorded and correlated as described in section 9.1, namely with one of the telemetry receivers to provide RSSI readings (recorded with dedicated computer), the antenna operation computer (running NYA-Sattrack) for commanding and recording of directions and a small program (by author) to correlate and edit the data files automatically.

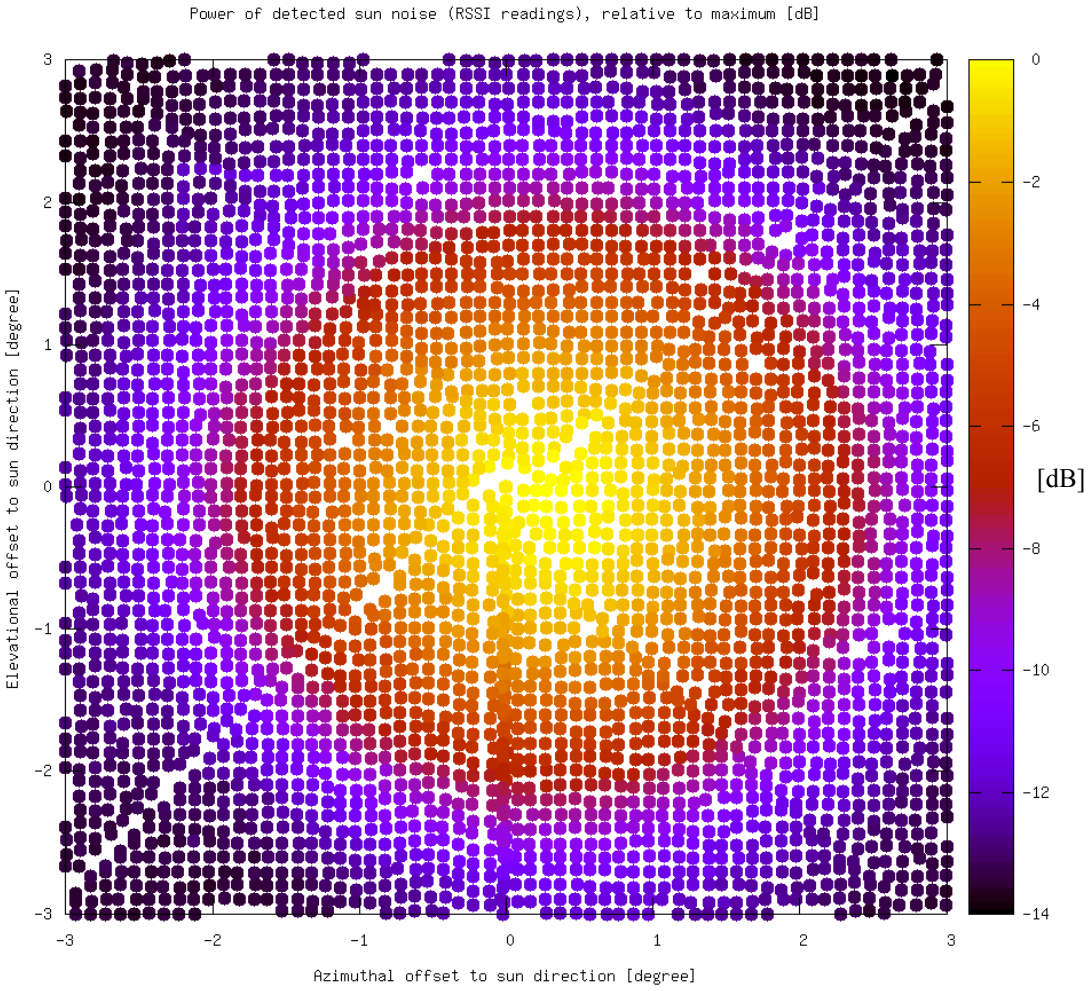

Figure 76: NYA-1 directivity w/o boresight offset compensation, square scan, 0.1° steps

Figure 76 and Figure 77 show graphics from experiments with the NYA-1 antenna. The experiments were combined sun-tracking / raster scans, using a raster resolution of 0.1° and a raster range of +/- 3°. The raster scan for Figure 76 followed the square scan scheme while the raster for Figure 77 was a stripe scan scheme. The boresight offset of NYA-1, as re-determined in this work (9.1), was not yet compensated during the measurements, but the previously determined boresight offset of NYA-1, from the time of installation (2001), was compensated by the NYA-1 ACU. The Figures thus show the error of the first offset determination, which was already considerably small. Both directivity patterns in the Figures are generally symmetrical but have a small offset to the right w.r.t. the midpoint of the graphics. This is in agreement with the results of the antenna boresight offset determination experiment (9.1) and with the boresight offset variation range as it was observed already previously.

The distribution of data points in Figure 76, as well as in some other Figures in this section, appears somehow surprisingly inaccurate, although the logged positioning commands were precise (Figure 75). All scans with the square type raster and NYA-1 also show a superimposed cross-shaped pattern and a vertical line from the midpoint to the bottom of the graphics. The vertical line pattern results from the square-type scan movement scheme in conjunction with the positioning system inexactness. Directions on this line were commanded twice (conjunction points in scan scheme, see Figure 53a) but achieved by the antenna system with different accuracies, which prevents the perfect coinciding of data points with the same nominal (commanded) directions. These lines are also visible on the graphics from square-type scans with NYA-2 (discussed below).

The cross-shaped pattern is formed at points where the antenna positioning system changes the direction of antenna movements, e.g., from vertical to horizontal and vice versa. Such “crosses” were not found on graphics from square type scans with NYA-2 (e.g., Figure 82). It was thus concluded that the observed effect is either connected with the NYA-1 positioning system or with the mode of its operation through NYA-Sattrack, e.g., the splitting of positioning commands into series of 5 steps (see 6.9.1), which is different to the NYA-2 operation mode (commanding of directions and corresponding axes rates, see 6.9.2). An argument for problems with the NYA-1 antenna positioning system is the fact that it evidently fails to adjust and / or to maintain an axis setting accurately (scattered points on lines), even when the commanded movements do not require any change of that axis setting. This

weakness is visible in all graphics from experiments with NYA-1, no matter which scan scheme was used.

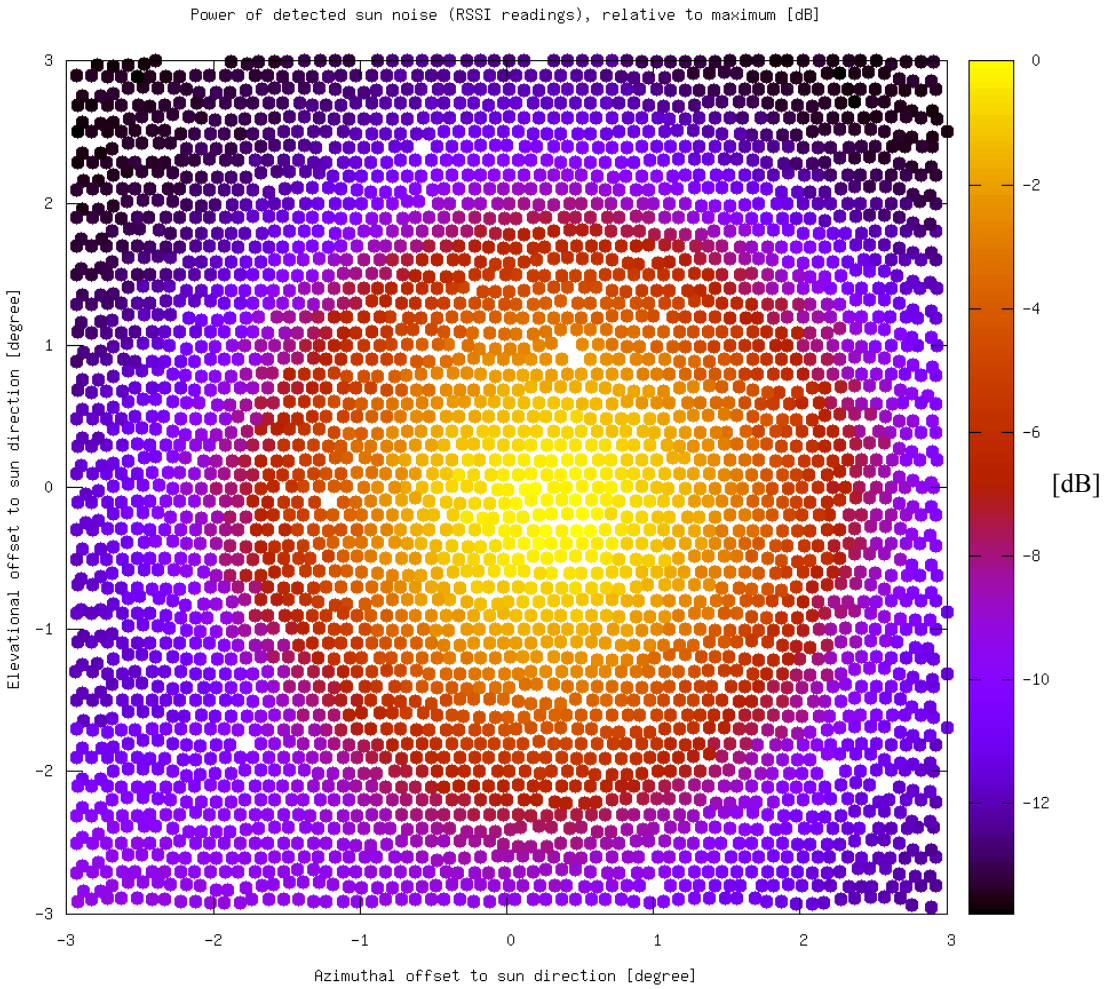

Figure 77: NYA-1 directivity w/o boresight offset compensation, stripe scan, 0.1° steps

Figure 77 shows data from a measurement with NYA-1 and the same scan raster step size and range as used for the measurements corresponding to Figure 76, but obtained one day later and with a different scan scheme (stripes instead of squares). The distribution of the data points again has a certain discrepancy to the commanded ideal raster, but there are no signatures as “crosses” or other lines. A small offset between all second horizontal scan lines and their directly neighbouring scan lines is detectable, best in the zone of transition from red to violet colours. The offset correlates with the actual direction of antenna movements (6.8.3, Figure 53 b), but was found with NYA-1 stripe scans only. The conclusion is that there was either a lose movement (azimuth direction) or a small delay of command execution in the positioning system of NYA-1. The stripe scans are very sensible for such effects, as every scan line is a kind of reference for the subsequent scan line. Timely effects or lost motion in

the direction of the scan lines thus become evident on the heat maps with double amplitudes. The found offset was not detectable on graphics from square type scans, which proved the benefit to perform the tests with two different scan schemes. The main lobe in Figure 77 shows basically the same pattern and offset to the graphic centre, but a 3 dB higher level of RSSI readings in the low region of the plot (violet colours), compared with the same region in Figure 76 (very dark colours, especially in corners at the bottom).

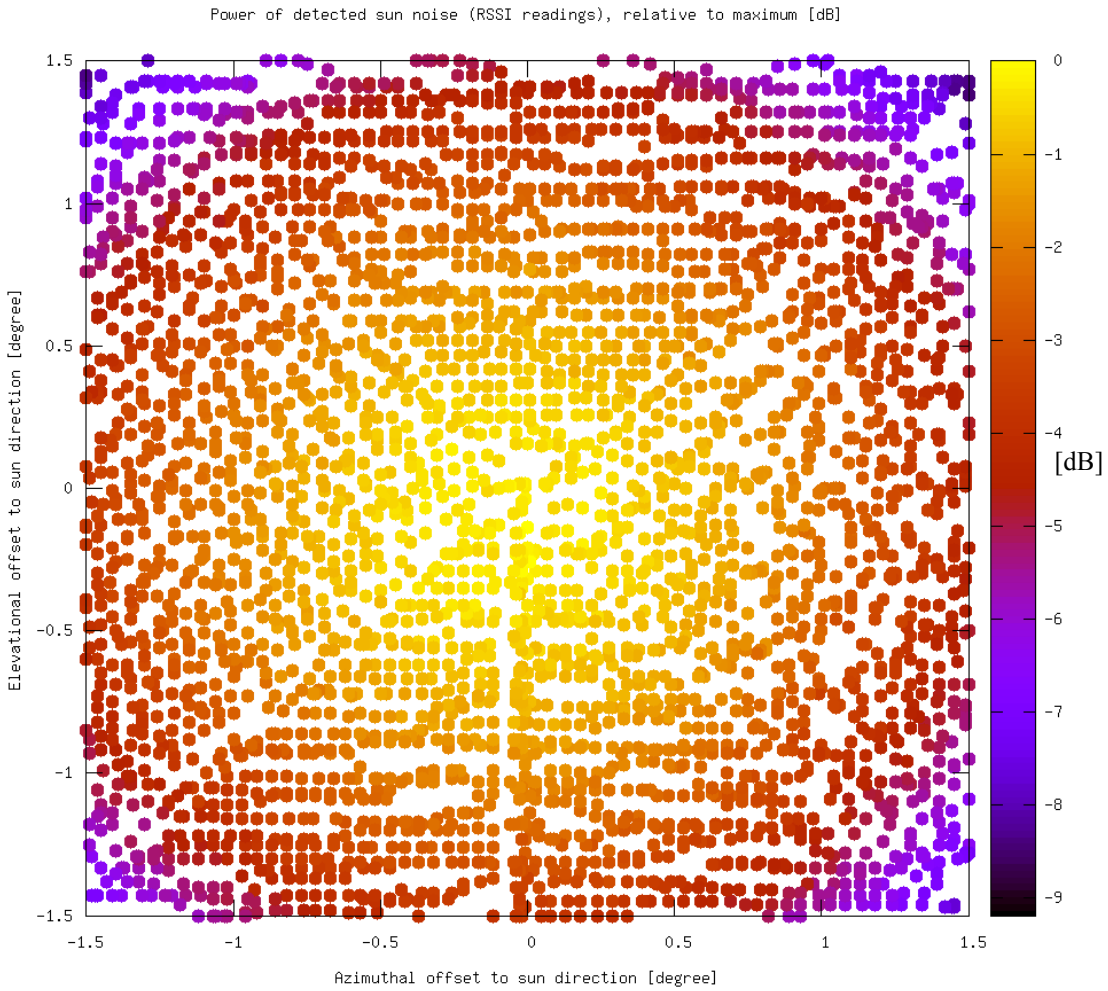

Figure 78: NYA-1 directivity with boresight offset compensation, square scan, 0.05° steps

A first guess of explanation was a suspected change of the solar flux over the time of the measurements for Figure 77. However, an increase of the solar flux should have a visible effect on the main lobe region also (same increase of signal levels) , e.g., at -2° elevational offset and 0° azimuthal offset, which is not the case. The measurements for Figure 77 were done at a different time of the day with lower sun elevations than the measurements for Figure 76 and thus smaller angular distances to the ground. This made the measurement prone to

receive more thermal noise from the ground and potentially stronger sun signal reflections due to the shallower incident angles.

Figure 78 shows data from another combined sun-tracking / square-type scan with NYA-1, using a raster resolution of 0.05° and a raster range of +/- 1.5°. The data set allows a more focussed view on the main lobe pattern. The determined antenna boresight offset (9.1) was already compensated by NYA-Sattrack during the measurement. The rotationally symmetric main lobe beam pattern appears to be well centred, which is regarded as a confirmation for a good directional calibration of the NYA-1 antenna system.

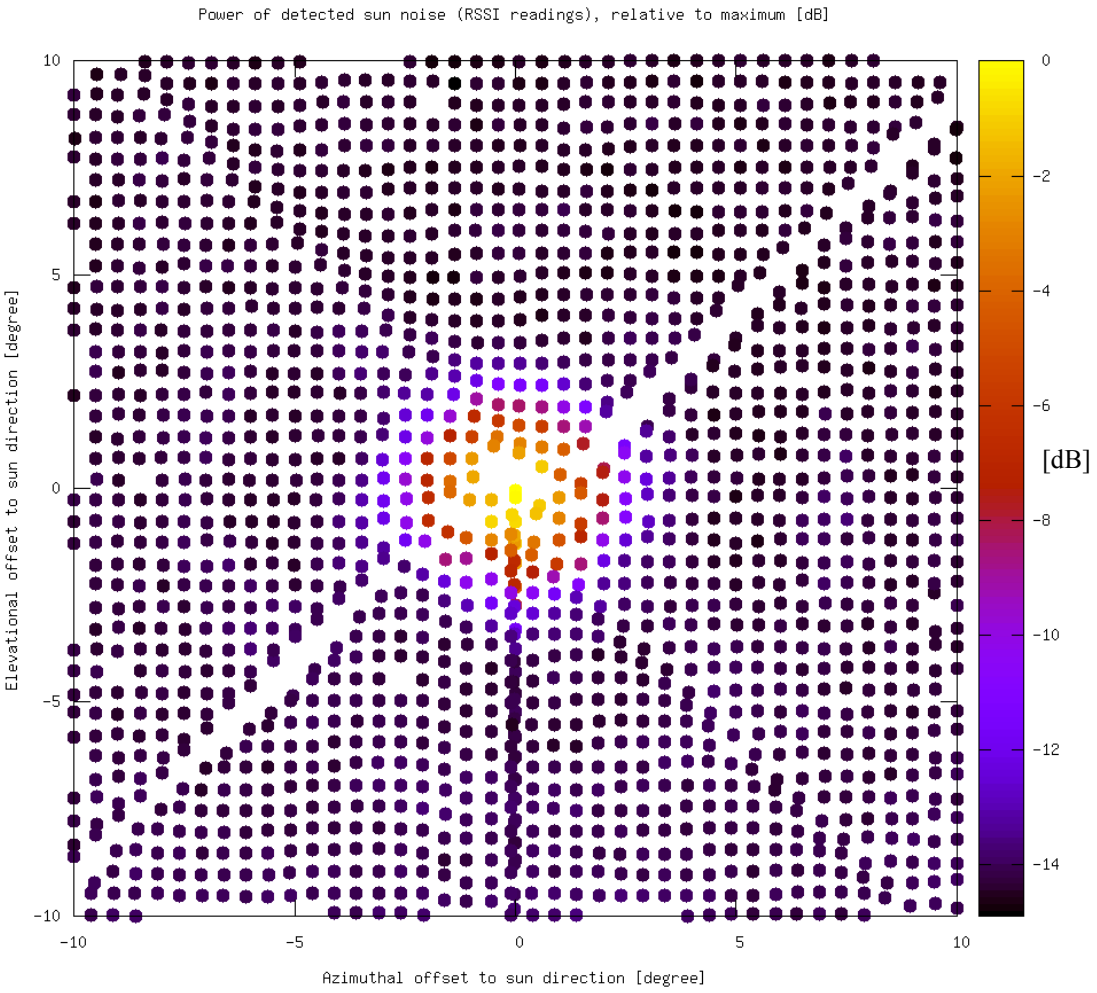

Figure 79: NYA-1 directivity with boresight offset compensation, square scan, 0.5° steps

Figure 79 shows data from a combined sun-tracking / square-type scan with a wider view around the main lobe direction of NYA-1, provided by a raster resolution of 0.5° and a raster range of +/- 10°. No side lobes are detectable in the graphic, but this does not mean that no side lobes exist in the scanned region. It can only be stated that the region shows no side lobes

with gain peaks of -15 dB or higher, relative to the main lobe's maximum gain. Side lobes with smaller gain peaks might exist in the scanned region, but are covered by the measurements noise floor. A cross-like structure is visible on the graphic, even more pronounced than in Figure 76 or Figure 78. The data of Figure 79 was thus chosen for analysis to investigate the origin of the cross-like pattern.

Figure 80 shows the positioning errors (commanded minus detected directions) for both axes (azimuth and elevation) and the actual antenna movement directions according to the 4 outmost scan squares of Figure 79. A first finding was azimuthal errors (blue graph) of about +/- 0.1°. The signs of the errors show a correlation with the actual azimuthal movement direction (clockwise or counter clockwise). The errors seem to correspond to a positioning delay as the achieved directions are always behind the commanded directions. A similar effect is found for the elevation axis (red graph), but with an even higher magnitude (+/- 0.2°). The suspected delay of positioning could be the result of a delayed positioning command execution, either caused by the NYA-1 ACU or the NYA-1 antenna, but not by NYA-Sattrack, as such problems were not observed with NYA-2.

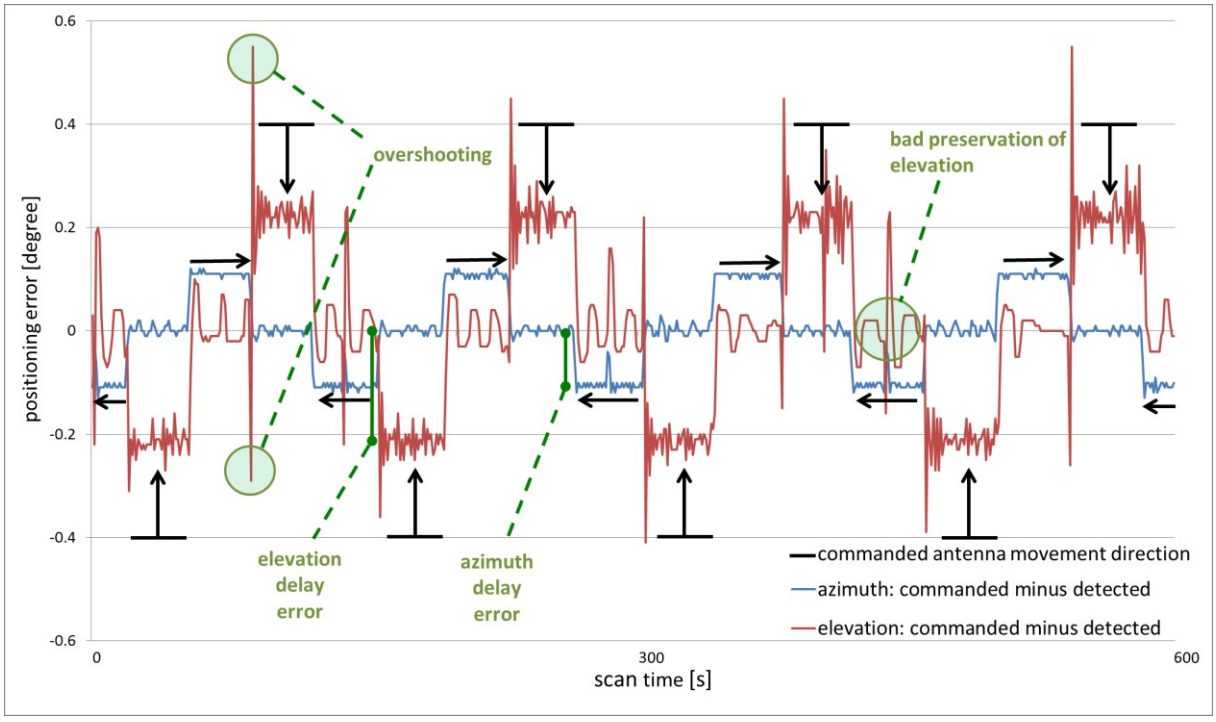

Figure 80: Analysis of positioning errors during square scan (0.5° steps) with NYA-1

Another elevational error was found at time intervals when the scan scheme only required a horizontal movement (horizontal arrows) and when no changes of elevation were

commanded. The positioning system apparently had problems to preserve constant elevations. The largest positioning errors (about +/- 0.5°) result from an overshooting on the elevation axis when an elevational movement follows an azimuthal movement, but not vice versa. A software bug in NYA-Sattrack as a possible explanation could be excluded, because it uses the same routines for both axes and turn directions. It was assumed that the degraded performance of the elevation axis was connected with a problem in the elevation servo loop, e.g., due to an imperfect resolver on the elevation axis (detection of actual angle) or vibrations in the system when the horizontal axis stops abruptly.

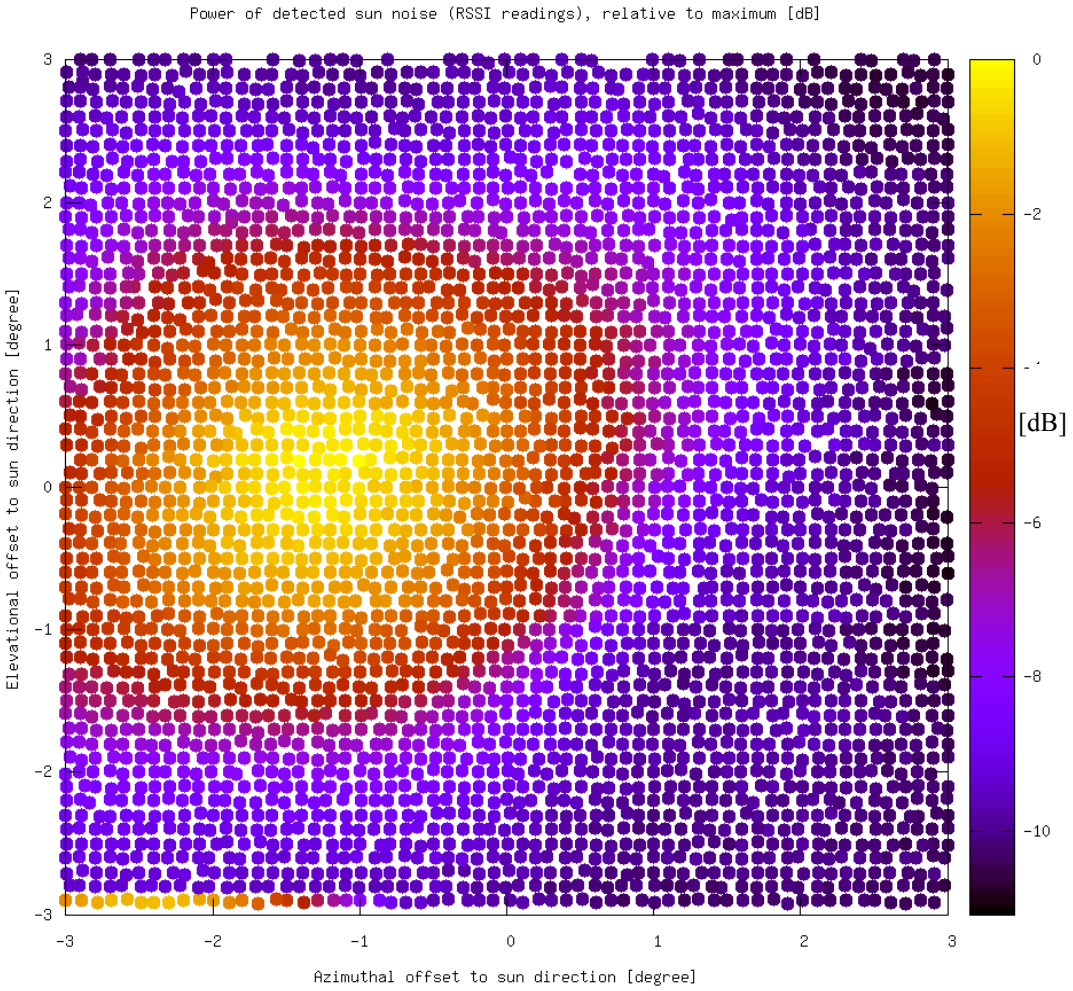

Figure 81: NYA-2 directivity w/o boresight offset compensation, stripe scan, 0.1° steps

Figure 81 (stripe scan) and Figure 82 (square scan) show results of NYA-2 experiments (sun-tracking combined with raster scan, no boresight offset compensation) with a raster step size of 0.1° and a raster range of +/- 3.0°. Both Figures show very similar patterns, which indicates again that the experiments basic results do not depend on the scan scheme. Figure 82 does not show a cross-style structure as seen with the square type scans with NYA-1. High signal

levels are displayed in the last scan line of Figure 81 (bottom), well outside the main lobe section. These high signal readings cannot be assigned to a side lobe, as the same signature then would appear on all other NYA-2 directional scans, which is not the case. A more likely explanation is the interpretation as a reflection from a local structure or the local environment, or as a signal from a satellite, which passed the antenna's field of view.

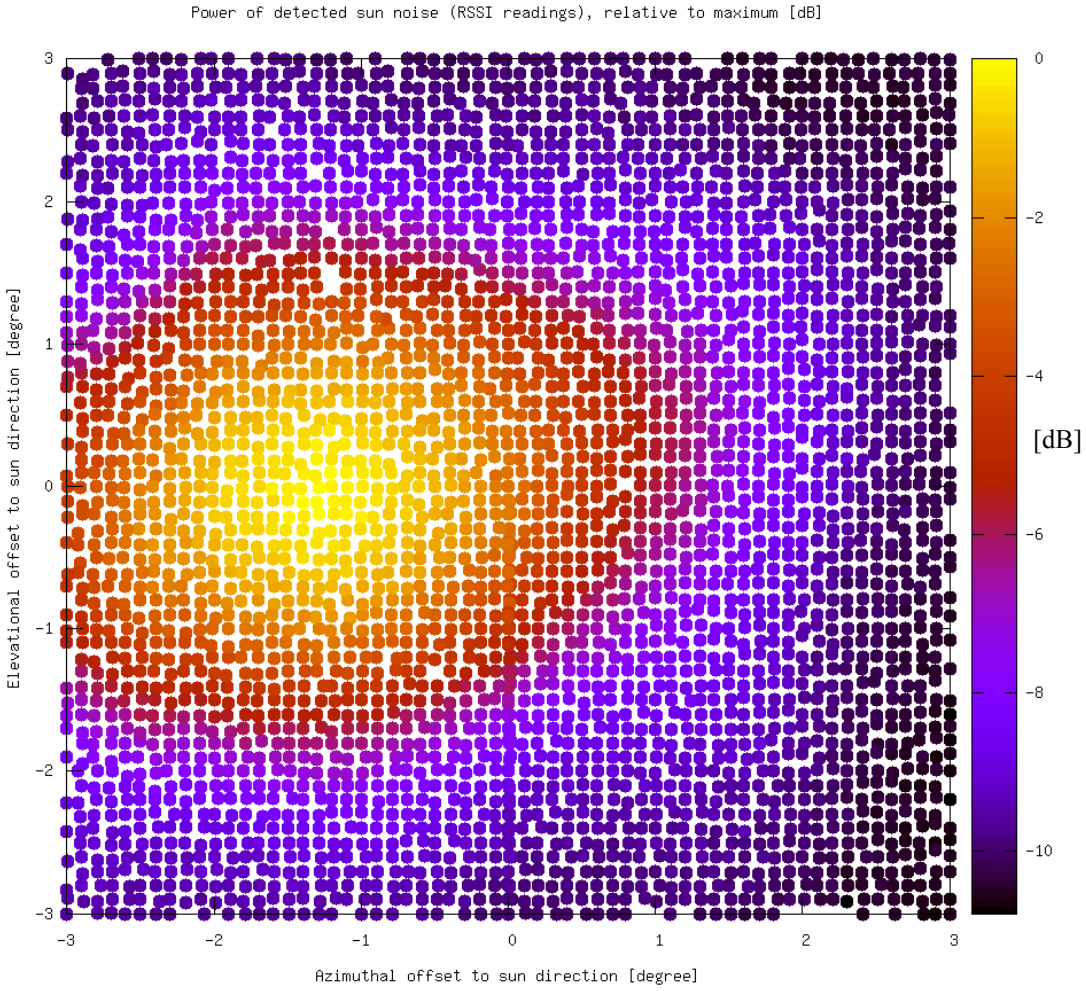

Figure 82: NYA-2 directivity w/o boresight offset compensation, square scan, 0.1° steps

Figure 83 focusses on the main lobe of NYA-2 with a raster resolution of 0.05° and a raster range of +/- 1.5° and shows a well-centred and rotationally symmetric beam pattern. The previously unknown but meanwhile determined boresight offset (9.1) was compensated during the scan. The resulting graphic is a confirmation of a correct boresight offset determination and compensation, respectively a good directional calibration of the NYA-2 antenna system.

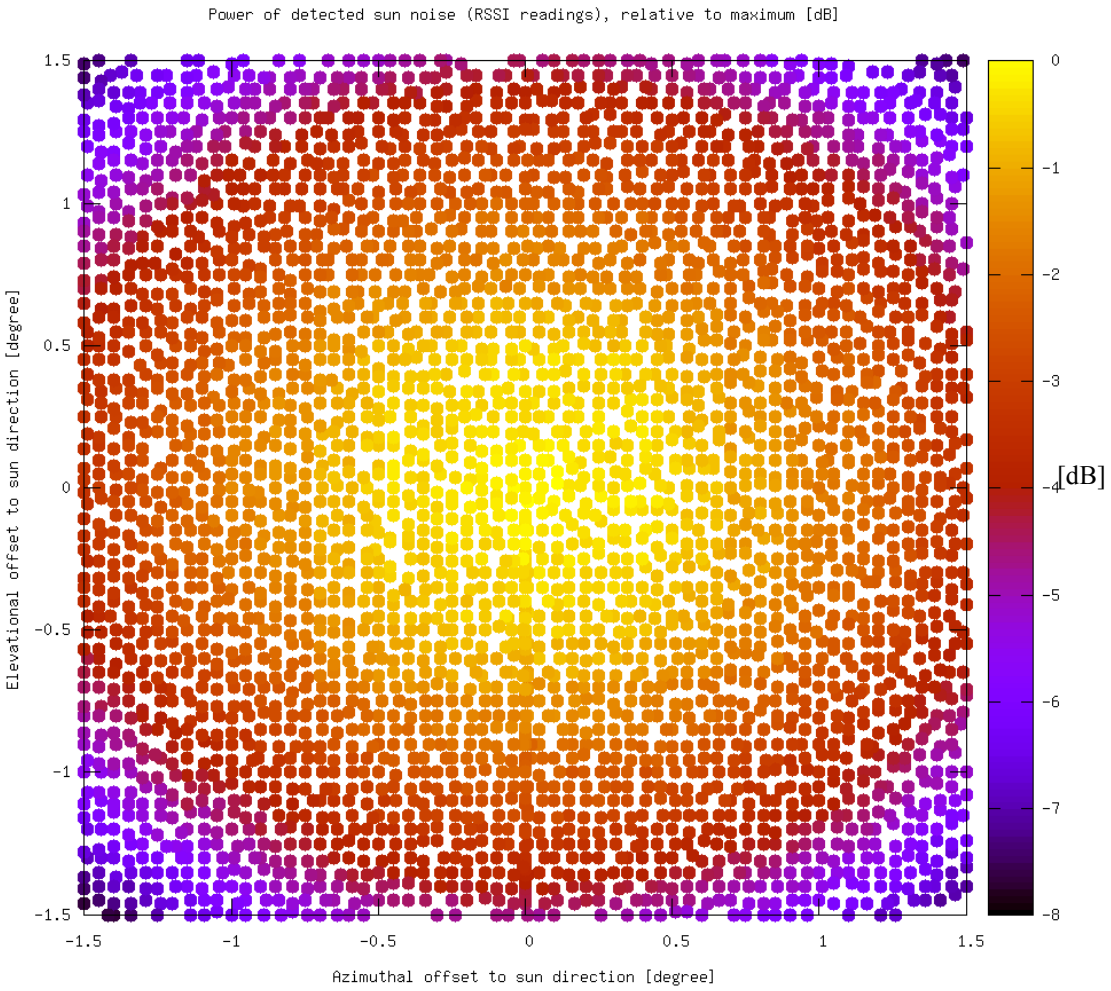

Figure 83: NYA-2 directivity with boresight offset compensation, square scan, 0.05° steps

Figure 84 shows a wider scan of the region around the boresight of NYA-2 (+/-10°). The measurement was made simultaneously with the corresponding NYA-1 measurements as shown in Figure 79. Both measurements used the same scan parameter and both graphics have the same colour scale range (0 to -15.5 dB). A remarkable difference between these two figures is the significantly higher "background noise" for NYA-2 at identical measurement conditions, as indicated by the purple colours in Figure 84. Similar observations can also be made by comparisons between other measurements with NYA-2 (Figure 83) and the corresponding measurements with NYA-1 (Figure 79), which suggests that NYA-2 generally picks up more noise than NYA-1.

The experiments in this section provided valuable results. However, the resume suggested some experimental improvements, which were realised with more experiments in 2016 (description in section 9.3.3).

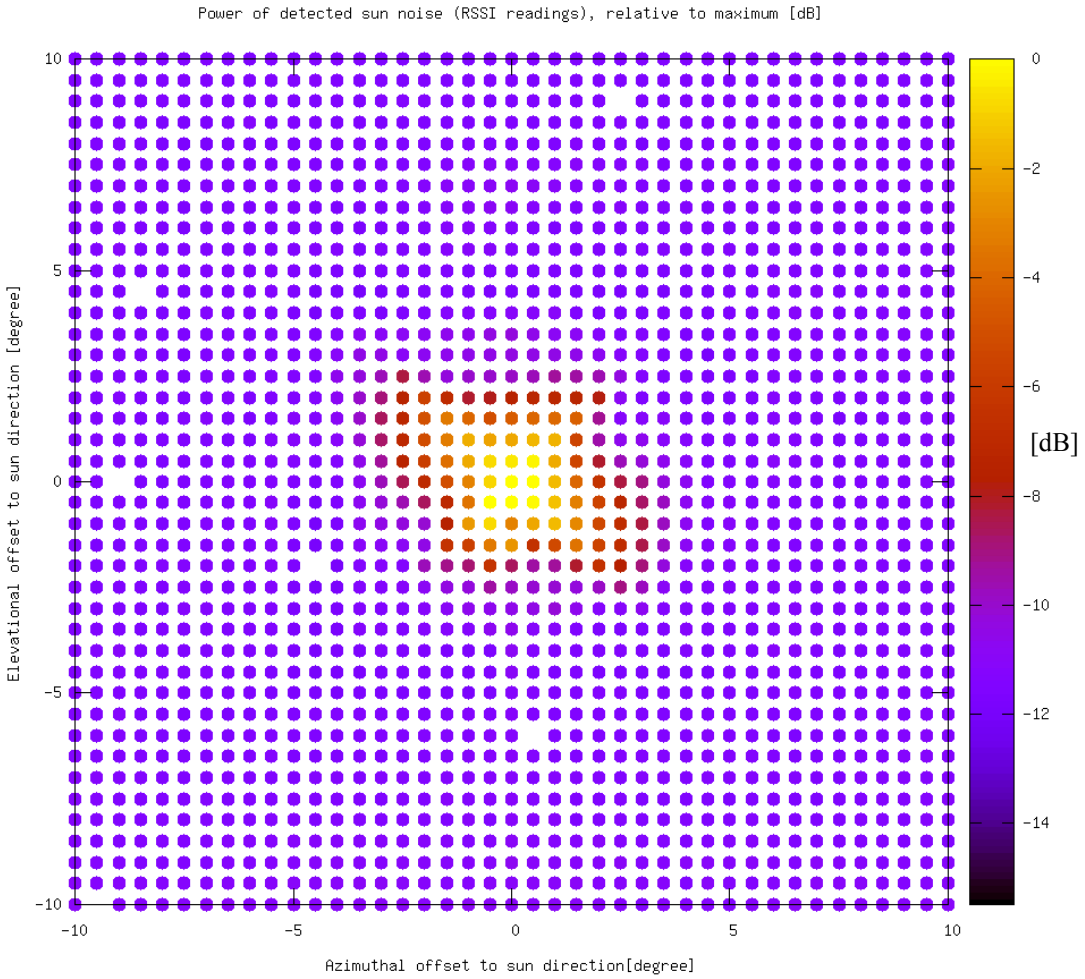

Figure 84: NYA-2 directivity with boresight offset compensation, square scan, 0.5° steps

9.3.3 Antenna directivity measurements in 2016

One of the findings from the antenna directivity measurements in 2015 was an increased noise level reception at low elevations. Another observation was that no side lobes could be detected, which was interpreted to result most probably from too low signal to noise ratios and / or the limited scan ranges. A weak point of the measurement setup was identified in the separated recording of RSSI readings and directions and the thus required correlation between the data sets. Another drawback was that the RSSI readings (received signal power) from the used telemetry receiver were not calibrated, which prevented a determination of the antenna's half power beam width Θ.

In 2016 the experiments of 2015 were continued with an improved experiment setup and increased scan ranges (up to +/- 30°) for the further investigation of side lobes. A calibrated spectrum analyser (FSP 13) was used to provide accurate measurements of received noise

power levels, instead of a telemetry receiver as in 2015. Analyser data was recorded through an additional software interface (6.10.4) in NYA-Sattrack[8]. In consequence the measurements of received solar noise power could be triggered timely correct (synchronised with readings of actual antenna directions) and the measurement results could be recorded directly (no data gaps as in 2015) in an additional column of the corresponding logfiles for sun-tracking.

The configuration of the spectrum analyser was the same as described in section 9.2 (determination of G/T). The antennas were moved with up to 1°/s. In consequence it could be expected that the received signal levels could change with a corresponding rate, due to the different antenna gain in different directions. According to equation (2) this would be 2.43 dB per second with NYA-2 when it was moved from boresight to an offset of 1°. Higher differences between individual measurements could be expected when the corresponding antenna directions were on the slope of the main lobe, e.g., up to 20 dB as suggested by typical directivity pattern as in Figure 27. The settings of the spectrum analyser for the experiment addressed several methods of averaging, which reduce the instrument's reaction time to signal changes. It was thus tested by experiment if the analyser's signal step response was good enough to measure the expectable rapid signal changes.

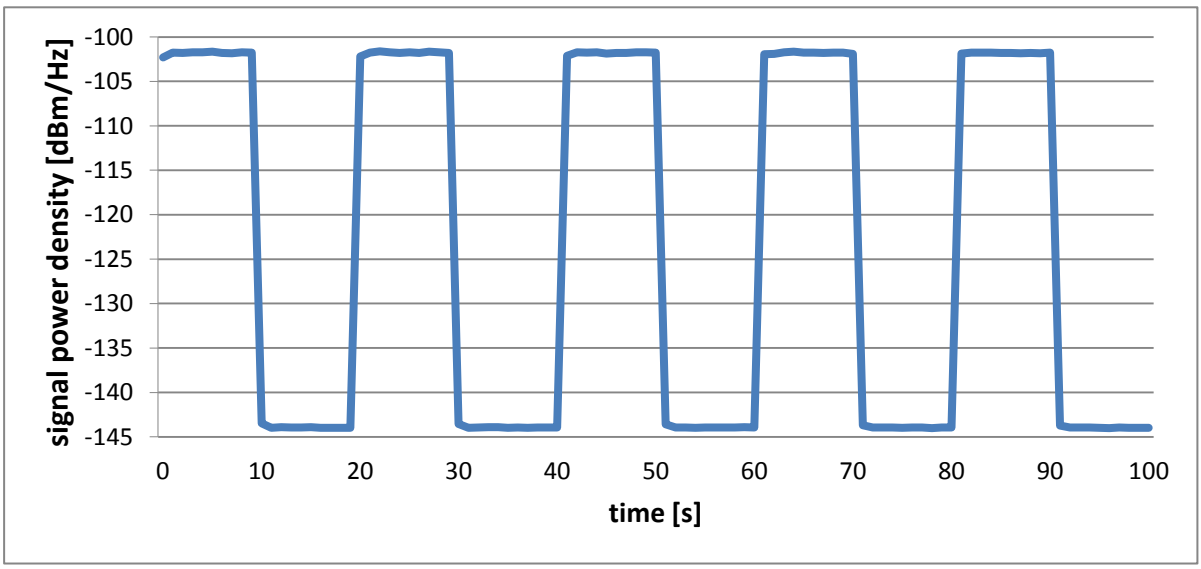

Figure 85: Signal step response of spectrum analyser with configuration for experiments

NYA-Sattrack operated one antenna in sun-tracking mode, to provide sun radio noise as a test signal. This test signal was connected and disconnected from the analyser input, by manual

[8] The same interface function was used also to determine the commanding timing accuracy (section 6.13.2).

switching of an RF relays, in intervals of about 10 seconds. This procedure was repeated several times and the recorded signal power density (sampled at 1 Hz) was plotted (Figure 85). The graphic shows that the instrument detected signal changes of 40 dB (from high to low and from low to high) after one second or earlier, which was more than sufficient. It was also concluded that the analyser sensitivity, which is limited by the internal instrument noise and represented by the lower signal levels, provided at least 40 dB of measurement range below the sun signal level (higher level). The required measurement range of the directivity experiments was defined by the difference of the signal levels from the sun and the noise floor with connected antennas. This was always less than 16 dB for all experiments (2015 and 2016), as it is evident from the signal scales of the diverse measurements (e.g., Figure 86 to Figure 90). It was thus concluded that the analyser configuration was suitable for the experiments, both, with respect to measurement range and agility.

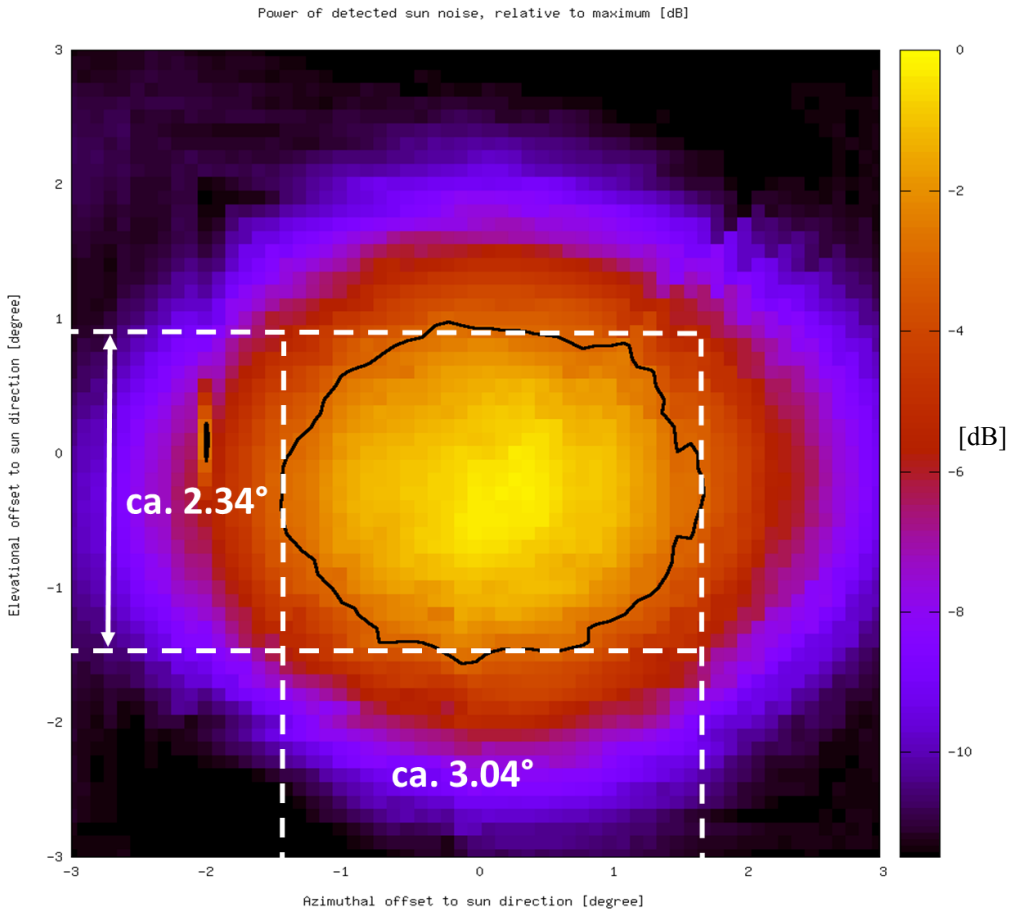

Figure 86: Half power beam width of NYA-1, determined from square scan with sun

Some of the measurements from 2015 were repeated in 2016 (same scan ranges etc.). The repeated measurement results were in agreement with the former measurements (shape of plotted RSSI data pattern etc.) and are thus not shown here, except of Figure 86 and Figure

87, which are square type scans (range +/- 3°, step size 0.1°), combined with tracking of the sun (both antennas). The "contour" function of the program "gnuplot" was used to draw isolines in plots of gridded measurement data, according to the -3 dB level of received signal power, to determine the antenna's half power beam width Θ.

The determined magnitude of Θ in vertical direction (NYA-1: 2.34°, NYA-2: 2.20°) is in good agreement with the corresponding theoretical values in Table 1 (NYA-1: 2.33°, NYA-2: 2.22°), which were calculated with equation (1). The Θ values in horizontal direction should be the same as in vertical direction, but were found to be higher for unknown reason.

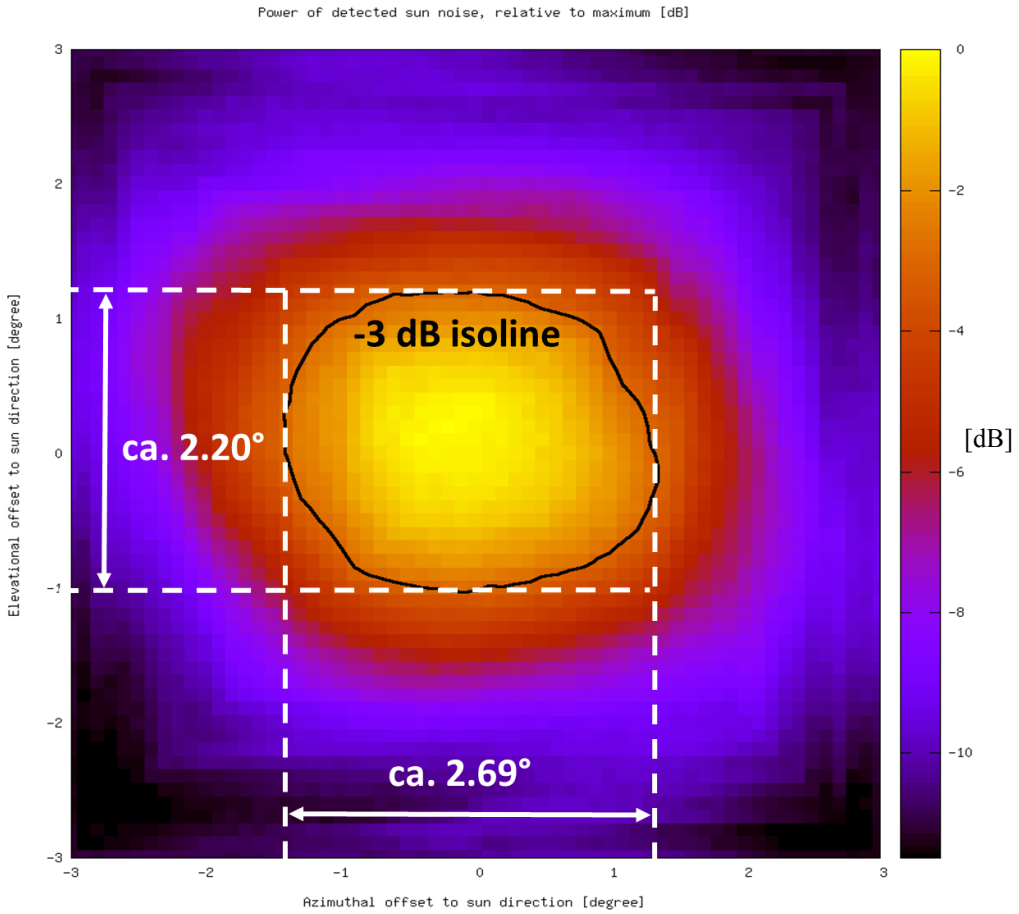

Figure 87: Half power beam width of NYA-2, determined from square scan with sun

Figure 88 shows the result of a combined sun-tracking with stripe scan and the NYA-1 antenna. The scan range (+/- 15°) was wider than for all measurements in 2015, to sense for side lobes with larger offsets to the boresight. Some patterns of slightly increased signal levels appear especially in the upper left quadrant of the graphic. However, these can hardly be interpreted as signatures from side lobes, as such must be expected to be present in all

quadrants, due the gain pattern of the antenna, which should have symmetries as in Figure 27b.

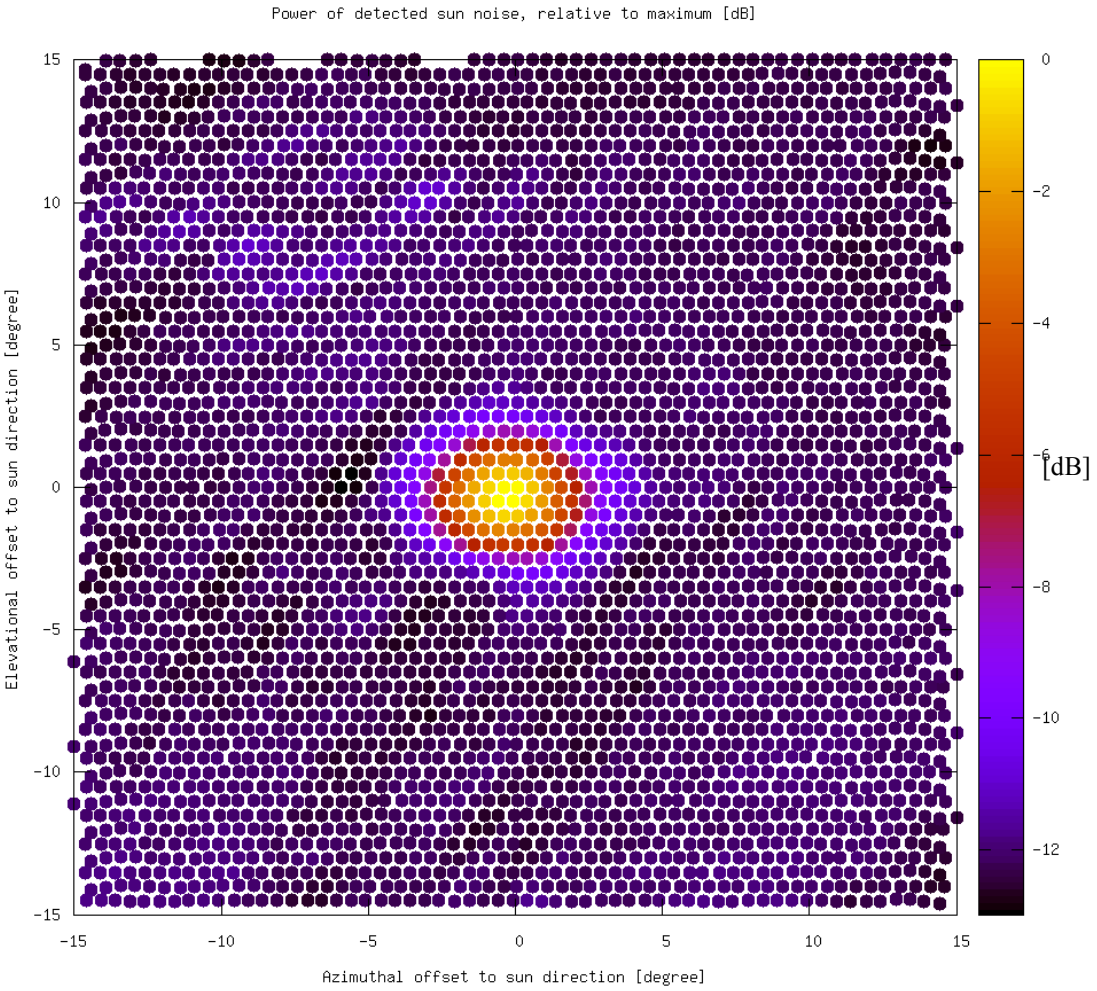

Figure 88: NYA-1 directivity with boresight offset compensation, stripe scan, 0.5° steps

A corresponding measurement with the same parameter and the NYA-2 antenna shows a similar unremarkable gain pattern (Figure 89). The colour code is the same in both figures, but the scale minimum for the signal power of the measurement with NYA-2 is about 1.5 dB higher than of the measurement with NYA-1. This is again, as already noticed in 2015, an indication for a higher system noise of the NYA-2 antenna, compared with the NYA-1 antenna. Both antennas were tested with the same variety of measurement setups timely close on the same days (applies separately for 2015 and 2016) or even simultaneous, but the noise floor with NYA-2 was always higher than with comparable NYA-1 measurements. It must thus be concluded that NYA-2 receives more noise from the environment than NYA-1 in general. One explanation for the observed higher NYA-2 noise levels could be a mismatch or misalignment of the NYA-2 antenna feed. This could generate an antenna reflector

illumination spill-over, including some areas outside the reflector rim. The feed would thus receive unwanted thermal noise energy from the area behind the reflector and not only wanted signal energy from the reflector front surface.

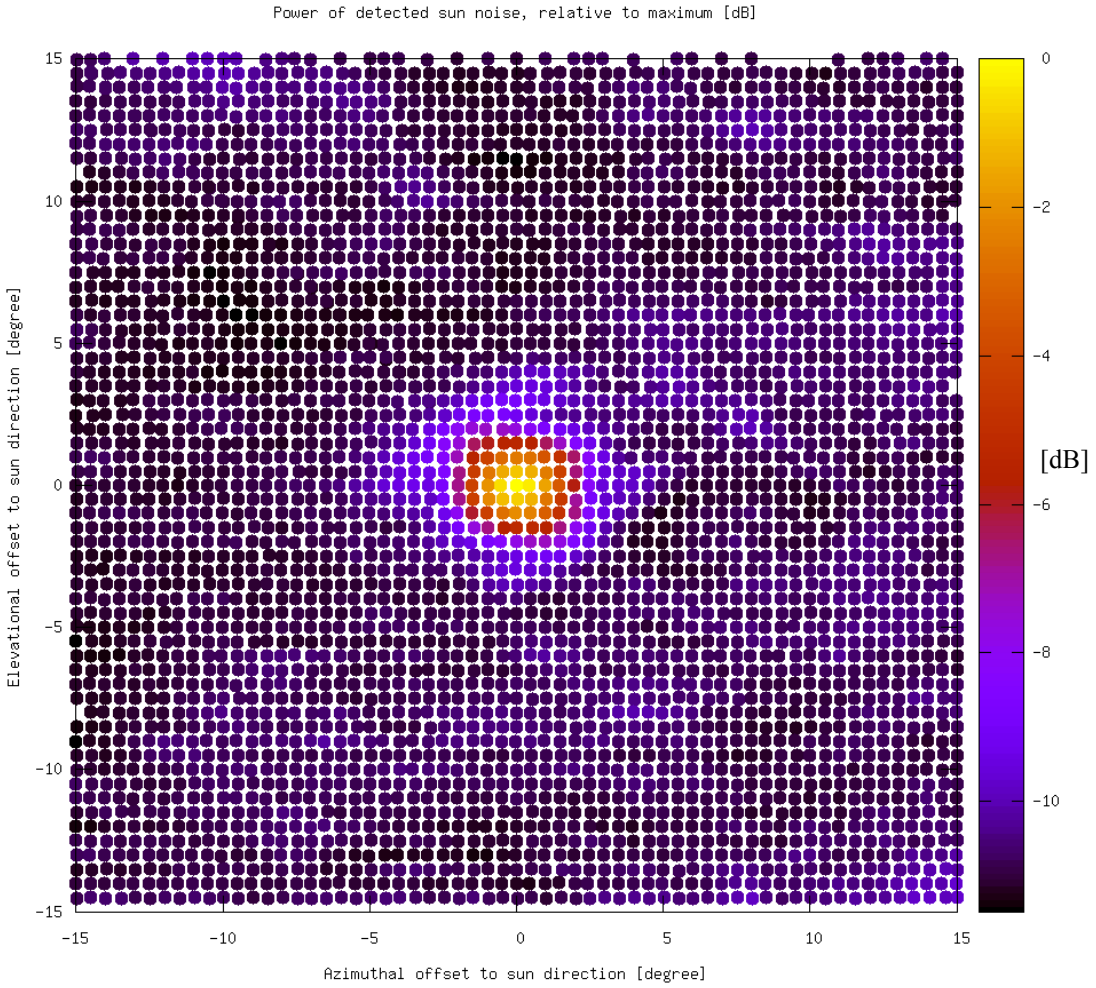

Figure 89: NYA-2 directivity with boresight offset compensation, stripe scan, 0.5° steps

Another explanation is the reception of additional noise through side lobes of NYA-2. This appears to be possible, even though no side lobes were detected during the experiments. However, it must be considered that the total background noise is the sum of all noise contributions as collected by multiple side lobes. Side lobes appear as spikes in a sectional view graph (Figure 27 a), but are effectively ensembles of ring-shaped zones (Figure 27 b) with a not negligible potential for noise power collection. The experiments had a limited and most probably insufficient sensitivity for the detection of individual side lobes, which must produce signal levels that are strong enough to peak out of the “background noise floor” to be detectable. Better results for such type of measurements and the used setup, especially for the detection of side lobes, should be achievable during times with increased solar activity, which

would produce stronger noise signals from the sun and thus a higher signal to noise ratio. The feed at the NYA-2 antenna was designed to work with RHCP and LHCP signals in the S-band and X-band, while the feed for the NYA-1 antenna was designed only for RHCP signals in the S-band. It can be assumed that the additional functionality of the NYA-2 feed, which is the result of a more complex feed design (compared to feed of NYA-1, see Figure 23), was achieved at the price of less adapted reflector illumination (e.g., higher spill-over) and less side lobes reduction. Also a higher feed-internal signal loss, compared with the simple feed of NYA-1, could arise from the more complex design, which is in detail unknown to the author. Another possible explanation is a reduced antenna gain, e.g., due to a small deformation of the reflector from the observed mechanical crashes during factory acceptance tests and the early installation phase (section 5.2.3). None of these assumptions could be verified, but a lower signal to noise ratio of the NYA-2 antenna, at least in the elevation intervals of the experiments, is one of the significant experiment results.

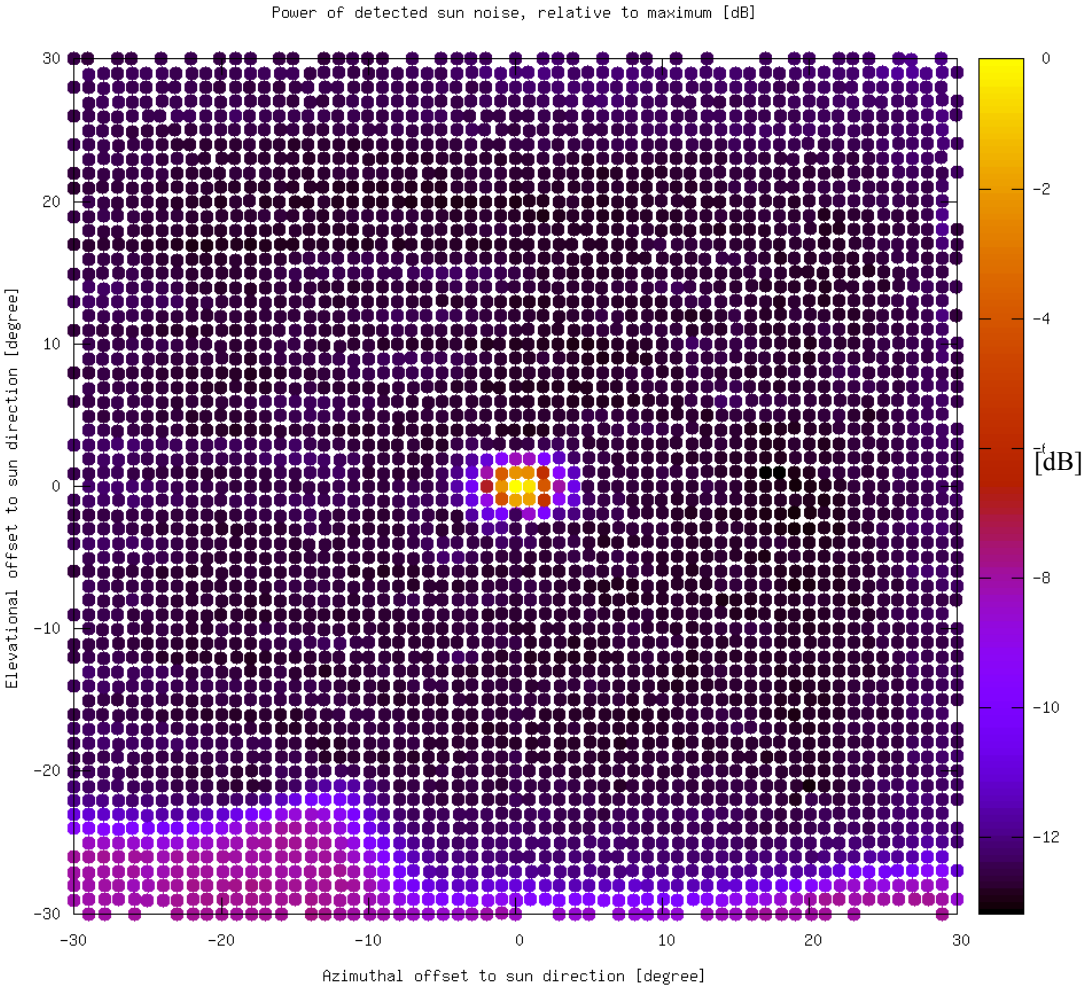

Figure 90: NYA-2 directivity with boresight offset compensation, square scan, 1° steps

Figure 90 shows a square scan around the sun direction with an offset range of +/- 30° in elevation and azimuth. No clear signs of side lobes can be found but an eye-catching zone of higher noise signals (increase of up to 5 dB) appear in the lower area of the plot at elevation offsets of about -21° and below. The profile of the noise zone correlates, at least in the corresponding direction interval, to some extent with the local horizon mask (Figure 49). The direction of the "noise profile peak" at about -21° (elevation offset) and -13° (azimuthal offset) has an absolute elevation of 13.2° and an absolute azimuth of 182° (absolute numbers from measurement data file) and corresponds indeed well to the direction of the Zeppelin-mountain peak, which has a true (geometrical) elevation of 12.6° and an azimuth of 183° from the viewpoint of the antenna. There are more correlations between the noise distribution pattern and the local horizon mask. However, they are less evident and the representation of the real local horizon by measured noise signals appears a bit diffuse. The reason is that the scan raster (square scan, Figure 53 a) was (virtually) moving with the actual sun direction during the measurement, which took more than one hour, resulting in more than 15° of azimuthal movement.

The measurement did not aim to, but draw attention to a local horizon of noise, produced by thermal noise of the environment. The noise horizon was found, at least in the investigated range, to correlate basically with the geometrical horizon mask, but also to have a certain vertical offset to it. This is certainly due to the antenna aperture angle, which causes the reception of noise from the local horizon even when the antenna aims shortly above it. It is also not unlikely that the distance and character of the local horizon cause different noise levels. Extreme examples might be a glacier in the distance (low noise) and the antenna operation cabin with several electronic devices (higher noise), which is close to the antennas. The noise horizon has a significant potential to reduce the signal to noise ratio during satellite reception, which could be avoided by the definition of increased vertical tracking exclusion angles to be considered for the planning of satellite contact schedules (contact times in jobfiles). Only a small segment of the local noise horizon could be made visible and thus a full scan of the local noise horizon, respectively the local environment (e.g., between 0° and 15° elevation) with respect to radio noise, was performed in November 2016 (section 9.4).

Another important result of the experiments in this section and section 9.3.2 is an assessment of an operational sun exclusion angle as explained below. The various scans with ranges of +/- 10° and more (e.g., Figure 89) show clearly that the signal from the sun was reduced down

to the background noise level (by about 12 dB) when the sun direction was more than 5° apart from the antenna boresight. This means that the sun has no negative impact on satellite tracking when it has a minimum offset of 5° to all tracked directions of a satellite contact. However, it reduces the antenna performance within that angular area and should thus be excluded from it. Taking into account that higher sun fluxes are likely to be met occasionally in the future, it makes sense that a slightly higher sun exclusion angle of 6° is respected for satellite tracking, which must be considered already by the contact planning procedure.

9.4 RF-scan of local environment

One conclusion of the measurements in section 9.3.3 was that the thermal noise of the local environment at Ny-Ålesund, respectively a certain contrast to the colder background above the local horizon, could be detected by the station's antennas. A series of measurements was performed in November 2016 to investigate and picture the local "RF-horizon" in more detail. The arctic winter time was assessed to be favourable for such kind of measurement as the sun, which could generate interfering signals directly or by reflections, was below the horizon full time. It was the first time that the antennas were operated for special measurements without local supervision and control, but the risk for damages to the antennas was considered to be small, since a proper and reliable operation of the antennas with NYA-Sattrack was already proofed.

A new software function was programmed for NYA-Sattrack to execute stripe-like scans with azimuth angles from 0° to 360° in a definable range of elevations with user selectable step sizes and angular resolutions. While this scan scheme was directly useable with NYA-1, it was found that it was not applicable with NYA-2 as the transitions over azimuths of 90° and 270° at low elevations caused significant deviations between commanded and achieved directions, due to the antenna's X over Y positioning system (explained in section 4.6). The horizon scans with NYA-2 were thus divided into two scans. The first scan covered directions with azimuths between 90° and 270° and turned over 180°. The second scan covered directions with azimuths between 270° and 90° and turned over 0°. In result there were no transitions over 90° and 270° during each of the scans. Both 180° scans were then combined to a full 360° scan, however, with a visible seam between them. The measurements with NYA-1 were limited to elevations equal or above 1.3°, because lower elevations were found to trigger the elevation axis protection switch occasionally.

There was no calibrated instrument for the measurements of received signal power on-site at the time of measurement, e.g., such as the spectrum analyser, which was used in summer times of 2015 and 2016. The received RF signal power (noise) was thus detected by the station's CORTEX receivers, logged on the receiver operation PCs, and finally correlated with separately logged antenna directions by data time stamps. One measurement of received signal power was recorded for each scanned direction, which was changed at a frequency of 1 Hz.

Figure 91 shows plotted data from the first horizon scan with NYA-1 (step-size Az = 0.5°, El = 1.0°). The local horizon is partly visible, e.g., with two peaks close to azimuths of 180° and 270° at about 12° elevation. These were identified with Figure 49 (NYA-1 optical horizon mask) as Zeppelin Mountain and Schetelig Mountain, but both appear less clear than expected. A more striking "V-shaped" signature extends in the azimuth range between about 70° and 150°. Even more surprising than the strong stamping of the signature in higher elevation directions was the fact that the pattern results from extreme small measurement values, peaking in a minimum of (less than) -75 dBm at about 115° azimuth and about 1° elevation. A straightforward interpretation of this data would suggest that the background in the corresponding directions was by far colder than the local environment (area below horizon contour) and the sky (area above horizon contour), which makes no physical sense.

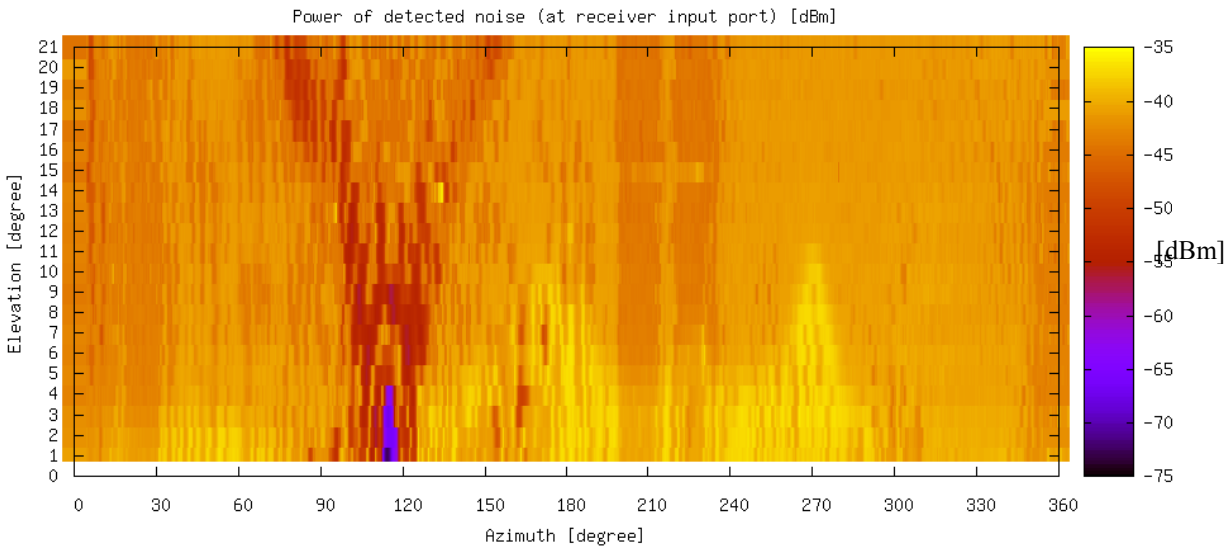

Figure 91: First scan of horizon with NYA-1 antenna (resolution Az = 0.5°, El = 1.0°)

The first horizon scan with NYA-2, as shown in Figure 92, and repeated scans with both antennas confirmed the strangely low measurement values. Both antennas detected signal minima at nearly the same azimuths and with low elevations in direction to Ny-Ålesund,

which implied that the source of the phenomenon was located in the village. It was found to be a DORIS beacon, which is used for tasks in the field of space geodesy (Jayles, Nhun-Fat and Tourain 2006). The beacon transmits permanently (24/7) with high power (10 W) on a frequency of 2.036 GHz and 401.25 MHz. Both DORIS frequencies (including harmonics of 401.25 MHz) were far away from the receiver frequency at the time of measurement (2.280 GHz) and thus the CORTEX receiver should not have received any DORIS emissions. Also the LNAs and preamplifiers were not specified for frequencies below 2.2 GHz.

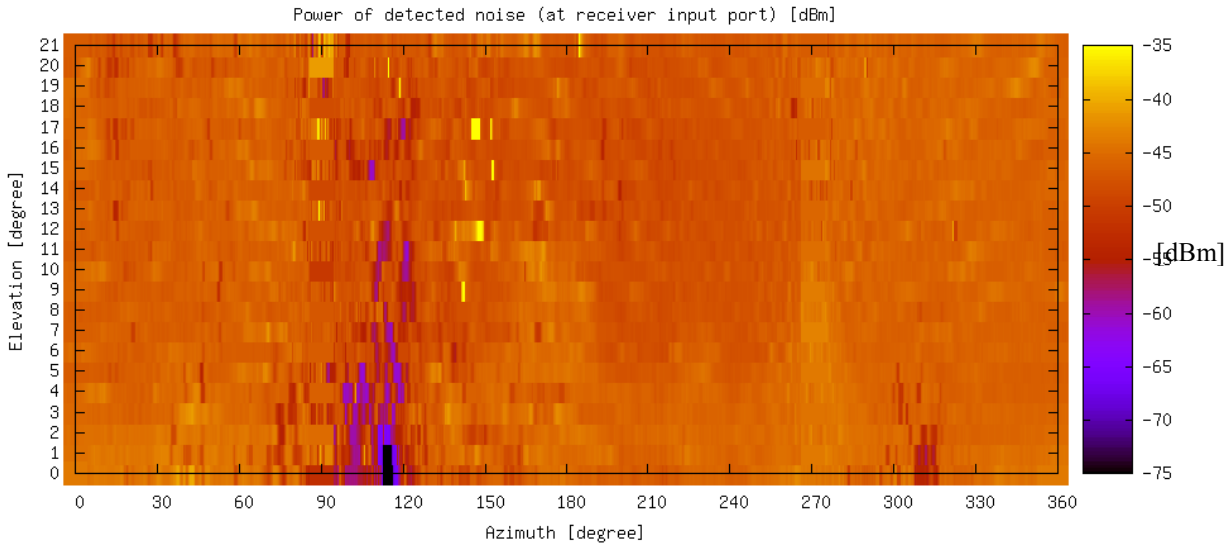

Figure 92: First scan of horizon with NYA-2 antenna (resolution Az = 0.5°, El = 1.0°)

The observed effect is explainable by an overloading of LNAs or other equipment in the receive signal path (Figure 31), e.g., the preamplifiers. Amplifiers have a limited capacity for amplification with respect to gain, but also with respect to the total output power, which is the power sum of all amplified signals. A strong input signal, in this case from the nearby DORIS beacon, can "occupy" an amplifier up to its power limit. The stronger the disturbing signal is, the less power is available to amplify other signals, in this case the noise signals from the sky and the local environment at the measurement frequency. The distance between the satellite-receiving station and the DORIS beacon is about 1.1 km only (Figure 37) and thus the NYA-1 and NYA-2 receiving antennas received very high signal energies. The DORIS frequencies are outside the specified bandwidths of the antenna feeds, LNAs and intermediate preamplifiers. However, this does not mean that these devices do not work at all at not specified frequencies, e.g., close to 2 GHz.

It was not clear if the described amplifier over steering reduced the performance of the LNAs at the antenna feeds or of the intermediate preamplifiers, which followed the LNAs in the

signal paths after some meters of coaxial cable. The intermediate preamplifiers were not directly exposed to the strong signals, but even worse, to the amplified signal output from the LNAs (gain = 60 dB), which made it probable that they were concerned. Also the input stages of the telemetry receivers could have been affected. These should be protected by internal filters but have to cope with again even higher signal levels, due to the additional gain of the intermediate preamplifiers (gain = 40 dB).

A possible counter measure for the reduction or elimination of DORIS signals and the described effect could be filters in front of the LNA or preamplifier inputs. Such filters were not available quickly and also not desirable, at least not in front of the LNAs, due to the expectable reduction of G/T antenna performance (explained in sections 4.5 and 5.3). Instead, it was arranged that the intermediate preamplifiers were removed from the signal paths (de-installation by AWI staff: NYA-2 on 7.11.2016, NYA-1 on 16.11.2016). The intermediate preamplifiers had initially been installed at the times of antenna installations and when LNAs with lower gain were used at the station (prior to 2014). They were now considered to be not required any longer, due to the higher gain of the meanwhile installed newer LNAs, and as supported by the calculations in section 5.3. First tests confirmed that the new setup worked well for satellite tracking while the disturbing effects were reduced significantly.

Figure 93 and Figure 94 show subsequently performed horizon scans with both antennas at a resolution of 0.5° (azimuth and elevation), this time limited to elevations of up to 15°. The contour of the local environment, respectively the local noise horizon mask as determined by the noise measurement, is clearly visible and in good agreement with the optical horizon (Figure 49). No unwanted signal signatures are found anymore, except in a small area around the direction to the DORIS beacon (azimuth between 115° and 120°) below the local horizon (2° and less), which has no relevance for satellite tracking. Some pattern with yellow colours appear in that area, according to signal levels that are higher than the thermal noise, which is different to Figure 91 and Figure 92, where they are smaller (black). The nature of the new pattern is thus not explainable by the described over steering of amplifiers. It is assumed that they correspond to weak spurious emissions of the DORIS beacon transmitter. Such spurious emissions are known to be, e.g., 40-50 dB weaker than the main emission, but with a broadband frequency spectrum.

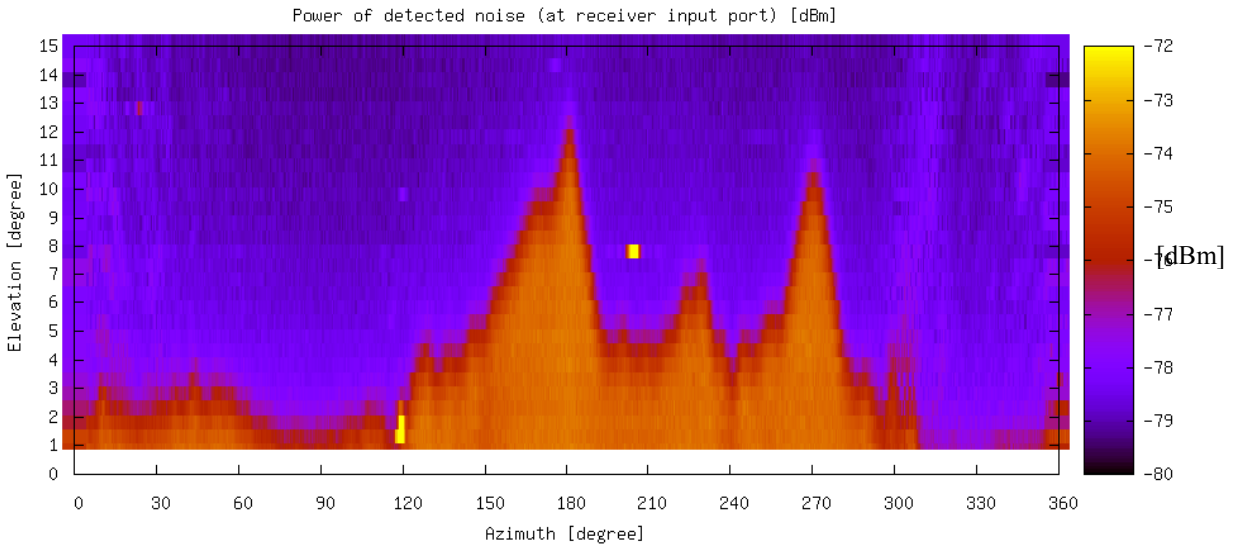

Figure 93: Scan of horizon with NYA-1, intermediate preamplifier removed

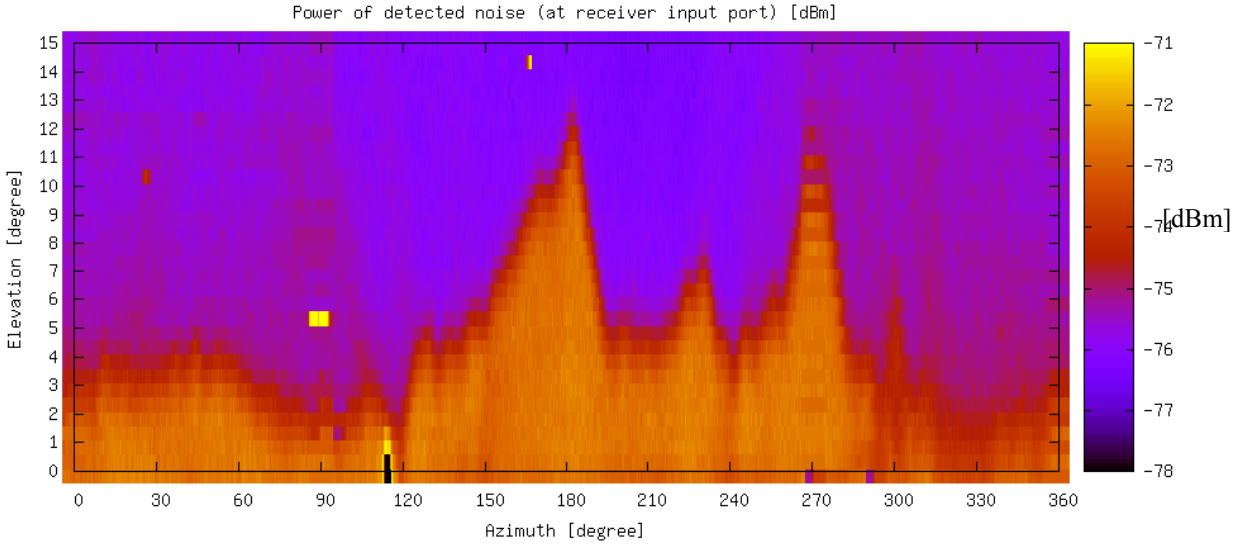

Figure 94: Scan of horizon with NYA-2, intermediate preamplifier removed

The other yellow spots in the plots, e.g., in Figure 94 at about 90° azimuth and 5.5° elevation, are believed to be emissions from satellites. These do not correlate with the orbits of the satellites that are received at NYA regularly, but each of the scans for Figure 93 and Figure 94 took more than 6 hours and many other satellites passed the station during that time. The ranges of displayed signal level data (colour codes) were adjusted for almost equal colours in the areas below the horizon mask, to highlight that the horizon scan with NYA-2 shows more noise (pattern with red shades over blue background) than the NYA-1 scan in the directions to the sky. This is in agreement with all other measurements in section 9 and can be interpreted as another evidence for a less good RF-related performance of NYA-2 compared with NYA-1.

It was suspected that some unresolved tracking problems at apparently good receiving conditions (e.g., high elevations above local horizon) in the past, such as high numbers of crc-errors which usually occur at too low S/N ratios (4.4), originated from the described effects. Corresponding analysis were performed with data from a new database for receiver-operation logs, which was implemented in August 2016 (by S. Reißland, GFZ). Figure 95 and Figure 96 show statistics of crc-errors per day (at roughly equal daily data volumes) which were detected by the CORTEX receivers during telemetry contacts with TerraSAR-X (with NYA-1), Tandem-X (with NYA-2) and GRACE-1 (with NYA-2 and some contacts with NYA-1). There are no statistics for GRACE-2 in the graphs because there were no contacts with GRACE-2 in the displayed time interval, due to problems with the satellite's on-board power system.

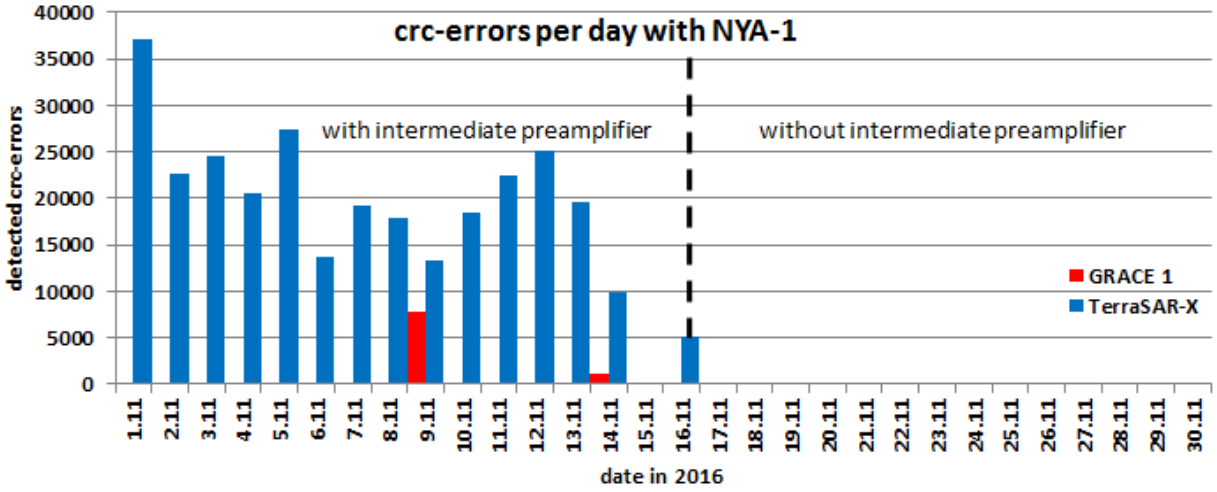

Figure 95: crc-errors with NYA-1, with and without intermediate preamplifier

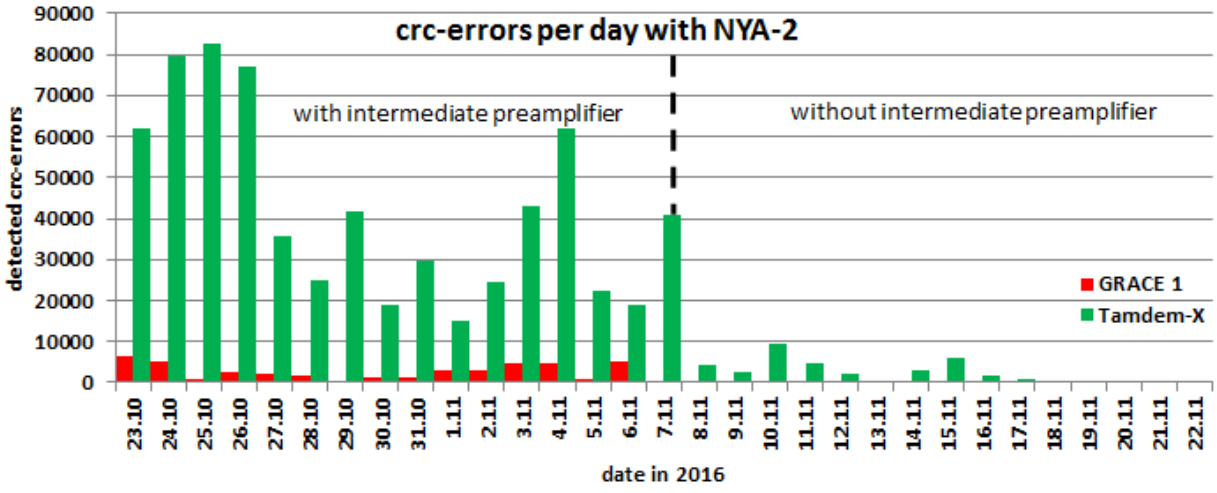

Figure 96: crc-errors with NYA-2, with and without intermediate preamplifier

The graphs cover the different dates when the preamplifiers were removed from NYA-1 and NYA-2 and about 2 weeks before and after that measure. It is evident that by far less (only about one-tenth) crc-errors were detected during the satellite tracking with both antennas since the removal of the intermediate preamplifiers.

The horizon scans discovered that the local DORIS beacon transmissions reduced the RF performance (sensitivity) of the satellite-receiving station significantly, which was a long searched explanation for so far unresolved receiving problems. Repeated measurements showed also that the simple changes of the technical setup (removal of intermediate preamplifiers) reduced the interferences effectively. In consequence the number of detected crc-errors in received satellite data decreased dramatically, which effect an increase of error-free received telemetry data.

10 NYA-Sattrack in praxis

10.1 Routine operation performance

NYA-Sattrack was tested to run as a 32-bit application and as designed on computers with 32 and 64 bit versions of Windows 2000, Windows XP, Windows 7 and Windows 10 operation systems. The program executables have a size of 250 KB for the main program and about 80 KB for one antenna interface DLL. About 3 MB of computer system memory (RAM) are used during normal operation. The computers for the routine operation of NYA-1 and NYA-2 with NYA-Sattrack currently use a Windows 7, 64 bit version.

The proper operation of the antennas at Ny-Ålesund was checked frequently, at least once per day, including weekends. This procedure was practised already before NYA-Sattrack was used, in order to ensure short reaction times in case of problems with the antenna systems. Some problems, as described in 8.2 and 8.3, showed up in the first days and after some months of program operation, but no significant problems afterwards. Generally it can thus be concluded that the program performance was and is very good. The automatic processing and update of jobfiles and twoline elements files works perfectly. This includes unplanned changes of tracking schedules, which was done a few times, just by sending the updated schedules to the antenna operation PCs. The program log, the individual satellite tracking logs and the graphical log (skyplots) are generated and stored as desired and the program GUI proved to be well designed for a frequent and low effort operator monitoring of all satellite tracking activities.

NYA-Sattrack is listed by the Windows task manager function on a dual core PC (Intel I3 processor) as an “idling” process, with “0%” CPU load during most of the time. Higher CPU load was observed only for intervals of about 1 second, when the program reads a jobfile and prepares a next satellite pass tracking, but not during active satellite tracking. All in all NYA-Sattrack is considered not only to fulfil all design goals, requirements and expectations, but to do this also in an even stable and resource saving manner.

An assessment of the practically achieved system internal positioning accuracy requires a comparison between desired (commanded) and detected directions under real operation conditions, which of course must include the operation of antennas. Positioning errors that are detected in this way thus indicate the sum of possible shortcomings of NYA-Sattrack and

other errors in the loop, e.g., from uncertainties of the positioning gears, the resolvers (positioning feedback) and the interaction between antennas and antenna controllers (ACU). Figure 97 and Figure 98 show azimuthal, elevational and total tracking errors based on logged positioning data (commanded directions in last second minus achieved directions in actual second, resolution 0.01°) of a GRACE-2 satellite contact, which was tracked by NYA-1 and NYA-2 simultaneously on 10th September 2016. The tracked pass had a culmination of 89° and is thus a good example for so called "keyhole passes", which are known to potentially cause high tracking errors with elevation over azimuth positioning systems.

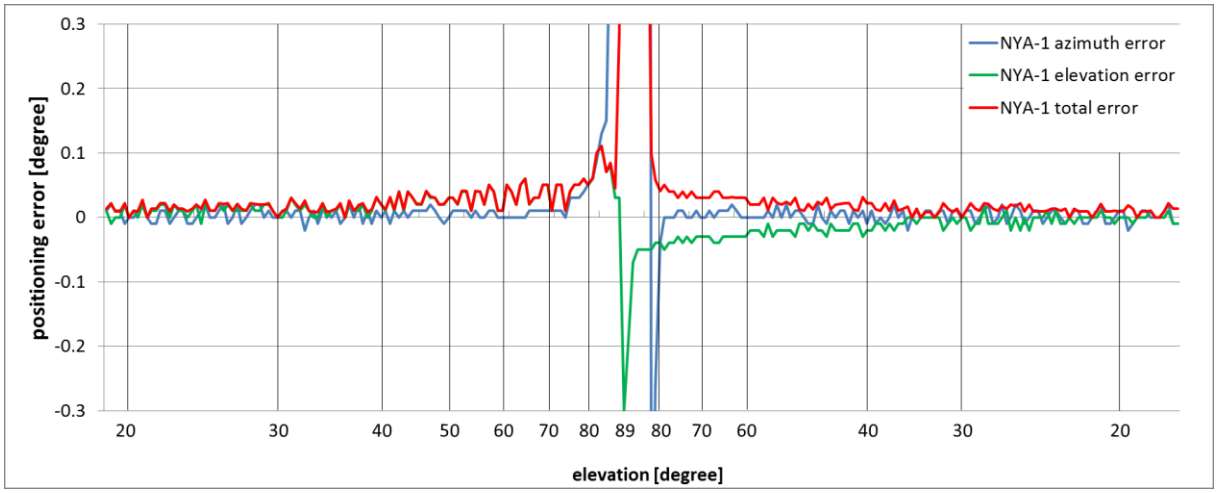

Figure 97: Tracking performance of NYA-1 during pass with 89° culmination

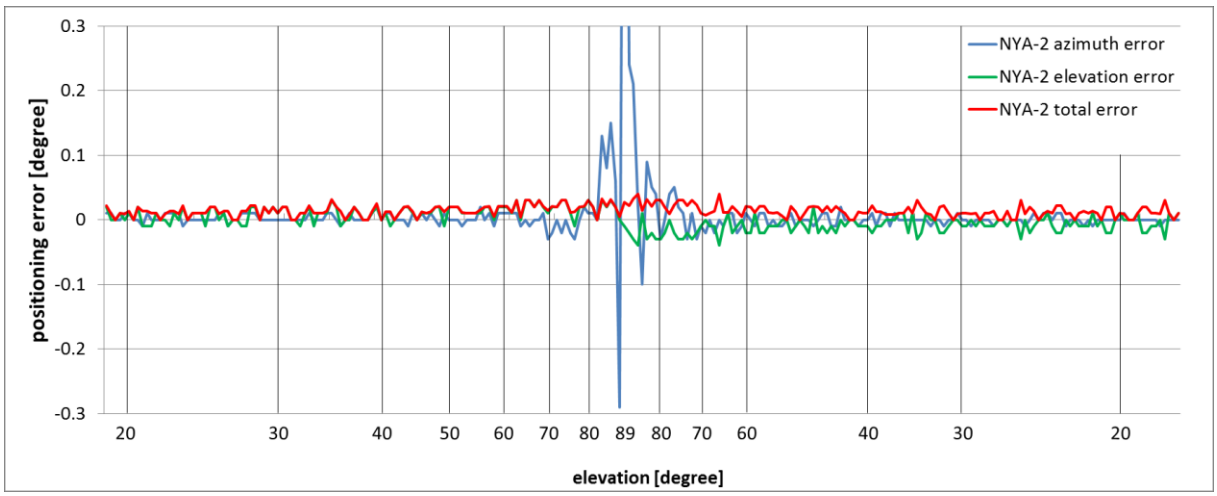

Figure 98: Tracking performance of NYA-2 during pass with 89° culmination

The graphs show that the azimuthal, elevational and total tracking errors of both antennas are clearly less than 0.1° for all elevations below 83°. The maximum azimuth errors above that

elevation in this example (not shown in graphs) are very large for NYA-1 (68°) and at least high for NYA-2 (1.27°). The elevational errors are much smaller than the azimuthal errors and stay below 0.1° in general, except of one negative peak (-0.3°) in the graph for NYA-1. However, the finally relevant errors for satellite tracking are the total errors, as shown with the red graphs in Figure 97 and Figure 98. These were calculated with equation (39) and their maxima are 3.17° for NYA-1 (at ~85° elevation) and 0.04° for NYA-2 (at about 65°), both on the descending leg of the pass.

The differences of observed tracking performance between NYA-1 and NYA-2 at high elevations are considered to origin from the different layouts of the positioning systems (El over Az and X over Y axes), as explained in section 4.6, but not from NYA-Sattrack. A small difference of tracking error mean values before culmination (error > 0°) and after culmination (error < 0°) is noticeable with both antennas. This error is interpreted to result from a not yet fully compensated command execution delay (introduced by the antenna system) and to be a function of the axis rates, which increase with elevation, but not of the elevation itself. The effect was not further investigated, as it was that small, but may be considered if higher accuracies are required in the future. In summary it can be stated that the tracking performance of both antennas at Ny-Ålesund, in the operational configuration with NYA-Sattrack, is very good. However, the satellite data reception at times with high elevations, e.g. over 83°, should be avoided with NYA-1. This has to be considered in the contact scheduling process, while there are no such limitations for regular satellite tracking with NYA-2.

10.2 Examples for benefit from in-house development of NYA-Sattrack

In spring 2015 GFZ was informed that the Norwegian authorities defined a new format for satellite tracking logfiles, mandatory to be used by all satellite ground stations under their control responsibilities. These logfiles must be provided to them during the regular (biannual) inspections at the NYA station, to be checked with certain routines (software of authorities, no details known to the author). The new released logfile format defined the structure and contents of logfiles as well as the logfile naming. The structure of the logfile names was defined as:

<satellite name)>_<orbit number>_<date>_<time>_<antenna system name>_.trk
with
satellite name: NORAD name (spaces not allowed, dashes to be converted to underscores)

orbit number: orbit number of logged satellite contact (since satellite start)
date: yyyymmdd (year, month, day of month)
time: hhmmss (hours, minutes, seconds)
antenna system name: antenna system identifier, but without dashes and spaces
“.trk”: filename suffix (extension)

Parts of the new tracking logfile format were already implemented in NYA-Sattrack by chance, but some other had to be included by additions and modifications to the program. The inclusion of actual satellite orbit numbers (at tracking time) into logfile names was not foreseen until then. A dedicated routine to calculate the orbit numbers from information in the twoline elements and AOS-times was programmed and integrated in NYA-Sattrack. Since then the orbit numbers are also displayed on the program main GUI. Problems or at least significant higher effort for the problem solution would have arisen if NYA-Sattrack had not been in place at that time, due to the lacking support for both previously used antenna operation software packets. After all the unexpected change of the logfile format could be handled with low effort and short reaction time. The described adaptation to changed operation conditions was a first example for the benefit that yields, also in this respect, from the in-house development of the new antenna operation software.

Another example for a required and executed modification of the antenna operation software was the adaptation to changes in the jobfile format. Jobfiles are used to configure antenna and receiver operations at Ny-Ålesund (5.5) and contained only a very small number of parameters (times and frequencies) for many years (old jobfile format example in Appendix). An extension of the jobfile parameter list was required in 2016, e.g., because the satellite Flying Laptop (3.4.2) can transmit on one or two frequencies, with different data rates and different antenna polarisations (RHCP and LHCP). A new jobfile format (Falck, Reißland, et al. 2017) was developed by GFZ to address these points and other new features of NYA-operations, e.g., the assignment of receiver channels to antenna signals. It uses new or partly modified keywords and units of the old format and a changed date/time format (new jobfile format example in Appendix). It was also praxis to use one jobfile per antenna, but only one jobfile in the new format will be used for both (or more) antennas at NYA in the future. The changeover to the new format, (scheduled for summer/autumn 2017) required modifications to the software for the jobfile generation as well as for the execution of jobfiles at NYA.

Changes as described above could and can be implemented easily into NYA-Sattrack and NYA-GPS-Sync by GFZ, because it is in-house developed software. The same or similar changes of software from other sources would require at least full insight in the related program source code or reliable support, which is usually connected with costs, if obtainable at all.

10.3 Operation reliability of NYA-Sattrack

Some software troubleshooting was required in the first time after installation of NYA-Sattrack and a second time some months later in 2014. These problems were not detected earlier, e.g., during the main programming and test activities before installation, because one problem was strongly related to antenna hardware issues (8.2) and the other showed up only after some weeks of uninterrupted antenna operation (8.3). These initial problems were solved as early as possible and NYA-Sattrack was observed to run in principle flawlessly with both antenna systems at Ny-Ålesund since then. Regularly problems with the formerly used software for NYA-1 during turns of the year were not experienced with NYA-Sattrack anymore (both antennas, 2014 to 2017). The azimuth axis limit stop events of the NYA-1 antenna, a formerly frequently occurring and annoying problem (5.2.2), never happened again, thanks to the implemented solution in NYA-Sattrack, which handles the problem with an adapted strategy (6.9.1). Also the different types of logfiles were generated and archived reliably, which was not always the case with the older antenna operation software. All these issues were solved completely with NYA-Sattrack.

The operation of the antennas at NYA was observed by the author since 2002, but it was found very difficult to generate authoritative absolute numbers for the reliability of antenna operation software, e.g., before and after the introduction of NYA-Sattrack in 2014, although this was much desired. One reason was gaps in the archive of operation logfiles for some periods before 2014, e.g., due to hard disc crashes. Another reason was the difficulty to distinguish if an observed problem was related to antenna operation software issues or to any other of many possible reasons. Examples are computer problems (e.g., computer OS, other software, hardware), problems with the antenna systems (including ACUs and interfaces), frequent main power outages (partly bridged by local UPS), communication problems (Internet) or human operating errors and other interactions, e.g., for test and maintenance works. There was no systematic documentation of anomalies at NYA to support related analyses.

The starting points for the assessment of the antenna operation reliability with NYA-Sattrack, as shown in Figure 99 and Figure 100, were accumulated numbers of completely tracked satellite contacts versus scheduled satellite contacts. These numbers were generated with a small program (programmed by author) that scanned the logfile archive for the existence and validity of logfiles, corresponding to all individual satellite contact entries in the jobfiles since July 2014 (more than 27000 per antenna). By nature this initial statistic represented all kind of operation problems. The numbers were thus revised according to problems that could be assigned reliably to other sources than the NYA-Sattrack software, e.g., from information in logfiles, related emails and other notes. In consequence these corrected numbers cover all software problems, but also all incidents with unidentified problem sources, which have a part of more than 50 % in Figure 99 and Figure 100. The graphs provide an overview over the full time of operation, including initial problems in the first months of operation, and correspond thus to a worst-case assessment of antenna operation reliability with NYA-Sattrack. This approach is to some extent comparable to the approach for the statistical graph that covers the first years of NYA-1 operation with the DLR-software (Figure 47).

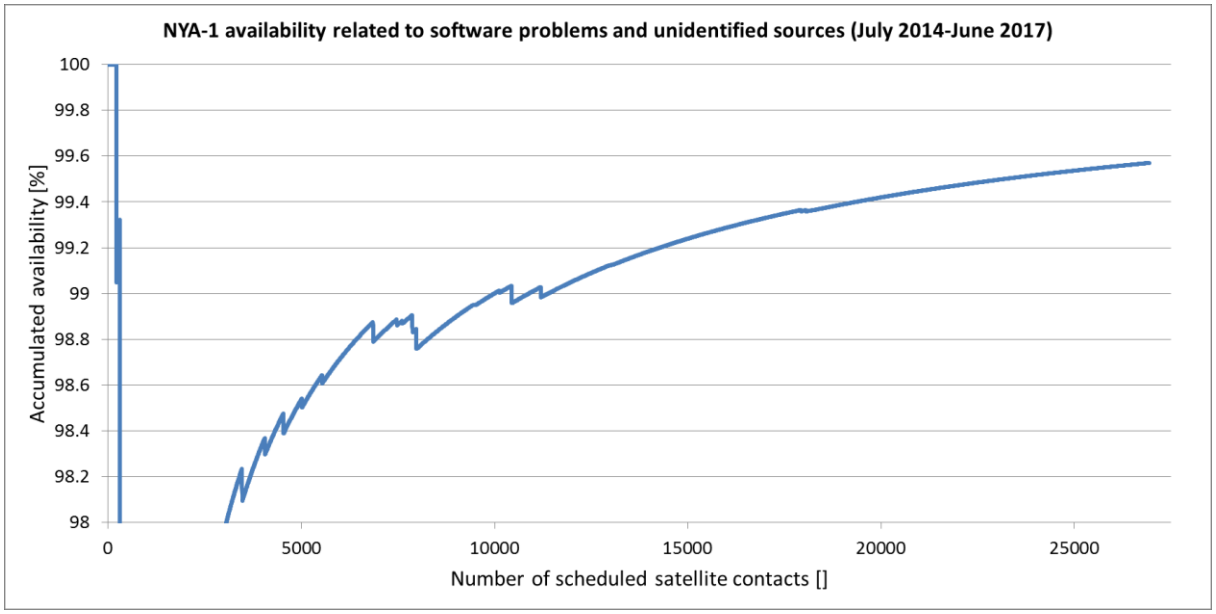

Figure 99: Accumulated availability of NYA-1 with NYA-Sattrack operation

The graph for NYA-1 (Figure 99) shows that several incidents occurred until contact number ~11000 (September 2015), which limited the corresponding total availability number to about 99 % at that time. The main reason was the difficult detection and management of the underlying problem, which was related to a discrepancy of the NYA-1 antenna system feedback (sections 8.2 and 8.3), but discussible not to a genuine software problem. Only one

noticeable period with a problem was observed later (about contact 18000, June 2016). The accumulated availability number approached 99.6 % in June 2017.

The graph for operation of NYA-2 in Figure 100 shows less many incidents than for NYA-1 in Figure 99. A more or less stable availability level of about 99.8 % was maintained from contact 5000 in January 2015 until June 2017 (end of graph). Both graphs (Figure 99 and Figure 100) are interpreted as proofs of good routine antenna operation reliability. The reduction of availability numbers result from only a few incidents per year, rather than a continuous lack of performance, but most incidents caused the loss of several contacts with a corresponding strong effect on the statistics.

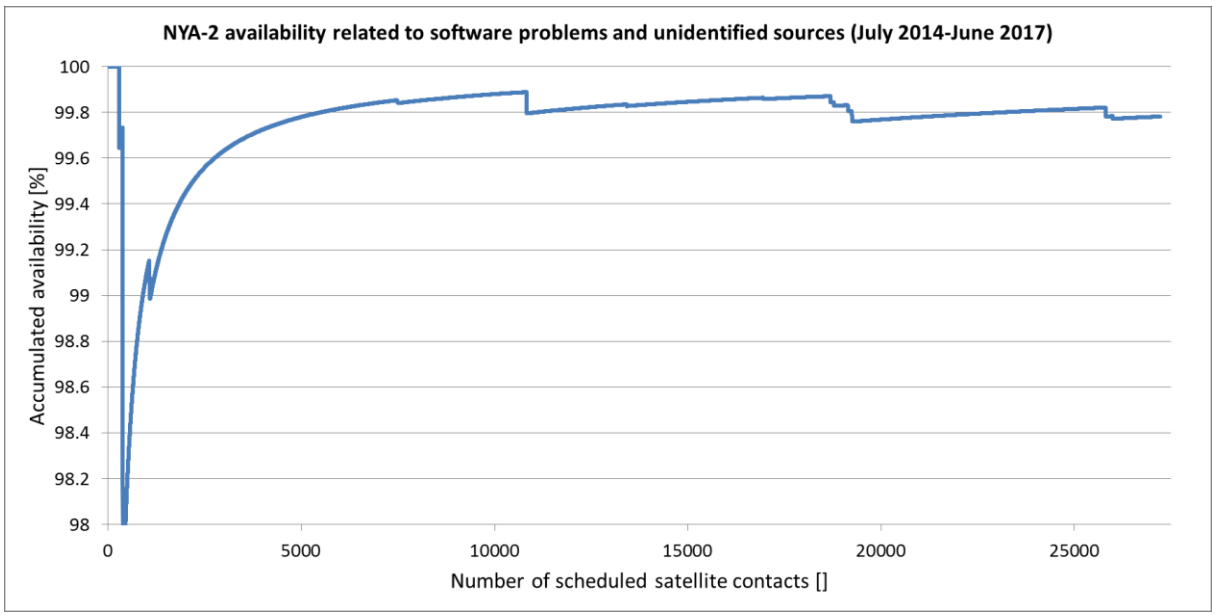

Figure 100: Accumulated availability of NYA-2 with NYA-Sattrack operation

The graphs above are based on records, which were practically accessible by the author only. An independent tool to monitor satellite reception activities with participation of GFZ is the so called Dump-Browser (Figure 101). This web based service displays, among many other parameters, the completeness of received data with respect to scheduled downlink data volumes. Each horizontal bar in Figure 101 represents data of one satellite and one day. The white timestamps correspond to the AOS times of contacts between the satellites and the NYA station. Some additional information is shown in different colours, e.g., detected crc errors of received telemetry data as vertical yellow dashes. All data losses in the scheduled downlink processes, no matter if caused by anomalies on the satellite, the active receiving antenna, including antenna operation software, the telemetry receiver or the contact scheduling, are

displayed as gaps (no colours). Examples of data gaps in Figure 101 are found for TerraSAR-X (TSX) on the 23rd of September 2015 (doy 266) and around 14:00 h on the next day (both not related to NYA-Sattrack). The absence of data gaps on the Dump-Browser display, on the other way round, thus indirectly attests a clean function of all components that were involved in the downlink, including the antenna operation software.

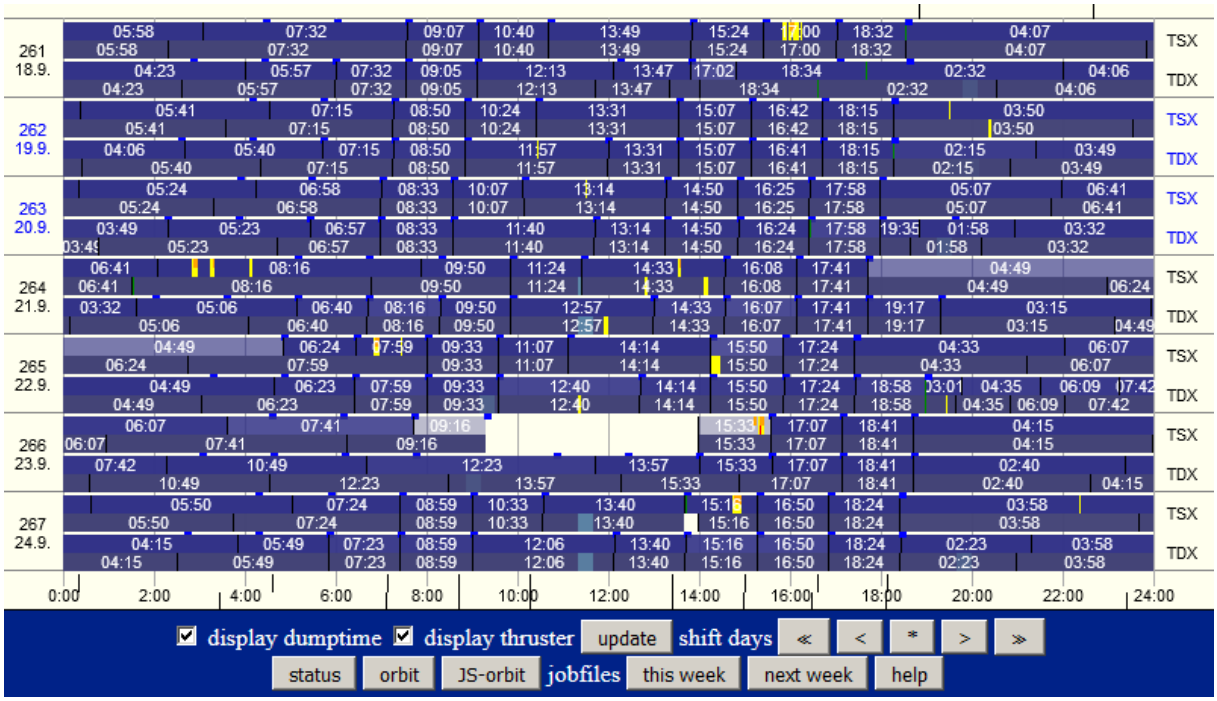

Figure 101: GFZ Dump-Browser screenshot from 2015 (© GFZ)

The Dump Browser was developed by GFZ (W. Köhler) for the CHAMP mission[9], but was still used for operational tasks, especially by staff at GFZ and GSOC for the missions GRACE, TerraSAR-X and Tandem-X. It was also accessible for other parties, e.g., JPL, which are partners of GZF in the missions GRACE and GRACE-FO. There is no comprehensive picture of antenna performance through the Dump-Browser functions which could directly support the findings from Figure 99 and Figure 100. However, the open access to the Dump-Browser allowed a kind of peer monitoring. Significant problems with the satellite reception at NYA, especially when they continue over longer terms, are usually detected by some of the mentioned parties (e.g. GSOC). The corresponding email traffic is traceable and does at least not contain any evidence that the NYA station performance decreased with NYA-Sattrack.

[9] A new Dump Browser is currently developed by GFZ (S. Reißland).

A reliability figure of 98%, as for NYA-1 in the early years (described in section 5.7), means that 1 contact out of 50 scheduled contacts failed. The regular mean working load for NYA-1 was 25 contacts per day (same as today) and this implies that one NYA-1 contact failed every second day on average. Such outage rates and the connected loss of data were not acceptable for any professional project participation. It also resulted in considerably high effort for problem analysis and troubleshooting.

A total system reliability of 99.5% or better is assumed to be applicable for each antenna at NYA in these days. On average this is only one (or less) of 200 contacts that fails (per antenna) every 8 days. This makes a significant difference in the end, both, for professional station support of satellite missions and with respect to maintenance effort. It is also considered to be a highly respectable figure for an unmanned station with regular, but not continuous, remote monitoring and control.

11 Summary

This work aimed on the proper preparation of the satellite-receiving station at Ny-Ålesund for future activities. The previously experienced station performance had several weak points and was threatened to get reduced even further due to aged components and the lack of support for important station operation software. As it was aspired to use the Ny-Ålesund station as the primary downlink station for the upcoming GRACE-FO mission, it became necessary to solve these problems and to prepare the station for a performance level that complies with the mission's requirements. The new antenna operation software NYA-Sattrack was developed, because this was identified as the key to achieve the required high operation performance, reliability and system sustainability.

NYA-Sattrack supported the determination of important station performance parameters at the NYA station with dedicated special functions, all for the first time. A combination of sun-tracking with raster scans was used to determine the effective antenna boresight offsets. The proper compensation of these offsets was then established and verified by NYA-Sattrack. The program was also used to investigate antenna radiation patterns, including half power beam widths, to derive a guideline for a sun exclusion angle, and for the determination of the antenna performance in terms of *G/T*, which is the most significant antenna parameter. Some shortcomings of the NYA-1 antenna positioning system were revealed also. The measurements could be made with fully installed radomes and with the sun as a natural source of radio signals, which was favourable or even required due to the special operation conditions at Ny-Ålesund. The new horizon scan function was the basis for the identification of an interfering radio signal (DORIS beacon) and for the verification that it does not reduce the NYA station RF-performance anymore (after changes in RF paths). All new functions are now valuable tools to maintain the established station performance, e.g., with regularly repeated control measurements.

The routine operation performance of the new software is excellent and the program GUI proofed to provide operational information and control in a task-adapted and very functional way. The basic activity logging fulfils the requirements of local (Norwegian) authorities while the extensive logging features, e.g., the novel graphical log, help to identify operation problems quickly, e.g., such resulting from faulty scheduling or hardware. The program execution requires minimal computer resources, which is the result of a careful software

design and the abstinence of unnecessary features, such as high-resolution graphics and high frequency display updates. The program NYA-GPS-Sync, other new software that was developed in this work, maintains computer system clock accuracies as good as required and corresponding to the investigated limits that are mainly defined by the computer hardware and the computer operation system.

Some new functions of NYA-Sattrack are not used for routine operations, e.g., the switching between two pass predictions and the interface for auto-tracking input, but show the potential of the software for future tasks. First useful applications of the switching function between different prediction tables (e.g., NORAD and GFZ predictions) can be expected for the LEOP of upcoming satellite missions to be received at Ny-Ålesund. The software design allows an adaptation to different antenna models and positioning systems, which supports the station sustainability, while the in-house development provides an independency from third parties w.r.t. matters of antenna operation. This point already proofed to be beneficial, when required changes of logfile- and jobfile formats were solved with low effort and in short times. The selected third party routines for the prediction of satellite pass directions ("Spacetrack report #3 software") is not considered to be a dependency, but as the application of a quasi-standard. These routines have a very high reputation since decades and should not need any improvements in the future. They are also based on publically available source code which can be modified as already done for the interaction with NYA-Sattrack.

This work covers a wide range of topics with relevance for a computerised antenna operation, from bit-level programming and antenna theory to graphical interfaces and system performance characterisation. There was no opportunity for testing activities with an involvement of antennas for most of the development time, which was a real challenge. Anyway the newly developed software NYA-Sattrack provides the projected performance as discussed in this work, offers several novel extra features and continues to pass the "litmus test" in a 24/7 operation at Ny-Ålesund with more than 25 satellite downlink contacts per day and antenna since July 2014. The demonstrated operation reliability, the theoretical assessments of the system performance and their software-aided determination by measurements were mandatory preconditions for NYA to be acceptable as the primary downlink station of the GRACE-FO mission. In consequence it will be possible to download all on-board data from both GRACE-FO satellites (a contractual obligation within the MOS

responsibilities of GFZ) and to provide it with very low latencies (e.g., for GNSS-RO data processing chains), all at comparable very low costs.

12 Ideas for future work

A possible improvement for the determination of antenna boresight offsets with NYA-Sattrack might be achieved by the replacement of the routine for the calculation of sun directions with a more precise routine, such as it was used in this work as a reference only. A consideration of radio wave refraction effects, which arise mainly due to the dispersive character of the Ionosphere, might be another improvement for measurements with the sun and for satellite tracking at low elevations. The accuracy of pedestal installations w.r.t. the alignment to zenith should be verified. This could be done with a clinometer at the antenna when it is turned around with constant elevation. Such measurements should also be helpful to investigate the detected inaccuracies of the NYA-1 antenna.

It might also be worth to try if the improved system performance (from improved boresight compensation, new LNAs, removal of intermediate preamplifiers) allows measurements with remote radio stars. Such radio stars are ideally small targets for the determination of boresight errors. Their electromagnetic flux is known precisely and has less fluctuation than the sun flux, which could thus also lead to more reliable *G/T* figures. Such measurements might be successful in the polar night when there is no sun at Ny-Ålesund and thus no sun noise signal reflections and less thermal noise from the environment.

The horizon scan function should be modified to conduct full scans of the local hemisphere in shorter times. Measurements in all seasons of the year might be interesting also. The obtained measurement data could be processed to maps of *G/T*. These could replace the currently practised antenna performance description by a single *G/T* value to provide an improved basis for the scheduling of satellite contacts. A beneficial combination of the used square and stripe type scan scheme could be a square scheme with turn directions that alternate after each transition to the next larger square.

An idea for a kind of auto-tracking function, without special auto-tracking devices, is the satellite-tracking with two antennas in a special configuration. One antenna would be used to receive satellite data while tracking the satellite with predicted satellite directions, in principle as usual, but with additional corrective positioning data from the second antenna. The second antenna would probe directions in a certain range around the predicted directions for a better

satellite reception, e.g., with respect to signal strength. Measured offsets between actual directions of the first antenna and directions of better signal reception as detected by the second antenna could be used for a stepwise adjustment of the tracking. This method supports a positioning of the first antenna according to the currently best information on the actual satellite directions, both, from predictions and the measurements of the second antenna. Thus the first antenna tracks the satellite always very close to its boresight direction with maximum antenna gain. The second antenna is operated around its boresight and thus effectively with reduced antenna gain. However, this has no negative impact on the reception result as it is used for direction correction only, but not for data reception.

All shown antenna measurements in the S-band should be repeated at other satellite communication frequencies, e.g., in the X-band, as this could pave the way for the support of more satellite missions with even more demanding requirements. Some corresponding prerequisites are already available at the station, e.g., radomes that are impedance-matched for S- and X-band. Also a new telemetry receiver for higher data rates, such as usually met at higher frequencies, was purchased by GFZ recently.

Appendix

Example of file with twoline elements ("15010702.tle")

Note: Orbit-related data is placed in the lines starting with "1" and "2", which are the twoline elements, while the first line of each block is for reference only (not part of official format definition).

```
GRACE1     Epoch: 20150107 06:00:00 ( Originator: GSOC )
1 27391U 02012A   15007.25000000 +.00011873  00000-0 +17702-3 0    00
2 27391  89.0027  88.8160 0011498  73.7005 156.9330 15.54928224717752

GRACE2     Epoch: 20150107 06:00:00 ( Originator: GSOC )
1 27392U 02012B   15007.25000000 +.00011816  00000-0 +17596-3 0    09
2 27392  89.0028  88.8548 0011894  74.1947 157.3763 15.54955471717753

TSAR-X     Epoch: 20150107 00:00:00 ( Originator: GFZ )
1 31698U 07026  A 15  7.00000000 0.00000690  00000-0  00000-0 0    14
2 31698  97.4451  16.3874 0000876  89.5989  12.6589 15.19148676419460

TDEM-X     Epoch: 20150107 00:00:00 ( Originator: GFZ )
1 36605U 10030  A 15  7.00000000 0.00000769  00000-0  00000-0 0    13
2 36605  97.4453  16.4291 0000969 215.8085 245.8140 15.19151125252161
```

Old NYA jobfile format (example: "nya_0515.gfz")

```
[System]
NrOfContacts=174

[NYA Kontakt 001]
Satellite=GR1
Acquisitn=02-FEB-2015 (doy033) 00:34:54 02-FEB-2015 (doy033) 00:39:24
Dump_____=02-FEB-2015 (doy033) 00:35:24 02-FEB-2015 (doy033) 00:38:54
Frequency=2211002

[NYA Kontakt 002]
Satellite=TSX
Acquisitn=02-FEB-2015 (doy033) 01:58:17 02-FEB-2015 (doy033) 02:00:47
Dump_____=02-FEB-2015 (doy033) 01:58:47 02-FEB-2015 (doy033) 02:00:17
Frequency=2280000
.
.
.

[NYA Kontakt 174]
Satellite=GR1
Acquisitn=08-FEB-2015 (doy039) 23:18:36 08-FEB-2015 (doy039) 23:23:06
Dump_____=08-FEB-2015 (doy039) 23:19:06 08-FEB-2015 (doy039) 23:22:36
Frequency=2211002
```

New NYA jobfile format (example)

```
[NYA Contact 001]
Ant=NYA1
Satellite=FLP
Acqn=20161017T00:19:46 20161017T00:24:46
Dump=20161017T00:20:16 20161017T00:24:16
Frequency=2.XXX
Polarization=R
Datarate=1XXXXX
Receiver=RX1-1 RX2-2

[NYA Contact 002]
Ant=NYA2
Satellite=FLP
Acqn=20161017T00:19:46 20161017T00:24:46
Dump=20161017T00:20:16 20161017T00:24:16
Frequency=2.XXXXXX
Polarization=L
Datarate=1XXXXXX
Receiver=RX1-2 RX2-1
.
.
.
```

Station configuration file for NYA-Sattrack (“station_config.txt”)

```
#
#   config file for NYA-Sattrack program
#
# - comment lines begin with "#"
# - the first entry in each line is a keyword and must not be modified
# - the keyword must begin at first position in a line and followed by at
#   least one space
# - multiple entries in one line must be separated by spaces
# - be careful when introducing changes
#
#
# user notes:
#
#
#
#
# CONFIG AREA STARTS BELOW THIS LINE
#
# station name, to be used for display and pass-logfiles
station   SRS-NYA, GFZ-Potsdam
#
# antenna acronym to be used for logfile naming
antacronym NYA1
#
# station latitude (degrees "dot" decimal degrees, F7.4)
#statlat   50.0000
statlat   78.9275
#
# station longitude (degrees "dot" decimal degrees, F7.4)
#statlon   10.0000
statlon   11.8825
#
# station altitude (meters "dot" cm, F7.2)
statalt      35.00
#
# timestep for antenna positioning table [s] (default is 001.00000000)
```

```
timestep  001.00000000
#
# number of interpolated points to be inserted between calculated positioning
# commands (if applicable)
interpoint   5
#
# which antenna DLL-file is to be used
ant_dll    SA_GPIB_150413.DLL
#ant_dll    SA_GPIB_150402.DLL
#ant_dll    SA_GPIB_141023.DLL
#ant_dll    CGC-XY_140815.DLL
#
# maximum allowed antenna axes angular rotation speed [deg/s]
maxspeed     4.0
#
# use autotrack information (0 = no, 1 = yes)
autotrack     0
#
# serial comport parameter for antenna steering (e.g., COM1  19200 8 N 1)
comporta COM1  19200 8 N 1
#
# serial comport parameter for autotrack offset input (e.g., COM2  19200 8 N 1)
comporto COM4  19200 8 N 1
#
# serial comport parameter for communication with analyser (e.g., COM6  9600 8 N 1)
comportz COM6   9600 8 N 1
#
# GPIB controller address (PC board, e.g., 0 for GPIB-0, if applicable)
gpib-co   0
#
# GPIB ACU primary address (used for SA-antenna, 0 - 30, e.g., 5)
gpib-pa   5
#
# GPIB ACU secondary address (used for SA-antenna, 0 or 96 - 126)
gpib-sa   0
#
# antenna elevation mask file (ascii, az, el)
elemask    antmask2.txt
#
# full or relative path and name of incoming jobfile directory
jobpath  E:\NYA-Sattrack\incoming
#
# full or relative path and name of incoming tlefile directory
tlepath  E:\NYA-Sattrack\incoming
#
# external pass prediction program 1 ececutable file
predict_1   E:\NYA-Sattrack\Vallado_WGS721.exe
#
# external pass prediction program 1 short name / description
p1_name   "Spacetrack Vallado-WGS721"
#
# external pass prediction program 1 output filename
calcout_1   E:\NYA-Sattrack\calc_out3.txt
#
# external pass prediction program 2 executable file
predict_2   E:\NYA-Sattrack\Vallado_WGS84.exe
#
# external pass prediction program 2 short name / description
p2_name   "Spacetrack Vallado-WGS84"
#
# external pass prediction program 2 output filename
calcout_2   E:\NYA-Sattrack\calc_out2.txt
#
# method for adjustment of prediction, e.g., autotracking
passadjust   no adjustment
#
# external program to be executed when tracking is initialised
pretrack
```

```
#
# external program to be executed when tracking was finished succesfully
pasttrack ftplogpush_NYA-1_170117.exe
#
# external program to be executed when tracking failed
failtrack failtrack_170118.exe
#
# automatic jobfile update interval [min] (0 - 1440, 0 = no auto update)
auto_job    1
#
# automatic tlefile update interval [min] (0 - 1440, 0 = no auto update)
auto_tle    1
#
# automatic generation of skyplot bitmap files at the end of each pass (379 KB)
skyplot     1
#
# static installation offset of antenna azimuth [degrees] (+/-0.00)
# (if not yet considered by the ACU)
stataz    0.00
#
# static installation offset of antenna elevation [degrees] (+/-0.00)
# (if not yet considered by the ACU)
statel    0.00
#
# static time offset, e.g. ACU processing time [s] (+/-0.00)
statti    -0.00
#
# start program normal or in testmode
# (no abort of tracking if no reply from antenna)
testmode  1
#
# end of file
```

Satellite database file for NYA-Sattrack (“satellites.txt”)

```
#
# satellite data base
#
# format:
# column 1 (1):  satellite acronym (A3)
# column 2 (10): NORAD ID as used in twoline element files (A5)
# column 3 (16): clear name of the satellite (A10)
#
CMP       26405 CHAMP
SAC       26620 SAC-C
GR1       27391 GRACE-1
GR2       27392 GRACE-2
TSX       31698 TerraSAR-X
TDX       36605 TANDEM-X
# end of file
```

Example of entries in NYA-Sattrack program activity logfile (“prog_log.txt”)

```
2015-05-26 13:53:59 E:\NYA-Sattrack, NYA-Sattrack, V. 26.5.2015 + SA_GPIB_150421.dll started
on FantechNYA1
2015-05-26 13:53:59 antenna: NYA1, Scientific Atlanta + 3860-Controller, GPIB: PC 0, ACU 5, 0
2015-05-26 13:53:59 predict_1 = E:\NYA-Sattrack\Vallado_WGS84.exe
2015-05-26 13:53:59 predict_2 = E:\NYA-Sattrack\Vallado_WGS721.exe
2015-05-26 13:54:05 update: GR1_20150526_144806, waiting for sat
2015-05-26 13:54:09 user opened test and maintenance window
2015-05-26 13:54:17 user closed test and maintenance window
2015-05-26 14:48:02 antenna status: ACU connected, antenna status available
2015-05-26 14:48:03 GR1_20150526_144806, start tracking
2015-05-26 14:53:06 GR1_20150526_144806, stop tracking
.
```

Example of logfile for regular satellite tracking ("TerraSAR_X_49043_20160418_110658_NYA2.trk")

```
# station:    SRS-NYA, GFZ-Potsdam,  78.9275 N   11.8825 E     35.00 m
# antenna:    NYA2, CGC, X/Y axes positioning system
# satellite:  TerraSAR-X, ID: 31698
# frequency:  2280.000
# program:    NYA-Sattrack, V. 18.8.2015 + CGC-XY_160418.DLL
# prediction: "Spacetrack Vallado-WGS84" + 16041802.tle
#
# date       time   ms    az-calc-el     az-off-el   az-comm-el   az-current-el
2016-04-18 11:06:59.002  68.06  18.02   0.00   0.00  68.06  18.02  68.06  18.02
2016-04-18 11:07:00.002  67.94  18.17   0.00   0.00  67.94  18.17  67.94  18.17
2016-04-18 11:07:01.002  67.81  18.32   0.00   0.00  67.81  18.32  67.81  18.32
.
.
.
```

Example of logfile for sun-tracking with recording of analyser data ("sun_track_NYA1_160419084039.txt")

```
# station:    SRS-NYA, GFZ-Potsdam,  78.9275 N   11.8825 E     35.00 m
# antenna:    Scientific Atlanta + 3860-Controller, GPIB: PC 0, ACU 5, 0
# program:    NYA-Sattrack, V. 18.4.2016 + SA_GPIB_150413.DLL
#
# sun tracking
#
# date       time   ms    az-calc-el     az-off-el   az-comm-el   az-current-el analyser
2016-04-19 08:40:42.003 140.39  20.35   0.00   0.00 140.39  20.35 140.39  20.35 -143.958
2016-04-19 08:40:43.003 140.39  20.35   0.00   0.00 140.39  20.35 140.39  20.35 -143.911
2016-04-19 08:40:44.003 140.39  20.35   0.00   0.00 140.39  20.35 140.39  20.35 -143.962
.
.
.
```

Extract from "toss2000" code for calculation of seconds in elapsed years

```
' step through the years from 2000 to (actual year - 1)
FOR I = 0 TO (actual year - 1)
  IF I MOD 4 = 0 THEN                       ' true for switch years
    ss2000out = ss2000out + 31622400        ' add seconds in switch year
  ELSE
    ss2000out = ss2000out + 31536000        ' add seconds in normal year
  END IF
NEXT I
```

Extract from "fromss2000" code to calculate the day number in the current month

At this point of code the ss2000in input value is already reduced according to fully elapsed years and months by preceding code

```
day = 1                             ' begin with first day of month
DO WHILE ss2000in > 86400           ' 86400 = number of seconds in one day
   day = day + 1                    ' count days in month
   ss2000in = ss2000in - 86400      ' reduce seconds according to counted days
LOOP                                ' loop until less seconds than for one day
```

List of figures

List of abbreviations and glossary

ACU	Antenna Control Unit (Interface system between steering PC and antenna)
AOS	Acquisition of signal (satellite)
ASC	Advanced Stellar Compass
ASCII	American Standard Code for Information Interchange
Astrofein	Astro- und Feinwerktechnik Adlershof GmbH
AWI	Alfred Wegener Institute, Helmholtz-Centre for Polar and Marine Research
AWIPEV	Joint French - German Arctic Research Base at Ny-Ålesund (AWI and Polar Institute Paul Emile Victor, IPEV)
BASIC	Beginner's All-purpose Symbolic Instruction Code (programming language)
BPSK	Binary Phase Shift Keying
CC-BY-SA	Creative Commons license with author attribution (BY) and share alike (SA)
CHU	Camera Head Unit (image sensor of ASC)
CONAE	Comisión Nacional de Actividades Espaciales (Space agency of Argentina)
COTS	Commercial off-the-shelf
CRC	Cyclic Redundancy Check
CSSI	Center for Space Standards and Innovation
DIDM	Digital Ion Driftmeter
DLR	Deutsches Zentrum für Luft- und Raumfahrt (national aeronautics and space research centre of Germany)
DLL	Dynamic Link Library (binary containing program resources that are used / linked by calling programs on demand only)
DORIS	Doppler Orbitography and Radiopositioning Integrated by Satellite
DOS	Disc Operation System (early computer operation system of Microsoft)
DSR	Data Set Ready (signal of RS-232 serial interface standard)
DTR	Data Terminal Ready (signal of RS-232 serial interface standard)
DWD	Deutscher Wetterdienst (German weather service)
ECEF	Earth-Centered, Earth-Fixed
ECMWF	European Centre for Medium-Range Weather Forecasts
EGSIEM	European Gravity Service for improved Emergency Management
FORTRAN	Formula Translating System (programming language)
GFZ	German Research Centre for Geosciences, Helmholtz-Centre Potsdam
GPS	Global Positioning System
GPS-RO	GPS radio occultation
GSOC	German Space Operation Center
GNSS	Global Navigation Satellite System (e.g., GPS)
GNSS-R	Global Navigation Satellite System Reflectometry
GNSS-RO	Global Navigation Satellite System Radio Occultation
GPMRC	Recommended Minimum Sentence C
GUI	Graphical User Interface

IEEE	Institute of Electrical and Electronics Engineers
IRS	Institut für Raumfahrtsysteme (Institute for space flight) Stuttgart
ISA	Industry Standard Architecture (computer interface-slot for extension boards)
ITU	International Telecommunication Union
KVM	Keyboard, Video, Mouse. A KVM-switch connects one set of KVM devices with multiple computers.
LEO	Low Earth Orbit (altitudes between 200 and 2000 km)
LEOP	Launch and Early Orbit Phase
LHCP	Left Hand Circular Polarisation
LNA	Low Noise Amplifier
LOS	Loss of (satellite) signal
MOS	Mission Operation System
NMEA-0183	National Marine Electronics Association (interface specification, v. 0183)
NORAD	North American Aerospace Defence Command
NTP	Network Time Protocol
NYSMAC	Ny-Ålesund Science Manager Committee
O-QPSK	Offset Quadrature Phase-Shift Keying
POD	Precise Orbit Determination
pps	Pulse Per Second
PRARE	Precise Range And range Rate Equipment
QPSK	Quadrature Phase-Shift Keying
RF	Radio frequency
RHCP	Right Hand Circular Polarisation
ROM	Radio Occultation Meteorology
SAF	Satellite Application Facility
SAR	Synthetic Aperture Radar
SCN	Satellite Catalog Number
STK	Satellite Tool Kit (Commercial Software)
SWR	Standing Wave Ratio
TEME	True Equator Mean Equinox
TIC	Time Interval Counter
UPS	Uninterruptable Power Supply
USB	Universal Serial Bus (computer interface standard)
TanDEM-X	TerraSAR-X add-on for Digital Elevation Measurement
TLE	Twoline elements (satellite orbit properties, noted in a two lines format)
VLBI	Very Long Baseline Interferometry

List of references

Andreas, A. *MIDC SPA (Solar Position Algorithm) Calculator.* 2008-2011. https://www.nrel.gov/midc/solpos/spa.html (accessed Dec. 17, 2015).

Baldesarra, M., Brieden, P., Danzmann, K., Daras, B., Doll, B., Feili, D., Flechtner, F., Flury, J., Gruber, T., Heinzel, G., Iran Pour, S., Kusche, J., Langemann, M., Lücher, A., Müller, J., Müller, V., Murböck, M., Naeimi, M., Pail, R., Raimondo, J.-C., *e2.motion - Earth System Mass Transport Mission (Square) - Concept for a Next Generation Gravity Field Mission - Final Report of Project Satellite Gravimetry of the Next Generation (NGGM-D).* München: Deutsche Geodätische Kommission der Bayerischen Akademie der Wissenschaften, Reihe B, Angewandte Geodäsie ; 318, 2014.

Briess, K., G. Kornemann, and J. Wickert. “MicroGEM: Microsatellites for GNSS Earth Monitoring.” Abschlussbericht Phase 0/A, 2009.

Buhl, M., J. Wickert, and M. Rothacher. "Machbarkeitsuntersuchung NanoX (ger.), Final Report." Berlin, 11 14, 2013. pp121.

Cakaj, S., W. Keim, and K. Malaric. "Sun Noise Measurement at Low Earth Orbiting Satellite Ground Station." *47th International Symposium ELMAR.* Zadar, Croatia, 2005.

California Polytechnic State University. "6U CubeSat Design Specification, Rev. PROVISIONAL." April 20, 2016.

Cardinali, C., and S. B. Healy. “Impact of GPS radio occultation measurements in the ECMWF system using adjoint-based diagnostics.” *Q.J.R. Meteorol. Soc., 140*, 2014: 2315-2320.

Carreno-Luengo, H., A. Camps, I. Perez-Ramos, G. Forte, R. Onrubia, and R. Diez. "3Cat-2: A P(Y) and C/A GNSS-R Experimental Nano-Satellite Mission." Melbourne, Australia, IEEE, 2013.

CelesTrak. *NORAD Two-Line Element Set Format.* 2004. http://www.celestrak.com/NORAD/documentation/tle-fmt.asp (accessed 12 16, 2016).

CGC Technology Ltd. "GFZ – Ny Alesund Antenna Control & Scheduling Software Manual." *Doc Ref: CGC/2004179/05/002/TD Issue 1.0.* April 11, 2005.

Cole, S., and A. Buis. *NASA PRESS RELEASE 17-084.* 27 October 2017. https://www.nasa.gov/press-release/prolific-earth-gravity-satellites-end-science-mission (accessed October 2017).

Danish Meteorological Institute. *ROM SAF - Monitoring of NRT Products.* 2015. http://www.romsaf.org/monitoring/index.php (accessed 12. 10., 2015).

Dietrich, Fred J., and Richard S. Davies. "Communication Architecture." In *Space Mission Analysis and Design (Third Edition)*, edited by Wiley J. Larson and James R. Wertz, Chapter 13. Microcosm Press and Kluwer Academic Publishers, 1999.

Falck, C. "NYA antennas G over T measurements." *Technical Report GFO-GFZ-TR-1002, Issue 1.0.* Potsdam, December 15, 2015.

Falck, C., F. Flechtner, F. H. Massmann, J. C. Raimondo, Ch. Reigber, and A. Scherbatschenko. “Betrieb des PRARE-Bodensegments für ERS-2 - Abschlussbericht 2003.” Potsdam, 2013.

Falck, C., S. Reißland, K. Snopek, and F. H. Massmann. “NYA Jobfile Description.” *Technical Report NYA-GFZ-SP-1001, Issue 1.0.* July 2017.

Flechtner, F., Neumayer, K. H., Dahle, Ch., Dobslaw, H., Fagiolini, E., Raimondo, J. C., Güntner, A. “What Can be Expected from the GRACE-FO Laser Ranging Interferometer for Earth Science Applications?” *Surveys in Geophysics*, March 2016: 453–470.

GARMIN International, Inc. "GPS 16/17 SERIES TECHNICAL SPECIFICATIONS." Olathe, USA, October 2005.

Gouweleeuw, B., T., Kvas, A., Grüber, C., Gain, A., K., Mayer-Gürr, T., Flechtner, F., Güntner, A. "Daily GRACE gravity field solutions track major flood events in the Ganges-Brahmaputra Delta." *Hydrology and Earth System Sciences (HESS)*, 2018: Accepted for review: 31 Jan 2017 – Discussion started: 07 Feb 2017.

Healy, S.B., J. Wickert, G. Michalak, T. Schmidt, and G. Beyerle. “Combined forecast impact of GRACE-A and CHAMP GPS radio occultation bending angle profiles.” *ATMOSPHERIC SCIENCE LETTERS*, 2007: Issue 8: 43 – 50.

Heise, S., N. Jakowski, A. Wehrenpfennig, Ch. Reigber, and H. Lühr. “Sounding of the topside ionosphere/plasmasphere based on GPS measurements from CHAMP: Initial results.” *Geophys. Res. Lett., 29(14)*, 2002.

Herman, J., A. Davis, K. B. Chin, M. Kinzler, S. Scholz, and M. Steinhoff. "Life with a weak Heart; Prolonging the Grace Mission despite degraded Batteries." Stockhom, Schweden, 11.-15. June, 2012.

Hoots, Felix R., and R. L. Roehrich. *Spacetrack Report #3: Models for Propagation of the NORAD Element Sets.* Colorado Springs, CO: U.S. Air Force Aerospace Defense Command, 1980.

IN-SNEC. “CORTEX-XL Series-RTR USER’S MANUAL.” *DTU 000499 Ver.2 – Rev. 0.* 17 1 2006.

International Organization for Standardization. "Data elements and interchange formats – Information interchange – Representation of dates and times, ISO 8601." 1988.

ITU Radiocommunication Assembly. "Determination of the G/T ratio for Earth stations operating in the fixed-satellite service." *Recommendation ITU-R S.733-2.* 1992-1993-2000.

ITU Radiocommunication Assembly. "Radio noise." *Recommendation ITU-R P.372-12.* July 2015 a.

ITU Radiocommunication Assembly. "Attenuation by atmospheric gases." *Recommendation ITU_R. P.676-10.* September 2013.

Jaeggi, A., Weigelt, M., Flechtner, F., Guentner, A., Mayer-Gürr, T., Martinis, S., Bruinsma, S., Flury, J., Bourgogne, S. “European Gravity Service for Improved Emergency Management - a new Horizon2020 project to serve the international community and improve the accessibility to gravity field products.” *Presentation at EGU.* 2015.

Jakowski, N., Wehrenpfennig, A., Heise, S., Reigber, C., Lühr, H., Grunwaldt, L., Meehan, T. K. "GPS radio occultation measurements of the ionosphere from CHAMP: Early results." *Geophys. Res. Lett., 29(10)*, 2002.

Jayles, C., B. Nhun-Fat, and C. J Tourain. "DORIS: system description and control of the signal integrity." *Journal of Geodesy*, 2006: Volume 80, Issue 8, pp 457–472.

Keil, N., and G. Altenburg. "Fehleranalyse CHAMP, Ereignis vom 28.01.03 (DOY 028)." CHAMP project-internal document, Jena-Optronik GmbH, 2003.

Klein, B., and K. Snopek. "Level 4 MOS Requirements." *GFO-DLR-RQT-1003, Issue 2.1.* 6 15, 2015.

livioflores-ga, google.com:. *Equation to know where the Sun is at a given place at a given date-time.* Nov. 2006. http://answers.google.com/answers/threadview/id/782886.html (accessed Dec. 17, 2015).

Maral, G., and M. Bousquet. *Satellite Communications Systems: Systems, Techniques and Technology (Third Edition).* Wiley, 1998.

Martin-Neira, M. "A Passive Reflectometry and Interferometry System (PARIS): Application to Ocean Altimetry." *ESA Journal., vol. 17*, 1993: pp. 331–355.

Massmann, F., H. "CHAMP Satellitenbetrieb Nov. 2009/Sep. 2010 (Missionsende)." *Schlussbericht Zeitraum 01.11.2009 bis 19.09.2010, FZ: 50 EE 0944.* March 2011.

Melbourne, W. G., Davis, E. S., Duncan, C. B., Hajj, G. A., Hardy, K. R., Kursinski, E. R., Meehan, T. K., Young, L. E., Yunck, T. P. "The application of spacebourne GPS to atmospheric limb sounding and global change monitoring." *JPL Publication 94-18*, 1994: 147 pp.

National Marine Electronics Association. "NMEA 0183." March 1983.

National Oceanic and Atmospheric Administration. "NOAA Global Vegetation Index User's Guide; APPENDIX L: Software to Calculate Relative Azimuth from Third Generation Weekly Composite GVI Date." Suitland, USA: Katherine B. Kidwell (editor), July 1997.

PowerBASIC, Inc,. "Visual Designer for PowerBASIC Windows Compiler, Version 2.01.0102." 2010.

PowerBASIC, Inc. "PowerBASIC 10 for Windows, PB/Win IDE, Version 10.04.0108." 2012.

Proakis, J., and M. Salehi. *Digital Communications.* McGraw-Hill Education, 2007.

Reda, I., and A. Andreas. "Solar Position Algorithm for Solar Radiation Applications." *Solar Energy. Vol. 76(5)*, 2004: pp. 577-589.

Reigber, C., Lühr, H., Grunwaldt, L., Förste, C., König, R., Massmann, F.-H., Falck, C. "CHAMP Mission 5 Years in Orbit." In *Observation of the Earth System from Space*, by J. Flury, R. Rummel, C. Reigber, M. Rothacher, G. Boedecker and U. Schreiber, p. 3-16. Springer, 2006.

Rohde & Schwarz. "Calibration Certificate 10300352529." Memmingen, 2015.

Rohde & Schwarz. *R&S FSP Spectrum Analyzer Operating Manual.* Munich, 2009.

Rolinski, A. J., D. J. Carlson, and R. J. Coates. "The X-Y Antenna Mount for Data Acquisition from Satellites." *IRE TRANSACTIONS ON SPACE ELECTRONICS AND TELEMETRY*, 1962: 159-163.

Ruf, C., Unwin, M., Dickinson, J., Rose, R., Rose, D., Vincent, M., Lyons, A. "CYGNSS: Enabling the Future of Hurricane Prediction." *IEEE Geoscience and Remote Sensing Magazine, Vol.1(2)*, 2013.

Schmidt, T., J. Wickert, G. Michalak. "The operational processing system for GPS radio occultation data from CHAMP and GRACE." In *System Earth via Geodetic-Geophysical Space Techniques*, by F. Flechtner, et al., 455-460. Springer, 2010.

Scientific Atlanta. "Scientific Atlanta X-band Remote Sensing Antenna System." *System Manual, Publication No. 55S576Z, Manual Part No. 535807.* October 1996 b.

Scientific Atlanta. "Scientific Atlanta Series 3860 Digital Controller Operation and Maintenance Manual." *Publication No. 55E616Z/6288, Manual Part No. 536003, First Edition.* October 1996 a.

Sheard, B. S., G. Heinzel, K. Danzmann, D. A. Shaddock, W. M. Klipstein, and W. M. Folkner. "Intersatellite laser ranging instrument for the GRACE follow-on mission." *Journal of Geodesy*, December 2012: Volume 86, Issue 12, pp 1083–1095.

Stanford Research Systems. “SR620 Universal Time Interval Counter.” Vol. Revision 2.7. Sunnyvale, California 94089, USA, 2 2006.

Stosius, R., G. Beyerle, A. Hoechner, J. Wickert, and J. Lauterjung. "The impact on tsunami detection from space using GNSS-reflectometry when combining GPS with GLONASS and Galileo on GNSS-Reflectometry tsunami detection from space." *Advances in Space Research, 47, 5,*, 2011: 843-853.

Thales Alenia Space. “Assessment of a Next Generation Mission for Monitoring the Variations of Earth’s Gravity.” Final Report SD-RP-AI-0688, 2010.

United States Naval Observatory, Her Majesty's Nautical Almanac Office, ed. *The astronomical almanac for the year 2014.* 2014.

Unwin, M., P. Jales, J. Tye, C. Gommenginger, G. Foti, and J. Rosello. “GNSS-Reflectometry on TechDemoSat-1: Early Mission Operations and Exploitation.” *IEEE Journal of Selected Topics in Applied Earth Observations and Remote Sensing, 9, 10*, 2016: 4525-4539.

Vallado, D. A., P. Crawford, R. Hujsak, and T. S. Kelso. "Implementing the Revised SGP 4 in STK." *AGI User Exchange.* Washington, DC and San Diego, CA, October 2006 b.

Vallado, D. A., P. Crawford, R. Hujsak, and T. S. Kelso. *Source Code and Readme file for paper AIAA 2006-6753.* https://celestrak.com/publications/AIAA/2006-6753/AIAA-2006-6753.zip, July 16, 2012.

Vallado, D. A., P. Crawford, R. Hujsak, and T.S. Kelso. "Revisiting Spacetrack Report #3." *AIAA/AAS Astrodynamics Specialist Conference, AIAA 2006-6573.* Keystone, CO, USA, August 2006 a.

Vallado, D.A. *Fundamentals of Astrodynamics and Applications.* 2007.

Wehrenpfennig, A., N. Jakowski, and J. Wickert. "A Dynamically Configurable System for Operational Processing of Space Weather Data." *Physics and Chemistry of the Earth (C), 26, 8*, 2001: 601—604.

Wickert, J. “Das CHAMP-Radiookkultationsexperiment: Algorithmen, Prozessierungssystem und erste Ergebnisse.”, Scientific Technical Report STR02/07, pp 147, Potsdam, 2002.

Wickert, J., Reigber, C., Beyerle, G., König, R., Schmidt, T., Grunwaldt, L., Galas, R., Meehan, T., Melbourne, W. G., Hocke, K. “Atmosphere sounding by GPS radio occultation: First Results from CHAMP.” *Geophysical Research Letters, 28, 17*, 2001: 3263-3266.

Wickert, J., Schmidt, T., Michalak, G., Heise, S., Arras, C., Beyerle, G., Falck, C., König, R., Pingel, D., Rothacher, M. "GPS Radio Occultation with CHAMP, GRACE-A, SAC-C, TerraSAR-X, and FORMOSAT-3/COSMIC: Brief Review of Results from GFZ." In *New Horizons in Occultation Research: Studies in Atmosphere and Climate*, by A. Steiner, B. Pirscher, U. Foelsche and G. Kirchengast, p. 3-16. Springer, 2009 a.

Wickert, J., G. Michalak, T. Schmidt, G. Beyerle, C.Z. Cheng, S.B. Healy, S. Heise, C.Y. Huang, N. Jakowski, W. Köhler, C. Mayer, D. Offiler, E. Ozawa, A.G. Pavelyev, M. Rothacher, B. Tapley, and C. Arras: “GPS radio occultation: Results from CHAMP, GRACE and FORMOSAT-3/COSMIC”, Terrestrial, Atmospheric and Oceanic Sciences, 20, doi: 10.3319/TAO.2007.12.26.01(F3C) 2009 b.

Wickert, J., M. Rothacher, K. Brieß, G. Wahnschaffe, and N. Pilz. “NanoGEM - Phase A, SAT-NanoGEM-1000-RP01_1-3_Schlussbericht.” Berlin, 29 Oktober 2011. pp 144.

Wickert, J., T. Schmidt, G. Beyerle, R. König, Ch. Reigber, and N. Jakowski. “The radio occultation experiment aboard CHAMP: Operational data analysis and validation of vertical atmospheric profiles.” *J. Met. Soc. Japan,Special issue 'Application of GPS Remote Sensing to Meteorology and Related Fields', 82(1B)*, 2004: 381-395.

Wickert, J., E. Cardellach, M. Martin-Neira, J. Bandeiras, L. Bertino, O.B. Andersen, A. Camps, N. Catarino, B. Chapron, F. Fabra, N. Floury, G. Foti, C. Gommenginger, J. Hatton, P. Høeg, A. Jäggi, M. Kern, T. Lee, Z. Li, H. Park, N. Pierdicca, G. Ressler, A. Rius, J. Rosello, J. Saynisch, F. Soulat, C.K. Shum, M. Semmling, A. Sousa, J. Xie,

and C. Zuffada, GEROS-ISS: GNSS REflectometry, Radio Occultation, and Scatterometry Onboard the International Space Station, IEEE Journal of selected topics in applied Earth observations and Remote Sensing, doi: 10.1109/JSTARS.2016.2614428, 2016.

Wiedemann, K. "GRACE Follow On RF Compatibility Test Plan and Procedure 1.0." Technical Report, 2014.

Williams, Edward A. (Editor-in-Chief). *National Association of Broadcasters Engineering Handbook.* Taylor & Francis, 2013.

Zus, F., L. Grunwaldt, S. Heise, G. Michalak, T. Schmidt, and J. Wickert. “Atmosphere sounding by GPS radio occultation: First results from TanDEM-X and comparison with TerraSAR-X.” *Advances in Space Research, 53, 2*, 2014: 272-279.